An Investigation into the Structure and Localisation of the Bacterial Twin Arginine Translocase (Tat) Complexes by Electron Microscopy

Sarah Marie Smith BSc

A thesis submitted for the degree of Doctor of Philosophy
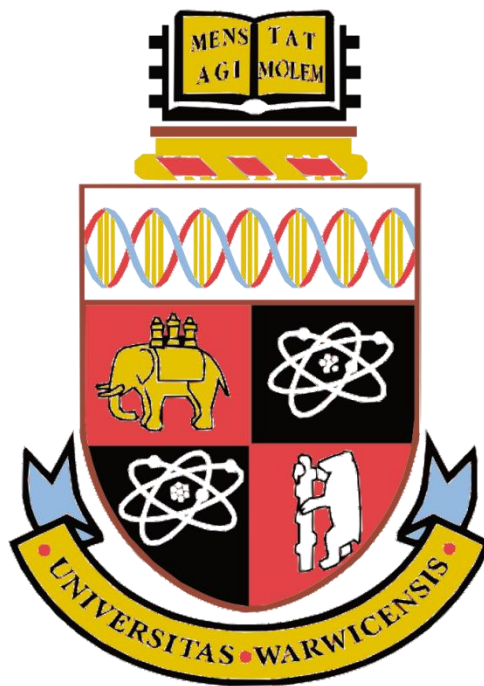
University of Warwick

School of Life Sciences

September 2015

Table of Contents

List of Figures

List of Tables

Acknowledgements

Firstly I would like to give my sincerest thank you to my supervisors, Professor Colin Robinson and Dr Corinne Smith for providing me with the opportunity to undertake this research project; and for their continual guidance and help throughout my 4 years as a PhD student.

I thank Ian Hands-Portman for his advice and assistance in the EM suite; and Andy Yarwood for help with the array tomography work- his input has been invaluable.

To Dr Roshani Patel and Dr Charlotte Carroll, thank you for being such wonderful friends, always providing me with much sound advice and encouragement (and plenty of laughs!).

Thank you to Harrison for his love and support throughout this endeavour and his patience when work (very frequently), took over the rest of my life!

Thank you to my close family for their continual love and support throughout my education, and life in general.

Thank you

Declaration

The work presented in this thesis is original, and was conducted by the author (unless otherwise stated), under the supervision of Professor Colin Robinson and Dr Corinne Smith.

None of the work presented in this thesis has been submitted previously for another degree.

All sources of information have been acknowledged by means of reference.

Collaborative work has been conducted contributing to material presented in this thesis. The extent of the collaborative work is indicated in the relevant chapters. In summary, collaborative work was carried out with the following:

Dr David Scott (Research Complex Harwell) performed the analytical ultracentrifugation.

Dr Cvetelin Vasilev (University of Sheffield) performed AFM analysis.

Andrew Yarwood (JEOL, UK) assisted in array tomography work.

Summary

The twin arginine translocase (Tat) pathway is expressed in the inner membrane of both Gram-negative and Gram-positive bacteria. The model organism for each of these bacteria is *Escherichia coli* and *Bacillus subtilis*, respectively.

In *B. subtilis* the Tat machinery is comprised of only TatA and TatC subunits. Namely, TatAdCd and TatAyCy translocases, which act in parallel, yet possess different substrate specificities. Little structural information is known about these multimeric integral membrane protein complexes owing to the difficulty in their purifications, small size and compositional heterogeneity. A primary structural investigation was performed on TatAyCy to gauge the true molecular weight and heterogeneity of this complex, providing fundamental insight into the effect that detergent solubilisation can have on a detergent-solubilised protein. Therefore, I circumvented the use of detergent and analysed Tat machinery in its native cellular environment. To achieve this, I developed a novel combinatorial approach of immunogold labelling with the volumetric microscopy technique- array tomography.

The *E. coli* Tat system is comprised of three proteins: TatA, TatB and TatC. TatA is believed to constitute the protein-conducting element of the translocase machinery. However recent structural data has cast doubt on the biological significance of the properties of this protein, and consequently its role in the translocation process. Therefore, by using array tomography, I endeavoured to directly visualise TatA in its native cellular environment to gain insight into the localisation and distribution of this protein in *E. coli*. TatA was shown to cluster along the inner membrane in a TatBC-dependent manner. This is the first time that any Tat component has been visualised in 3D space, *in situ*.

Additionally, the detailed insight into the exploitation of Tat machinery for the export of high value, biotechnologically-relevant protein was investigated; with a potential for this translocase to be used in cell surface display technologies revealed.

Abbreviations

Å	Ångströms
AFM	Atomic force microscopy
APH	Amphipathic Helix
APS	Ammonium persulphate
ATP	Adenosine triphosphate
BN-PAGE	Blue Native PAGE
BSA	Bovine serum albumin
C-	Carboxy terminus
C	Cytoplasmic fraction
$C_{12}E_9$	Nonaoxyethylene n- dodecyl ether
CMC	Critical Micelle Concentration
CpTat	Chloroplast Tat
Δ (Delta)	Gene deletion
DDM	n-Dodecyl-β-D-maltoside
DMSA	Dimethyl sulfoxide reductase
DOPC	1,2-Dioleoyl-sn-glycero-3-phosphocholine
E	Elution fraction
ECL	Enhanced chemifluoresence
EDTA	Ethylenediaminetetraacetic acid
EM	Electron microscopy
FT	Flowthrough
g	Grams
GF	Gel-Filtration
GFP	Green fluorescent protein
His/h	Hexa-histidine tag
hr	Hour
HRP	Horseradish peroxidise
kDa	Kilodaltons
LB	Luria Bertani medium
L:P	Lipid-to-protein ratio
M	Membrane fraction
mAU	Milli-absorbance unit

min	Minutes
MWCO	Molecular weight cut off
nM	Nanometres
N-	Amino terminus
OD	Optical density
P	Periplasmic fraction
PAGE	Polyacrylamide gel electrophoresis
PBS	Phosphate buffered saline
PMF	Proton motive force
PVDF	polyvinylidene fluoride membrane
rpm	revolutions per minute
s	seconds
Sec	General secretory pathway
SRP	Signal recognition particle
Strep-Tag	Strep II tag
SEM	Scanning electron microscopy
Tat	Twin arginine translocation
TBS	Tris buffered saline
TEM	Transmission electron microscopy
TorA	Trimethylamine-N-oxide reductase
Vo	Void Volume
v/v	Volume per volume
W	Wash fraction
WT	Wild type
w/v	Weight per volume
YFP	Yellow fluorescent protein

Chapter 1:
Introduction

1.0 Introduction

1.1 Protein translocation in bacteria

All organisms transport proteins into or across biological membranes to reach their final cellular location. In bacteria, 20-30% (Holland, 2004; Pugsley, 1993) of proteins synthesized in the cytoplasm are destined for extra-cytoplasmic locations. To reach such destinations, the protein(s) must traverse the inner membrane (Figure 1.1.1): a phospholipid bilayer which serves to compartmentalise the cell.

Bacteria are prokaryotes which can be sub-divided into 2 broad classifications based upon a bacterium's ability to retain a Gram-stain. Gram-positive bacteria, as the name suggests, are those that retain the dye, as opposed to those that lack the ability which are termed: Gram-negative bacteria. The ability to retain the dye is owed to a differing composition of the bacterial cell wall.

Gram-positive bacteria have a 'simple' cell-wall structure of a single cell membrane which is enclosed by a thick peptidoglycan layer. Therefore, non-cytoplasmic proteins only have to traverse a single bilayer to enter the extracellular space/growth medium. However, Gram-negative bacteria have a more complicated cell-wall structure. The peptidoglycan layer is much thinner, which is surrounded by an outer membrane, thus generating an extra cellular compartment called the periplasm. Some proteins reside in this periplasmic space, or they can be inserted into the outer membrane. A schematic depicting the differences between these two types of bacteria is presented in Figure 1.1.1.

3 major transport systems exist in Gram-negative bacteria, for the translocation and insertion of proteins across or into the inner membrane, namely: Sec translocase, YidC insertase and Tat translocase. This thesis focuses on the translocation of proteins by the Tat pathway and will be discussed in detail (§1.3).

Outer membrane

Peptidoglycan layer

Periplasm   Inner membrane
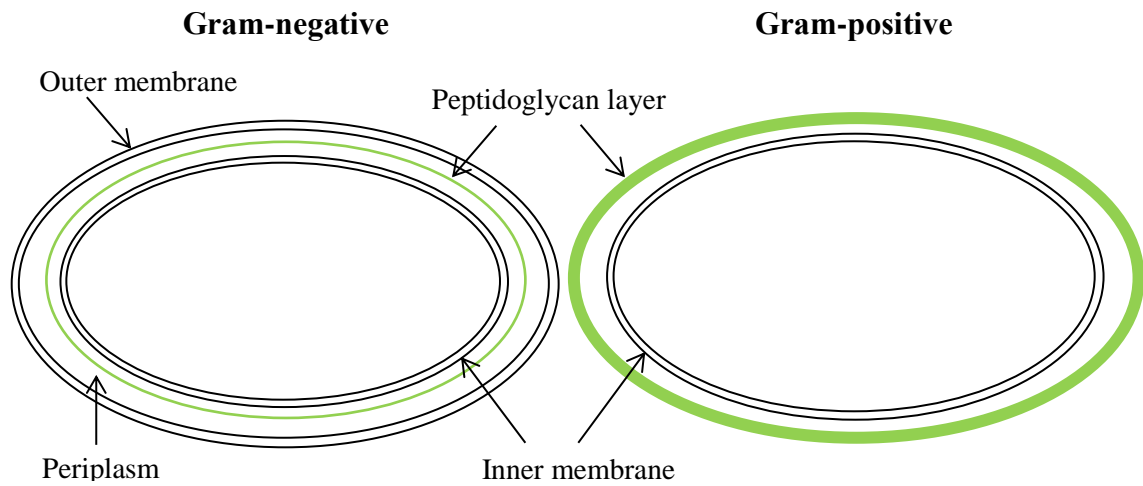
Figure 1.1.1. The cell walls of Gram-negative and Gram-positive bacteria.
A schematic representation of the cell walls of Gram-negative (left) and Gram–positive (right) bacteria. Both contain and inner membrane and a peptidoglycan layer; however this layer is much thicker in Gram-positive bacteria. Gram–negative bacteria have an outer membrane thus creating an additional cellular compartment: the periplasm.

1.2 The Sec translocase

The Sec translocase is a heterotrimeric integral membrane protein complex that serves to transport unfolded proteins either into the lipid bilayer of the inner membrane, or into the periplasmic space. It is a highly conserved system present in all bacteria, archaea and the ER membrane of eukaryotic cells (Pohlschröder *et al.*, 1997). Only the bacterial Sec system will be discussed in this thesis.

Proteins are targeted to the Sec pathway by virtue of an N-terminal signal peptide. Inner membrane proteins that require lateral transfer into the phospholipid bilayer possess an N-terminal signal anchor sequence (SA) which lacks a signal peptidase cleave site that would otherwise be present in signal peptides of less hydrophobic, secretory proteins that are to traverse the inner membrane.

The Sec translocon consists of three main components: SecY, SecE and SecG (Figure 1.2.1). SecY is a 48 kDa protein which consists of 10 α-helical transmembrane helices (TMH) forming a clam-shell arrangement in the inner membrane, and constitutes the aqueous channel of the Sec translocase (Berg *et al.*, 2004). The channel forms an hourglass shape with the central constriction region being lined with 6 isoleucine residues (Park & Rapoport, 2012). This hydrophobic

ring in the middle of the channel is predicted to form a seal around the passenger protein, preventing ion leakage during transport. Additionally, an extension of TMH2 of SecY blocks the channel forming a "plug" on the periplasmic side of the constriction site (Berg *et al.*, 2004; Tsukazaki *et al.*, 2008) and has been proposed, through its hydrophobic surface, to guide the substrate through the channel. Cross-linking data has led to the idea that upon substrate binding this plug is displaced to open the channel for translocation (Berg *et al.*, 2004). TMH2 of SecY (along with TMH7) forms what is termed the 'lateral gate' of the Sec translocon. Contact of the preprotein with this region of SecY induces separation of the two halves of this protein, allowing the lateral partitioning of TMHs and signal sequences into the lipid bilayer (du Plessis *et al.*, 2011).

SecE is a small integral membrane protein of 14 kDa that clamps the two halves of SecY together (Berg *et al.*, 2004). It is essential for Sec transport and cell viability, since in its absence, SecY is unstable and is degraded (Kihara *et al.*, 1995).

SecG is the third, and smallest, component of the Sec translocase being only 12 kDa. Whilst it is not essential for translocation in the *E. coli* system (Nishiyama *et al.*, 1994), it has been shown to increase the stability of the SecYE complex (Belin *et al.*, 2015).

This translocase interacts with different cytosolic proteins depending on the nature of the substrate to be transported. For example, if the nascent polypeptide chain emerging in the ribosome tunnel (RNC) displays a high degree of hydrophobicity (Heijne, 1986) and helicity (Bruch *et al.*, 1989), it is bound by the signal recognition particle (SRP).

1.2.1. The SRP pathway

The SRP is a ribonucleoprotein complex comprised of a 48 kDa GTPase protein, Ffh, and 4.5S RNA. Ffh is a tri-domain protein, whose C-terminal M domain is responsible for substrate binding (Batey *et al.*, 2000; Koch *et al.*, 2003; Zheng & Gierasch, 1997). This is a methionine-rich region which is predicted to provide a flexible hydrophobic surface for interaction with signal sequences (Bernstein *et al.*, 1989).

Once bound to the RNC, the RNC-SRP complex is targeted to the inner membrane (hence co-translational pathway) (Figure 1.2.1.) for interaction with SRP receptor, FtsY, which is located in a ribosome-binding site on SecY for efficient delivery of the nascent polypeptide chain to the Sec machinery (Kudva *et al.*, 2013; Ng *et al.*, 1996). SRP binds to FtsY, displacing its receptor from SecY and promotes GTP hydrolysis. This hydrolysis drives the dissociation of RNC-SRP complex such that the RNC fully docks onto the SecYEG machinery, aligning with the SecY channel (Beckmann *et al.*, 2001; de Leeuw *et al.*, 2000; Valent *et al.*, 1998).

The SA sequence of the RNC then inserts into the SecY channel and moves towards lateral gate (Egea & Stroud, 2010). It is predicted this movement is followed by displacement of the plug domain in the central constriction site thus opening the Sec translocon (Kudva *et al.*, 2013). The protein is then able to exit via the lateral gate into the inner membrane (Figure 1.2.1).

1.2.2. The Sec pathway

Alternatively, if the nascent polypeptide signal peptide is less hydrophobic, cytosolic Trigger Factor (TF) binds to the signal peptide to prevent SRP binding. SecB then binds the fully-synthesized protein (hence post-translational pathway), keeping the protein in a translocation-competent state, and subsequently targets the unfolded protein to SecA at the inner membrane (Figure 1.2.1).

SecA is the soluble receptor of SecB, and is the motor protein of the Sec translocase. Upon release of SecB and consequent transfer of preprotein to SecA, ATP is hydrolysed and translocation is initiated (Fekkes *et al.*, 1999). Repeated cycles of ATP hydrolysis push the preprotein through the SecY channel approximately 30-40 amino acids at a time (Schiebel *et al.*, 1991) resulting in a step-wise translocation of the substrate across the inner membrane (Tomkiewicz *et al.*, 2006).

Some membrane proteins insert into the inner membrane independently of Sec machinery, and instead use the membrane-localised insertase YidC (Dalbey *et al.*, 2011; Wang & Dalbey, 2011; Welte *et al.*, 2012). However, this mechanism of translocation is largely unknown.
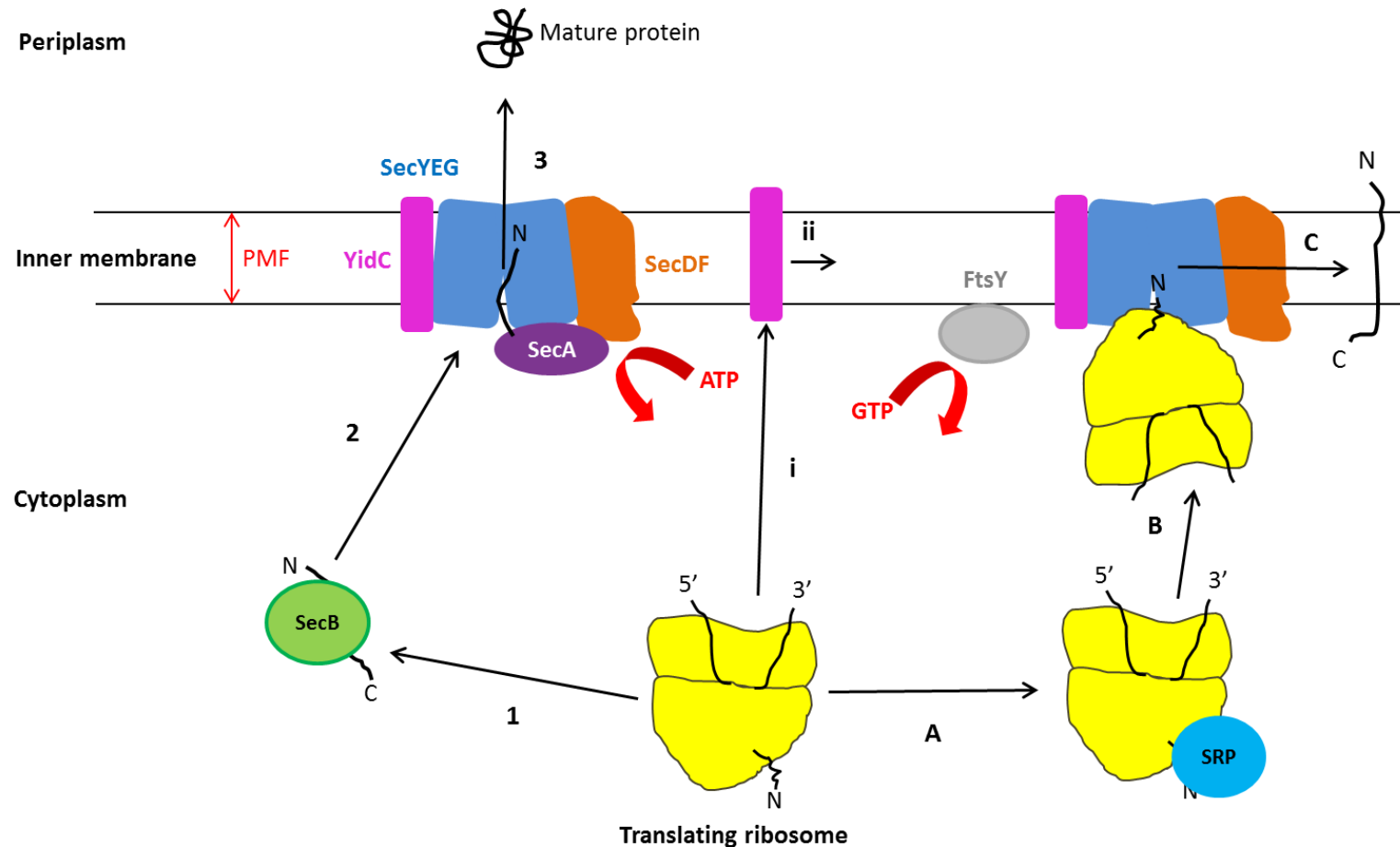
Figure 1.2.1. Overview of protein transport by the Sec machinery
Post-translational transport: 1- the nascent polypeptide chain (NPC) is bound by SecB and 2- transported to the Sec translocase where it is transferred to SecA. 3- the unfolded protein is threaded through the SecY channel, powered by repeated cycles of ATP hydrolysis. The protein gains entry into the periplasm and folds to form a mature protein. Co-translational transport: A- SRP binds to the NPC as it exits the ribosome. B- the SRP-bound ribosome is then targeted to the Sec machinery. SRP binds its receptor FtsY, and is displaced from the ribosome complex. The ribosome aligns with the SecY channel and translocation is initiated. C- The protein exits the translocase via a lateral gate and gains entry into the inner membrane. The proton motive force (PMF) is also important for translocation. Some membrane proteins use YidC as an alternative insertion: (i) the NPC is directly targeted to YidC (ii) the mechanism of YidC insertion is largely unknown. YidC also has the capability to cooperate with the Sec translocon during membrane protein insertion.

1.3 The Twin arginine translocase pathway

1.3.1. Introduction to Tat

In contrast to the aforementioned Sec translocase the twin arginine translocase (tat) pathway transports fully-folded proteins. This translocase was discovered in the thylakoid membrane of chloroplasts in the early 1990s (Mould & Robinson, 1991), and was found to require three essential protein components: (Tha4 (Mori *et al.*, 1999; Walker *et al.*, 1999), Hcf106 (Settles *et al.*, 1997), and cpTatC (Cline & Mori, 2001)), and a proton motive force (Klösgen *et al.*, 1992) for the translocation of fully-folded proteins (Clark & Theg, 1997; Creighton *et al.*, 1995; Hynds *et al.*, 1998). The complex was subsequently found to be expressed in some bacteria, archaea and mitochondria (Yen *et al.*, 2002). The bacterial homologues are TatA, TatB and TatC, respectively (Bogsch *et al.*, 1998; Sargent *et al.*, 1998; Sargent *et al.*, 1999), and will remain the focus of this introduction. For a recent review of the chloroplast Tat pathway see (Albiniak *et al.*, 2012).

The bacterial Tat pathway is essential for many processes—including energy metabolism (Bernhardt & De Boer, 2003; Ize *et al.*, 2003), formation of the cell envelope (Bernhardt & De Boer, 2003; Ize *et al.*, 2003), biofilm formation (Ize *et al.*, 2004), heavy metal resistance (Ize *et al.*, 2004), nitrogen-fixing symbiosis (Meloni *et al.*, 2003) and bacterial pathogenesis (Ding & Christie, 2003; Ochsner *et al.*, 2002; Pradel *et al.*, 2003).

This unique system has been studied intensively over the past two-and-a-half decades; yet the understanding of the mechanism of translocation remains unsolved. This is owed to the innate difficulties in working with large, heterogeneous, multimeric integral membrane protein complexes. Recent studies have utilised structural and localisation experiments in their endeavours to gain more information on this translocase. Undoubtedly these avenues of research, in combination with the fast-developing world of both light and electron microscopy will provide invaluable tools to help decipher this unique translocase's mechanism.

1.3.2. Bacterial Tat genes

The most intensively studied bacterial Tat pathway is that of the Gram-negative bacterium, *Escherichia coli* (*E. coli*). This translocase's proteins are constitutively

expressed from the *TatABC* operon (Santini *et al.*, 1998; Sargent *et al.*, 1998; Weiner *et al.*, 1998) (Figure 1.3.1.) and reside in the inner membrane. Another gene *tatD* is expressed downstream, encoding a DNase protein TatD (Wexler *et al.*, 2000). Despite this protein originally not being thought to operate within the Tat pathway, data has revealed that this protein is implicated in the proof-reading of Tat substrates (Matos *et al.*, 2009). Another *tat* gene, *tatE*, is also expressed elsewhere in the genome. This gene is thought to be a cryptic gene duplication of *tatA* and not possess an important role in Tat translocation; however recent data has shown the TatE protein to be capable of substituting for TatA , efficiently translocating the largest Tat substrate in *E. coli*: TorA (90 kDa) (Baglieri *et al.*, 2012).

The Gram-positive model organism, *Bacillus subtilis* (*B. subtilis*), expresses two minimal pathways comprised of only TatA and TatC proteins, TatAdCd and TatAyCy (Jongbloed *et al.*, 2004). The genes encoding these proteins are organised in 2 operons: *tatAd*, *TatCd* and *phoD* (the only known substrate of this complex). Similarly, for the second operon: *tatAy*, *tatCy* and *ywbN*, respectively (Figure 1.3.1.). A third *tatA*-type gene, *tatAc*, is expressed on its own and its role in the translocation of fully-folded substrates remains unknown; however a recent study by (Beck *et al.*, 2013) showed that the TatAc protein can functionally replace TatA and TatE providing strong evidence for a physiologically-relevant role of this protein.

A

B
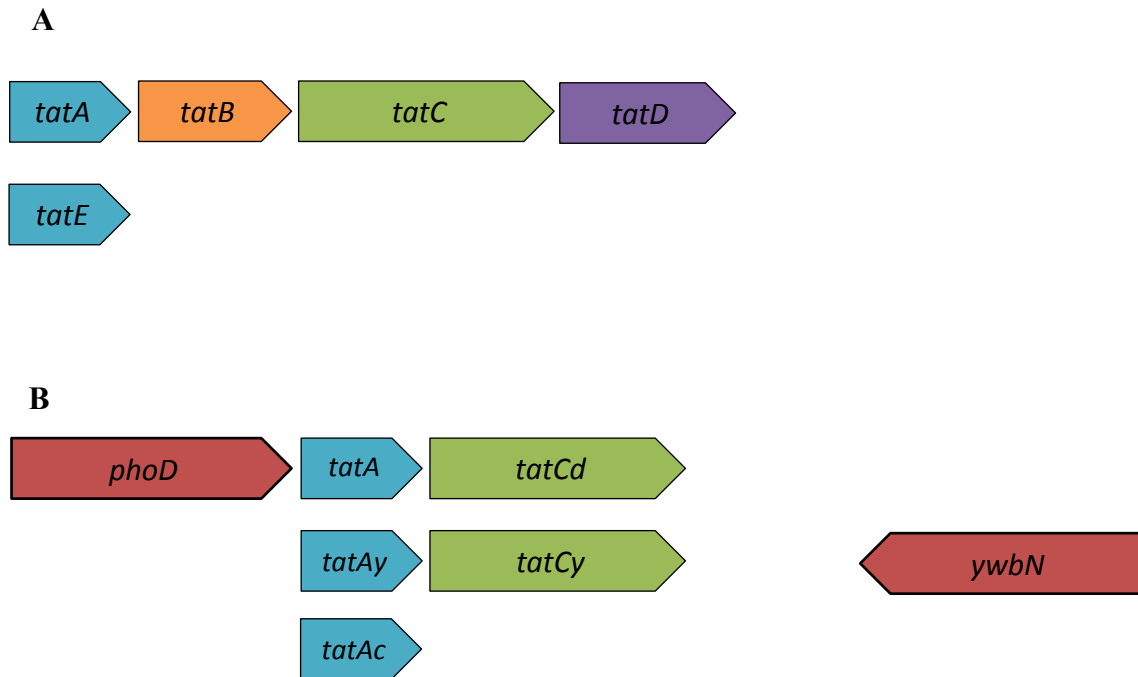
Figure 1.3.1. Organisation of bacterial *tat* genes from *E. coli* and *B. subtilis*
A) The *tatABC* genes are constitutively expressed from a single operon in *E. coli* and express the essential TatABC proteins of the Tat translocase. The *tatD* gene is also expressed in this operon. The *tatE* gene is a paralog of *tatA* and is expressed elsewhere in the genome. B) The two minimal Tat systems of *B. subtilis* are expressed in separate operons alongside their respective substrates. The first is: *tatAd* and *tatCd* genes alongside substrate *pho*D. Secondly, *tatAy* and *tatCy* genes are expressed with substrate YwbN elsewhere in the genome. There a third *tatA* gene, *tatAc*, which is not expressed with any of the other *tat* genes.

1.3.3. Tat subunits

The *E. coli* TatA subunit is the most abundant component of the Tat machinery, expressed in 20-fold excess of TatB and TatC (Sargent *et al.*, 2001). This 9.6 kDa protein of 89 amino acids is a single transmembrane-spanning protein with an N-out topology (Porcelli *et al.*, 2002). Further biophysical analysis by (Lange *et al.*, 2007) used a multi-construct approach to confirm the conformation and alignment of TatA from *B. subtilis* in the inner membrane. CD spectroscopy showed TatA to possess a short -terminal alpha-helix connected to a central transmembrane helix (TMH), which is linked via an amphipathic helix (APH) to an unstructured C-terminus (Lee *et al.*, 2002; Sargent *et al.*, 1998; Settles *et al.*, 1997) (Figure 1.3.2.).

Protease accessibility experiments probed the topology of the TatA protein in the inner membrane and found that the non-essential TatC region exhibited a dual topology (Chan *et al.*, 2007; Gouffi *et al.*, 2004).

NMR experiments on the TatA protein from *B. subtilis* confirmed the L-shaped arrangement of this protein in the inner membrane (Müller *et al.*, 2007). Further analysis also revealed that the TMH (14-16 residues in length) tilts 17° with respect to the membrane normal, which bears implications for predicted mechanisms of Tat translocation (discussed in section 1.5). Such arrangement was supported by (Walther *et al.*, 2010) who then went on to reveal that the APH exhibits a slanted alignment relative to the membrane normal. This is contrary to the membrane-parallel orientation predicted by (Lange *et al.*, 2007), and alludes to the idea that the APH does not simply serve as a flexible linker between the TMH and C-terminal region, and instead adopts a conformation key to the translocase assembly.

The 7 kDa TatE protein shares over 50% sequence similarity with TatA (Sargent *et al.*, 1998), and thought to arise from a cryptic gene duplication of *tatA* gene (Yen *et al.*, 2002). Despite this similarity, TatE is much shorter than TatA, possessing only 67 amino acids (Sargent *et al.*, 1998). Given its low abundance, it was anticipated that TatE is largely redundant regarding Tat translocation (Jack *et al.*, 2001); however data has shown that this protein is capable of functionally substituting for TatA protein (Baglieri *et al.*, 2012); and for some substrates, the absence of TatE significantly hinders translocation into the periplasm (Sargent *et al.*, 1998), proposing a specific role for the TatE protein.

TatB protein of *E. coli s*hares a 20% sequence similarity to TatA (Hicks *et al.*, 2003), and is predicted to adopt a similar secondary structure and membrane topology to TatA in the inner membrane (Bolhuis *et al.*, 2001)(Figure 1.3.2.). However, the two proteins exhibit functionally distinct roles within the inner membrane: TatA is predicted to form the pore-forming element of the translocase (Gohlke *et al.*, 2005), whereas TatB forms part of the substrate binding site (Tarry *et al.*, 2009) and is thus an essential component for translocation of native *E. coli* substrates (Blaudeck *et al.*, 2005; Ize *et al.*, 2002) (discussed in section 1.4). At 171 amino acids in length (18.4 kDa), this protein is a lot longer than TatA, possessing a long, unstructured C-terminus (Lee *et al.*, 2002); however the hinge region and APH are essential for function with single amino acid substitutions causing significant effects on translocation (Barrett *et al.*, 2003; Hicks *et al.*, 2003; Lee *et al.*, 2006). Interestingly, Tat has been shown to tolerate the translocation of non-native fusion proteins in the absence of TatB (Blaudeck *et al.*, 2005; Ize *et al.*, 2002); implying that lack of TatB

activity could be compensated for by TatA. This would mirror the situation in the Gram-positive bacterium *B. subtilis* that contains only TatAC-type translocases(Barnett *et al.*, 2008). In fact- N-terminal, single amino acid mutations have been shown to induce bifunctionality in *E. coli* TatA (Barrett *et al.*, 2007; Blaudeck *et al.*, 2005).

Finally, TatC is the largest and most conserved subunit of the Tat translocase, forming part of the substrate-binding complex (Tarry *et al.*, 2009) (discussed in section 1.4.1). Primary sequence analysis of this 32 kDa protein has predicted that the 258 amino acids possess a secondary structure of 6 TMH in the inner membrane, with an N-in C-in topology (Behrendt *et al.*, 2004) (Figure 1.3.2.). Site-directed mutagenesis studies have revealed that residues essential to the functionality of this protein (and thus the Tat translocase), are localised to the cytoplasmic N-region and the first cytoplasmic loop of the TatC protein (Allen *et al.*, 2002; Barrett *et al.*, 2005; Buchanan *et al.*, 2002; Holzapfel *et al.*, 2007; Punginelli *et al.*, 2007).
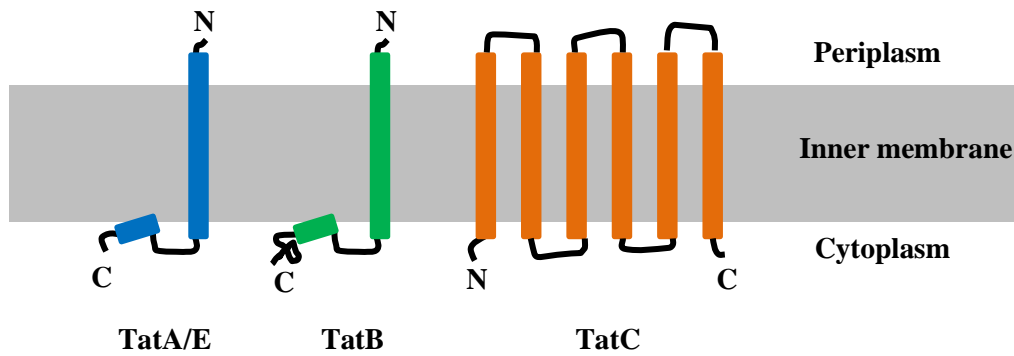
Figure 1.3.2. Organisation of TatA, TatB and TatC proteins in the inner membrane
Three integral membrane proteins, encoded by the *tatABC* operon, are the essential components of the twin arginine translocase in Gram-negative bacteria. TatA and TatB possess similar topologies: they have a short periplasmic N-terminal region connected to a single pass transmembrane helix (TMH), which is linked via a hinge region to an amphipathic helix (APH) and a highly charged, unstructured C-terminus on the cytoplasmic side of the inner membrane. Recent evidence (Walther *et al.*, 2010) suggests that the APH is tilted relative to the membrane normal. TatC is predicted to contain 6 TMH, with both the N- and C-terminus residing at the cytoplasmic side of the inner membrane. *E. coli* expresses a TatA paralog, TatE which is expressed elsewhere in the genome. The Gram-positive bacterium, *B. subtilis* possesses both TatA (TatAy and TatAd) and TatC (TatCy and TatCd) proteins with identical topologies in the inner membrane. They lack a TatB protein.

1.3.4. Signal peptides

Substrates are targeted to the Tat translocase by virtue of an N-terminal signal peptide. Tat signal peptides possess a tripartite structure of a: basic N-terminal region, central hydrophobic region and a polar C-terminal region (Figure 1.3.3.). It is within this latter region that a signal peptidase cleavage site is located for cleavage of the precursor protein in the periplasm to produce a mature protein (Lüke *et al.*, 2009; Yahr & Wickner, 2001). Sec and Tat signal peptides actually possess the same basic structure; however there are important differences that target a particular substrate to its specific translocation machinery.

The Tat translocase derives its name from the presence of a highly conserved twin arginine motif, **SRR**xFLK (where x is any polar amino acid), located immediately before the hydrophobic region of the signal peptide (Figure 1.3.3.) (Berks, 1996; Cristóbal *et al.*, 1999).

The **RR** residues are completely invariant and are essential for transport. Substitution of one of the arginine residues to lysine slowed transport, whereas substitution of both residues abolished Tat activity (Buchanan *et al.*, 2001; DeLisa *et al.*, 2002; Ize *et al.*, 2002; Mendel *et al.*, 2008; Stanley *et al.*, 2000). Therefore, at least one arginine in the consensus motif is a prerequisite of Tat transport. These results are in contrast to mutations affecting the overall charge of the N-terminal consensus region of Sec signal peptides, which did not affect transport efficiency at all (Sasaki *et al.*, 1990); supporting the idea that these twin-arginine residues play important roles in specific interactions of substrate signal peptide with Tat machinery. Although, these residues are not the only factor that play an important role in directing Tat substrates specifically to Tat machinery. The hydrophobic domains of Tat signal peptides are less hydrophobic than Sec signal peptides (Cristóbal *et al.*, 1999). In fact- a Tat substrate can be redirected to Sec machinery by increasing the hydrophobicity of its signal peptide (Cristóbal *et al.*, 1999); demonstrating the importance of this factor to targeting to Tat machinery. Additionally, the C-terminal region contains basic residues that are rarely found in Sec signal peptides, and are predicted to prevent interactions with the Sec machinery (Blaudeck *et al.*, 2003; Bogsch *et al.*, 1997; Cristóbal *et al.*, 1999).

Aside of RR, the other residues within the consensus motif are important for directing the substrate to the Tat machinery. The phenylalanine residue (+3 Figure 1.3.3.) is the most highly conserved residue in the consensus motif, present in 80% of Tat signal peptides (Stanley *et al.*, 2000). Results of single amino acid substitutions have shown that it is the hydrophobicity of this region, as opposed to the side chain functionality, that is important for efficient export (Stanley *et al.*, 2000). The remainder consensus motif residues occur at an average frequency of >50% (Berks, 1996).

Substitutions of serine, leucine and lysine amino acids (-1, +4 and +5 positions, respectively (Figure 1.3.3.), have varying effects on transport efficiency. Substitutions of serine to cysteine substantially slowed Tat export; suggesting that low hydrophobicity of this region of the signal peptide, is important for efficient export. In contrast, the high hydrophobicity of leucine at position +4 is important for efficient export (Stanley *et al.*, 2000). The importance of these residues varies

between substrates; particularly lysine, where the presence of this particular residue abolishes export in one substrate yet is important in another (Stanley *et al.*, 2000).

Interestingly, the expression of an N-terminal signal peptide is not an absolute prerequisite for Tat transport; some proteins are able to traverse the inner membrane via "hitchhiking" i.e. they form complexes with other proteins which express a Tat signal peptide (Jack *et al.*, 2004; Rodrigue *et al.*, 1999; Sargent *et al.*, 1998).
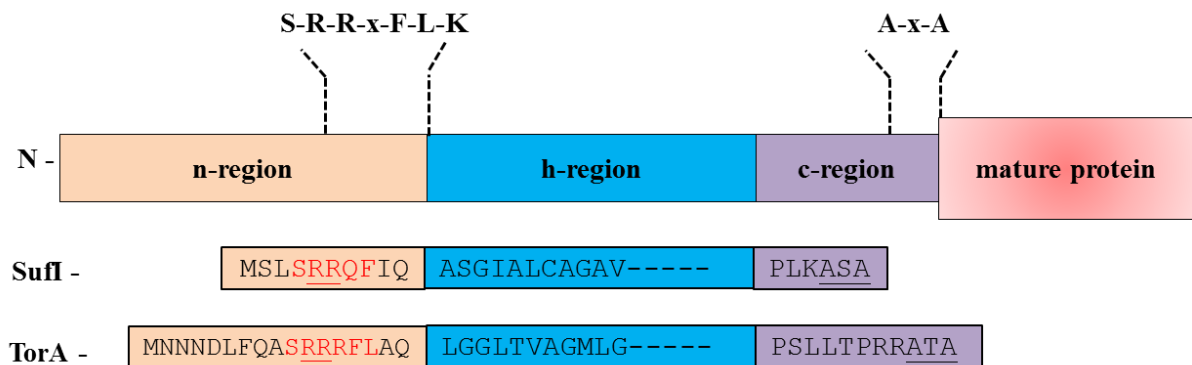
Figure 1.3.3. Tat signal peptide
Schematic to depict the tripartite structure of a Tat signal peptide. A positively-charged N-terminal region (n-region), a hydrophobic core (h-region) and a polar c-region which contains an A-x-A motif which encodes a peptidase cleavage site for removal of the signal peptide in the periplasm (indicated). The consensus motif is located at the junction of the n- and –h region (indicated). Signal peptide sequences of typical Tat substrates are shown as an example (SufI and TorA). Residues that match the consensus motif are in red font (twin arginine underlined), and C-terminal signal peptidase recognition sites are underlined in black.

1.3.5. Tat substrates

The extent to which Tat is utilised for transport of fully-folded proteins varies in different organisms. Gram-positive bacteria generally contain very few substrates; for example, *B. subtilis* expresses two minimal translocases that each only transports one substrate (Widdick *et al.*, 2006).However, *Streptomyces* is an exception in this type of bacteria, since it can transport over 100 secretory proteins into the periplasm (Joshi *et al.*, 2010; Widdick *et al.*, 2006). Enteric bacteria are different still, expressing in the range of Tat 20-30 substrates (Palmer *et al.*, 2010).

Despite the significant variation in substrate numbers, the reasons why different substrates require transport via the Tat machinery is largely unknown; however a few

motives have been proposed. Firstly, substrates may non-covalently bind cofactors, more specifically metal-sulphur clusters or nucleotide-based cofactors (Berks *et al.*, 2003), in the cytoplasm prior to export. This offers the advantage that the co-factor and substrate do not need to be separately transported into the periplasm (Berks, 1996).

Some substrates that lack cofactors may still require Tat translocation due to rapid folding kinetics and therefore must be transported fully-folded. An example is *E. coli* proteins AmiA and AmiC that are required for normal cell wall biosynthesis. *E. coli* mutants that lack Tat machinery and therefore unable to correctly localise AmiA and AmiC resulted in cells growing in a filamentous morphology since normal cell division is prevented (Bernhardt & De Boer, 2003; Ize *et al.*, 2003).

Interestingly, halophilic archaea secrete a large proportion of their secretome via the Tat pathway. It is predicted that use of Tat machinery, and thus full folding of substrates in the cytoplasm, avoids the complications of protein aggregation and misfolding that arises as a result of high extracellular salt conditions (Pohlschröder *et al.*, 2004), or that high internal salt conditions promote cytoplasmic folding of nascent polypeptides (Bolhuis, 2002; R. Wesley Rose, 2002).

Furthermore, cytoplasmic folding would avoid interaction with periplasmic metal ions that could otherwise compete for binding site(s) in the protein. For example, the bacterial SoxYZ protein *Paracoccus pantotrophus* that contains an iron-sulphur cluster is targeted via Tat so as to avoid competing periplasmic Co^{2+} and Cu^{2+} ions (Sauvé *et al.*, 2007).

Finally, Tat has been shown to transport heterooligomeric complexes. More specifically, some Tat substrates actually lack a Tat signal peptide, yet are able to traverse the inner membrane by binding to a partner protein which bears an N-terminal Tat signal peptide, a mechanism termed "hitch hiking". These proteins must be fully-folded to successfully hitchhike as oligomeric proteins.

The vast majority of Tat substrates are secretory proteins however some remain anchored in the inner membrane via N- or C-terminal transmembrane domains (Bachmann *et al.*, 2006; De Buck *et al.*, 2007; Hatzixanthis *et al.*, 2003; Jormakka *et al.*, 2002). Recent evidence that used a signal peptide mutant of a native *E. coli* Tat

substrate, YedY, confirmed that Tat is capable of lateral membrane insertion of some substrates (Ren *et al.*, 2013).

1.4. The Tat complex

In a steady-state situation, the three essential components of the *E. coli* Tat machinery arrange themselves in the inner membrane as a TatBC complex (at 1:1 stoichiometric ratio) (Bolhuis *et al.*, 2001) and a heterogeneous pool of TatA that is expressed at a 20-fold excess over TatBC (Sargent *et al.*, 2001). Briefly, binding of a signal peptide-bearing substrate to the Tat machinery, in the presence of a proton motive force, triggers the translocation of substrate (Cline & McCaffery, 2007; Cline & Mori, 2001) through the large 370-700 kDa heterooligomeric TatABC complex (Bolhuis *et al.*, 2001; Oates *et al.*, 2005; Oates *et al.*, 2003) (discussed in more detail in section 1.5).

Early 2D structural analysis of TatABC complexes from *E. coli*, *Agrobacterium tumefaciens* and *Salmonella typhimurium* revealed structural conservation of this machinery, with the TatABC particles possessing dimensions of approximately 9 – 13 x 10 nm (Oates *et al.*, 2003). These negatively-stained particles had a central pool of stain surrounded by 5-7 stain-excluding densities, each 4 nm wide. A flexible modular assembly of this machinery was alluded to since there was a correlation between particle size and the number of 4 nm densities in the structure. Since the stain excluding region was too small to accommodate a fully-folded protein it is sensible to assume that more TatA subunits or TatABC would be needed to create a full-sized channel (Oates *et al.*, 2003).

1.4.1. The TatBC complex

It is broadly accepted that the TatBC complex serves as the substrate binding site of this translocase. Cross-linking data revealed TatC to be the primary interaction site between Tat machinery and substrate (Alami *et al.*, 2003; Gerard & Cline, 2006; Kreutzenbeck *et al.*, 2007; Maurer *et al.*, 2010; Richter & Brüser, 2005). Specifically, it is the N-terminal region of the TatC protein and the first cytoplasmic loop that are important in making contact to the signal peptide of the substrate (Zoufaly *et al.*, 2012).

The exact role of TatB in the substrate binding complex has remained uncertain. This is plagued partly by a lack of high resolution structural information. However, recent structural NMR data revealed the extended C-terminal region of TatB to exhibit significant flexibility relative to the TMH and APH. This flexible region contains amino acid residues that have been shown to be in close proximity to the substrate during translocation, and they therefore occupy a large conformational space. This significant structural plasticity of TatB potentially facilitates the substrate-binding complex to adapt for substrates of differing sizes and shapes (Zhang *et al.*, 2014).

Furthermore, recent cross-linking data has unveiled new insight into the potential role of this protein. Data showed that in the absence of TatB, the signal peptide of a translocation-incompetent substrate was removed; suggesting that this protein could be implicated in preventing the premature cleavage of signal peptides (Frobel *et al.*, 2012). Also, (Maurer *et al.*, 2010) showed precursors to become surrounded by TatB and make contact to its TMH and APH, which were then lost upon translocation; suggesting that the interaction between TatB and substrate occurs at an early stage in substrate-binding.

Recent crystal structure data of TatC revealed this protein to possess a "glove-like" structure, owed to the TMH5 and TMH6 of this protein being much shorter in length than the other TMHs (Ramasamy *et al.*, 2013; Rollauer *et al.*, 2012) (Figure 1.4.1). A potential role for this concave region of TatC was further elucidated in light of cross-linking data showing that the TMH5 and TMH of TatB interact (Rollauer *et al.*, 2012). Also, this region is rich in aromatic residues which would have the potential to bind the lysine residue of the signal peptide consensus motif (SRRxFLK) (Ramasamy *et al.*, 2013).

It remains uncertain about the mechanism of insertion of the signal peptide; however there are now numerous studies in favour of a hairpin-like insertion of the signal peptide. Firstly, the N-terminus of TatB was found to cross-link to Tat substrates prior to translocation (Maurer *et al.*, 2010). Also, mutations in this same region of TatB were found to suppress defective translocation of translocation-incompetent substrates (Kreutzenbeck *et al.*, 2007; Lausberg *et al.*, 2012). These data demonstrate the interaction of the precursor to the *trans*-side of the inner membrane, which would only be possible by a deep insertion of the signal peptide in the inner membrane prior

to translocation. The *trans*-region of TatB has also been demonstrated to strongly crosslink to precursors directly (Gerard & Cline, 2006); presenting evidence for deep insertion of signal peptide once it has made contact to TatC.
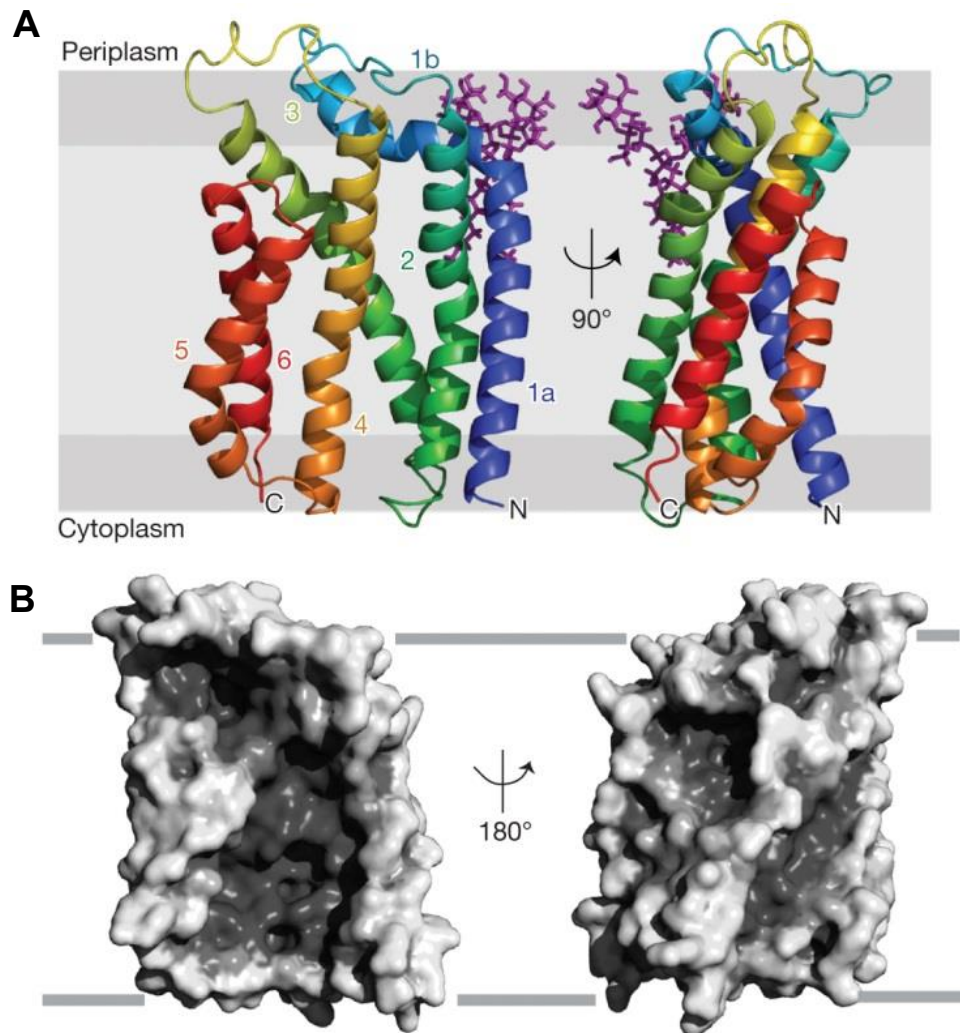
Figure 1.4.1 Crystal structure of TatC from *Aquifex aeolicus*
A – cartoon representation of *A. aeolicus* TatC structure coloured in dark blue from the N-terminus to red at the C-terminus. The position of the bilayer is indicated in grey. A molecule of Lauryl Maltose Neopentyl Glycol (LMNG) detergent is shown in purple. The crystal structure revealed that transmembrane helices (TMH) 5 and 6 are shorter than the other TMH in the TatC protein, which generates a concave region in the TatC structure.
B – Surface representation of the *A. aeolicus* TatC structure highlighting the concave structure within TatC. Cross-linking data elude to a TatB-accommodating role for this concave region. This figure has been adapted from Rollauer *et al.,* 2012.

Low resolution EM structures of the TatBC complex revealed a hemispherical morphology of 11-17 nm in diameter (Tarry *et al.*, 2009) (Figure 1.4.2). The presence of an internal cavity was identified, which was too small to accommodate a fully-folded substrate, and thus a potential role for signal peptide insertion was predicted. Analysis of this reconstruction demonstrated that the dimensions were consistent with the presence of 7 copies of TatBC, and thus contain 7 potential signal peptide binding site. However, when TatBC was expressed in the presence of Tat substrate, interestingly, there were only two copies of a Tat substrate bound at a single time. Not only does this support evidence that the preliminary binding site is superficially exposed (since the individual substrates protruded out from the TatBC complex), and that more than one substrate can bind the substrate-binding complex at one time (Ma & Cline, 2010), it presents evidence in favour of a negative cooperativity of substrate binding (Tarry *et al.*, 2009).
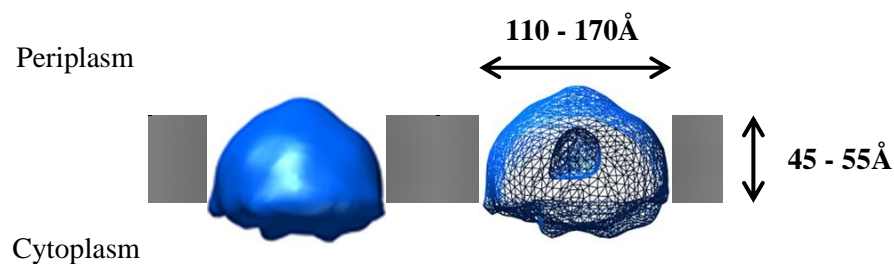
Figure 1.4.2. Low resolution 3D model of TatBC complexes generated by single particle reconstruction

The low resolution structure shown shows hemispherical TatBC-his complexes that are 11-17 nm in diameter. The structure possesses a central cavity, which is too small to house Tat substrates. The height of the complexes are between 45 and 55Å, which is consistent with the thickness of the phospholipid bilayer of the inner membrane (added in grey). This figure has been adapted from Tarry *et al.* (2009).

Until recently highly detailed information in the architecture of the TatBC complex was lacking. However, recent photo crosslinking data has shown TatBC oligomers to form enclosed chambers consisting of a core of TatB surrounded by outer rings of TatC monomers (Blümmel *et al.*, 2015). More specifically, the TMH of each TatB protein bridges TMH5 of one TatC and the TMH2 and -4 of an adjacent TatC (illustrated in Figure 1.4.3.). These data, in combination with data of Cline et al

(Cline, 2015) who showed the movement of the thylakoidal TatA proceeded from TatB peripheral position near TMH5 to concave face of TatC (TMH2 and TMH4), is consistent with the idea that TatA inserts between TatC monomers consequently increasing the diameters of the dome-shaped TatBC complex, thus increasing space for internal oligomerisation of TatA and potentially a pore through which the substrate can pass (Figure 1.4.3.) (Cline, 2015).
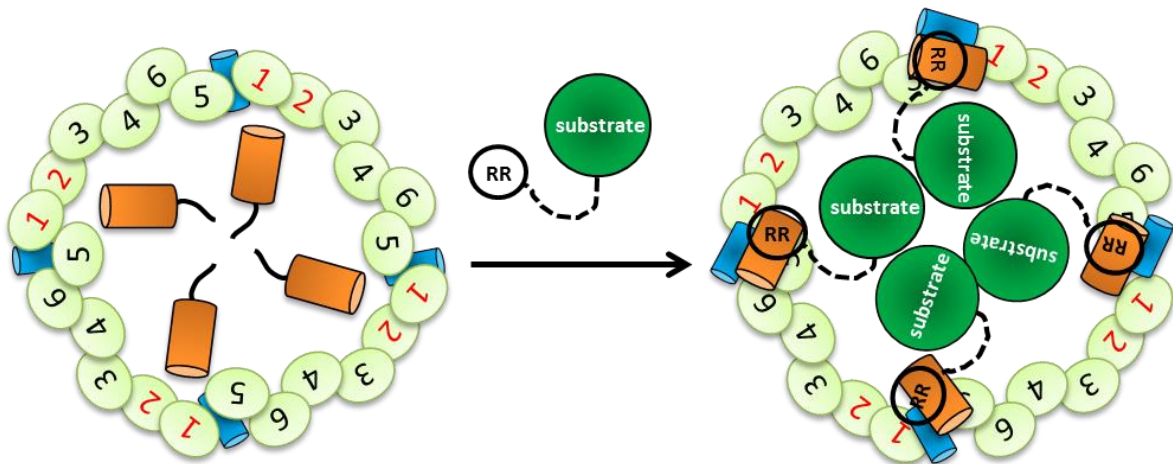
Figure 1.4.3. Arrangement of TatBC protein complex in the inner membrane
Schematic depicting the arrangement of TatABC proteins in the inner membrane before (left) and after (right) substrate binding. TatC (green), transmembrane helices (TMH) are labelled 1-6. TatA = blue cylinder. TatB = orange cylinder. Upon binding of substrate (green circle), the arrangement of the TatABC proteins in the inner membrane changes. The arrangement shown is based on the results of numerous cross-linking data of signal peptide (labelled RR) to TatB and TatC (Alami *et al.*, 2003; Aldridge *et al.*, 2014; Blümmel *et al.*, 2015; Gerard & Cline, 2006; Ma & Cline, 2013; Zoufaly *et al.*, 2012). Briefly, TatA moves from a peripheral position (near TMH5 of one TatC and the TMH2 and TMH4 of an adjacent TatC), to the concave face of TatC, inserting between TatC monomers. This increases the internal space of the TatBC complex (where the TatA pore is thought to subsequently assemble), creating a channel through which the substrate can pass.

1.4.2. The TatA complex

The TatA component of the Tat complex in *E. coli* exhibits significant heterogeneity of $100 - 500$ kDa, identified Blue Native-polyacrylamide gel electrophoresis (BN-PAGE). These complexes resolved at 34 kDa intervals, supporting the idea of a modular formation of 3 to 4 units of TatA at a time.

Low resolution structures of TatA revealed this protein to form channel-containing complexes of varying diameters (Gohlke *et al.*, 2005) (shown in Figure 1.4.4.). The complexes ranged from 8.5 – 13 nm in diameter, which accommodates for the significant heterogeneity witnessed for TatA by gel electrophoresis. The channels ranged from 3 – 7 nm in diameter, which would accommodate even the largest Tat substrates. A lid-type feature was also identified on the cytoplasmic side of the inner membrane which has been predicted to prevent ion leakage during transport. This information forms the biggest support of the most accepted, yet unproven, mechanism of Tat translocation: the pore forming model (discussed in section 1.5) where TatA forms the translocation channel.
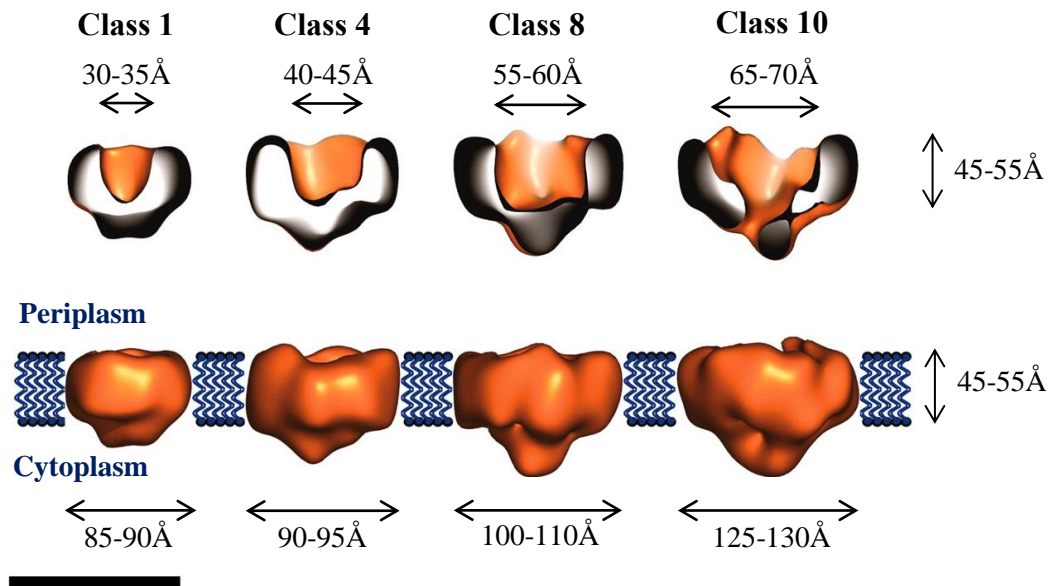
Figure 1.4.4. Low resolution 3D models of TatA complexes generated by single particle reconstruction
The low resolution 3D models show TatA complexes to possess (detergent-inclusive) diameters of 85 – 130Å. The structures possess a channel that is occluded on the cytoplasmic face of the inner membrane. The pores are 30 – 70Å in diameter, meaning that even the largest Tat substrates can traverse the inner membrane fully-folded. The cytoplasmic-lid is proposed to gate entry of the substrate to the translocase. The height of the complexes are between 45 and 55Å, which is consistent with the thickness of the phospholipid bilayer of the inner membrane (shown in blue). Scale bar = 100Å. This figure has been adapted from Gohlke *et al.* (2005).

However such conclusions have been questioned in light of structural data from the TatA paralog, TatE. Export assays have shown TatE to functionally substitute for TatA in *E. coli*, supporting efficient translocation of native Tat substrates (Baglieri *et al.*, 2012). Low resolution EM structures revealed this protein to form complexes that were much smaller and more homogeneous than seen for TatA, which precludes the capability of TatE to possess a pore-forming role (shown in Figure 1.4.5). Therefore these data question the functional relevance of the TatA heterogeneity, and goes against the pore-forming model of Tat translocation.
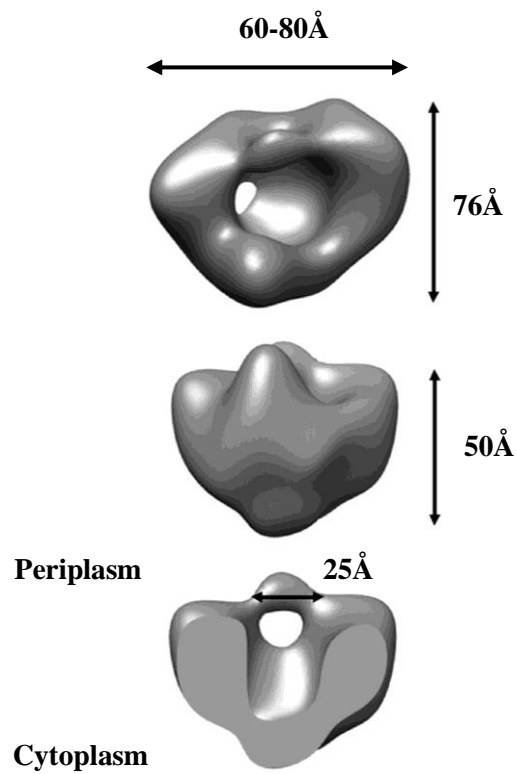
Figure 1.4.5. Low resolution 3D model of TatE complexes generated by single particle reconstruction
The low resolution structure shows TatE complexes that are 60-80Å in diameter. The structure possesses a central cavity, 25Å in diameter, which is too small to house Tat substrates and is occluded at one end. This diameter of this central cavity is smaller than the lowest class size of TatA complexes (30Å). The height of the complex is 50Å, which is consistent with the thickness of the phospholipid bilayer of the inner membrane. This figure has been adapted from Beck *et al.* (2013).

Whilst EM structures showed TatA to possess a pore-like feature, we remain unaware of what specific structural features of TatA contribute to the pore or the cytoplasmic-exposed lid of this complex. Biophysical analyses showed that upon oligomerisation of the TatA protein, the highly conserved polar residue at position 8 of the TMH remains in the middle of the pore and water accessible (Hicks *et al.*, 2003). Consequently, the pore of the TatA complex would consist of TMHs that are only hydrophobic for half the length of a typical membrane. This thinned and distorted bilayer within the TatA pore would provide a translocation pathway through the Tat machinery (Chan *et al.*, 2011).

Aside of constituting the pore-forming component of this translocase, TatA has been shown to be an early interacting partner with the substrate. These cross-links were not obtained in the absence of TatBC, and were sensitive to the PMF; suggesting a functional hierarchy of precursor binding exists i.e. TatBC makes contact to substrate which then triggers the interaction of TatA (Fröbel *et al.*, 2011). This would be consistent with the transient coalescence model of Tat translocation (discussion in section 1.5).

1.5. The Tat mechanism

As previously mentioned, it is well established that the first interactions between substrate and Tat machinery is the substrate precursor binding to the TatBC complex. This is subsequently thought to trigger the recruitment of TatA (Cline & Mori, 2001) to form the active TatABC translocase though which the substrate can pass. It is at this point where our uncertainty in the Tat translocation event arises, owed to our inability to "capture" the translocase in any sense i.e. analyse the full translocon whilst it is engaged with substrate.
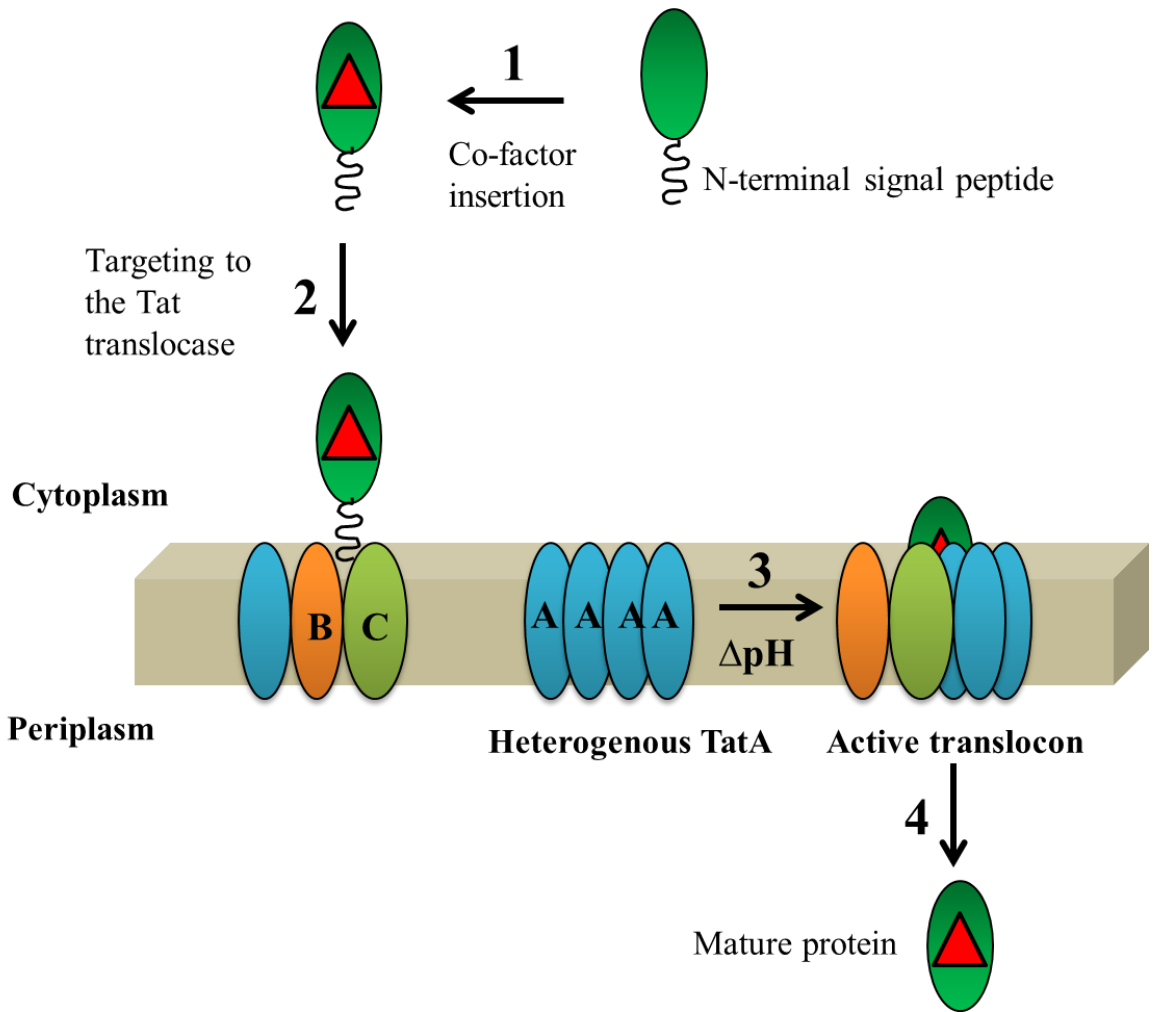
Figure 1.5.1. Generalised model for the pore-forming mechanism of the Tat translocase. Tat-dependent substrates often require post-translational insertion of a co-factor in the cytoplasm (step 1) – to form a fully folded Tat substrate with its exposed twin-arginine-containing signal peptide (black helix) that will be recognised by the homooligomeric TatBC-containing substrate-binding complex (in Gram-negative bacteria step 2). The presence of a bound substrate and a proton motive force is thought to trigger the transient coalescence of TatA subunits to form the active translocon in the cytoplasmic membrane (step 3). The substrate is then exported into the periplasm where it is processed to its mature form (step 4).

Whilst we do not yet fully understand the mechanism of Tat translocation, it is clear that TatA forms an integral part of the translocation machinery and thus any model of Tat translocation varies in their predictions of how TatA is able to permit passage of substrate through the Tat machinery. There are two main models for Tat translocation: the trap door model and the membrane destabilisation model.

1.5.1. Trap-door model

Low resolution structural data of TatA showed this protein complex to possess channels of varying diameters and a cytoplasmic lid (Gohlke *et al.*, 2005), which formulated the hypothesis of a trapdoor mechanism of translocation. The authors predicted that the walls of the channel were formed by the TMH of TatA and the cytoplasmic-exposed APH formed the cytoplasmic lid, which would gate access to the translocase and maintain an ionic seal around the substrate (White *et al.*, 2010).

The ability of TatA to flip its APH into the membrane bilayer from its resting position at the cytoplasmic face of the membrane (Gouffi *et al.*, 2004) further supports the idea of a trap-door model since this movement would result in a hydrophilic coating of the TatA channel enabling passage of substrate through the membrane bilayer (Figure 1.5.2.).

1.5.2. Membrane-destabilisation model

In light of recent structural data of the smaller and more homogeneous *E. coli* TatA paralog, TatE, which showed that this protein forms complexes that are too small to constitute a protein-conducting element of a translocase, the functional relevance of the TatA heterogeneity was questioned (Baglieri *et al.*, 2012). Additionally, the EM structure of a TatA protein from *B. subtilis* which is smaller and more homogeneous than *E. coli* TatA lacked a channel-like feature. Given the TatAdCd translocase, when heterologously expressed in *E. coli*, is capable of translocating even the largest Tat substrate (TorA 94 kDa); the fore-forming property of TatA is questioned.

These data support an alternative mechanism of Tat translocation: the membrane-weakening hypothesis. Initially proposed by Brüser and Sanders (Brüser & Sanders, 2003), this model predicts that TatA aggregates in an unordered manner at the membrane to form a translocase large enough that would result in the destabilisation of the membrane enabling passage of substrate to the periplasmic side of the membrane.

Furthermore, the structure of TatAd was further resolved by NMR, again showing that the APH was able to partially incorporate into the membrane bilayer (Walther *et al.*, 2010); however, in contrast to previous data for TatA, these data suggested that

the topology of TatAd is not as flexible as originally anticipated (Gouffi *et al.*, 2004; Porcelli *et al.*, 2002; Walther *et al.*, 2010). This implies that the movement of the TatA APH into the membrane bilayer would be consistent with a 'lipid disrupting property' of this protein; and thus support the membrane destabilisation theory of Tat translocation (Walther *et al.*, 2010) (Figure 1.5.2.).

A) Trap-door model
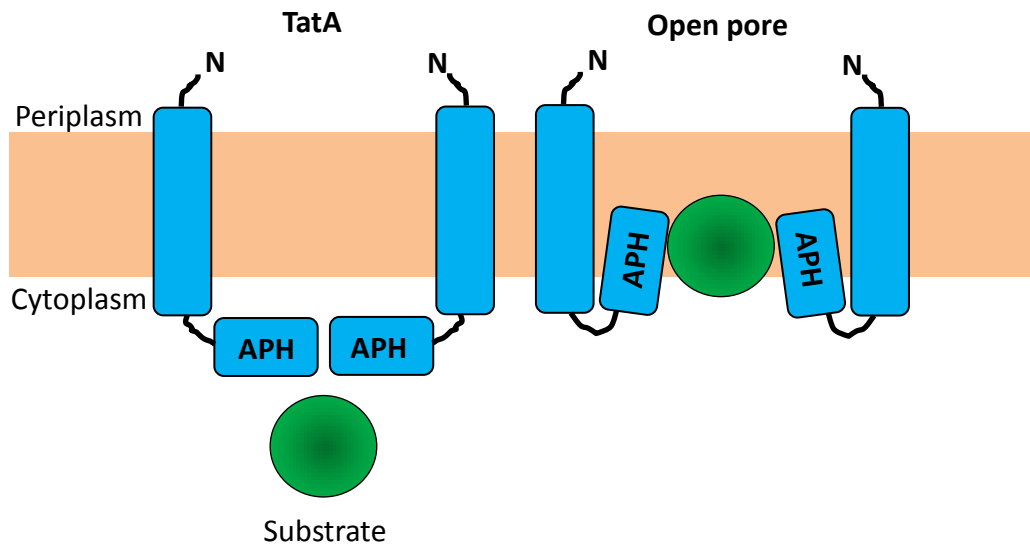
B) Membrane-weakening model
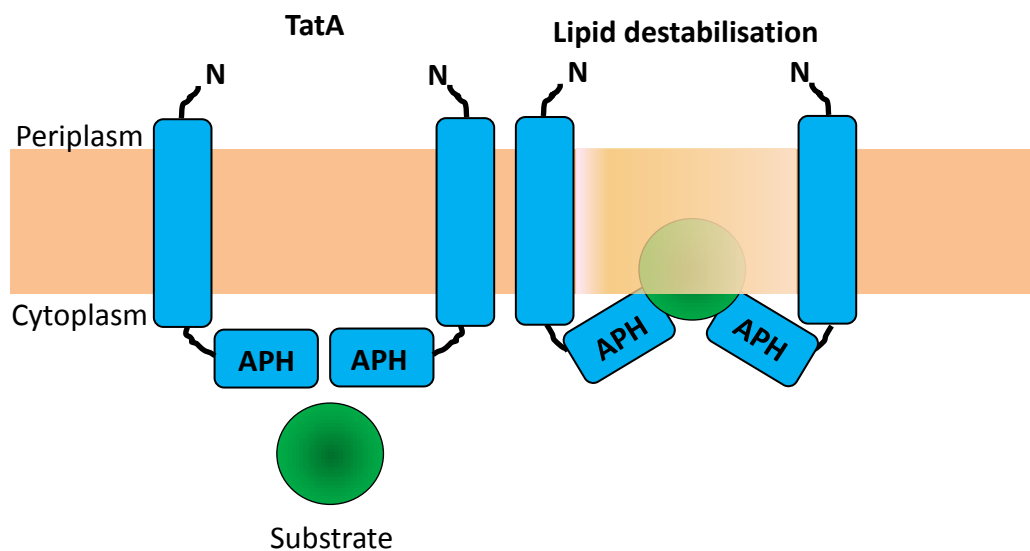
Figure 1.5.2. Mechanism of Tat translocation

Figure adapted from . A substrate bearing an N-terminal signal peptide is targeted to the inner membrane and makes contact to Tat machinery. The figure depicts two hypothesised mechanisms of translocation across the inner membrane, both of which focus on the TatA protein. A) The amphipathic helix (APH) of TatA has a dual topology. In a steady-state situation where there is no substrate to traverse the membrane, the APH lies parallel to the membrane. However, when a substrate binds to TatBC the APH of TatA flips into the membrane to form a hydrophilic pore through which the substrate can pass. B) The dual topology of TatA's APH is a lot less flexible than predicted in the previous model. The APH alters orientation to slightly perturb the membrane bilayer, resulting in lipid destabilisation and thus membrane weakening. The substrate can then be transported through this disrupted lipid patch to gain entry to the periplasm.

1.6. Gram-positive Tat systems

Most of our understanding on the Tat translocase is derived from investigations focusing on the Gram-negative system of *E. coli*, TatABC, which has proven to be a good model owed to the conserved features of this system across Gram-negative bacteria (Oates *et al.*, 2003). However, recent investigations into the Gram-positive organism *B. subtilis* have yielded significant insight into the potential differences between Gram-positive and Gram-negative bacteria.

All Gram-positive bacteria (expect *actinomycetes* (Schaerlaekens *et al.*, 2001)), contain only *tatAC* genes (Jongbloed *et al.*, 2004; Pop *et al.*, 2002); indicating a fundamental difference compared to Gram-negative Tat systems. *B. subtilis* contains two TatAC-type translocases (TatAdCd and TatAyCy) that operate in parallel yet possess different substrate specificities (Jongbloed *et al.*, 2004). TatAdCd is expressed under phosphate-limiting conditions (Pop *et al.*, 2002) and is present in the inner membrane as a 230 kDa TatAdCd complex, and a separate TatAd complex of ~270 kDa (Barnett *et al.*, 2008). The situation is mirrored with the constitutively expressed TatAyCy (200 kDa), where a separate TatAy complex (200 kDa) is also expressed in the membrane (Barnett *et al.*, 2009). The organisation of the *tatAC* genes encoding these proteins is shown in figure 1.3.1 of section 1.3. TatAd and TatAy proteins have an almost identical topology to *E. coli* TatA in the inner membrane; although their APH regions are shorter (Hu *et al.*, 2010; Lange *et al.*, 2007; Müller *et al.*, 2007). Recent NMR studies confirmed this predicted topology of TatAd (Walther *et al.*, 2010). Akin to TatC, TatCd and TatCy are predicted to contain 6 TMH (Nolandt *et al.*, 2009). The topologies of these Gram-positive Tat components are depicted in Figure 1.3.2.

These complexes are markedly different from their Gram-negative counterparts in *E. coli*, since they are smaller, more homogeneous and lack a TatB component (Barnett *et al.*, 2008; Barnett *et al.*, 2009), and it remains questionable whether such differences are indications of different mechanisms of Tat translocation between Gram-positive and –negative bacteria.

A lack of TatB is compensated for by the bifunctionality of TatAd and TatAy proteins (Barnett *et al.*, 2008). Furthermore, heterologous expression of TatAdCd in *E. coli* was found to support the translocation of native substrates (Barnett *et al.*,

2008). The TatAyCy complex, although not as flexible as TatAdCd, was able to transport GFP-tagged substrates (Barnett *et al.*, 2009). Therefore despite these systems only possessing a single substrate in their native cellular environment, these data clearly show the inherent flexibility of these complexes and suggests that a discrete translocase is sufficient to efficiently transport folded substrates.

The biological relevance of the heterogeneity witnessed in *E. coli* TatA complexes is further questioned in light of EM structural data of the TatAd protein. Detergent-solubilised TatAd complexes were revealed to be 7.5 − 9 nm in diameter and possess cavities of 2.5 − 3 nm which were occluded at the cytoplasmic face of the membrane (Gohlke *et al.*, 2005). These features, contrary to those of TatA, were consistent with the TatE complex of *E. coli* (Baglieri *et al.*, 2012), and suggest that TatAd cannot form the translocation channel alone. Therefore, an alternative translocation mechanism is suggested which involves the coalescence of numerous, homogenous TatA/E complexes to TatBC complexes.
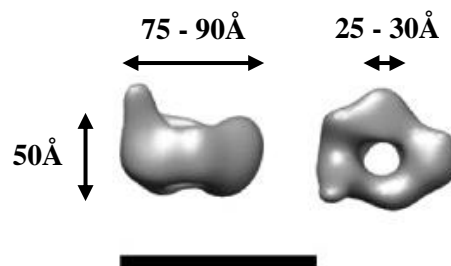
Figure 1.6.1. Low resolution 3D model of TatAd complexes generated by single particle reconstruction
The low resolution structure shown shows TatA complexes that are 75-90Å in diameter. The structure possesses a central cavity, 25-30Å in diameter, which is too small to house Tat substrates. The height of the complex is 50Å, which is consistent with the thickness of the phospholipid bilayer of the inner membrane Scale bar = 100Å. This figure has been adapted from Baglieri *et al.* (2012).

A third TatA protein is constitutively expressed in *B. subtilis*, TatAc. Until recently this protein was thought to be functionally redundant since *tatAC* mutant strains failed to show any phenotype (Jongbloed *et al.*, 2004; Jongbloed *et al.*, 2002; Tjalsma *et al.*, 2000); however when expressed in *E. coli* this protein was able to functionally substitute for TatA in TatAcCd and TatAcCy; forming fully functional

29

complexes that were capable of translocating endogenous Tat substrates (including AmiA, AmiC and TorA) (Monteferrante *et al.*, 2012). It was also able to substitute for *E. coli* TatA and TatB (Beck *et al.*, 2013).

Available data points to differences in both structure and mechanism of Tat machinery between Gram-positive and Gram-negative bacteria. Clearly, more effort needs to be employed to extend and deepen our knowledge of Gram-positive Tat systems so that our understanding is on par with that of TatABC systems.

1.7. Importance of the Tat pathway

1.7.1. A novel antimicrobial target?

Given that bacteria are major contributors to infectious diseases, the rapid increase in antibiotic-resistant bacteria over recent years now limits the therapeutic options for such diseases. Consequently, the issue of antibiotic-resistant pathogenic bacteria is now a major public health concern and now more than ever, do we need to we need to source new antibiotics and novel antimicrobial targets.

Tat serves a potential novel antimicrobial target owing to its ability to secrete virulence factors to the periplasm of numerous pathogenic bacteria. Such proteins would subsequently gain access to secondary protein secretion machinery for export across the outer membrane for cell-surface display or gain entry to the extracellular medium. Tat has been shown to be required for the virulence of numerous pathogenic bacteria including: enterohemorrhagic *E. coli* O157:H7 (Pradel *et al.*, 2003), *Salmonella enterica* (Mickael *et al.,* 2010), *Legionella pneumophila* (De Buck *et al.*, 2005), *Pseudomonas syringae* (Caldelari *et al.*, 2006), and *Agrobacterium tumefaciens* (Ding & Christie, 2003). Since Tat is not expressed in human or animal cells, this machinery has potential as a valuable antimicrobial target.

Some bacterial genomes (E.g. *Mycobacterium tuberculosis*, *Mycobacterium smegmatis* and *Burkholderia pseudomallei*) encode β-lactamases which contain Tat signal sequences and are translocated by Tat machinery (Rholl *et al.*, 2011; Saint-Joanis *et al.*, 2006). Several studies have been conducted that impaired the presence or functionality of the Tat machinery, in numerous pathogenic organisms such as those mentioned, to determine confirm dependence on this translocase for virulence.

For example - the signal peptide mutation (RR➔RK) of Tat-dependent PenA protein of *B. pseudomallei* increased the susceptibility of this bacterium to β-lactam antibiotics (McDonough *et al.*, 2005; Rholl *et al.*, 2011; Saint-Joanis *et al.*, 2006). *B. pseudomallei* are Gram-negative bacteria that cause meloidosis in plants and animals (Northfield *et al.*, 2002). In humans, without successful antibiotic treatment, septicaemia has over a 90% mortality rate (Warner *et al.*, 2007). Likewise, mutation of *tatABC* genes in *Mycobacterium tuberculosis* increased susceptibility of this pathogenic bacterium to β-lactam antibiotics (Saint-Joanis *et al.*, 2006).

Given this evidence, it is sensible to assume that specific inhibitors of the Tat machinery could serve as novel antimicrobial compounds, or specifically β-lactamase inhibitors, that could potentially be used in combination with β-lactam antibiotics. Design of such inhibitors is a complicated task owed to the fact that currently, there are no high resolution structures available for the Tat components or the machinery in its entirety; therefore design of specific Tat inhibitors via molecular modelling is a difficult task. (Vasil *et al.*, 2012) developed a titration assay (which analysed the ability of the compound's inhibition to be overcome by increasing the levels of Tat expression) to test a library of small molecular weight compounds for potential as Tat inhibitors. From over 80,000 initial compounds, 2 were isolated that displayed specific Tat inhibition.

Available evidence presents a strong case for the involvement of Tat machinery in the virulence of numerous pathogenic bacteria. Whilst our understanding of the full extent of this involvement is still at an early stage, there is definitely merit for further investigations and investment of designing novel Tat inhibitors.

1.7.2. The biotechnology industry

The ability of the Tat translocase to transport fully-folded proteins into the periplasmic space has captured the interest and investment of the biotechnology industry, which serves to produce high-value therapeutic proteins. Owing to its rapid growth, high yield, easiness of scale-up and cost-effectiveness, *E. coli* is currently used as the host organism for the production of ~30% of therapeutic proteins (Huang

et al., 2012). A preferred method of protein purification from these cells is to export the recombinant protein into the periplasmic space since this cellular compartment contains only ~4% of the total proteome (Pooley *et al.*, 1996), thus simplifying purification and downstream processing. To translocate a recombinant protein, a signal peptide can be fused to its N-terminus to target it to the inner membrane. Sec and SRP pathways require the substrate to be in a partially-unfolded form; however many therapeutic proteins fold rapidly in the cytoplasm prior to export or, even if they are maintained in a partially unfolded state in the cytoplasm, they fail to correctly refold in the periplasm. The Tat system is of interest to the biotechnology industry since it circumvents this issue by transporting large, fully-folded proteins across the inner membrane, thus simplifying downstream processing.

Initial studies tested Tat's capability of transporting a heterologous protein on a large scale. Results showed high levels of TorA-GFP export at ~0.35 g.L^{-1} with no large-scale release of cytoplasmic contents (Matos *et al.*, 2012), confirming this translocase's potential as a viable method of producing therapeutic protein. More recent data showed Tat to successfully transport biopharmaceuticals including human growth hormone (hGH), interferon α2b and antibody fragments (Alanen *et al.*, 2015). Current efforts are focusing on transporting these biopharmaceuticals on a large, industrial-relevant scale.

1.8. Electron microscopy

Overexpression of recombinant integral membrane proteins often results in low expression levels, as is the case with Tat proteins. Consequently, techniques such as 3D crystallisation are incredibly difficult since they require high yields of highly pure protein as starting material. In contrast, electron microscopy requires very little starting material for extensive analysis; therefore this investigation used EM as a core technique to directly visualise Tat proteins under a variety of experimental conditions.

For clarity in subsequent chapters, the main techniques utilised in this investigation will be introduced.

1.8.1. Negative staining

Negative staining is a routine sample preparation technique for biological samples, whereby the sample is coated in a thin layer of dried heavy metal salt, to give high contrast under the electron microscope. The advantages of this preparation technique are: the sample is very resistant to beam-induced degradation; it is a very high throughput technique owed to the easiness and rapidity of sample staining. Finally, negative staining has proven very useful for analysis of Tat proteins since they are very small biological macromolecules (Baglieri *et al.*, 2012; Beck *et al.*, 2013; Gohlke *et al.*, 2005; Oates *et al.*, 2003; Tarry *et al.*, 2009), thus analysis via other EM preparation techniques such as cryo-EM [reviewed in (Milne *et al.*, 2013)] is very difficult as these proteins have very low contrast under the electron beam in ice. Therefore, staining with heavy metal salts remains a first vital step in the characterisation of Tat proteins.

1.8.2. Chemical fixation and resin embedding

Fixation is the first and most crucial step in the preparation of samples for analysis under the EM. It serves two crucial purposes: firstly, biological preparation of the cells with minimal alteration from living state. Secondly, protection of the sample to maintain stability in subsequent preparative conditions (e.g. embedding) and from damage induced by irradiation from the electron beam.

Conventional fixatives include glutaraldehyde and osmium tetroxide. The former, owed to the abundance of free aldehyde groups available, rapidly and irreversibly fixes samples by cross-linking to proteins; whereas osmium tetroxide binds irreversibly to lipids in the sample. Therefore, the combination of these fixatives generates optimal contrast under the electron beam (Franke *et al.*, 1969). However, antigenicity of the sample is severely diminished since osmium has the potential to extract proteins and the high-density cross linking by glutaraldehyde has the potential to render many antigenic sites inaccessible to antibody binding (De Paul *et al.*, 2012). Antigenicity was vital to the latter half of this investigation (discussed in section 1.8.3); therefore a gentle fixation regime was adopted which involved low percentage of glutaraldehyde fixative and omitted the use of osmium tetroxide.

It has been found that many epitopes are sensitive to high concentrations of glutaraldehyde (Miller, 1972; Smit *et al.*, 1974); therefore a gentle fixation with 2-4% formaldehyde and 0.1-1% glutaraldehyde is a sufficient compromise to obtain ultrastructural and antigenicity preservation (Tokuyasu, 1984).

The final step in sample preparation is embedding in resin. Individual plastic monomers are slowly and gradually incubated with the sample and polymerised to form a solid resin, which provides a protective medium for the sample under the electron beam. Mild aldehyde fixation in combination with LR gold resin was used, since lightly cross-linked samples enrobed in hydrophilic resins have been shown to facilitate access of the labelling agent (antibody) to the antigenic site; thus improving the immunogold signal achieved (Philimonenko *et al.*, 2002).

1.8.3. Immunogold labelling

Immunogold labelling is a powerful technique for the specific localisation of antigenic sites within a biological sample. Identification of the cellular context of a particular protein can provide insight into its structure and/or function within the cell.

In this investigation immunogold labelling was used to unambiguously identify the TatA protein of TatABC in *E. coli* and a heterologous substrate that was transported by the same machinery (chapters 3 and 4, respectively). The immunolabelling process involved the sequential labelling of the sectioned sample with antibodies raised against a specific antigen. This already-labelled sample then undergoes a second round of labelling, this time with a gold-conjugated secondary antibody. It is the gold particle that generates high contrast under the electron beam, thus enabling identification of the protein in the sample. This process is outlined in Figure 1.8.1.
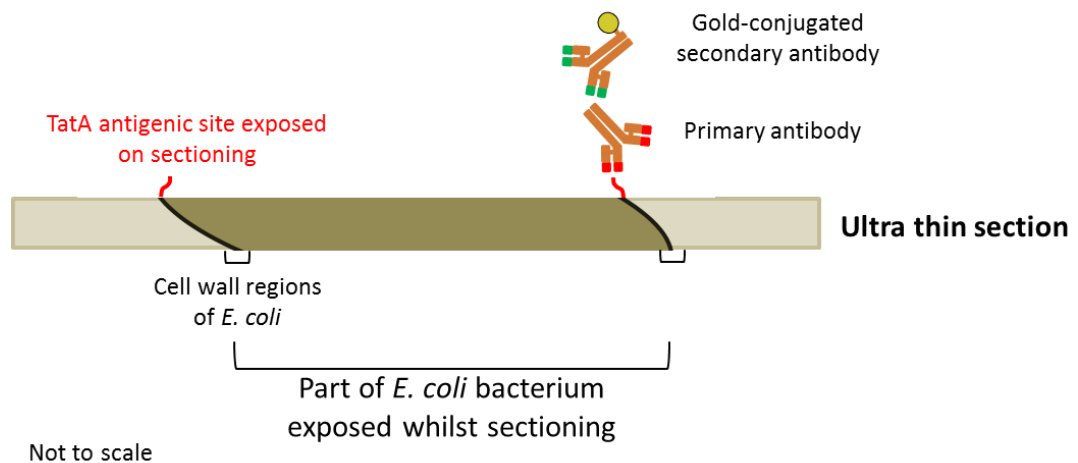
Figure 1.8.1. Immunogold labelling of Tat-expressing *E. coli* cells
Schematic to depict immunogold labelling of resin-embedded, Tat-expressing *E. coli* cells. Serial sections are firstly immunolabelling with a primary antibody raised against a specific antigen – in this case – TatA protein. The primary anti-TatA antibody, which was raised in rabbit host, was then immunolabelled with a goat anti-rabbit, gold-conjugated secondary antibody. The gold particle generates high contrast under the electron beam, thus enabling direct identification of protein of interest.

1.8.4. Array tomography

Derived from the Greek works *tomos* – to cut or section and *graphein* – to write, array tomography involves the physical, serial sectioning of a resin-embedded biological sample. These sections are sequentially imaged under the scanning electron microscope (SEM) to obtain 2D electron micrographs which are then computationally aligned and reconstructed to generate a 3D volume for visualisation.

Imaging in this manner avoids the conventional pitfalls of imaging using conventional TEM in that the imaging conditions are non-destructive to the sample since the electrons do not completely pass through the sample. Also, much larger cell volumes can be analysed, such that in this instance, a whole *E. coli* cell can be reconstructed from a single image acquisition.

The novel combinatorial approach of immunogold labelling of *E. coli* cells with array tomography has enabled us to gain new insight into the 3D localisation and distribution of Tat complexes in their native cellular environment.

1.9. Overall aims and objectives of this investigation

The overall aim of this investigation was to gain insight into the structure and localisation of the Tat translocase.

The experiments utilised individual Tat proteins and/or complexes from both *E. coli* and *B. subtilis*, since they are the model organisms for both Gram-negative and – positive bacteria, respectively; therefore a considerable amount of pre-existing data is available to assist in the design of experiments and data analysis.

To achieve this overall aim, electron microscopy was the main technique used to enable visualisation of Tat protein and/or substrates under numerous experimental conditions.

1. Detergent-induced variability in the appearance of Tat proteins has been reported (Porcelli *et al.*, 2002); therefore what is the true extent of detergent contribution to the molecular weight and heterogeneity of detergent-solubilised Tat complexes?

2. Can I develop and fully-optimise a technology that enables the investigator to circumvent the used of detergent in the analysis of Tat machinery, and thus analyse Tat components in their native cellular environment?

3. Data using fluorescently-conjugated Tat proteins is to be treated with caution, owed to the tendency of these proteins to be inactive or aggregate at the inner membrane (Alcock *et al.*, 2013; Ray *et al.*, 2005). The available confocal data does not give high-resolution information of the localisation of the particular Tat protein, or an appreciation of its 3D localisation in the cell (Alcock *et al.*, 2013; Leake *et al.*, 2008; Ray *et al.*, 2005; Rose *et al.*, 2013). What is the localisation of particular Tat protein in their native cellular environment? Is the localisation dependent on other Tat proteins? Given the remarkable feat that this machinery accomplishes, is there a higher order of organisation of Tat machinery?

4. Tat is of interest to the biotechnology industry owed to its ability to transport fully-folded proteins into the periplasm (Matos *et al.*, 2012). Tat has been shown to successfully transport heterologous biotherapeutics (Alanen *et al.*, 2015). What are the limitations to the expression of heterologous proteins in *E. coli*, specifically by Tat machinery?

Chapter 2:

Materials and Methods

2.0 Materials & Methods

2.1 Suppliers of chemicals, reagents and materials used

All reagents and materials were obtained from the companies listed below.

Abcam (UK): Goat anti-mouse (10 nm gold conjugate); Goat anti-rabbit (10 nm gold conjugate); Rabbit anti-Strep.

Agar Scientific (UK): formvar/carbon coated copper grids (300 mesh).

Antibody Production Services Ltd (UK): Rabbit anti-TatA and Rabbit anti-hGH

Avanti lipids (USA): Mini extruder and *E.coli* lipids

BioRad: Bio-beadTM SM-2 adsorbent,

GE healthcare (UK): Superdex 200 10/300 GL pre-packed gel filtration column; ECL™ detection reagents; Native protein markers for gel electrophoresis and gel filtration chromatography; Hybond TM-P PVDF membrane.

Calbiochem (Germany): *n*-Dodecyl-*ß*-D-maltoside (DDM)

Expedeon (UK): Instant Blue ready-to-use Coomassie® stain.

Fermentas (UK): Bradford Reagent ready-to-use

Fisher Scientific (UK): Acetic acid (glacial); Acetone; Ethanol; Formaldehyde; Glycerol; Glycine; Hydrochloric acid; Methanol; Sodium chloride; sodium dodecyl Sulphate (SDS); Sucrose, and Tris.

Fuji (Japan): Super RX film.

Hamilton (Switzerland) 1ml syringes (for extruder)

IBA (Germany): Buffer E; Strep-tactinTM HRP-conjugate, and Strep-tactinTM affinity chromatography resin, Biotin blocking buffer.

Invitrogen (USA): Mouse anti-His (C-terminal) antibody, Mouse anti-Strep (C-terminal) antibody.

Melford (UK): Isopropyl-*ß*-D-thiogalactoside.

New England Biolabs (USA): Pre-stained broad range protein markers.

Premier International Foods (UK): Marvel milk powder.

Promega (UK) Anti-rabbit-HRP and anti-mouse-HRP conjugates

Roche applied science (UK): CompleteTM protease inhibitor cocktail tablets.

Sigma-Aldrich (UK): Ampicillin; L-arabinose; Avidin; Bis-Tris;

β-mercaptoethanol; Bovine serum albumin; $C_{12}E_9$; Ethanol (absolute); Kanamycin; Lysozyme; Normal goat sera; Silver nitrate; Sodium cacodylate; Sodium carbonate; Sodium thiosulphate; Tannic acid; TEMED; Tricine; Triton X-100, Trizma,

SPI-Chem™ : Uranyl Acetate

VWR (UK): 40% Acrylamide solution; Ammonium persulphate; Bromophenol blue; Calcium chloride; Disodium hydrogen phosphate; EDTA; Glucose; Magnesium chloride; Potassium chloride; Sodium dihydrogen phosphate; Sodium hydroxide pellets; Trichloroacetic acid and Tween 20.

Whatmann (UK): 3mm filter paper and membranes (0.1nm, 0.2nm, 0.6nm, 0.2um)

2.2 Growth and storage of *E. coli* cells

2.2.1. *E. coli* strains used

The *E. coli* strains used in this work are presented in table 2.2.1.

Strain	Properties	Reference
MC4100	*F-, araD139, Δ(ara-leu)7696, Δ(lac)x74, galU, galK, hsdR2, mcrA, mcrB1, rspL*	Casadaban and Cohen, 1980
Δ*tatABCDE*	MC4100 Δ*tatABCDE, Ara^r*	Sargent *et al*., 1988
DH5α	*supE44, ΔlacU169 (80lacZΔM15), hsdR17, recA1, endA1, gyrA996, thi-1, relA1*	Sambrook *et al.*, 1989

Table 2.2.1. Bacterial strains used
All bacterial strains used in this work, the relevant properties and initial reference where they were first used are outlined in the table above.

2.2.2. *E. coli* plasmids used

The *E. coli* plasmids used in this work are presented in table 2.2.2.

Construct	Properties	Reference	Source
TatAyCy_S	pBAD24 + *B. subtilis* TatAyCy-Strep in *ΔtatABCDE*	Barnett *et al.*, 2009	Robyn Eijlander (University of Groningen)
TatABC_S	pBAD24 + *E. coli* TatABC-Strep in *ΔtatABCDE*	Bolhuis *et al.*, 2001	Robyn Eijlander (University of Groningen)
TatABC_S	pEXT22 + *E. coli* TatABC-Strep in *ΔtatABCDE*	Barrett *et al.,* *2003*	Claire Barrett (University of Warwick)
TatA_h	pBAD24 + *E. coli* TatA-his in MC4100	Barnett *et al.,* 2008	Robyn Eijlander (University of Groningen)
pHAK14	pET23 + TorA signal peptide human growth hormone-6His in MC4100	Alanen *et al.,* 2015	Heli Alanen (University of Kent)
pHAK77	As pHAK14 but with substitution of	Alanen *et al*.,	Heli Alanen

	A39L in TorAsp in MC4100	2015	(University of Kent)

Table 2.2.2. Bacterial plasmids used
All bacterial plasmids used in this work, the relevant properties and initial reference where they were first used are outlined in the table above.

2.2.3. LB supplements

Luria Broth (LB) media (10 g/L NaCl, 10 g/L bactotryptone and 5 g/L yeast extract) was supplemented with ampicillin (100 μg/μl) with pBAD24; kanamycin (50 μg/μl) with pEXT22 and/or pET23.

2.2.4. Competent Tat cells

The *E. coli* strains listed in table 2.2.1. were inoculated in 5 ml LB media and cultured overnight at 37°C with shaking (220 rpm). The overnight pre-culture was then diluted 1/10 into fresh LB and cultured for 3hr at 37°C with shaking. Cells were harvested via centrifugation at 3000 g for 10 min. Cells were resuspended in 10 ml of 0.1 M MgCl$_2$ and incubated on ice for 10 mins before harvesting as previous. Cells were resuspended in 1 ml 0.1 M CaCl$_2$ and incubated on ice for 30 min. Once competent, the cells remain viable for 24 hours.

2.2.5. Transformation of *E. coli* cells

100 μl of competent *E. coli* cells were incubated with ~100 ng of DNA on ice for 30 min before mixing. After an additional 15 min incubation, the competent cells were subjected to heat shock: the cells were incubated at 42°C for 1 min and then immediately placed back on ice for 2 min.

2.2.6. Storage of *E. coli* cells

Glycerol stocks of *E. coli* cultures were prepared by mixing 2 parts liquid culture with 1 part 50% (v/v) glycerol and placed immediately on dry ice. Once frozen, the stocks were stored at -80°C.

2.3 Protein expression and purification

2.3.1. Cell culture and induction of plasmids

A 5ml overnight pre-culture of *E. coli* cells containing the appropriate plasmid, was used to inoculate (at 1/100 dilution) fresh LB media, and cultured to OD_{600} of 0.1-0.2. At this OD, cells were induced with 0.1 mM IPTG and cultured until they reached stationary phase (OD_{600} 0.6-0.8). For cells containing the pBAD plasmid, induction occurred upon addition of 200 μM arabinose until the cells reached mid-exponential growth phase (OD_{600} 0.6-0.8).

2.3.2. Fractionation of the *E. coli* cell

E. coli cells were fractionated into periplasm, cytoplasm and membrane fractions using the lysozyme/cold osmotic shock method (Randall and Hardy 1986). Cells (transformed with the appropriate plasmid), were cultured in 10 ml LB media and induced with 1 mM arabinose (or 1 mM IPTG) and cultured until mid-exponential growth phase. Cells were harvested via centrifugation at 6000 rpm for 20 min at $4^{o}C$, and resuspended in 1 ml disruption buffer (100 mM Tris-acetate pH 8.2, 500 mM sucrose and 5 mM EDTA). The periplasmic fraction was obtained by adding lysozyme (20 µg/ml) to this resuspension and kept on ice for 5 min. 1 ml of ice-cold dH_2O was then added to introduce osmotic pressure; resulting in lysis of the *E. coli* outer membrane. 40 µl of 1M $MgSO_4$ was added at the same time to inhibit enzyme activity. The resulting spheroblasts were harvested by centrifugation at 4000 g for 1 min. The periplasm (supernatant fraction) was collected, and pellet resuspended in 0.5 ml wash buffer (50 mM Tris-acetate pH 8.2, 2.5 mM EDTA) and centrifuged at 4000 g for 1 min. The washed pellet was resuspended in 1 ml sonication buffer (50 mM Tris-Acetate pH 8.2) and sonicated for 3 cycles at 8 microns per cycle, for 10 secs with 30 sec intervals. The broken cell membranes were separated from the cytoplasm by ultracentrifugation at 70,000 rpm for 35 min (Beckman TLA 100.3). The resulting membranes were resuspended in 0.5 ml solubilisation buffer (20 mM Tris-HCl pH 8.0, 10% Glycerol, 50 mM NaCl and 1% DDM) for a minimum of 1 hr at $4^{o}C$.

2.3.3. Membrane isolation and solubilisation for Tat purification

For a 0.5 L culture, the Tat-expressing *E. coli* cells were harvested by centrifugation at 6000 rpm for 20 min at 4°C. The cells were resuspended in 24 ml pre-chilled disruption buffer (100 mM Tris-acetate pH 8.2, 500 mM sucrose and 5 mM EDTA) with 1 protease inhibitor tablet (Roche) added to the suspension. The *E. coli* outer membrane was disrupted using 1 mg/ml of lysozyme, followed by immediate addition of 24 ml ice-cold dH_2O. Finally 1ml of 1M $MgSO_4$ was added to the suspension. The resulting spheroblasts were harvested by centrifugation at 4000 g for 15 min at 4 ^{o}C and resuspended in 10 ml sonication buffer (50 mM Tris-acetate pH 8.2 and 2.5 mM EDTA). The membranes were broken by 4 sonication cycles of 30 secs at 10 microns (with 1 min interval between each cycle). The membranes were separated from the cytoplasm by ultracentrifugation at 70,000 rpm for 35 min at 4 ^{o}C (Beckman TL80.6 rotor). The resulting membrane pellet was solubilised in 10 ml solubilisation buffer (20 mM Tris-HCl pH 8.0, 10% glycerol, 50 mM NaCl and 2% DDM) overnight at 4 ^{o}C.

2.3.4. Export assays of Tat substrates in *E. coli* cells

E. coli cells (transformed with the appropriate plasmid), were cultured in 1L LB media and induced with 1 mM arabinose (or 1 mM IPTG) and cultured for 3 hours. At appropriate intervals (i.e 1 hr, 1hr 15 min, 1hr 30 – 3hrs) the optical density of the culture was measured at 600 nm. 10 ml of culture was removed from the flask and harvested by centrifugation at 6000 rpm for 20 min at 4°C. Each cell pellet was normalised against $OD_{600} = 10$, (e.g. OD_{600} of 0.6), then resuspended in 0.6 ml disruption buffer (and later sonication and solubilisation buffers). *E. coli* cells were fractionated into periplasm, cytoplasm and membrane fractions using the lysozyme/cold osmotic shock method (Randall and Hardy 1986). The same protocol as described in section 2.3.2. of this chapter was followed.

2.4 Protein chromatography

2.4.1. Purification using anion exchange Q-sepharose chromatography

5 ml of Q-sepharose resin (GE healthcare) was equilibrated in 10 ml of equilibration buffer (20 mM Tris-HCl pH 8.0, 50mM NaCl and 10% Glycerol). A solubilised membrane sample from a 0.5 L culture of *E. coli* (overexpressing the protein of interest), was applied to the Q-sepharose column and flow through was collected. To remove loosely bound material the column was washed 5X each with 5ml of wash buffer (20 mM Tris-HCl pH 8.0, 100 mM NaCl, 10% Glycerol and 0.02% DDM). The protein was eluted in 5X 2 ml elutions using high-salt elution buffer (20 mM Tris-HCl pH 8.0, 300 mM NaCl, 10% glycerol and 0.02% DDM). To neutralise the high-salt condition (by reducing final salt concentration to 150 mM), the elutions were eluted directly into 2ml of no salt buffer (20 mM Tris-HCl pH 8.0, and 0.02% DDM).

2.4.2. Affinity tags

For the purification and detection of recombinant proteins, C-terminal tags were sued. Either the 10 amino acid *Strep*-tag II (IBA, Germany) or a hexa-histidine tag were used where stated, denoted by –s or –h, respectively.

2.4.3. Purification using a Streptactin[TM]-Sepharose affinity chromatography

Solubilised membranes were incubated with 1μM avidin for a minimum of 30 min prior to loading onto the Streptactin column to prevent non-specific binding of biotinylated proteins. Prior to sample loading, the Streptactin resin was equilibrated with 2 column volumes (CVs) of equilibration/wash buffer (20 mM Tris-HCl pH 8.0, 150 mM NaCl and 0.02% DDM). Blocked, solubilised membranes were applied to the Streptactin resin and flow through collected. Unbound proteins were washed from the column by washing with 5 CVs (5X 4ml) of equilibration/wash buffer. Finally, the Strep-tagged proteins were eluted from the column, in 10X 1ml elutions, using the elution buffer (20 mM Tris-HCl, 150 mM NaCl, 2.5 mM desthiobiotin and 0.02% DDM).

2.4.4. Purification using a Talon^{TM} affinity chromatography

Talon affinity chromatography was used to purify his-tagged proteins. 10 ml of Talon resin was equilibrated with 10 ml (1 CV) of equilibration buffer (20 mM Tris-HCl pH 8.0, 400 mM NaCl, 5 mM imidazole and 0.02% DDM) and left rotating overnight at 4°C. The resin was separated from the equilibration buffer by centrifugation at 2000 rpm for 5min. A solubilised membrane sample or pooled Q-sepharose elutions were gently mixed with the Talon resin and left rotating for ~4 hr at 4°C. The slurry of protein sample/Talon resin was poured into a plastic gravity column and allowed to settle. The flow through was then collected from the column. The column was washed in 6 CVs of buffer 1 (equilibration buffer) and then eluted with 2.5 CV of elution buffer (20 mM Tris-HCl pH 8.0, 400 mM NaCl, 150 mM imidazole and 0.02% DDM). Each elution fraction was 0.5 ml.

All fractions from either Streptactin or Talon affinity columns were separated by SDS-PAGE and visualised by Western blot. Peak fractions were pooled and concentrated using: 30 kDa VivaSpin concentrators for TatAyCy and TatABC complexes; and 5 kDa cut off for TatAd.

2.4.5. Gel-filtration chromatography

Size-exclusion chromatography was used as the final purification step to isolate Tat proteins, and an analytical tool to estimate the mass of protein complexes. A Superdex200 10/300 GL column (protein separation range: 10-600 kDa) was used with an ÄKTA purifier FPLC system (GE healthcare), operated by the UNICORN® v.4.00 software. The column was equilibrated with 2 CVs of gel filtration (GF) buffer (20 mM Trizma-HCl pH 7, 150 mM NaCl +/- 0.02% DDM). The concentrated protein sample was centrifuged at 10000 rpm for 10 min prior to loading onto the column. Sample separation was performed at 0.5 ml/min and the elution volume was collected in 0.5 ml fractions. Between sample runs, the column and loading loop was washed in 2 CVs of GF buffer. Resin purity and column performance was maintained by a daily cleaning protocol: 2 CV dH$_2$O, then 2 CVs 0.5 M NaOH then 2 CVs dH$_2$O.

2.4.6. Gel filtration calibration

Calibration of the Superdex200 column was performed using proteins of known molecular mass to generate a standard curve for molecular weight estimation. Blue dextran was used to estimate the column void volume (Vo) (the volume at which all matter too larger to enter the resin is eluted). The protein standards and their elution volume (Ve) are shown in table 2.4.1.

Molecular weight (kDa)	Molecular weight (Da)	Protein standard	Ve (ml)	Ve/Vo
669	669000	Thyroglobulin	9.30	1.13
440	440000	Ferritin	10.92	1.32
158	158000	Aldolase	12.87	1.56
66	66000	Albumin	14.03	1.70
			Vo	
2000	2000000	Blue Dextran	8.25	

Table 2.4.1. Elution volumes of protein standards on Superdex200
Protein standards with their molecular weight and corresponding elution volume (Ve) are shown. The void volume (Vo) of the Superdex200 column was shown to be 8.25 ml. A linear plot of Ve/Vo is used to estimate the molecular weight of unknown protein sample.

2.5. Protein electrophoresis

2.5.1. SDS polyacrylamide gel electrophoresis (SDS-PAGE)

Gel electrophoresis was used to resolve protein samples. It was performed using the C.B.S vertical gel system and a uniform running buffer (25 mM Tris, 250 mM glycine and 0.1% SDS). SDS-PAGE gels consisted of a 17.5% resolving gel (17.5% acrylogel, 375 mM Tris-HCl pH 8.8, 0.1% APS and 0.06% TEMED) and 4% stacking gel (4% acrylogel, 125 mM Tris-HCl pH 6.8, 0.1% SDS, 0.6% APS and 0.06% TEMED). Protein samples were prepared by diluting aliquots 1:1 with 2x loading dye (125 mM Tris-HCl pH 6.8, 20% glycerol, 4% SDS, 0.02% bromophenol

blue and 5% β-mercaptoethanol) and heated at 70°C for 5 minutes. Gels were run at 35 mA for ~2 hr 15 mins (until the blue dye from had reached the bottom of the gel).

2.6. Protein detection

2.6.1.Silver staining

Having resolved proteins by SDS-PAGE, the gel was incubated in fixer solution (50% acetone, 1.25% trichloroacetic acid and 0.015% formaldehyde) for 15 minutes at room temperature. Fixer was washed off with 3x 5 min washes in dH$_2$O. The gel was washed for a further 5 mins in 50% acetone, followed by 1 minute incubation in 0.02% (w/v) sodium thiosulphate enhancer solution. Enhancer solution was removed by washing in dH$_2$O for 5 min. Staining of the gel followed, by an 8 min incubation in staining solution (0.25% (w/v) silver nitrate and 0.4% formaldehyde (v/v)). Protein bands were visualised by developing the gel in developing solution (0.2 mM sodium carbonate, 0.004% sodium thiosulphate (w/v) and 0.015% formaldehyde). Once the bands were visible, developing was stopped by rinsing the gel in 1% acetic acid. Finally, the gel was rinsed in water.

2.6.2. Coomassie staining

SDS-PAGE gels were incubated with ~50 ml of Instant Blue Coomassie stain for at least 1 hr before washing with dH$_2$O until background is clear.

2.6.3. Protein transfer to PVDF membranes

Once proteins had been resolved on a SDS-PAGE gel, they were transferred to a PVDF membrane using a semi-dry Western blotting system (Sigma, UK). Two sheets of Whatman paper soaked in transfer buffer (A Towbin transfer buffer was used: 25 mM Tris, 192 mM glycine and 20% methanol [Towbin et al., 1979]) and placed on the pre-wet positive electrode. A methanol-soaked PVDF membrane was then layered on top of the Whatman paper, followed by the gel. Finally, two more pieces of buffer-soaked Whatman paper were placed on top ensuring no air bubbles

remained in the stack. The blotter was closed, completing contact between the positive and negative electrode. Proteins were transferred at 200 mM over 2 hours.

2.6.4. Immunoblotting

Once proteins have been transferred to a PVDF membrane it is blocked overnight in a solution of 5% (w/v) dried milk in PBS-T (or 3% BSA for strep-tagged proteins) at 4°C. Membranes were then rinsed in PBS-T prior to the addition of 20 ml of the appropriate primary antibody (see table 2.6.1.) for 1 hr at room temperature (RT). For StrepII-tagged proteins, the membranes were blocked in biotin-blocking buffer (1:10000 dilution) before adding the anti-Strep-HRP antibody for 2 hours. For other primary antibodies, the post-incubation with antibody, the membranes were washed frequently for 1 hour in PBS-T. Then, the appropriate secondary HRP-conjugated antibody (table 2.6.1.) was incubated with the membrane for 1 hour at RT. Finally, all membranes were washed frequently in PBS-T for at least 1 hour at RT. Immunoreactive bands were detected using ECL^{TM} detection reagents according to the manufacturer's instructions. X-ray films were developed using an AGFA Curix 60 automatic developer as directed by the manufacturer's instructions.

Antibody	Dilution	Source
Mouse anti-*his* (C-terminal)	1:10000	Invitrogen, USA
Mouse anti-*strep* II HRP conjugate	1:10000	IBA, Germany
Anti-TatA	1:6000	Colin Robinson (University of Kent)
Anti-hGH	1:20000	Colin Robinson (University of Kent)
Anti-rabbit IgG HRP conjugate	1:10000	Promega, USA
Anti-mouse IgG HRP conjugate	1:10000	Promega, USA

Table 2.6.1. Antibodies used in this investigation
List of antibodies used in Western Blotting protocol, alongside working dilution and source.

2.6.5. Estimation of protein concentration

Estimation of protein concentration was achieved using Bradford's reagent (Fermentas) as per the manufacturer's instructions: 20 µl of protein sample mixed with 1 ml of room-temperature Bradford's reagent. Assay readings were recorded at 595 nm after 5 min incubation. Standard curves were prepared using BSA dilutions.

2.7. Protein reconstitution in liposomes

2.7.1. Liposome preparation

1 ml (~25 mg) of chloroform-dissolved *E. coli* polar lipids (Avanti) was dried in a 50 ml round-bottom flask using gentle nitrogen airflow (flask incubated in 60°C waterbath). Residual solvents were removed by placing the remaining thin lipid film under a vacuum overnight. The lipid film was hydrated in nitrogen-saturated liposome buffer (20 mM Tris-HCl pH 8 and 150 mM NaCl) to give a 2 mg/ml lipid solution for 4-6hr with gentle agitation to form multilamellar vesicles. Once fully hydrated, the lipid layer was subjected to 5 cycles of freeze-thaw. The liposomes were extruded through a 600 nm (3 X) and 200 nm (20 X) membranes, forming uniform 200 nm liposomes.

2.7.2. Protein reconstitution

The liposomes were subjected to 0.12% Triton-X-100 disruption via incubation for 15 min, whilst rotating. Protein was added to 2mg liposomes at differing ratios (lipid:protein – 1:1, 60:1 and 90:1) and further incubated for 45 min at room temperature for the protein to be incorporated. Detergent was removed via the addition of SM2 Biobeads: 30 mg of wet Biobeads were added gradually to the 1 ml liposome mixture and incubated at RT for 30 min. An additional 60 mg of beads were added and incubated for a further 1 hr. A final 60 mg of biobeads were added and rotated overnight at 4°C. The liposome solution was extracted from the Biobeads and concentrated by ultracentrifugation at 55,000 rpm for 1.5 hour (Beckman TLA 100.3 rotor).

2.8 Atomic Force Microscopy

all atomic force microscopy (AFM) work was carried out by Cvetelin Vasilev (University of Sheffield).

2.8.1. Sample preparation

Purified proteoliposome sample was diluted in imaging buffer (10 mM Tris pH 7.4, 120 mM KCl, 0.02% DDM) and 40 µl was deposited onto a freshly cleaned mica surface, which is attached to an AFM sample support. Protein was left to adsorb onto the mica surface for ~15 min. The sample was then rinsed 3X with imaging buffer, and imaged under the AFM tip.

2.8.2. AFM measurements

PeakForce QNM mode was operated on a Multimode 8 AFM instrument. The microscope was connected to a 15 µm E-scanner and a NanoScope Vcontroller (Bruker). NanoScope software (v8.15, Bruker) was used for data collection. OriginPro (v8.5.1, Origin Lab Corp.) software was used for data processing and analysis. All measurements were collected in imaging buffer at room temperature using BL-AC40TS probes (Olympus). Z-modulation amplitude was set to 20-24 nm, with the frequency set to 2 kHz. Tip-sample force was maintained between 60 – 80 pN.

2.8.3. Preparation of Wet Bio-beads SM-2

Biobeads SM-2 are adsorbent beads that capture detergent molecules. Biobeads (1 mg) are prepared for detergent extraction by washing in methanol for 15 min with rotation at RT. The methanol is discarded and a further 16 ml is added to the same beads and washing continued for 30 min. Residual methanol was removed by multiple washes in 30 ml dH_2O for 30 min. Finally, the beads were equilibrated in liposome buffer (20 mM Tris-HCl pH 8.0 and 150 mM NaCl) until ready to use.

2.8.4. Sucrose density gradient centrifugation (SDGC)

Sucrose density gradient was used to separate protein and liposomes given their differing densities. A sucrose gradient is prepared by: adding 400 µl 60% sucrose (in 20 mM Tris-HCl pH 8.0 and 150 mM NaCl buffer) to 200 µl liposome solution (final

sucrose concentration is 40%); then 2 ml of 20% sucrose (in 20 mM Tris-HCl pH 8.0 and 150 mM NaCl buffer) is layered on top. The final layer is 0% sucrose/400 µl liposome buffer. The gradient is subjected to ultracentrifugation at 55,000 rpm (Beckman TLA 100.3) for 1.5 hr at 4°C. Low-density liposomes shall resolve in the upper layers of the sucrose gradient, yet the unincorporated proteins will remain at the bottom sucrose layers.

2.9. Analytical ultracentrifugation

Analytical ultracentrifugation experiments (AUC) were conducted in a Beckman Optima XL-A analytical ultracentrifuge equipped with absorbance optics using a 60Ti rotor. Sedimentation equilibrium experiments were performed at 7000 rpm - 12000 rpm for purified TatAyCy complexes. Data was collected at 230 and 280 nm in step scan mode using a separation of 0.001 cm. Five readings were averaged for each scan, and a baseline scan was taken at 360 nm to correct for optical imperfections. Readings were taken at 6hr intervals until no difference could be detected between consecutive scans. The equilibrium distributions from three different loading concentrations (10, 20 and 50 µg/ml) were globally analysed using single species fit model in SEDPHAT software (Schuck, 2005). Solvent density was adjusted to that of DDM detergent by adding 29% (w/v) sucrose. Measurement of buffer density was measured to 1.01 g/mL using a density meter (Anton Paar DSA5000).

2.10 Electron microscopy

2.10.1. Sample preparation

2.10.1.1. Sample preparation for negative staining

20 µl aliquots of purified protein sample (previously stored at -20°C) were used for each imaging session. Any dilutions and/or washes were performed using the GF buffer (20 mM Trizma-HCl, 150 mM NaCl) +/-0.02% DDM detergent. All solutions were filtered through a 0.2 µm filter prior to use as a wash or dilution buffer.

2.10.1.2. Glow discharge

A hydrophilic surface of carbon-coated grids was generated by glow discharging. Glow discharge was performed with an EMtech K100x unit, running at $3x10^{-1}$ mbar and 25ma for 15 seconds of negative discharge in air.

2.10.1.3. Touching drop gridding method

4 µl of protein sample was pipetted onto a freshly glow-discharged Formvar/carbon coated copper grid (300 mesh), for 1 min. Washing excess sample off the grid was achieved by touching the grid to the convex face of a 8 µl drop of GF buffer for ~10 secs with gentle agitation. Post-washing, excess liquid was removed from the grid by blotting with filter paper. This process of washing and blotting was repeated again. Next, the grid was washed for ~10 secs in an 8 µl drop of uranyl acetate stain (1 or 2% (w/v)) before blotting and staining in a fresh drop of uranyl acetate for 20 secs. The grid was blotted for a final time and then left to air dry for ~10 min before insertion into the electron microscope. This protocol is an adaptation of a previously published method (Rubinstein, 2007) using a Parafilm® drop support and Whatman® paper for blotting.

2.10.1.4. Cryogenic plunging of biological samples

7 µl of biological sample was pipetted onto a glow-discharged lacey carbon grid and allowed to adsorb for 1 min. Lacey carbon grids were used since they contain irregularly-shaped holes in the carbon layer in which vitreous ice can form. After 1 min, both sides of the grid are blotted for 5 secs with filter paper. Immediately after blotting, the sample is plunged into liquid ethane to freeze in vitreous ice. An in-house pneumatic plunge system was used for this plunging step.

2.10.1.5. Chemical fixation of *E. coli* cells

Following immediate induction with 100 uM arabinose, 1L of *E. coli* cells (overexpressing his-tagged TatA [TatA-his] or strep-tagged TatABC [TatABC-strep]), were cultured to an OD_{600} of ~0.6. Bacterial cells were harvested via centrifugation at 6000 rpm for 20 minutes. The cell pellet was divided into aliquots (the cell volume no larger than an equivalent of 100 µl), and resuspended in 0.5 ml aldehyde fixative(s) (prepared in dH_2O) of varying concentrations. An equal volume

of low melting temperature agarose was added to the sample and re-suspended quickly. Samples were centrifuged at 15000 rpm for 1 min and placed onto ice for 10-15 minutes until the agarose had set. Once set, the agarose plug was extracted and any agarose lacking bacterial cells was trimmed and discarded. The remaining agarose-enrobed cells were sliced to pieces no larger than 1 mm^3. The specimen cubes were resuspended in fresh 0.5 ml aldehyde fixative overnight (o/n) at 4°C. The following day, cells were centrifuged at 2000 rpm for 2 mins. Aldehyde supernatant was discarded and cell pellet resuspended and subsequently rotated in 0.15 M sodium cacodylate/HCl buffer pH 7.4 (now termed cacodylate buffer) for 10 minutes at 4°C. A total of 5 washes were conducted.

2.10.1.6. Heavy metal staining of *E. coli* cells: Osmium tetroxide and Tannic acid staining

Post-washing of chemically fixed *E. coli* cells, cells were quenched via washing in cacodylate buffer containing 0.1 M glycine for 1 hour (2x 30 mins) at 4°C. To stain, cells were resuspended in 2% osmium tetroxide for 2 hours at room temperature (RT). Cells were then rinsed in 3x 5 min in cacodylate buffer. This was followed by a second staining of 1% buffered Tannic acid (TA) for 1 hour at 4°C. Washing of the cells was again necessary in cacodylate buffer for 1x 5 min and 1x 10 min period at RT. The *E. coli* cells were then dehydrated in an ethanol series (70% -100%) for a period of 2 hrs. The cells were then embedded in LR-Gold resin (London Resin Company Ltd.; Berkshire, UK).

2.10.1.7. Heavy metal staining of *E. coli* cells: Tannic acid and Uranyl acetate staining

The protocol was identical to section 2.1.2; however instead of osmium tetroxide followed by TA, 1% buffered TA was used followed by 1% aqueous uranyl acetate (UA) at 4°C in darkness. Also- the washing after the first staining period was dH$_2$O instead of cacodylate buffer.

2.10.1.8. Heavy metal staining of *E. coli* cells: The 'Berrymann' method

This method used fixative: 1% glutaraldehyde, 4% formaldehyde, 0.2% picric acid and 0.5 mM in 0.1M phosphate buffer, pH 7.4 for fixation of *E. coli* cells. Removal of phosphates was necessary following quenching of the sample(s). Staining

consisted of solely 2% buffered (0.1 M maleate-sucrose, pH 6.5) UA at 4°C in darkness.

2.10.1.9. Infiltration of resin

Ethanol was removed via centrifugation at 2000 rpm for 2 minutes. The following rotating incubations at 4°C were conducted:

- 1:1 LR gold:ethanol, 1 hr
- 7:3 LR gold:ethanol, 1 hr
- 100% LR gold, 1hr
- 100% LR gold, o/n
- 100% LR gold + 0.5% benziyl (polymerisation initiator), 1 hr
- 100% LR gold + 0.5% benziyl, 1 hr
- 100% LR gold + 0.5% benziyl, o/n

Sample was then transferred into 0.5 ml Eppendorf with fresh 100% LR gold +0.5% benziyl and left to stand for ~1 hr so that the *E. coli* cells deposited at the bottom of the Eppendorf. Samples were then polymerised via exposure to UV light for ~ 72 hours at 4°C.

2.10.1.10. Serial sectioning of resin blocks for imaging under the EM

A glass knife was used to 'square-off' the resin block (using an ultramicrome [Ultracut E, Reichert-Jung; Vienna, Austria]), providing a flat 0.5 mm^2 surface which could then be sectioned. Using the same microtome and a diamond knife, ultrathin (50 nm) serial sections were cut. Using a metal loop, these sections were transferred to either: carbon-coated (~80 nm thickness) glass coverslips (13 mm diameter) for scanning EM work, or 200-mesh carbon-coated copper grids (Agar Scientific, Stansted Essex) for transmission EM work.

2.10.2. Immunolabelling of serial sections

2.10.2.1. Optimised immunolabelling procedure for unambiguous identification of overexpressed TatA-his and TatABC-strep in the *E. coli* inner membrane

Using the touching-drop method serial sections were blocked in TBS/T buffer (0.24% Tris (w/v), 0.8% NaCl (w/v) and 0.1% Tween-20 (v/v)) pH 8.4 containing 1% BSA (w/v) and 4% normal goat sera (v/v) (Abcam Plc, Cambridge UK) for 30 min at RT. Grids/Glass coverslips were directly transferred to a 10µl drop of primary antibody ((table 2.9.1.) (diluted in TBS/T buffer + 1% BSA (w/v)) for 2hrs at RT. Sections were washed (with blotting with filter paper in between) for 3x 2 min with TBS/T buffer + 1% BSA at RT. Incubation with secondary antibody (diluted in TBS/T buffer + 1% BSA (w/v)) followed (table 2.9.1.) for 1hr at RT. Sections were washed for 3x 10 min with TBS/T+BSA buffer at RT, followed by 4x 3min washes in dH$_2$O at RT. Finally, grids were allowed to air dry before insertion into the EM.

2.10.2.2. Berryman immunolabelling procedure

Using the touching-drop method serial sections were blocked in TBS buffer (0.24% Tris (w/v) and 0.8% NaCl (w/v)) pH 7.5 containing 1% BSA (w/v) for 30 min at RT. Grids/Glass coverslips were directly transferred to a 10µl drop of primary antibody (table 2.9.1.) (diluted in TBS buffer) for 1hr at RT. Sections were washed (with blotting with filter paper in between) for 5x 3 min with TBS buffer at RT. Incubation with secondary antibody (diluted in TBS buffer) followed (table 2.9.1.) for 1hr at RT. Sections were washed for 5x 3 min with TBS buffer at RT, followed by 5x 3min washes in dH$_2$O at RT. To fix antibodies in place, sections were incubated in 2% aqueous glutaraldehyde for 5 min at RT. Counterstaining to improve section contrast was performed by staining sections in 2% aqueous osmium tetroxide for 5 min at RT. Residual stain was washed off sections by washing for 5x 3min with dH$_2$O at RT. Further staining in lead citrate for 3 min at RT followed, with removal of excess stain achieved by washing sections in dH$_2$O for 1x min. Finally, sections were allowed to air-dry before inserting into the EM.

2.10.2.3. Optimised immunolabelling procedure for the unambiguous identification of overexpressed Tat substrate (TorAspHGH) in *E. coli*

To identify the Tat substrate in the *E. coli* cell, the anti-hGH antibody was used (table 2.9.1.). The same methodology applies as (§2.10.2.1.), however a different TBS/T buffer was used: (0.24% Tris (w/v), 2.5% NaCl (w/v) and 2% Tween-20 (v/v)) pH 8.4.

Antibody	Host	Dilution	Source
anti-His	Mouse	1:20	Life Technologies, UK
anti-Strep	Mouse	1:20	IBA, Germany
anti-Strep	Rabbit	1:20	Abcam plc, UK
anti-TatA	Rabbit	1:20	Colin Robinson, Kent University
anti-hGH	Rabbit	1:1000	Colin Robinson, Kent University
Anti-rabbit IgG pre-adsorbed (10-nm gold)	Goat	1:10	Abcam plc, UK
Anti-mouse IgG pre-adsorbed (10-nm gold)	Goat	1:10	Abcam plc, UK

Table 2.9.1. Antibodies used for immunolabelling of serial sections with their optimised working dilution and source.

2.10.3. Transmission electron microscopy (TEM)

2.10.3.1. JEOL 2010F TEM

200 kV JEOL transmission electron microscope with a field emission gun electron source, operating a Gatan Ultrascan™ 4000 CCD camera with a pixel size of 14 μm.

2.10.3.2. Imaging software

The microscope was controlled via the FasTEM software suite (ver.3) and the CCD camera was operated using the Digital Micrograph package (ver.1.81.78).

2.10.3.3. Density profiling

The Density Profile tool in Digital Micrograph software (ver.1.81.78) was used to measure particle diameter in the electron micrographs.

2.10.4. Scanning electron microscopy (SEM)

2.10.4.1. JEOL 7401F SEM

A cryo-scanning electron microscope with a field emission electron source. The "in-lens" solid state back scatter detector provides ultimate resolution with low kV performance.

2.10.4.2. Imaging software

The microscope was controlled by SEMSupporter software (SiFi), which also enabled the acquisition of image montages from each serial section.

2.10.5. Computational reconstruction

2.10.5.1. Alignment of image stack

SiFi Panorama Mapping module in SEM supporter software was used to manually refine alignment of montage stack. The greyscale of the images was reset for each montage to make refinement of alignment easier in later steps. In eTomo software (IMOD (Kremer *et al.*, 1996)), Align Serial Sections/Blend Montages tab was selected and the relevant .mrc image stack uploaded. Midas module was used to further manually refine montage alignment; correcting for magnification, stretch and rotation. Under the 'Make Stack' tab in Align Serial Sections, Global Alignments was selected, and Make Aligned Stack option selected to generate aligned volume stack.

2.10.5.2. Segmentation of aligned image stack for generation of volume image

Following alignment using Midas, the Z-stack was opened using 3DMod (set to Model). The first Z-plane was selected, and the first bacterium centred, ensuring it filled the screen. A new Object was created for each bacterium.

For each Z-plane (1 to 20), the perimeter of a single *E. coli* bacterium was manually traced. Any immunogold labels were each marked as single points in each contour.

Points were edited and deleted as necessary to make sure that the contour matched the visible perimeter as accurately as possible. Once the contour was complete, any immunogold labels were each marked in a new Object as separate contours. The perimeter tracing and gold-point marking was repeated for each Z-plane until all were successfully contoured.

The contours were stitched together using the meshing feature in 3DMod. Mesh One was used to generate the surface for each bacterium. The final model was saved and exported into UCSF Chimera for visualisation.

2.10.6. Quantification of immunogold

2.10.6.1. Multi-random sampling approach to quantifying immunogold

Having sampled randomly and selected the optimal operating magnification of 12,000X on the JEOL 2010F TEM, raw gold counts were retained as numerical frequency distributions from 200 randomly imaged *E. coli* (from 2 biological and 2 technical replicates) and assigned to one of the two compartments: inner membrane and cytoplasm. A compromise between precision of intracellular location, or more specifically- inner membrane localisation, and noise of the EM image was achieved by counting any gold particle within a 25 nm radius of the inner membrane.

2.10.6.2. Statistical evaluation of immunogold distributions

Raw gold counts were used to construct a numerical frequency distribution table. Observed numbers of gold particles in each compartment were compared by use of contingency table analysis with 'g' groups (arranged in columns) and 'c' compartments (arranged in rows). This analysis generated predicted gold particles and, hence, partial chi-squared values, for each group and each compartment. Comparison of the total chi-squared value against a Chi-squared table determined whether the null hypothesis (of no difference in immunolabelling between TatA-overexpressing and Δ*tat* cells) could be rejected ($p<0.005$).

Chapter 3:

Primary structural insight into prokaryotic twin arginine translocase complex TatAyCy

3.1 Introduction

Bacillus subtilis contains two discrete Tat systems that operate in parallel, yet possess different substrate specificities (Jongbloed *et al.*, 2006): TatAyCy and TatAdCd (Jongbloed *et al.*, 2004). Reminiscent of the situation in *E. coli*, the TatAyCy system is comprised of two types of membrane protein complexes: TatAyCy and TatAy that have been reported to form ~200 kDa complexes (as judged by gel filtration chromatography) (Barnett *et al.*, 2009; van der Ploeg *et al.*, 2011). Likewise, TatAdCd exists as a ~230 kDa complex (Barnett *et al.*, 2008) , alongside a separate and discrete TatAd complex of ~160 kDa (Barnett *et al.*, 2008) .

In addition to differences in size, composition and organisation, the smaller TatAdCd and TatAyCy systems, which possess discrete, homogeneous TatA complexes, were found to translocate *E. coli* Tat substrates in the range of 63 kDa to 85 kDa (Barnett *et al.*, 2008; Barnett *et al.*, 2009). This further complicates the translocation process, since these data argue against the pore-forming model of Tat; instead suggesting a primary translocon that is flexible in accepting substrates of different sizes (Robinson *et al.*, 2011). There remains a lack of knowledge regarding the structural properties of TatAyCy and TatAdCd, which will assist in the elucidation of the Tat mechanism in Gram-positive bacteria.

Previous published structural information has largely focused on individual Tat constituents: TatE, TatAd and TatA (Baglieri *et al.*, 2012; Beck *et al.*, 2013; Gohlke *et al.*, 2005); whereas structural information on entire Tat complexes is severely lacking. Pursuit of a 3D reconstruction of TatABC, TatAyCy or TatAdCd is limited by several factors. Firstly, the interaction of the Tat constituents at the inner membrane is transient and it is therefore difficult to capture the active translocase at the membrane. Also, the small size of the Tat complexes makes it difficult to obtain electron microscopy images of sufficiently high contrast and information content to average for computational reconstructions. This is further complicated by the known heterogeneity of the Tat machinery since thousands of particles would have to be classified to gain enough structural data to represent the entire size range of the protein complex. The latter difficulties do not make it impossible to generate a 3D reconstruction − low resolution reconstructions of TatA were resolved despite

significant heterogeneity of 8.5 nm to 13 nm (Gohlke *et al.*, 2005) – however it is vital to thoroughly characterise the sample prior to pursuit of a 3D reconstruction.

Given the aforementioned evidence suggesting a difference in Tat mechanism between Gram-positive and Gram–negative bacteria (Baglieri *et al.*, 2012; Beck *et al.*, 2013), I decided to conduct preliminary 2D structural characterisation of the TatAyCy complex.

Initial results presented in this chapter demonstrate the use of EM to unambiguously identify the detergent-solubilised TatAyCy complexes. This is necessary when analysing a detergent-solubilised protein since lipid/detergent micelles are also present in the purified sample. These need to be identified so that they can be excluded from subsequent structural analysis. Size distribution analysis confirmed that TatAyCy protein-detergent complexes (PDCs) are 12-14 nm in diameter. This required further analysis to investigate whether this heterogeneity is intrinsic to the TatAyCy complex or an artefact of detergent solubilisation.

Analytical ultracentrifugation (AUC) (in collaboration with Dr David Scott, Research Complex, Harwell) was used to gain a detergent-free molecular weight of TatAyCy. This technique involves the application of a centrifugal force to a macromolecule in solution. Over time the solute will move towards the bottom of the cell and start to sediment. Simultaneously the process of diffusion opposes the sedimentation and eventually these two processes reach a state of equilibrium, thus the solute does not move (Figure 3.2.8.). Therefore, the concentration of the solute increases exponentially towards the bottom of the cell. This distribution is dependent on the buoyant molecular weight of the solute (molecular weight of the sample corrected by a buoyancy factor due to displaced solvent). Measurement of concentrations at different points leads to the determination of molecular weight of solute. Data from several experiments (run at different speeds, loading concentrations and measured at different wavelengths) are examined simultaneously to obtain the most accurate molecular weight possible.

AUC revealed a true molecular weight of TatAyCy to be 101 kDa, excluding detergent contribution. However, further analysis revealed that this protein is heterogeneous. This is the first time that TatAyCy has been analysed in such manner,

and these results bear implications for future structural studies on this complex, and the Tat mechanism of Gram-positive bacteria.

3.2 Results

3.2.1. Affinity chromatography of TatAyCy

Preliminary characterisation of TatAyCy complexes required a highly pure sample. Affinity chromatography was performed using a C-terminal strep tag on the TatCy component of the TatAyCy complex. As described in Materials and methods (§2.4.3.), solubilised membranes from *E. coli* cells overexpressing TatAyCy were applied to an equilibrated Streptactin™ affinity column (that specifically binds the strep-tag on TatCy). Bound proteins were eluted from the column and analysed by SDS-PAGE and blotting using antibodies to strep-tag on TatCy. The results are presented in Figure 3.2.1.

Strep-tagged proteins were detected in all wash fractions, implying that they bound to the column only weakly. The tightly bound TatCy-strep specifically eluted from the column over elution fractions 2-5. Silver staining of SDS-PAGE gel confirmed that TatAy had co-eluted with the TatCy complex (middle panel, Figure 3.2.1.). There are very few other migrating bands present on the gel, indicating a good level of purity of these isolated TatAyCy complexes after application to just a single column.
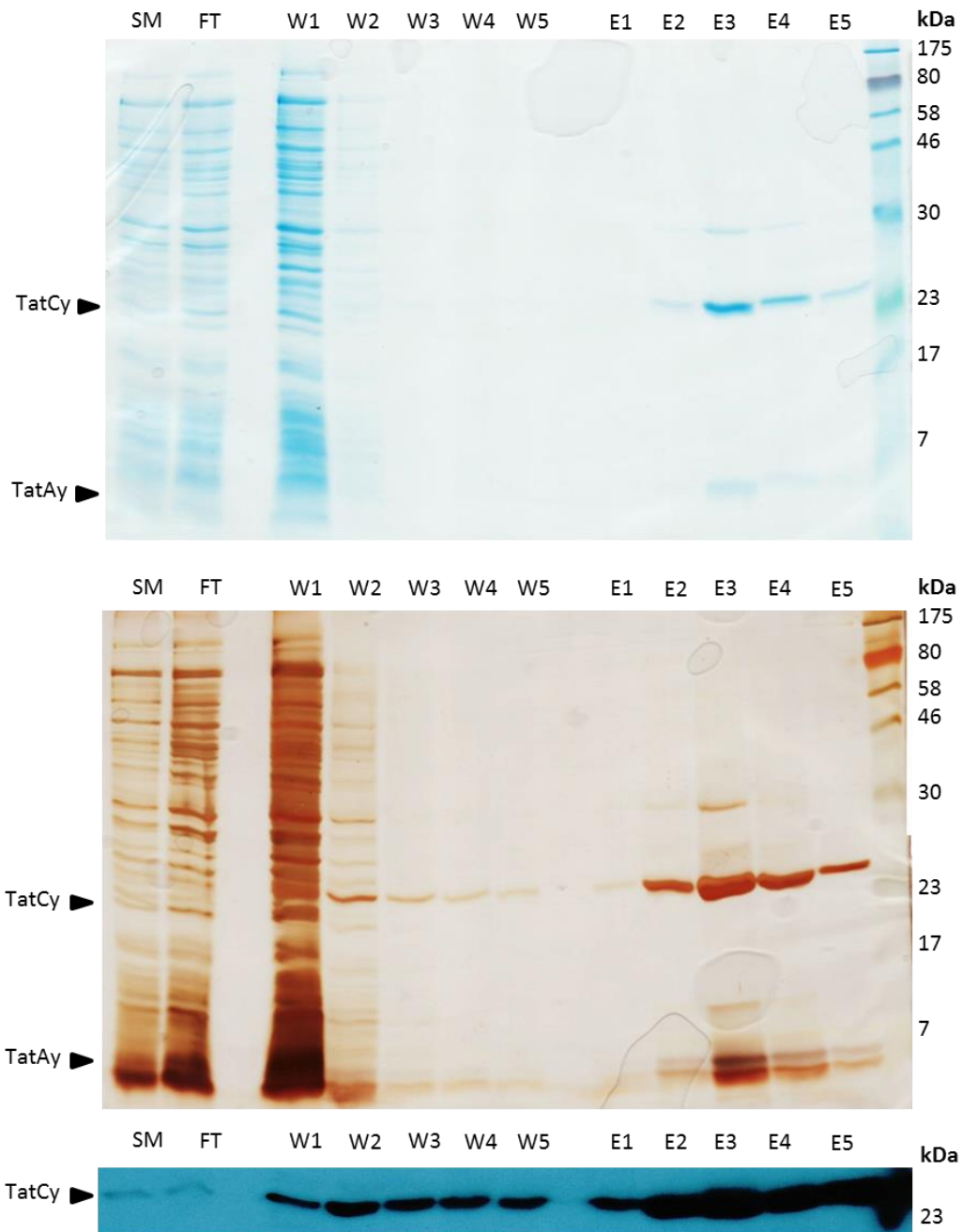
Figure 3.2.1. Affinity chromatography of WT TatAyCy-strep

SDS-Polyacrylamide gel electrophoresis analysis of purified TatAyCy-strep. *E. coli* membranes were isolated from *ΔtatABCDE* cells expressing WT TatAyCy-strep from the pBAD plasmid and solubilised in DDM. Solubilised membranes were applied to a StrepTactin column as described above. The column flow-through (FT), wash fractions (W1-5) and elution fractions (E1-5) were analysed by Coomassie staining (A) and silver-stain (B). The same samples were immunoblotted with antibodies against the Strep-tag on TatCy(C). Positions of TatAy and TatCy are indicated on the left-handside of the figures and molecular-weight markers on the right.

3.2.2. Gel filtration chromatography of TatAyCy complex

Affinity purified TatAyCy was subjected to size exclusion chromatography for further purification to obtain a homogeneous complex for EM analysis. Purified TatAyCy was applied to a gel filtration column and eluted in 0.5 ml fractions (Figure 3.2.2.). Peak fractions were immunoblotted with antibodies against the strep-tag on the TatCy protein (Figure 3.2.2., B). The blot shows TatCy strep eluting in 11 fractions between 8 and 14 ml. By using a calibration curve (generated from elution profiles of soluble standards), the mass of the TatCy complex (in 0.02% DDM detergent) can be estimated to be ~320 kDa. This is similar to previous molecular weights reported for the same complex in DDM detergent (Patel *et al.*, 2014). Fractions 15-24 were pooled and concentrated to a final concentration of 85 μg/ml. An aliquot of this final sample was resolved by SDS-PAGE and silver stained (Figure 3.2.2., C). The blot shows a pure fraction of a TatAyCy complex which will be used for subsequent analysis under the TEM.
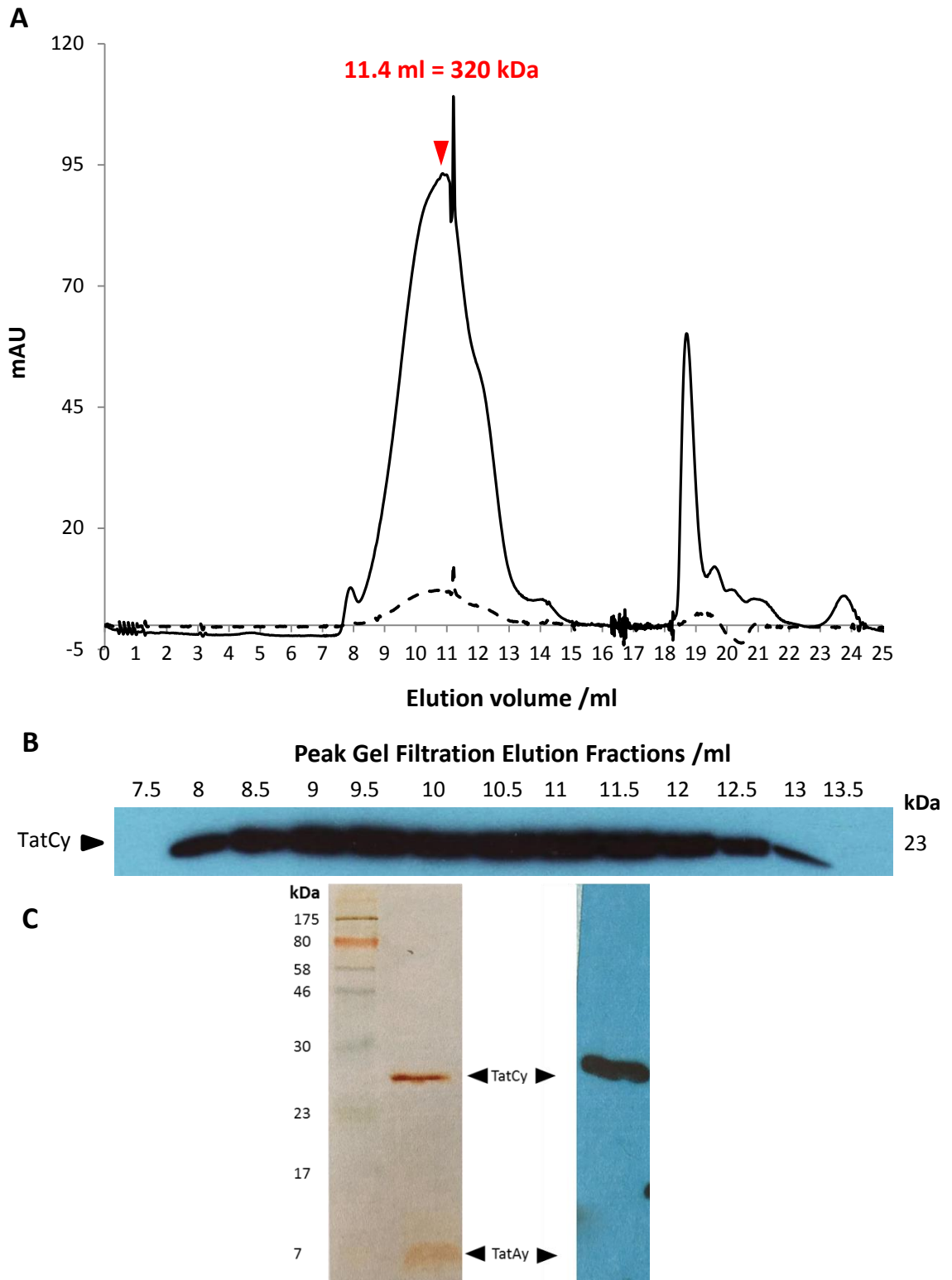
Figure 3.2.2. Size exclusion chromatography of WT TatAyCy-strep
Purified TatAyCy is a 320 kDa complex. (A) Affinity purified TatAyCy-strep was applied to a 24ml Superdex 200 (HR 10/300) gel filtration column as described in Materials and Methods and eluted in 0.5 ml fractions. Absorbance was measured at 230 nm (solid line) and 280 nm (dotted line). Peak elution fractions (14-26 / 7ml-13ml) were immunoblotted using antibodies against the strep-II tag on TatCy. (B) The TatCy immunoblot shows the presence of TatCy in all peak fractions. (C) Fractions 15-24 were pooled and concentrated to a final concentration of 85µg/ml. Silver stain of the pooled fraction shows the presence of TatAy and TatCy with no other contaminating proteins.

3.2.3. Electron microscopy of TatAyCy complexes

3.2.3.1 Optimisation of sample preparation for imaging of TatAyCy under the TEM

With the aim of gaining preliminary structural insight into the TatAyCy complex, TEM was employed to analyse particles of purified protein-detergent complexes (PDC) of TatAyCy.

Membrane proteins are notorious for low yields of purification. Therefore electron microscopy was deemed an appropriate technique for the preliminary structural characterisation of TatAyCy complexes, as only a few microliters of sample are required for analysis. Optimisation of sample preparation was required to minimise the number of contaminating aggregates and obtain an even spread of particles in the field of view. Both of these affect the level of staining that a particular PDC receives and consequently the contrast of particles under the electron beam.

Initial viewing of the concentrated gel filtration fractions containing pure, detergent-solubilised TatAyCy complexes revealed a sample containing a dense lawn of roughly-spherical TatAyCy particles and a large number of aggregates (large white, irregularly sized bodies) (Figure 3.2.3., A, yellow circles). In an attempt to minimise the number of aggregates, the washing of the sample, after being adsorbed to a copper grid, was increased. Results showed the density of particles decreased, yet the aggregates remained (Figure 3.2.3. B). Further optimisation by increasing dilution to 25X minimised the number of aggregates (Figure 3.2.3. C), and increased staining time of this sample with 2% uranyl acetate increased particle contrast (Figure 3.2.3., D).
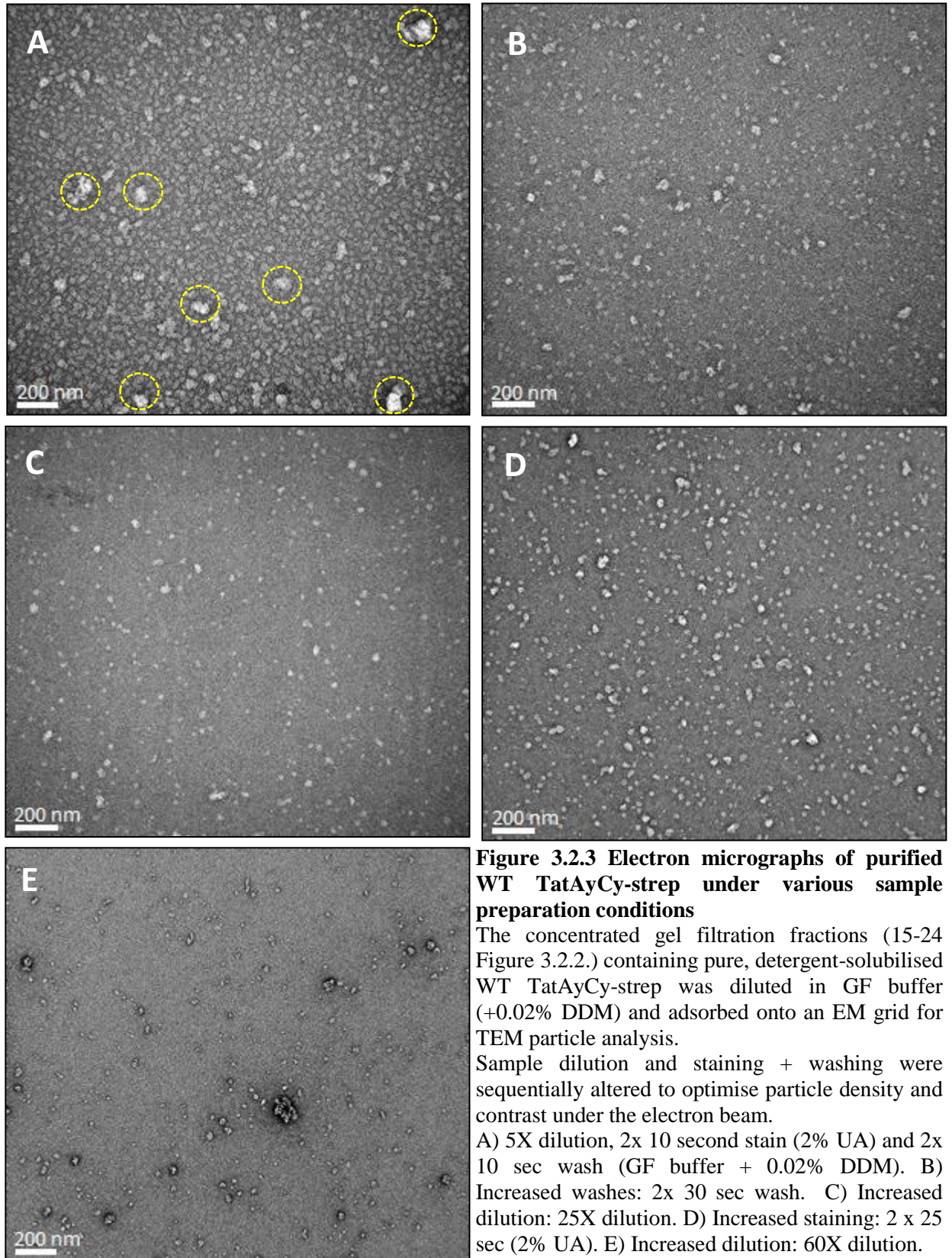
Figure 3.2.3 Electron micrographs of purified WT TatAyCy-strep under various sample preparation conditions

The concentrated gel filtration fractions (15-24 Figure 3.2.2.) containing pure, detergent-solubilised WT TatAyCy-strep was diluted in GF buffer (+0.02% DDM) and adsorbed onto an EM grid for TEM particle analysis.

Sample dilution and staining + washing were sequentially altered to optimise particle density and contrast under the electron beam.

A) 5X dilution, 2x 10 second stain (2% UA) and 2x 10 sec wash (GF buffer + 0.02% DDM). B) Increased washes: 2x 30 sec wash. C) Increased dilution: 25X dilution. D) Increased staining: 2 x 25 sec (2% UA). E) Increased dilution: 60X dilution.

Magnification = 40000X. Scale bar = 200 nm
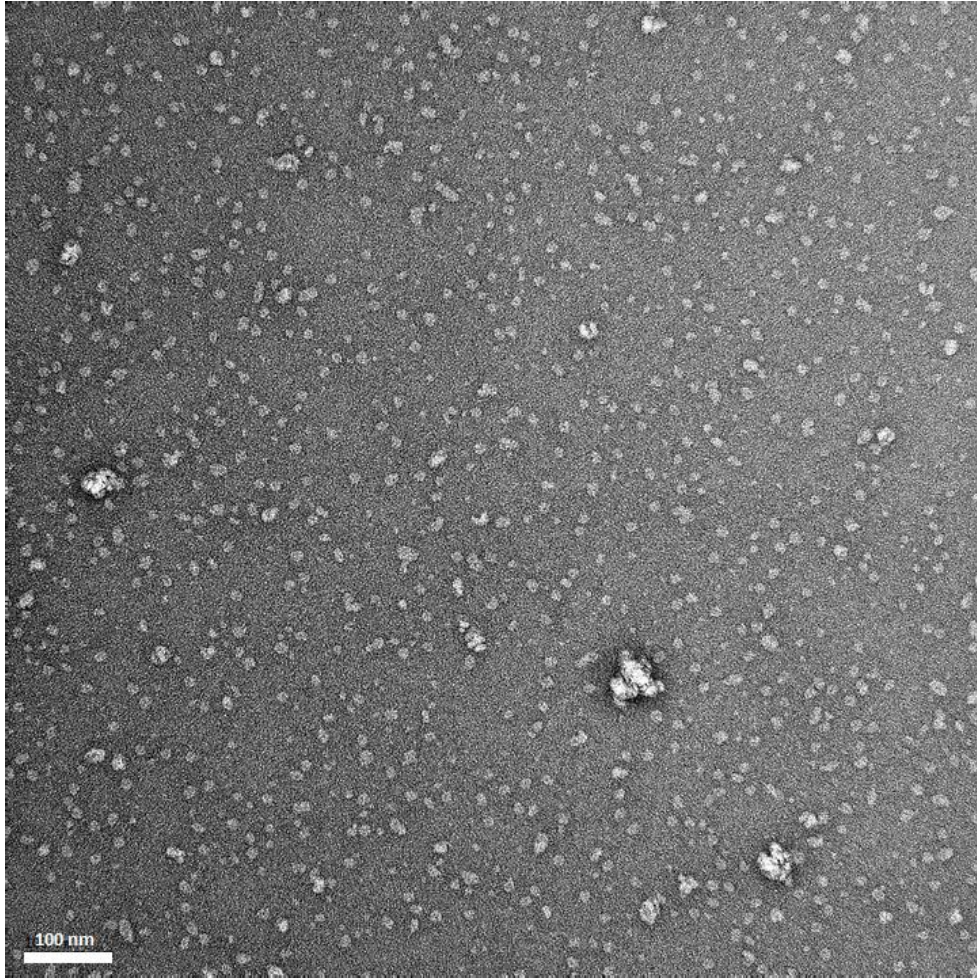
Figure 3.2.4. Electron micrograph of purified WT TatAyCy-strep in optimal sample preparation conditions

The peak gel filtration fraction (B4) containing pure, detergent-solubilised WT TatAyCy-strep was diluted in GF buffer (+0.02% DDM) and adsorbed onto an EM grid for TEM particle analysis. A 25X dilution in GF buffer (+0.02% DDM), 3x 25 sec 2% UA stain and 2x 30 sec washes in GF buffer (+0.02% DDM) gave the optimal particle density and density contrast under the electron beam. The micrograph shows a lawn of spherical protein-detergent complexes of varying diameters. Magnification = 40000X. Scale bar = 100 nm

Increasing the dilution of the sample to 60X in an effort to eradicate the aggregates drastically altered the appearance of the protein, since particles appeared significantly smaller. The stability of a solubilised protein depends on the protein:detergent (P:D) ratio. At higher detergent concentrations lipids distribute themselves amongst the detergent micelles, resulting in the formation of a heterogeneous mixture of lipid/detergent and protein/detergent micelles. With increased detergent concentration, delipidation occurs and solubilisation no longer increases. The removal of lipid head groups from a PDC alters stability of the PDC and thus the solubilised protein. Therefore, the 60X dilution of the TatAyCy protein (solubilised in 0.02% DDM) is evidence of this effect. A lowered protein concentration increased detergent ratio, clearly decreasing the stability of the TatAyCy PDC and causing it to disassemble (Figure 3.2.3., E).

The optimised sample of DDM-solubilised TatAyCy is shown in Figure 3.2.4. A heterogeneous population of circular TatAyCy-detergent complexes was observed. Aggregates could not be completely removed from the sample. However, to avoid disturbing the P:D ratio and thus the stability of the observed PDCs, minimising the number of aggregates was deemed to be sufficient.

Further analysis of these particles revealed the full extent of TatAyCy heterogeneity (Figure 3.2.5.). The diameters of 400 randomly selected TatAyCy particles from independent purifications was measured (Figure 3.2.5., C). Results showed that particles as small as 7 nm in diameter and in excess of 20 nm were present. Quantification of these measurements showed that 12-14 nm particles were the most abundant. Interestingly, the 12-14 nm particles (magnified in boxes for clearer observation) exhibited a similar density pattern: the central density across all of the particles shows a "W-shaped" pattern (Figure 3.2.5., B). Given that the particles have been negatively stained (i.e. stain is most dense where there is no sample), this W-shaped density profile is consistent with the presence of a central cavity/pore-like feature in the complex. Similar staining profiles have been observed previously for TatAd and TatE components of the *B. subtilis* and *E. coli* Tat systems, respectively, whose later reconstructions revealed the presence of a pore/cavity-like feature (Baglieri *et al.*, 2012; Beck *et al.*, 2013).
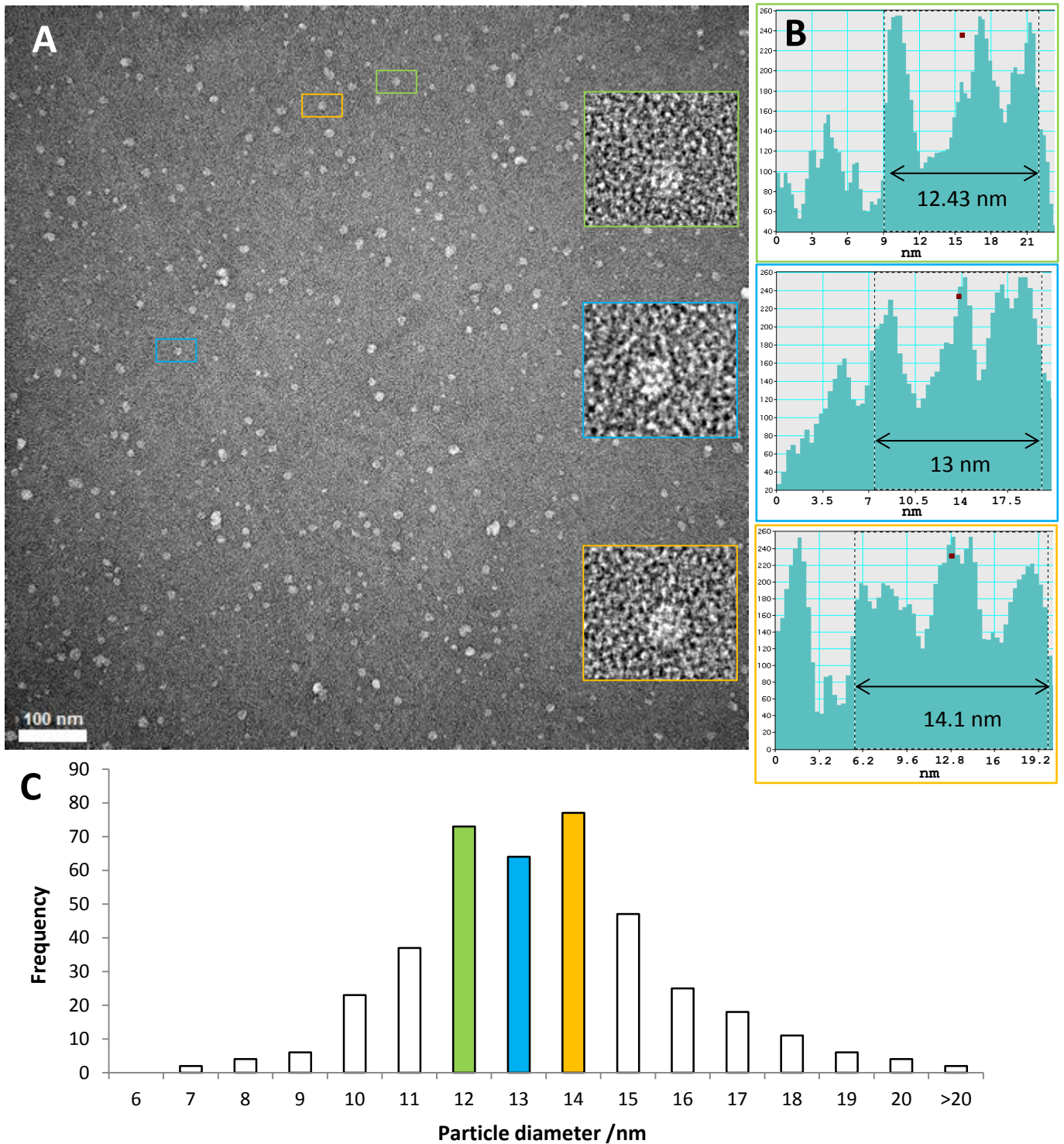
Figure 3.2.5. Size distribution analysis of WT TatAyCy-detergent complexes under the electron microscope

A) Electron micrograph of heterogeneous TatAyCy-detergent complexes. The peak gel filtration fraction (B4) containing pure, TatAyCy-strep was diluted in GF buffer (+0.02% DDM) and adsorbed onto an EM grid for TEM particle analysis. The micrograph contains spherical protein-detergent complexes of varying diameters. B) Density profiling (using Digital Micrograph software) of the WT TatAyCy complexes shows a "W-shape" profile indicating a stain-excluding region in the particle. C) 400 randomly selected particles had their diameters measured using ImageJ software to gauge the most abundant particle diameters. Magnification = 40000X. Scale bar = 100 nm

70

3.2.3.2 Preliminary characterisation of TatAyCy particles under the EM

The next stage was to ensure that the 12-14 nm particles are definitely detergent-solubilised TatAyCy complexes and not just detergent micelles, since any subsequent structural analysis on this complex would have to encompass the entire size distribution of the TatAyCy complexes. Serial dilutions of the purified TatAyCy protein were prepared for size-distribution analysis. As previously described, 400 TatAyCy particles were randomly selected from each dilution and its diameter was measured. Results are shown in Figure 3.2.6.

The amount of protein in each sample halves with respect to the previous and the concentration of DDM detergent remains constant (2.3X above the CMC); therefore PDCs are still able to form, just at a lowered frequency. If the 12-14 nm diameter range is a true reflection of TatAyCy size, these particles should be the most abundant in the sample.

Such a trend is observed in Figure 3.2.6: particle density is reduced as dilutions increase. Data also shows that for each dilution, the most abundant particle diameter was in the range of 12-14 nm. Interestingly, as the dilution increased from 1:10 to 1:40, the most abundant particle diameter increased in size from 12 to 14 nm, respectively (Figure 3.2.6., green bar on histogram). This is most likely due to the detergent ratio increasing relative to the amount of protein with each dilution. An increase in detergent ratio could result in more detergent molecules being incorporated into each PDC and thus increase particle diameter.
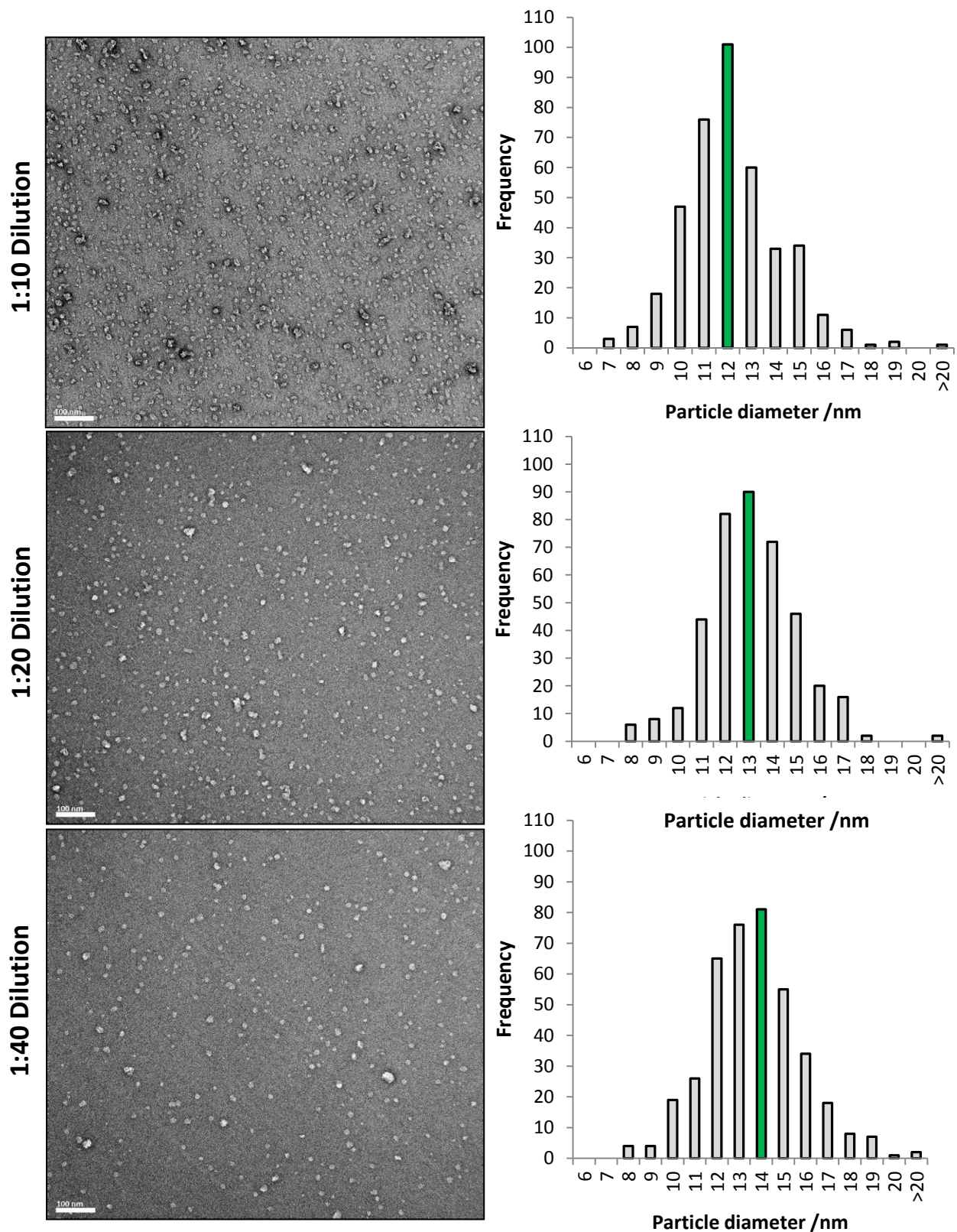
Figure 3.2.6. Size distribution analysis of serially diluted heterogeneous WT TatAyCy-detergent complexes under the electron microscope.

Left: Electron micrographs of TatAyCy sample. The peak gel filtration fraction (B4) containing pure, detergent-solubilised WT TatAyCy-strep was serially diluted (1:10, 1:20 and 1:40) in GF buffer (+0.02% DDM) and adsorbed onto an EM grid for TEM particle analysis. The micrograph contains spherical protein-detergent complexes of varying diameters. Right: 400 randomly selected particles had their diameters measured using ImageJ software to gauge the most abundant particle diameters for each dilution. Magnification = 40000X. Scale bar = 100 nm

Whilst 12-14 nm particles were the most abundant, there were also other particle sizes visualised. PDCs are not the only components present in the sample. When a protein is solubilised in detergent, there will be lipid-detergent micelles lacking protein incorporation. It is important to identify which particles these are and consequently confirm the extent of the heterogeneity of the TatAyCy complex. Therefore, a size distribution analysis of a detergent-only sample was conducted.
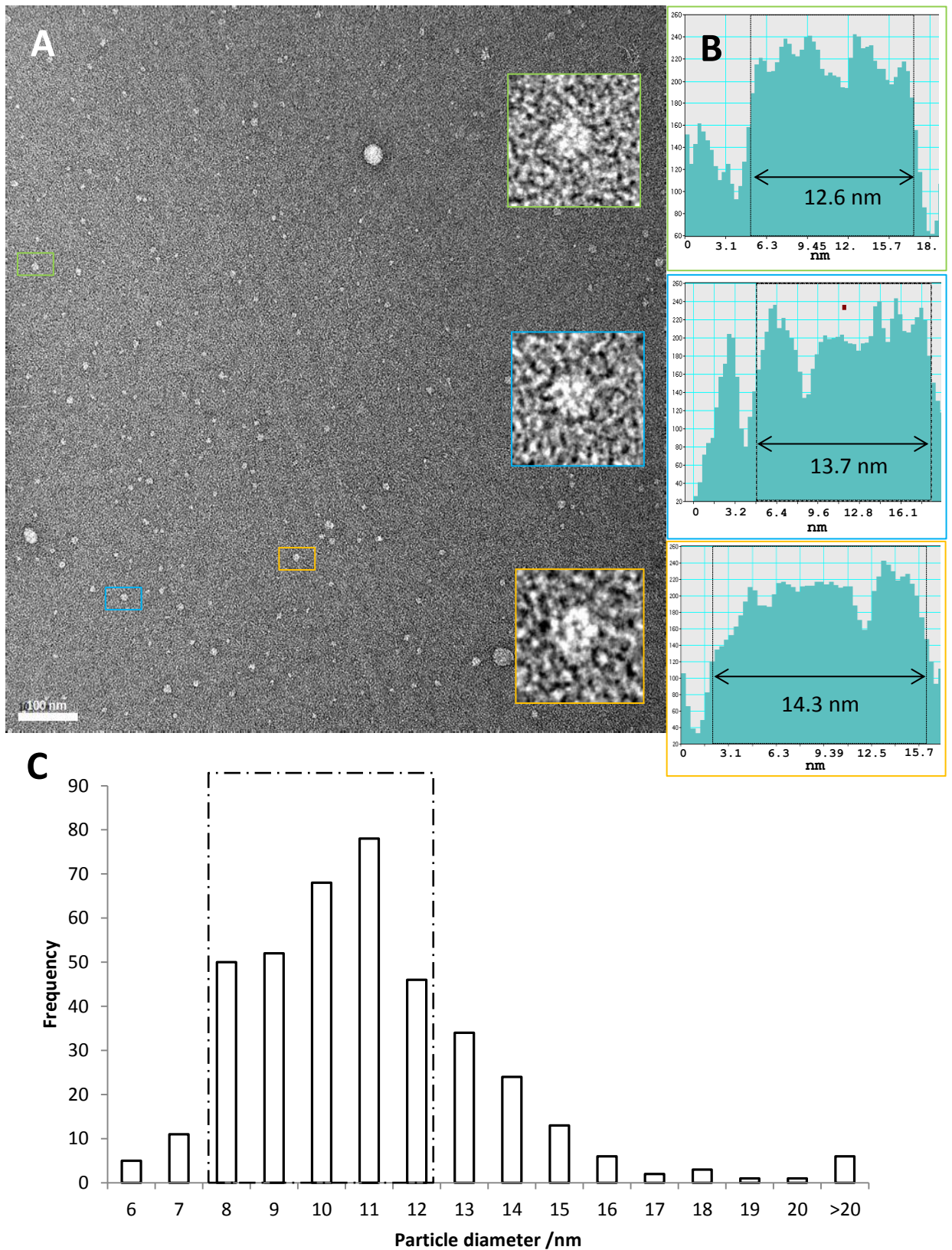
Figure 3.2.7. Size distribution analysis of buffer-only sample under the electron microscope.
A) Electron micrograph of detergent-only sample. Gel filtration buffer (+0.02% DDM) was adsorbed onto an EM grid for TEM analysis. The micrograph contains spherical detergent complexes of varying diameters. B) Density profiling (using Digital Micrograph software) of the detergent complexes shows varying profiles, not consistent with a "W-shape" profile. C) 400 randomly selected particles had their diameters measured using ImageJ software to gauge the most abundant particle diameters. Magnification = 40000X. Scale bar = 100 nm

74

EM analysis revealed a lawn of heterogeneous spherical particles (Figure 3.2.7., A) magnified in boxes for clearer observation). Quantification of particle size showed that, compared to the TatAyCy-detergent sample (Figure 3.2.5.), the most abundant particles had smaller diameters in the range of 8-11 nm (Figure 3.2.7 C). This shift in size distribution is likely attributable to the lack of protein incorporation into the detergent-micelles.

However, 12-14 nm particles were still present in the sample, albeit at a much lower frequency than in TatAyCy-containing samples (1.7X, 1.9X and 3.2X, respectively). Surface density analysis of these particles revealed that they exhibit a different average surface profile compared to TatAyCy-containing samples: the detergent-only samples lack the characteristic "W-shaped" profile. Instead surface density exhibits a more evenly shaped profile, lacking any deep stain-excluding regions like those observed in the TatAyCy sample. This profile could be explained by the fact that detergent micelles would have a more uniform surface density surface owed to the lack of protein incorporation.

Data presented this far provides evidence for spherical TatAyCy detergent-solubilised complexes to exhibit diameters of 12-14 nm. However, the observed increase in particle diameter with increasing dilutions demonstrates how alteration of protein/detergent ratio can alter complex size. Therefore, it remains questionable whether the observed heterogeneity is an intrinsic property of the TatAyCy complex or a consequence of detergent solubilisation. Confirmation of an intrinsic heterogeneity could provide insight into the translocation mechanism of a Tat system from Gram-positive bacteria.

3.2.4. Analytical Ultracentrifugation of purified TatAyCy

Whilst we know that detergent solubilisation contributes to the molecular weight of a protein upon the formation of PDCs, thus increasing the size of the protein when visualised under the electron microscope, it is unclear what the exact contribution of the detergent is. Also, regarding TatAyCy protein, we do not know whether the 12-14 nm particle heterogeneity is an inherent property of this protein complex, or an artefact of detergent solubilisation. Therefore, analytical ultracentrifugation (AUC) was employed to find the true molecular weight of the TatAyCy complex, and whether this complex possesses any inherent heterogeneity.

AUC is an extremely versatile technique for the quantitative analysis of macromolecules in solution. Sedimentation equilibrium (SE) was performed on purified, detergent-solubilised TatAyCy particles.

20 μl of highly pure TatAyCy (Figure 3.2.2., C) (10-50 ug/ml) was spun at 7000, 10000, and 12000 rpm until the measured (absorbance at 230 and 280 nm) concentration profile remained unchanged for at least 24 hours (§2.7 methods section). Density matching of the detergent-containing solvent was necessary to make the DDM neutrally buoyant. This was achieved by the addition of 29% sucrose (w/v) to the buffer. Global analysis (simultaneous analysis data measured at varying concentration and speeds) of the SE data was performed using SEDFIT and SEDPHAT software (Schuck, 2005). Results presented in Figure 3.2.9 presents SE data for the TatAyCy molecule, showing concentration as a function of position within the cell as monitored by absorbance at 230 and 280 nm (Figure 3.2.9, top and bottom, respectively).
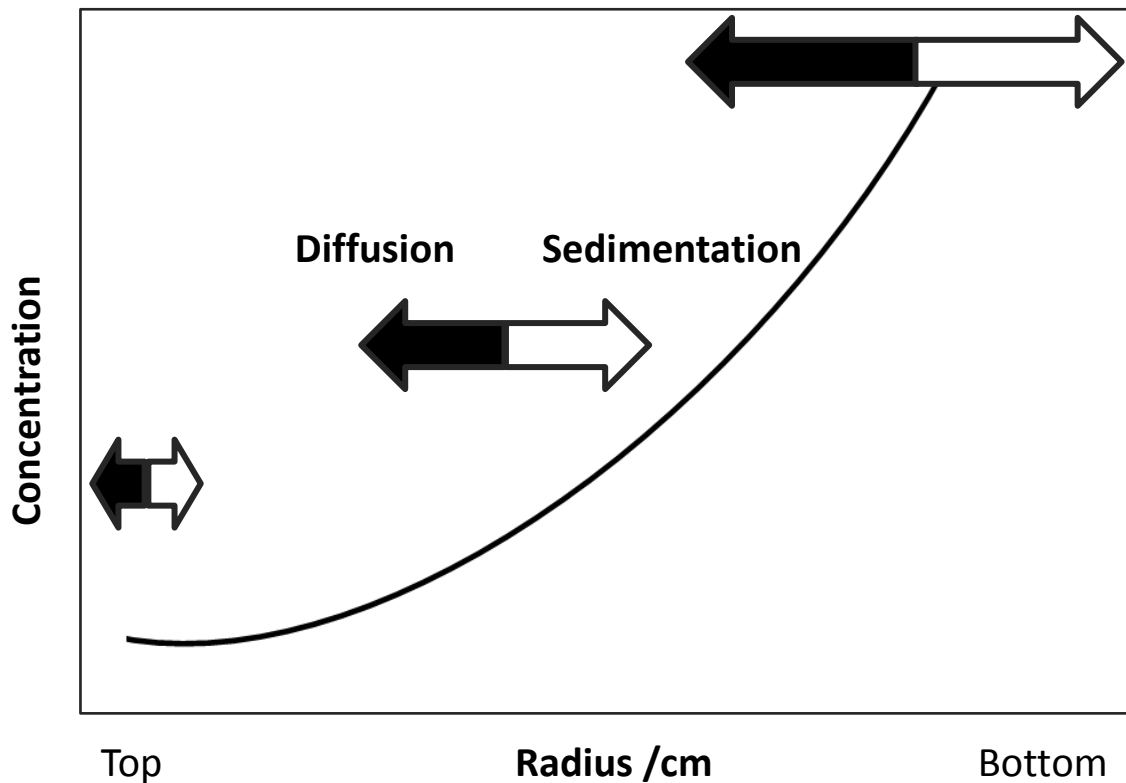
Figure 3.2.8. Schematic representation of sedimentation equilibrium of biological macromolecules

Upon application of centrifugal force the solute begins to sediment towards the bottom of the cell (white arrows). Simultaneously, this process is opposed by diffusion (black arrows). Eventually a point of equilibrium is reached and the solute no longer moves in the cell. The resulting concentration gradient of the solute increases exponentially towards the bottom of the cell (black line). Measurement of concentration at different points leads to the determination of molecular weight.
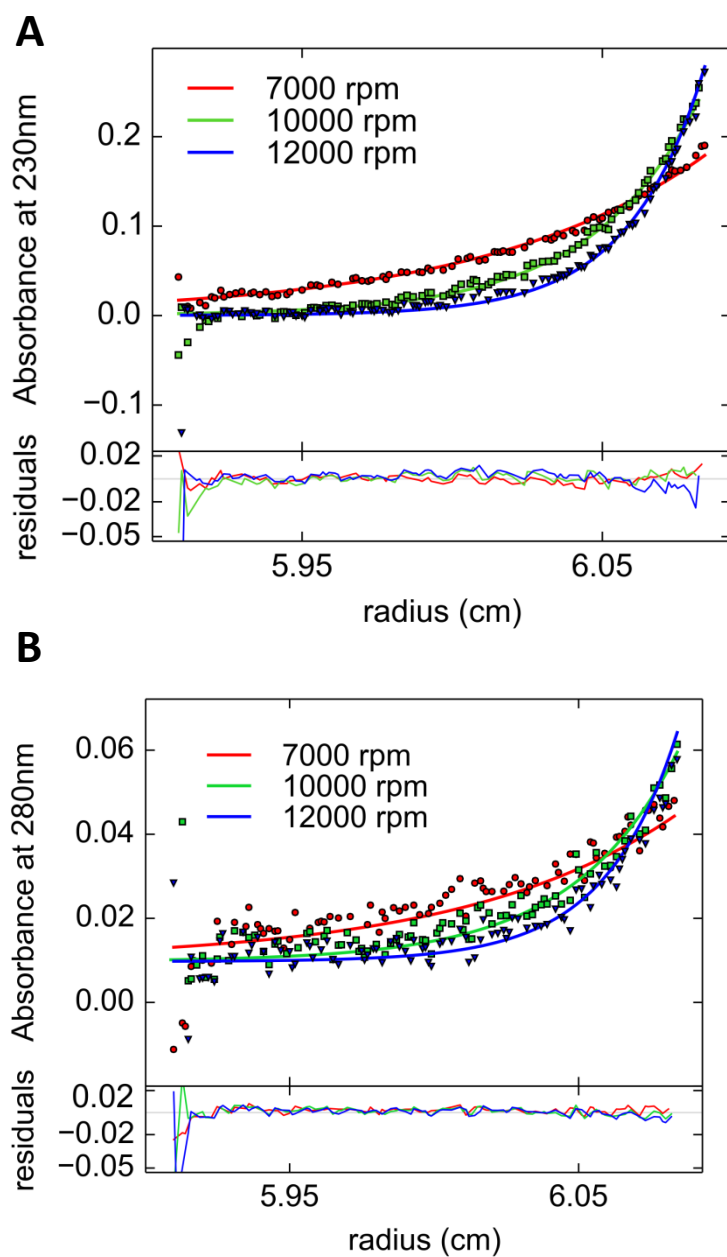
Figure 3.2.9 Sedimentation equilibrium analysis of purified TatAyCy complexes
Sedimentation equilibrium (SE) profile of 10-50 μg/ml TatAyCy purified in buffer containing 0.02% DDM. A molecular weight of 101 kDa was determined from fitting data at rotor speeds of 7000 rpm (red circle), 10000 rpm (green square) and 12000 rpm (blue triangle). Absorbance measurements of SE experiments were taken at 230nm and 280nm. The continuous lines represent best fits described single ideal species model of SEDPHAT software, and the residuals are indicated at the bottom of each chart.
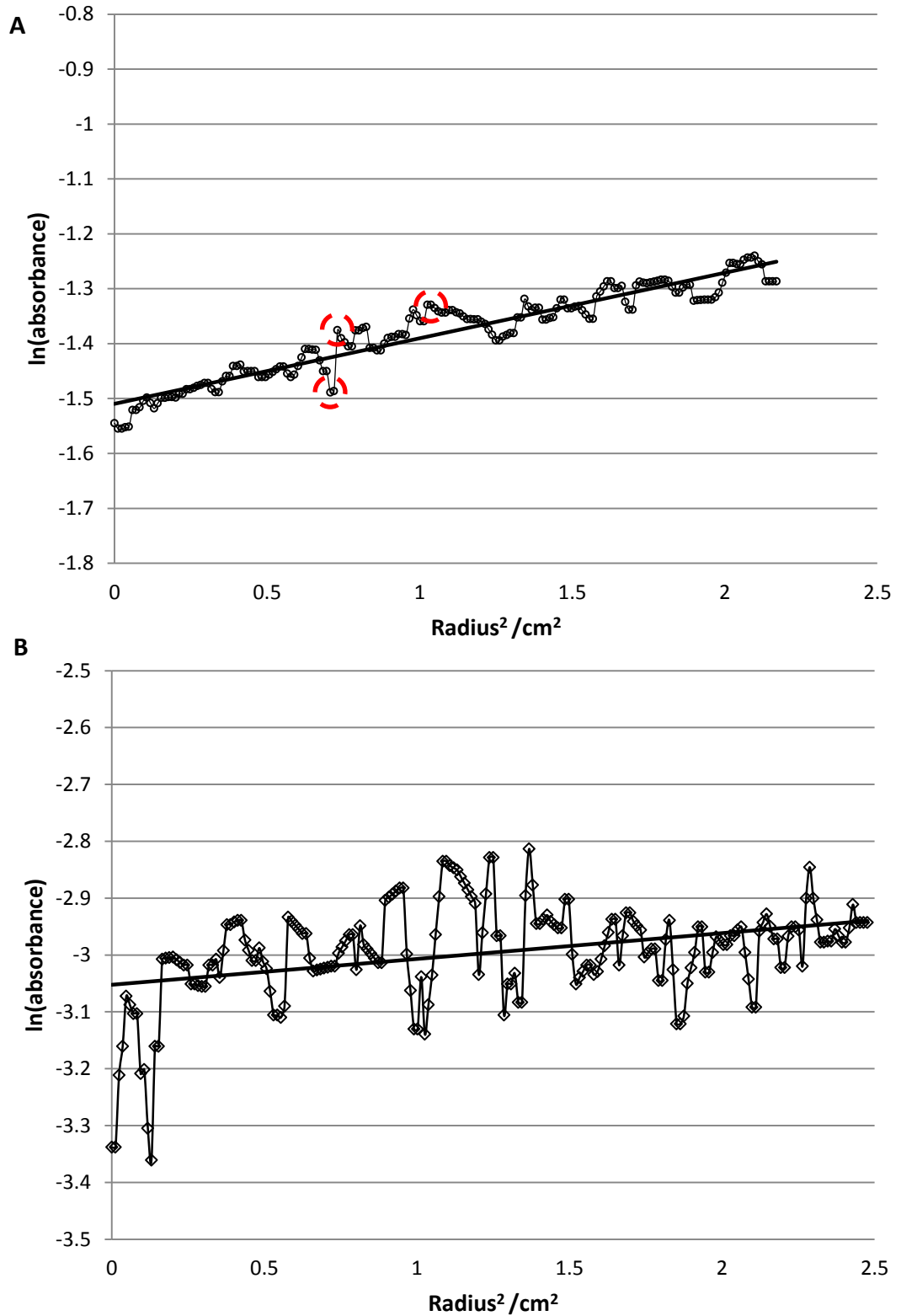
Figure 3.2.10 Sedimentation equilibrium analysis reveals TatAyCy behaves as a non-ideal species in solution

A plot of ln(abs) *vs.* r^2 for purified TatAyCy complexes revealed the complex to possess properties of a non-ideal solute. A single species would exhibit a linear concentration distribution. Absorbance data measured at 230 nm (A) and 280 nm (B) failed to yield a straight line with a significant number of residuals possessing non-linear value.

Analysis of this profile via fitting a single species model revealed the TatAyCy protein complex to exhibit a detergent-free molecular weight of approximately 101 kDa. The goodness of fit of this model is judged by two parameters. First are residuals which are the difference between each experimental data point and the corresponding point on the calculated curve from the model. Residuals for both 230 nm and 280 nm (Figure 3.2.9, bottom panel of each graph), are randomly distributed about point zero which is an indication of a relatively good fit for this particular model. The second parameter that tests for goodness of fit- Chi-squared analysis- mirrors this finding since statistical analysis of the residual points relative to the fitted model by the SEDPHAT software gave a value of Chi-squared value of 4 (a score of 1.0 would be a perfect fit).

Qualitative analysis of the SE data at 230 nm shows data points that fit the model well. This is indicated by a good overlay of individual data points to the fitted model (straight lines for each speed). As expected, the absorbance of the sample at 280 nm was virtually zero due to a lack of aromatic amino acids which would otherwise absorb UV light at this wavelength.

Given the heterogeneity revealed by EM analysis, data was replotted with the natural log of absorbance versus radius^2. In this type of plot, if a single species is present it should generate a straight line whose slope is proportional to its mass. Results are presented in figure 3.2.10. At 230 nm (Figure 3.2.10 A), whilst the overall trend would appear to be linear, a significant proportion of the residuals are non-linear (highlighted in red circles). In light of previous data from this sample at 280 nm (Figure 3.2.10 B), it is unsurprising that there are a significant number of non-linear residuals at this wavelength.

The identification of the TatAyCy sample exhibiting behaviour akin to a non-ideal species warrants further investigation into the full identification of species present. There appears to be a deviation from the 101 kDa molecular weight calculated by the single-species fit model of SEDPHAT software. Only upon identifying the different species present will the correct molecular weight range be determined (discussed in section 3.3).

3.3. Discussion

Most structural studies on the Tat system have focused on components from the Gram-negative bacterium, *E. coli* (Gohlke *et al.*, 2005; Ramasamy *et al.*, 2013; Rollauer *et al.*, 2012; Tarry *et al.*, 2009; Zhang *et al.*, 2014a; Zhang *et al.*, 2014b). However in light of recent evidence elucidating differences in Tat mechanism between Gram-positive and Gram-negative bacteria (Baglieri *et al.*, 2012; Beck *et al.*, 2013), structural insight into the Tat machineries from Gram-positive bacteria has potential to elucidate further details. The data presented in this chapter represents the first experimental evidence for an inherent heterogeneity of the TatAyCy complex from *B. subtilis*. Additionally, AUC data suggested that the average, detergent-free molecular weight of this complex was ~100 kDa.

Previous purifications of the TatAyCy complexes have yielded molecular weights of ~300 kDa (this study – Figure 3.2.2.) and 200 kDa (Barnett *et al.*, 2008). These molecular weights were predicted from gel filtration chromatography purifications of TatAyCy that had utilised different detergents for solubilisation from the inner membrane, namely: DDM and digitonin. These are non-ionic detergents that each form large micelles of 70 kDa (Smith & Pickels, 1940; VanAken *et al.*, 1986).

Despite the same micellar molecular weight of these detergents, significantly different TatAyCy-detergent molecular weights were predicted. Clearly there are varying contributions of the number of detergent monomers to the PDC. This highlights the significant and varying contributions a detergent can make to the overall molecular weight of a PDC and consequently the value of obtaining true molecular weights of insoluble proteins.

Given that the predicted 100 kDa value is smaller than the detergent-inclusive weights mentioned above, and the residuals of the fitted model and chi-squared goodness of fit analyses demonstrated a reasonably good fit, it seems that this predicted molecular weight of TatAyCy is feasible.

Since this is the first AUC study on entire Tat complexes, true molecular weight data for other complexes is lacking; nor has there been much characterisation of the TatAyCy complex prior to this study. A 100 kDa complex size would not accommodate for many copies of TatAy and TatCy proteins given their individual molecular weights: 6 kDa and 28.4 kDa, respectively. Hypothetically- if the

substrate-binding complex contained a 1:1 stoichiometric ratio of TatA and TatC components (akin to the situation in *E. coli* (Bolhuis *et al.*, 2001; Oates *et al.*, 2003)), then the TatAyCy complex would contain only approximately 3 copies of TatAyCy protomers. This is very different to the situation in *E. coli* where low resolution EM structures of the TatBC substrate binding complex alluded to a complex arrangement consisting of 7 copies of TatBC (Tarry *et al.*, 2009).

This makes the mechanism of transport of the TatAyCy complex more intriguing, given that such a small complex is capable of transporting not only its native substrate in *B. subtilis* (YwbN 45 kDa), but also Tat-precursor-tagged GFP substrates (native to *E. coli*) when heterologously expressed in *E. coli* (Barnett *et al.*, 2009). Perhaps such arrangement of TatA and TatC protein could be a reflection of a difference in Tat complex composition between Gram-positive and Gram-negative bacteria?

To add further validation to this predicted detergent-exclusive molecular weight, additional AUC SE experiments should be conducted on TatAyCy that has been purified in a different detergent, to establish whether the same molecular weight is predicted.

The most supported – yet still unproven – hypothesis for Tat translocation is the pore forming mechanism. The key factors in this model (which predicts that TatA is the pore-forming element of the translocase (Gohlke *et al.*, 2005)) are the size and heterogeneity of the Tat components. It is the heterogeneity exhibited by the TatA components which explains how fully-folded substrates of varying sizes are able to traverse the inner membrane without ion leakage. However- this model is complicated by the finding that TatAdCd and TatAyCy (when heterologously expressed in *E. coli*), are capable of transporting TatABC substrates between 63 kDa and 82.6 kDa (Barnett *et al.*, 2009). Furthermore, in light of evidence that TatAd lacks a pore large enough to support translocation (Beck *et al.*, 2013), it suggests that a different model of Tat translocase exists in Gram-positive bacteria, which is sufficiently flexible to transport a wide range of substrates. For example, there could be coalescence of relatively homogeneous TatA-type complexes to TatAC complexes; thus weakening the phospholipid bilayer.

The finding that the TatAyCy complex is a non-ideal species alludes to the idea that this complex possesses heterogeneity. However, since detergent (despite being neutrally buoyant), is still present we are unable to rule out the possibility that the detergent molecules are influencing the structure of the TatAyCy complex.

Given the small size of the TatAyCy complex, which as explained above would not accommodate many copies of TatAy and TatCy proteins, it remains unknown how TatAyCy complexes are able to permit the translocation of non-native substrates in *E. coli*. If TatAyCy was confirmed to possess an inherent heterogeneity, this flexibility explain how this complex is capable of transporting substrates other than its endogenous YwbN (45 kDa) (Barnett *et al.*, 2009). It could be possible that different numbers of TatAy monomers (from the pool of TatAy in the inner membrane (Barnett *et al.*, 2009) could be recruited to the main substrate-bound TatAyCy complex. Additional recruitment of TatAy, creating a larger TatAyCy complex, would cause greater perturbation to the inner membrane for transport of larger Tat substrates. However this is speculation and additional investigations would have to be conducted to confirm the intrinsic heterogeneity of the TatAyCy complex to determine what the true size range of this complex is, and how each species present in solution differs.

Sedimentation velocity (SV) is a technique that can address this question. Unlike SE, this technique relies on the application of a high centrifugal force to a macromolecule in solution which causes it to sediment towards the bottom of the cell. This process is information-rich since proteins of different sizes and components will exhibit different sedimentation profiles. Therefore this technique is able to separate samples according to size, shape and density; and consequently determine the oligomeric state of a heterogeneous membrane protein sample (Dorwart *et al.*, 2010). For example, insight into the different sizes of oligomeric TatAyCy complexes would reveal the true molecular weight range for this complex. Furthermore, based on the differences in molecular weight between each oligomeric complex, the relative contributions of each TatAy or TatCy proteins could be inferred.

The data presented in this chapter revealed a small detergent-free molecular weight of the TatAyCy complex *in vitro* and the importance for structural characterisation of

detergent-solubilised membrane proteins, prior to pursuit of 3D reconstructions, was demonstrated.

The increase of Tat complex size upon alteration of P:D ratio highlights the variability that detergent solubilisation can have on the structure of a solubilised protein. Such variability does not reside solely with TatAyCy, a striking difference in Tat behaviour between native and detergent solubilised states has been reported for TatA. Despite evidence showing that TatA complex formation requires the TatBC complex in the inner membrane (Alcock *et al.*, 2013), detergent-solubilised TatA forms complexes even when expressed in the absence of Tat components (Porcelli *et al.*, 2002), suggesting that extraction of TatA from the inner membrane using detergents induces the polymerisation of the TatA proteins. Therefore, data derived from detergent solubilised proteins should be treated with caution.

Due to heterogeneity and difficulty in distinguishing detergent-solubilised complexes a 3D reconstruction of TatAyCy complexes was not pursued. Results presented in this chapter reiterate the need to circumvent the use of detergents in this field of research. Therefore, the remainder of findings presented in this thesis have endeavoured to analyse the Tat machinery and/or its substrates avoiding the use of detergent-solubilised complexes.

Chapter 4:

Attempted reconstitution of TatAyCy into lipid bilayers

4.1 Introduction

Results presented in the previous chapter highlighted the variability that detergent solubilisation can have on the structure of an insoluble protein. Such variability has also been observed for the TatA protein of *E. coli* (Porcelli *et al.*, 2002), where detergent-solubilised TatA protein formed complexes even when expressed in the absence of other Tat components (TatB and TatC), which are compulsory for Tat complex assembly (Mori & Cline, 2002). These data highlight the caution that should be taken when analysing data from detergent-solubilised proteins.

The mechanism of Tat translocation is still very much unsolved, and approaches to elucidate how this system accomplishes the remarkable feat of transporting fully-folded proteins will undoubtedly involve structural analysis of Tat constituents. To obtain high-value, unambiguous information we need to circumvent the use of detergent-solubilisation for structural analysis. Therefore, the results presented in this chapter demonstrate the attempted reconstitutions of the TatAyCy system of *B. subtilis* into liposomes. Structural analysis of the TatAyCy-incorporated liposomes by atomic force microscopy (AFM) has the potential to elucidate topological details of this Tat complex in a lipid bilayer. Insight into the arrangement of a Tat complex in the inner membrane would add to our understanding of the mechanism of a Tat system from a Gram-positive bacterium.

Liposomes are spherical vesicles that contain a single lipid bilayer and are therefore able to serve as a mimic of the phospholipid bilayer of the cytoplasmic membrane of bacteria. Reconstitution of proteins into liposomes is a complicated task, which contains many parameters that are each vital to the success of the reconstitution. Therefore the approach to find the optimal reconstitution for a given membrane protein has long been entirely empirical.

There is an abundance of literature covering the formation of bacterial membrane protein proteoliposomes, detailing the diverse approaches to successful protein reconstitution into a liposome bilayer. The vast majority of these consist of a detergent-mediated approach since a detergent has already been used to extract the protein of interest from its native phospholipid bilayer. Therefore, the reconstitution process involves the incubation of a purified detergent-solubilised membrane protein

with liposomes. This approach was adopted in this study to attempt the reconstitution of TatAyCy into liposomes (Figure 4.2.2).

No published data exists on the reconstitution of whole Tat complexes into liposomes. The data presented in this chapter show, for the first time, the attempted reconstitution of TatAyCy complexes into liposomes; highlighting several parameters that are vital for successful reconstitution. Additionally, the analysis of TatAyCy proteoliposomes under the AFM tip is presented. AFM work was performed by Dr Cvetelin Vasilev (University of Sheffield).

4.2 Results

4.2.1. Affinity purification of TatAyCy for reconstitution into lipid bilayers

Affinity purification of TatAyCy complexes was necessary to obtain a highly pure sample of a Tat complex for reconstitution into a phospholipid bilayer. Affinity chromatography was performed using a C-terminal strep tag on the TatCy component of the TatAyCy complex. As described in Materials and methods (§2.4.3.), solubilised membranes from *E. coli* cells overexpressing TatAyCy were applied to an equilibrated Streptactin™ affinity column (that specifically binds the strep-tag on TatCy). Bound proteins were eluted from the column, and consequently analysed by SDS-PAGE and immunoblotting using antibodies to the strep-tag on TatCy. The results are presented in Figure 4.2.1.

Weakly-bound Strep-tagged proteins were eluted from the column in the first wash fraction. The tightly bound TatCy-strep specifically eluted from the column over fractions 2-5 (Figure 4.2.1., A+B). Silver staining of the SDS-PAGE gel confirmed that TatAy had co-eluted with the TatCy complex (Figure 4.2.1., B). The purity of these isolated TatAyCy complexes after application to just a single column is highlighted, since aside from the TatAy and TatCy bands, there are very few other migrating bands present on the gel.

Given the high purity of the TatAyCy complexes, and the fact that additional purification steps are likely to increase the dilution of the sample, a single affinity purification step was deemed sufficient to purify TatAyCy-strep before reconstitution into liposome vesicles. Therefore, elution fractions 2-5 were pooled and concentrated to 0.12 mg/ml.
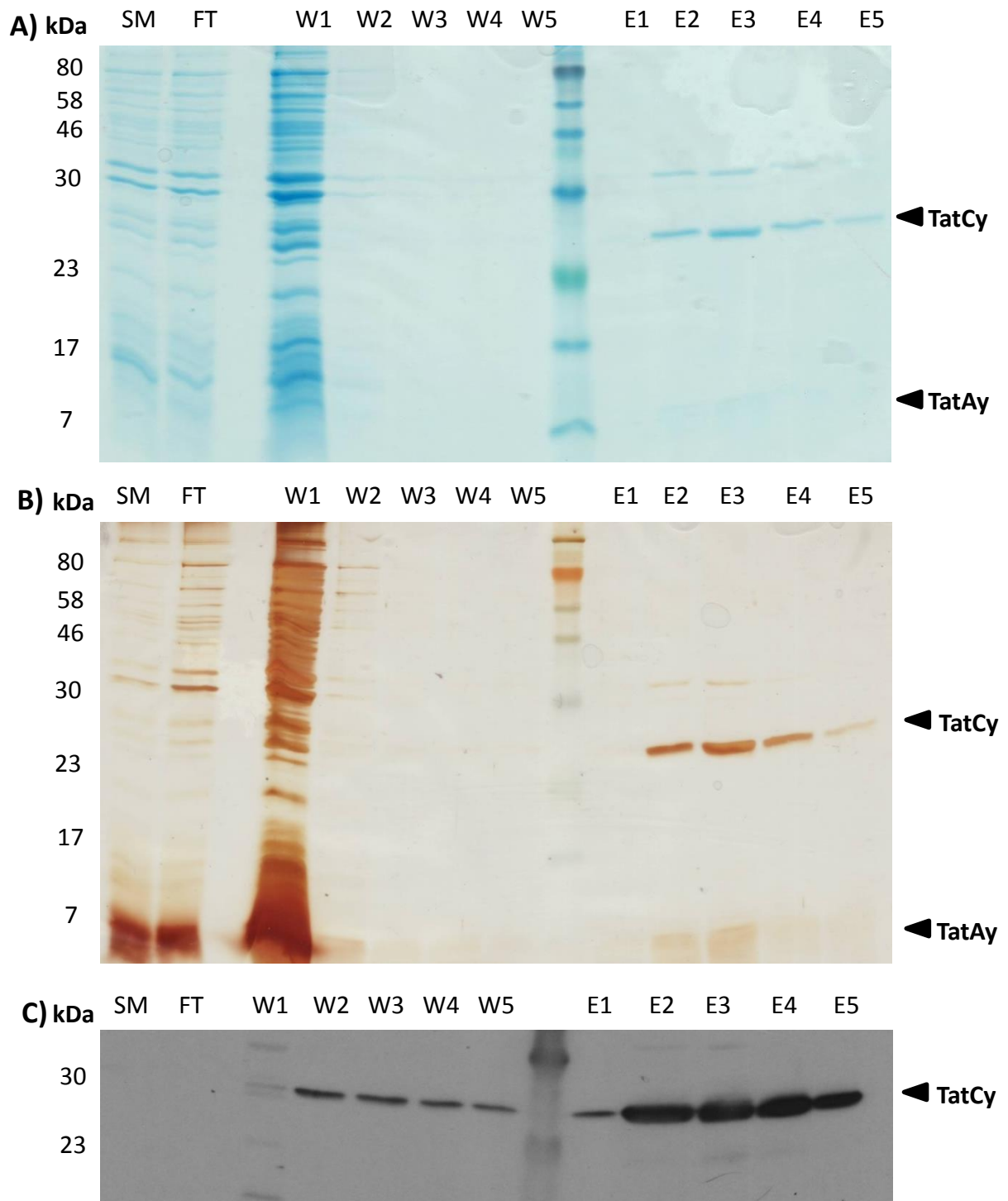
Figure 4.2.1. Affinity chromatography of TatAyCy-strep

E. coli membranes were isolated from *ΔtatABCDE* cells expressing WT TatAyCy-strep from the pBAD plasmid and solubilised in DDM. Solubilised membranes were applied to a StrepTactin column as described above. The column flow-through (FT), wash fractions (W1-5) and elution fractions (E1-5) were analysed by Coomassie staining (A) and silver-stain (B). The same samples were immunoblotted with antibodies against the Strep-tag on TatCy(C). Positions of TatAy and TatCy are indicated on the right-handside of the figures and molecular-weight markers on the left.

4.2.2. Reconstitution of purified TatAyCy into liposome vesicles

To reconstitute purified TatAyCy complexes into a membrane mimetic, liposomes were used. Liposomes are small, spherical artificial vesicles formed from phospholipids in aqueous solution and serve to mimic the native cellular environment of a lipid bilayer. An *E. coli* polar lipid extract was used to produce liposomes since an environment of similar physiological condition to that *in vivo* will be provided.

Multi-lamellar liposomes were formed upon hydration of a thin film of *E. coli* lipids, which were then subjected to 5 cycles of freeze-thaw to form large multi-lamellar liposomes. These liposomes were subsequently extruded through membranes, possessing pores of 600 nm and 200 nm, for a total of 30 cycles, to obtain a homogeneous population of single lamellar vesicles.

Once liposomes were formed, the next stage was to make them amenable to protein reconstitution. The most successful and frequently used strategy to achieve this is using a detergent-mediated approach (Figure 4.2.2.), since membrane proteins are extracted from their lipid bilayer and purified in the presence of detergents.

The approach adopted in this study is outlined in Figure 4.2.2. The liposome bilayer was destabilised by the addition of 10% Triton-X-100; a detergent that is commonly used for this purpose (Helenius & Simons, 1975). Upon increasing concentration of Triton detergent, the liposomes undergo structural changes and a subsequent phase transition from a lamellar structure to phospholipid-detergent micelles (Lichtenberg *et al.*, 2013). At the end of the incubation with Triton-X-100, the phospholipids are completely solubilised into mixed micelles. Purified TatAyCy was then introduced into the disrupted liposome solution (Figure 4.2.2., strep 2) and incubated with the mixed micelles.

To drive protein reconstitution into the micelle bilayer, excess detergent was removed by incubation with SM2 Biobeads. Biobeads contain small pores that capture excess detergent molecules, and it is this removal that drives the process of protein reconstitution.

Given the significant number of parameters to be optimised for an individual membrane protein reconstitution, different reconstitution procedures have yielded proteoliposomes of many different sizes and compositions. Therefore the best approach is to empirically determine the optimal conditions for the protein of interest. One parameter is the lipid-to-protein ratio (henceforth denoted L:P). Depending on required use of the proteoliposomes, the density of reconstituted protein may vary, which could influence the amount of protein to be added into the reconstitution mixture and consequently the L:P ratio. The initial reconstitution attempt used a L:P ratio of 60:1 and was performed as described in §2.7 of Materials and Methods. The TatAyCy proteoliposomes were separated from Biobeads and concentrated by ultracentrifugation. The resulting liposome pellet was resuspended in liposome buffer to a final concentration of 0.12 mg/ml.
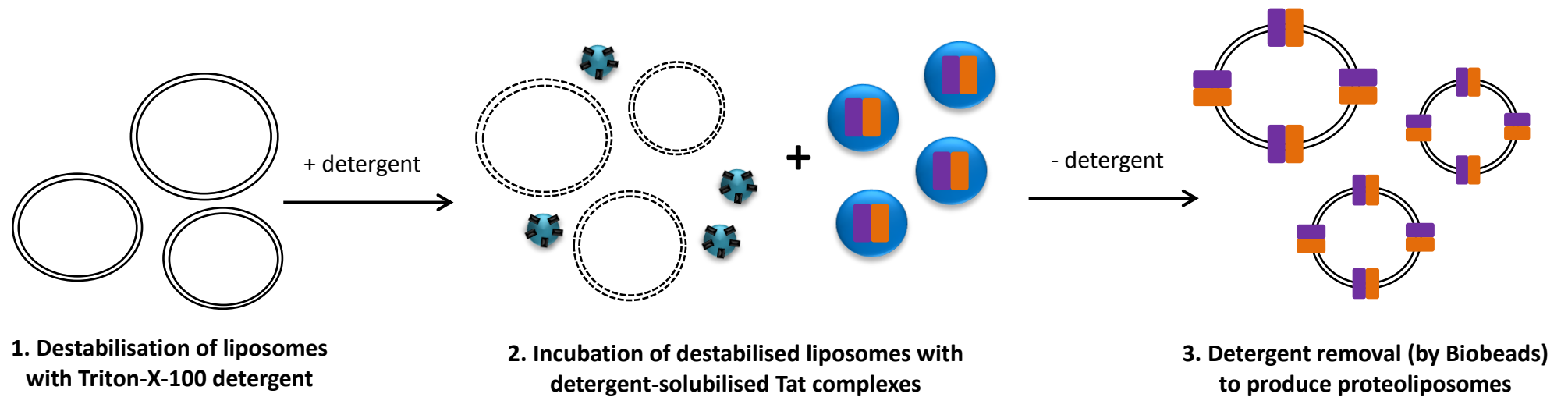
Figure 4.2.2. Schematic of proteoliposome formation
Schematic to illustrate the protocol adopted for the formation of TatAyCy-containing proteoliposomes. Liposomes were produced by extrusion through 100 nm pores (step 1). Addition of Triton-X100 destabilised the liposomes (indicated by dashed lines) to enable protein incorporation when incubated with a detergent-solubilised Tat sample (blue circles [detergent micelle] containing orange/purple rectangles [Tat complexes]) (step 2). Detergent extraction from the solution mixture (by Biobeads) drives the formation of Tat-containing proteoliposomes (step 3).

4.2.3. Sucrose density gradient centrifugation of TatAyCy liposomes

To evaluate the effectiveness of protein reconstitution, sucrose density gradient centrifugation was used. This technique separates particles based on their densities, and is therefore capable of separating free protein from that which is reconstituted into liposomes. The sucrose gradient was prepared as shown in Figure 4.2.3., A. The liposome sample was suspended in the 40% sucrose layer at the bottom of the centrifuge cell, with 20%, 10% and 0% deposited on top. Upon application of a centrifugal force, proteoliposomes should float to the meniscus of the 20% layer; whereas free protein that does not reconstitute into liposomes will aggregate at the bottom of the cell (Figure 4.2.3., A, right-hand-side).

Aliquots from each layer were resolved by SDS-PAGE and the presence of TatAyCy was detected by immunoblotting against the strep-tag on TatCy. The results of protein reconstitution at 60:1 L:P ratio show that whilst some TatAyCy aggregated at the bottom of the cell (Figure 4.2.3, B), some appeared to incorporate into liposomes, being present in higher sucrose layers of 10% and 20%. The difference in final position in the cell is owed to the size of the liposomes: smaller liposomes will have a lower density and thus resolve in lower percentages of sucrose.

The negative control sample, of empty liposomes, contained no protein detected by Western blotting, but the liposomes still floated to the middle 20% layer indicated by a cloudy meniscus in the centrifuge tube.

Despite the partial success of protein reconstitution at 60:1 ratio, preliminary AFM analysis reported that the liposome sample (which resolved at the 20% sucrose layer), contained large lipid patches with no protein. Since I endeavoured to reconstitute a sufficient amount of TatAyCy into liposomes for structural analysis via AFM, the amount of protein reconstituted needed to be greatly increased. Therefore, reconstitution was repeated but with a L:P ratio of 1:1. The reason for adding fewer lipids per unit of protein at this stage was in attempt to increase the efficiency of reconstitution: it is possible that at the previous L:P ratio (60:1), there was not enough protein to form densely packed Tat proteoliposomes. Results of this reconstitution are shown in Figure 4.2.3., C. The Western blot shows that all of the TatAyCy had aggregated at the bottom of the cell, remaining in the 40% sucrose layer.
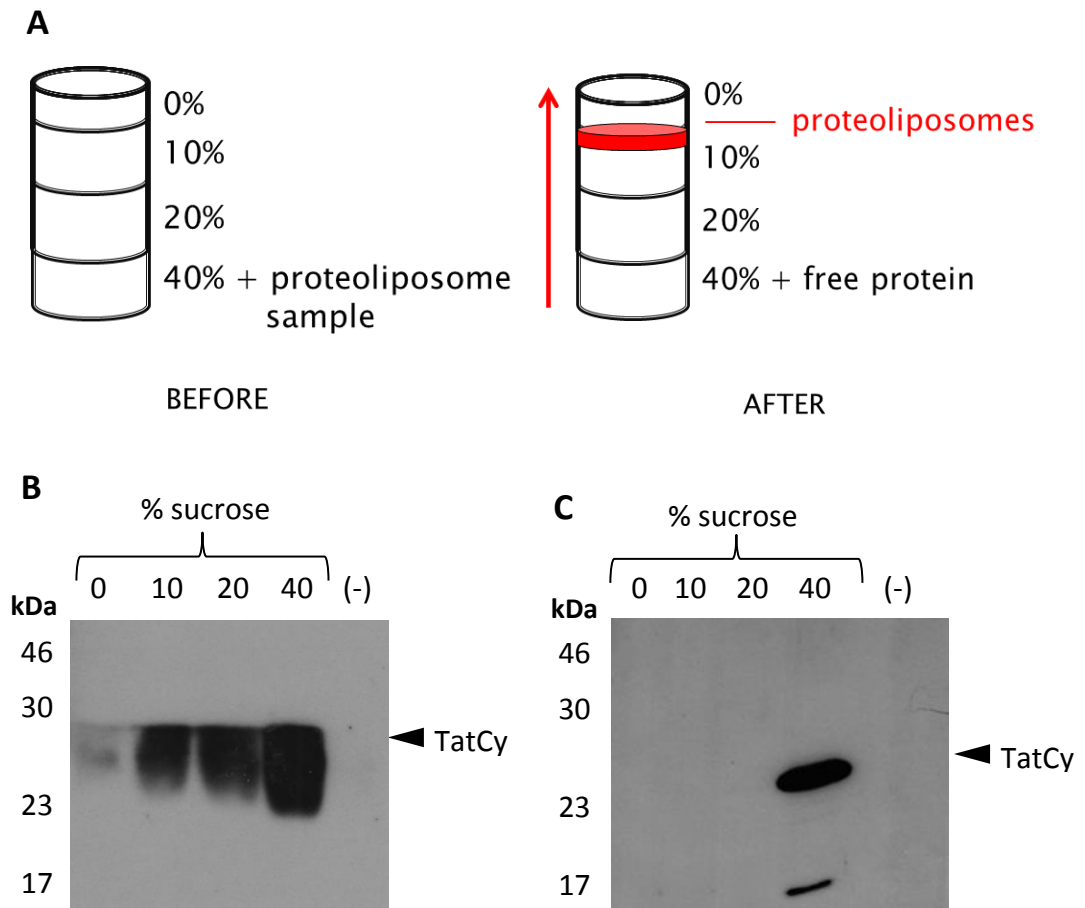
Figure 4.2.3. Analysis of protein incorporation into liposomes.
A) Successful protein incorporation into liposomes was analysed by sucrose density gradient centrifugation. Proteoliposome samples were applied to a sucrose gradient (0-40%) and centrifuged at high speeds (50000 rpm). Proteoliposomes should resolve in lower sucrose regions (0-20%) due to their greater buoyancy, whereas non-incorporated protein will aggregate at the bottom of the cell in the 40% layer. Control liposomes (lacking protein incorporation) were used to confirm liposome formation (indicated by a cloudy meniscus – not shown); hence lack of immunolabelling in the (-) lane of B and C. Aliquots from each layer were resolved by SDS-PAGE and TatAyCy protein identified by Western blotting using anti-Strep antibody. B) Western Blot to show results of protein reconstitution at lipid-to-protein ratio of 60:1. Some protein incorporated into liposome vesicles, yet a large proportion aggregated at the bottom of the cell. C) Western Blot of reconstitution at 1:1 ratio. No protein incorporated into liposomes, and aggregated at the bottom of the cell.

4.2.4. Cryo-EM of TatAyCy liposomes

To check whether liposomes were definitely being formed, and whether attempted protein reconstitution under the given conditions (§2.7.2) hindered liposome formation, aliquots from the negative liposome control and the liposomes in the 20% layer of the 60:1 reconstitution were imaged by cryo-EM. Results showed that both samples contained liposomes (Figure 4.2.4.).

Despite undergoing multiple extrusions through a 100 nm membrane, both samples contained a heterogeneous population of unilamellar vesicles that possessed diameters in the range of ~30 nm to 140 nm. This heterogeneity could affect the distribution of reconstituted protein in the liposomes resulting in a low protein density; and thus difficult AFM analysis. Furthermore, most of the liposomes are unilamellar, with the odd exception of bilamellar vesicles (Figure 4.2.4, yellow circles). The presence of such vesicles would not hinder structural analysis under the AFM.
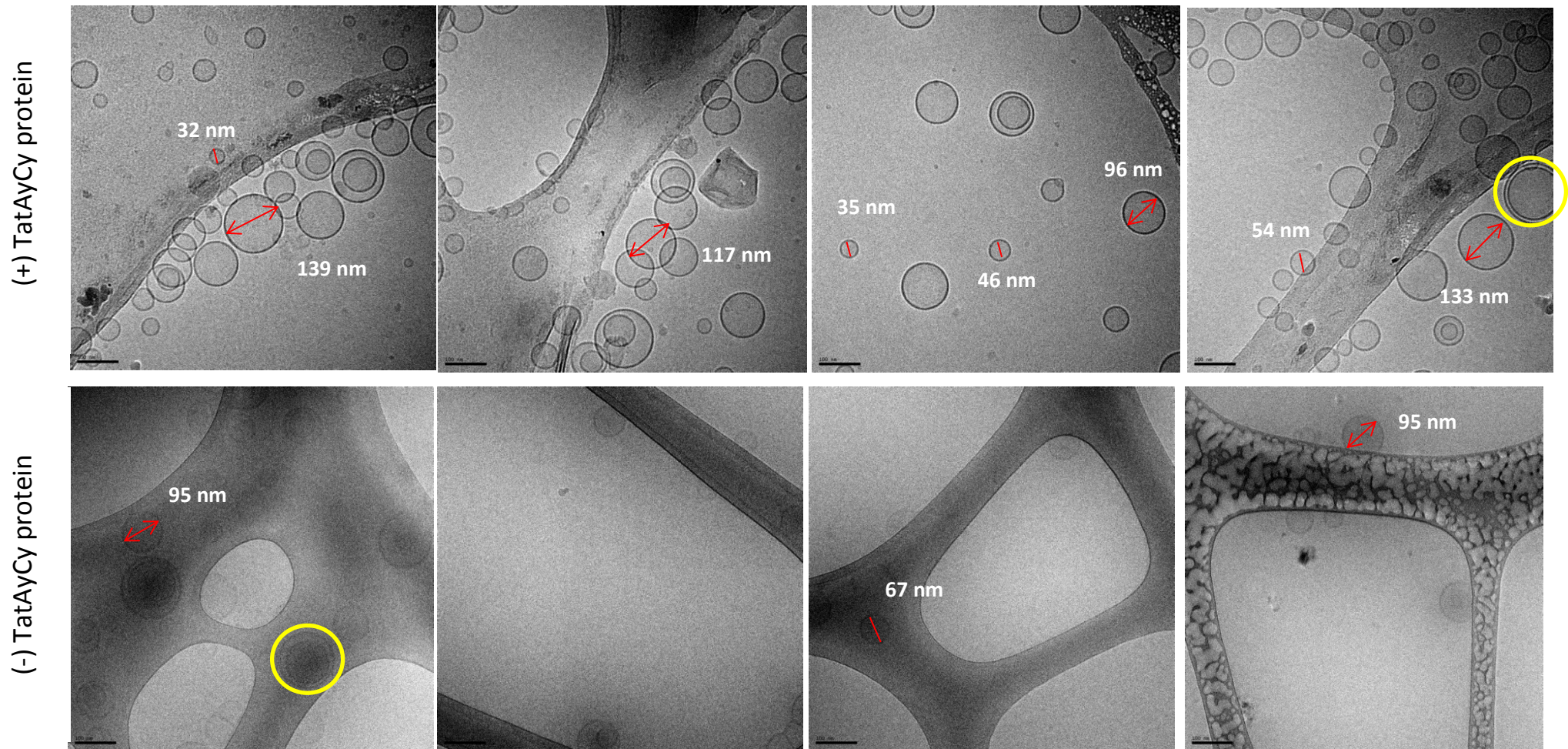
Figure 4.2.4. Digital electron micrographs of liposomes +/- the reconstitution of TatAyCy protein visualised by cryo-EM

Freshly formed liposomes +/- TatAyCy protein were cryogenically frozen and imaged under the EM. The presence of liposomes in both samples confirmed their successful formation. The presence of protein (top row) did not alter the stability of the liposomes or their formation since both samples were stable under the EM. Largely, unilamellar vesicles were formed with a few multilamellar vesicles present in solution (highlighted in yellow circles). The liposomes were heterogeneous in size, ranging from ~30 to 140 nm (size indicated in representative particles). Images were taken at 40000X mag on a JEOL UK 2010F. Scale bar = 100 nm.

4.2.5. Purification of TatAd for reconstitution into lipid bilayers

Given the unsuccessful reconstitution of TatAyCy protein into liposome vesicles, a smaller and more homogeneous Tat protein, TatAd-his (Beck *et al.*, 2013), was purified for reconstitution into liposomes to determine whether these properties aided protein reconstitution.

A two-step purification procedure of TatAd-his was performed to reduce the amount of contaminating proteins onto the affinity column. Initially, solubilised membranes from *E. coli* cells overexpressing TatAd-his were applied to an equilibrated ion exchange column (Q-sepharose column). Bound proteins were eluted from the column by an increasing gradient of salt concentration. All fractions were analysed by SDS-PAGE and immunoblotted using antibodies to the TatAd protein itself. The results are presented in Figure 4.2.5.. TatAd was present in all fractions of the Q-sepharose column (Figure 4.2.5., B and C). Elution fractions 2-5 were pooled and concentrated, and subsequently applied to an equilibrated Talon column. Weakly-bound his-tagged proteins were eluted from the column in washes 1-3. Tightly-bound his-tagged proteins were eluted in fractions 1-5, with most TatAd-his eluting in fractions 3-5 (Figure 4.2.5., C).

Coomassie staining of the Talon column elutions confirmed the presence of other minor migrating proteins; however TatAd was in definite excess. The presence of minor contaminant proteins will not hinder protein reconstitution; although they would introduce ambiguity when analysing the sample under the AFM. However, this part of the experiment aimed to test whether protein properties influence reconstitution. Therefore, elution fractions 3-5 were pooled and concentrated to 0.2 mg/ml.
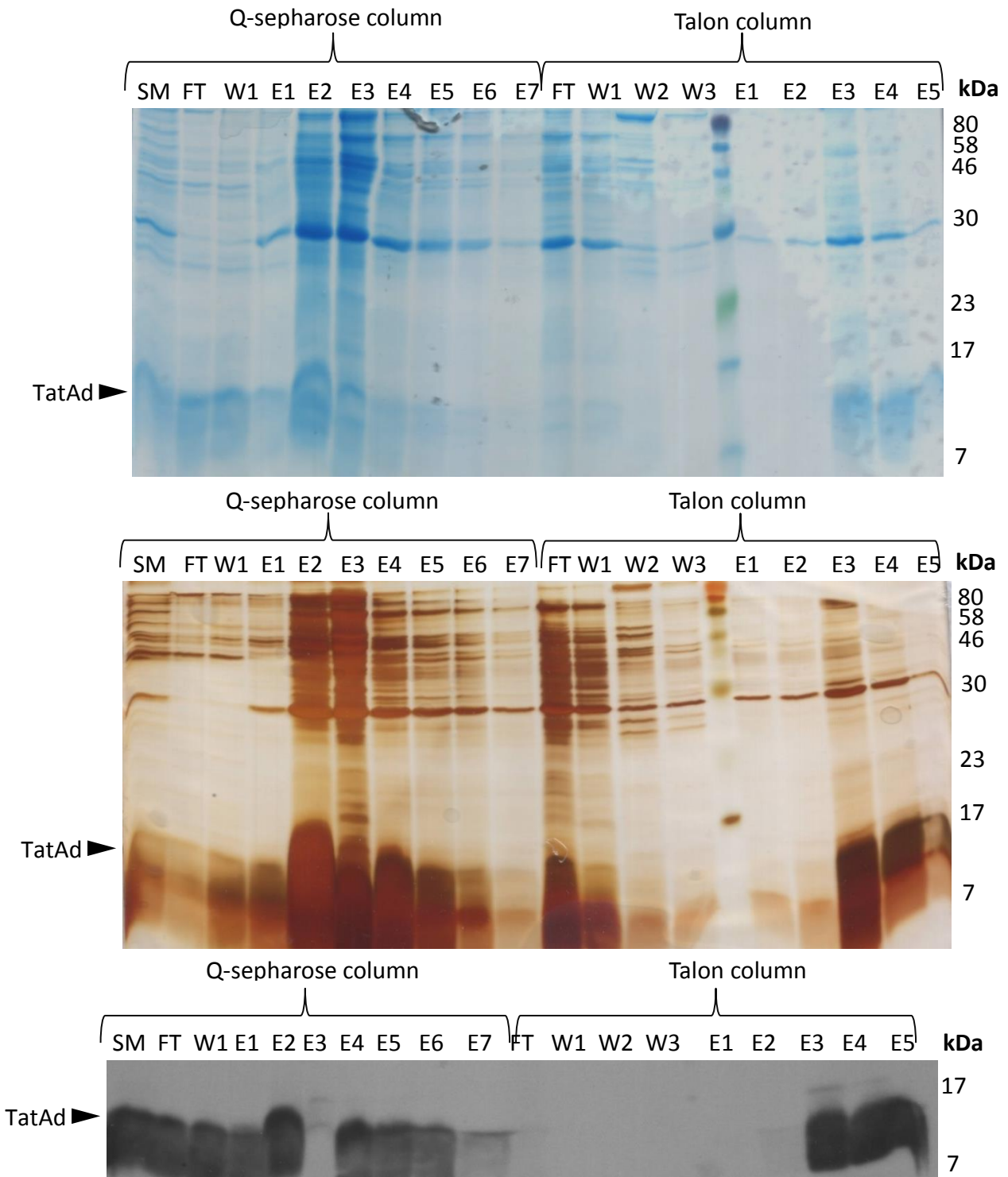
Figure 4.2.5. Purification of TatAd-his

E. coli membranes were isolated from *ΔtatABCDE* cells expressing TatAd-his from the pBAD plasmid and solubilised in DDM. Solubilised membranes were first applied to a Q-sepharose column. Elution fractions 2-5 (E2-E5) were pooled, concentrated and applied to a Talon column. The column flow-through (labelled FT), wash fractions (labelled W) and elution fractions (labelled E) of the Q-sepharose and Talon column were analysed by Coomassie staining (A) and silver-stain (B). The same samples were immunoblotted with antibodies against the TatAd protein. Positions of TatAd are indicated on the left-handside of the figures and molecular-weight markers on the right.

4.2.6. Sucrose density gradient centrifugation of TatAd liposomes

To evaluate the effectiveness of protein reconstitution, sucrose density gradient centrifugation of the TatAd-reconstituted liposomes was performed as described previously (§4.2.3). The L:P ratio was reverted back to 60:1 since a 1:1 ratio resulted in all of the TatAyCy aggregating at the bottom of the cell (Figure 4.2.6.). Also, the parameter change in this part of the investigation was the protein (TatAd instead of TatAyCy). Reconstitution showed evidence of liposomes floating up to the 20% layer. Results of Western blot analysis for the detection of TatAd indicated that most of the protein had successfully reconstituted into liposomes and resolved at the 20% layer. However, some did not reconstitute and aggregated at the bottom of the cell. Some non-specific binding was also witnessed. AFM analysis of the proteoliposomes that resolved in the 20% sucrose layer, akin to TatAyCy proteoliposomes reconstituted at the same ratio, was reported to contain large lipid patches with no protein detected.
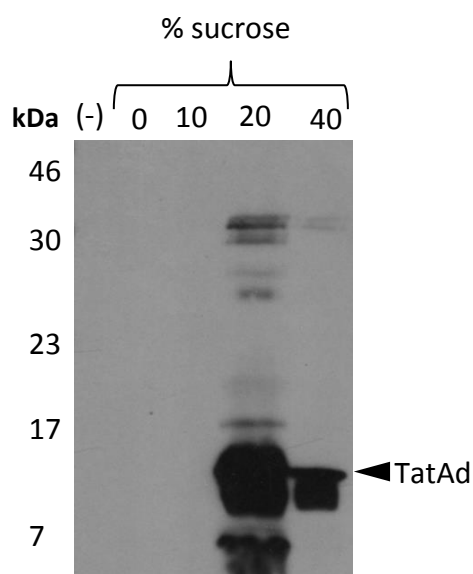
Figure 4.2.6. Analysis of successful TatAd incorporation into liposomes
Western Blot to show results of TatAd reconstitution at lipid:protein ratio of 60:1. Aliquots from each layer of a sucrose gradient were resolved by SDS-PAGE and TatAd protein identified by Western blotting using an anti-TatAd antibody. Some non-specific binding was detected. A proportion of TatAd was incorporated into liposome vesicles indicated by TatAd detection in the 20% sucrose layer. Some TatAd had also aggregated and remained at the bottom of the cell in the 40% layer. Control liposomes (lacking protein incorporation) were used to confirm liposome formation (indicated by a cloudy meniscus – not shown); hence lack of immunolabelling in the lane (-).

4.2.7. Further optimisation of Tat protein reconstitution

Given the lack of success with protein reconstitution for both TatAyCy and TatAd at 60:1 and 1:1 L:P ratios, further optimisation was conducted whereby numerous parameters were sequentially altered, including type of lipid, choice of detergent and L:P ratio. These conditions are shown in Figure 4.2.7.

	Lipid-to-protein ratio	0.3:1	0.55:1	**Detergent**
Lipid type	*E. coli* total lipid	A	B	Triton-X-100
	DOPC	C	D	
		E	F	OG

Figure 4.2.7 Optimisation of Tat reconstitution by alteration of numerous experimental parameters.
Table detailing which parameters were altered in attempt to increase Tat protein reconstitution into liposomes. Three main factors were sequentially altered: the lipid type (either DOPC lipid, or *E. coli* polar lipid extract) (orange shading), the lipid:protein ratio (blue shading) and the presence of octylglucoside (OG) for liposome destabilisation (samples E and F).

Lower L:P ratios were examined in light of data showing that bacterial membrane proteins reconstituted more efficiently at L:P ratios (Parmar *et al.*, 1999). Also, in addition to *E. coli* polar lipid extract, DOPC lipids were used to prepare liposomes. This is because DOPC has only a single lipid composition and therefore will provide a flatter bilayer under the AFM. Any perturbations can be attributed more confidently to protein in the lipid bilayer. Finally, in samples that showed signs of reconstitution, octylglucoside (OG) was used instead of Triton-X-100, which is another detergent frequently used in detergent-mediated reconstitution. OG has a high CMC (23 mM) which slows the, usually rapid, rate of detergent removal by the Biobeads. This more gentle treatment, may aid protein reconstitution. Once prepared under the appropriate condition, each of the samples were analysed by AFM.

4.2.8. AFM analysis of TatAyCy proteoliposomes

Reconstitution of TatAyCy into liposomes was performed under different experimental conditions (Figure 4.2.7. A-F), and subsequently analysed for protein reconstitution using AFM. Samples that contained liposomes prepared from *E. coli* polar lipid extract were examined first (Figure 4.2.7. A and B). Results are shown in Figure 4.2.8.

The green arrows indicate equivalence points between AFM view (left-hand-side) and the measured height in the sample (right-hand-side). In both samples, the green arrow is positioned at a point where the lipid bilayer ends and the mica surface is exposed; hence the true sample height can be measured. AFM analysis revealed that both samples (L:P 0.3:1 [top panel] and 0.5:1 [bottom panel]) contained a sample height of 5 nm, which is consistent with an empty lipid bilayer surface. Additionally, these 5 nm surfaces had a significant lateral dimension of ~ 600 nm in both samples, consistent with a vast empty lipid deposition on the mica surface. Therefore, protein reconstitution was largely unsuccessful. A 10 nm feature was identified that protruded from the lipid bilayer surface in the 0.55:1 sample; however this was the only one identified; and therefore deemed unreliable.

Furthermore, reconstitutions of TatAyCy into liposomes that were prepared from DOPC lipid, at 0.3:1 and 0.55:1 L:P ratios (Figure 4.2.7. C and D) were unsuccessful since- similar to the previous AFM data, the sample contained vast empty lipid patches that were 5 nm in height and up to 1 μm wide in lateral space (Figure 4.2.9). Very large features, approximately 20 nm in height were also identified in the liposome sample (Figure 4.2.9., bottom panel, right-hand-side), which are too large to be individual proteins and are therefore most likely unopened liposomes or protein aggregates.

Despite the above samples (Figure 4.2.7. C and D) failing to reconstitute TatAyCy protein, they were easier to analyse under the AFM tip compared to liposomes which were prepared from *E. coli* polar lipid extract. More specifically, the lipid bilayer of the liposomes made from DOPC lipids could be clearly distinguished from the surrounding substrate surface. Therefore, reconstitution of liposomes produced from this lipid was repeated; although in an attempt to eliminate the presence of large aggregates and promote protein reconstitution, OG detergent was used instead of

Triton-X-100. Results are presented in Figure 4.2.10. These proteoliposome samples contained protein-like features that were 10-12 nm in height (top and middle panel). A control sample of empty liposomes contained features that were distinguishably larger in height (~18 nm), which are likely to be liposomes aggregates.

The lateral dimensions of the protein-like features are difficult to reliably measure owed to an inherent artefact of AFM analysis termed, 'profile broadening'. This is effect arises due to tip-sample convolution. More specifically, the tip of the AFM that makes contact to the sample is not a perfect point, it is rounded, and thus any AFM image is a convolution of the shape of the probe and the shape of the sample. The effect of this is that the protruding feature is measured wider than its true width. Whereas, the height measured in Z-axis is high resolution, and if the particles are assumed to be roughly spherical, this measurement would correspond to the diameter of the feature.

Despite these 10 − 12 nm protein-like features being distinct from those in negative control samples, they were not abundant within the sample. Therefore, improving the quantity of Tat protein being reconstituted into liposomes remains important future work. A high density of Tat protein in liposome bilayer is important to reliably measure the topology of this protein in a membrane environment.
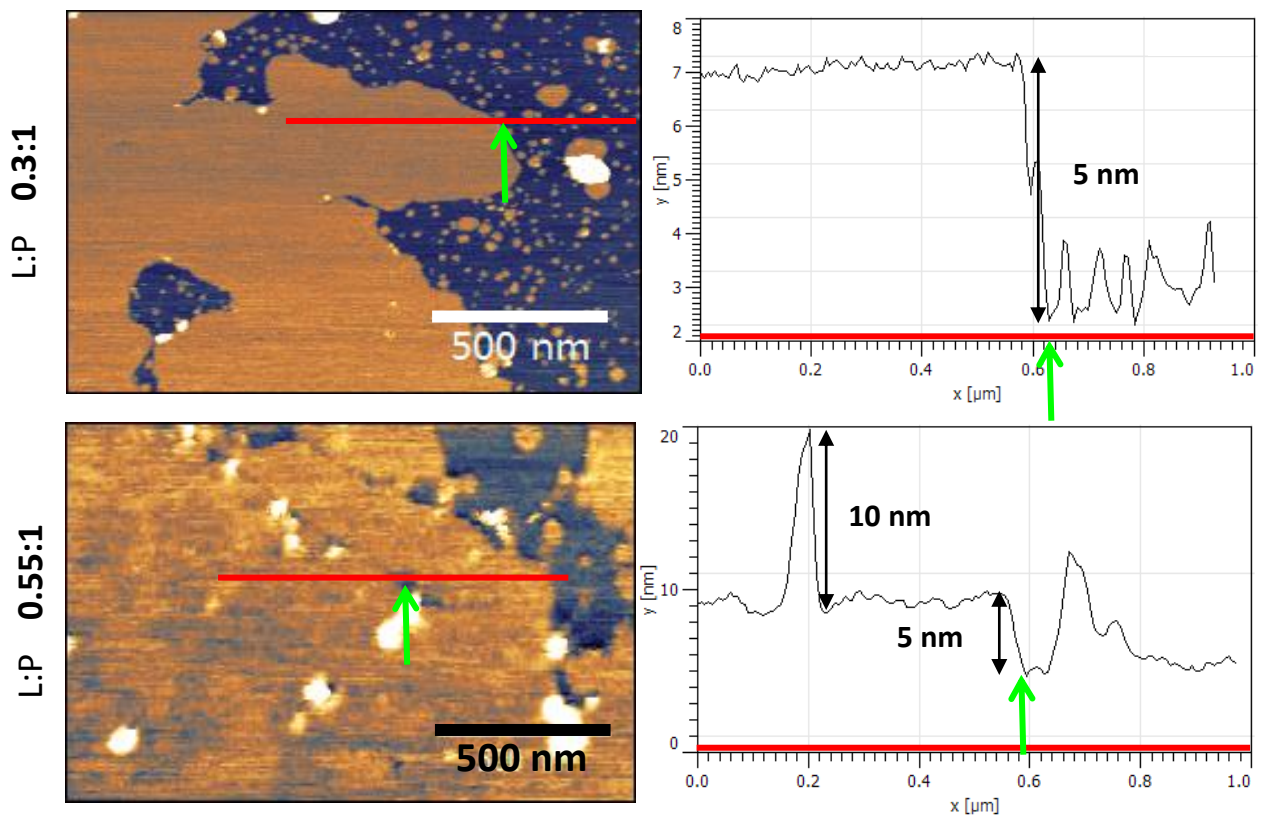
Figure 4.2.8. TatAyCy reconstitution into liposomes (of *E. coli* polar lipid extract)
TatAyCy proteoliposomes (orange surface on left-hand-side panels) were adsorbed onto mica surface (blue surface on left-hand-side panels) for topography analysis under the atomic force microscope (AFM) tip. Randomly-selected cross-sections (red line) were measured with the AFM and examined for protein reconstitution.

Top panel: TatAyCy protein reconstituted at a lipid-to-protein ratio (L:P) of 0.3:1 was unsuccessful. AFM measurements (right-hand-side) showed largely vast flat areas that are approximately 5 nm in height, which are attributable to empty lipid surfaces. Scale bar = 500 nm.

Bottom panel: TatAyCy protein reconstituted at a L:P ratio of 0.55:1 was unsuccessful. Again, 5 nm empty lipid bilayer was largely detectable. A 10 nm protrusion was detected (labelled, right-hand-side); however this was the only one in the sample. Scale bar = 500 nm.

The green arrows indicate equivalence points between AFM view (left-hand-side) and the measured height in the sample (right-hand-side).
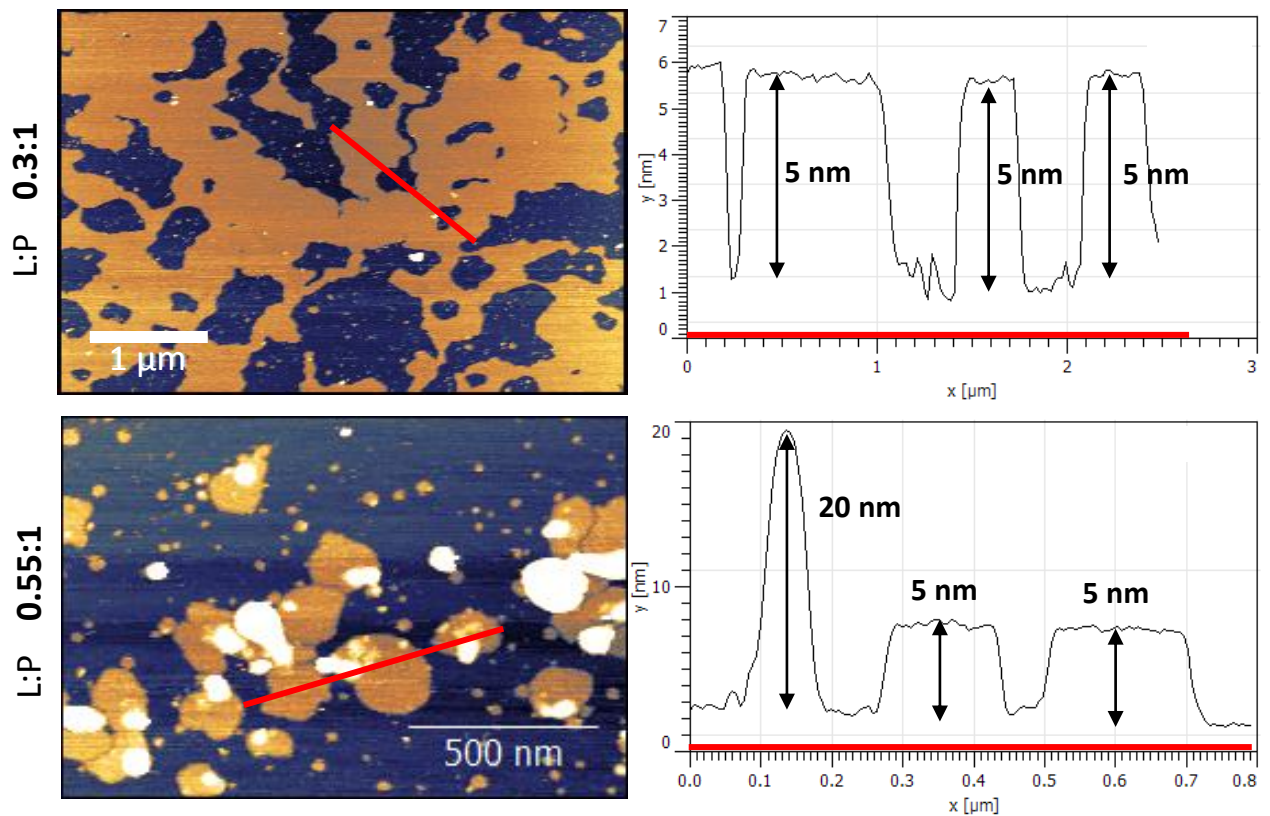
Figure 4.2.9. TatAyCy reconstitution into liposomes (of DOPC lipid)
TatAyCy proteoliposomes (orange surface on left-hand-side panels) were adsorbed onto mica surface (blue surface on left-hand-side panels) for topography analysis under the atomic force microscope (AFM) tip. Randomly-selected cross-sections (red line) were measured with the AFM and examined for protein reconstitution.
Top panel: TatAyCy protein reconstituted at a lipid-to-protein ratio (L:P) of 0.3:1 was unsuccessful. AFM measurements (right-hand-side) showed largely vast flat areas that are approximately 5 nm in height, which are attributable to empty lipid surfaces. Scale bar = 1 μm.
Bottom panel: TatAyCy protein reconstituted at a L:P ratio of 0.55:1 was unsuccessful. Again, a 5 nm empty lipid bilayer was largely detectable. 20 nm protrusions were frequently detected, which is likely to be protein aggregates or unopened liposomes. Scale bar = 500 nm.
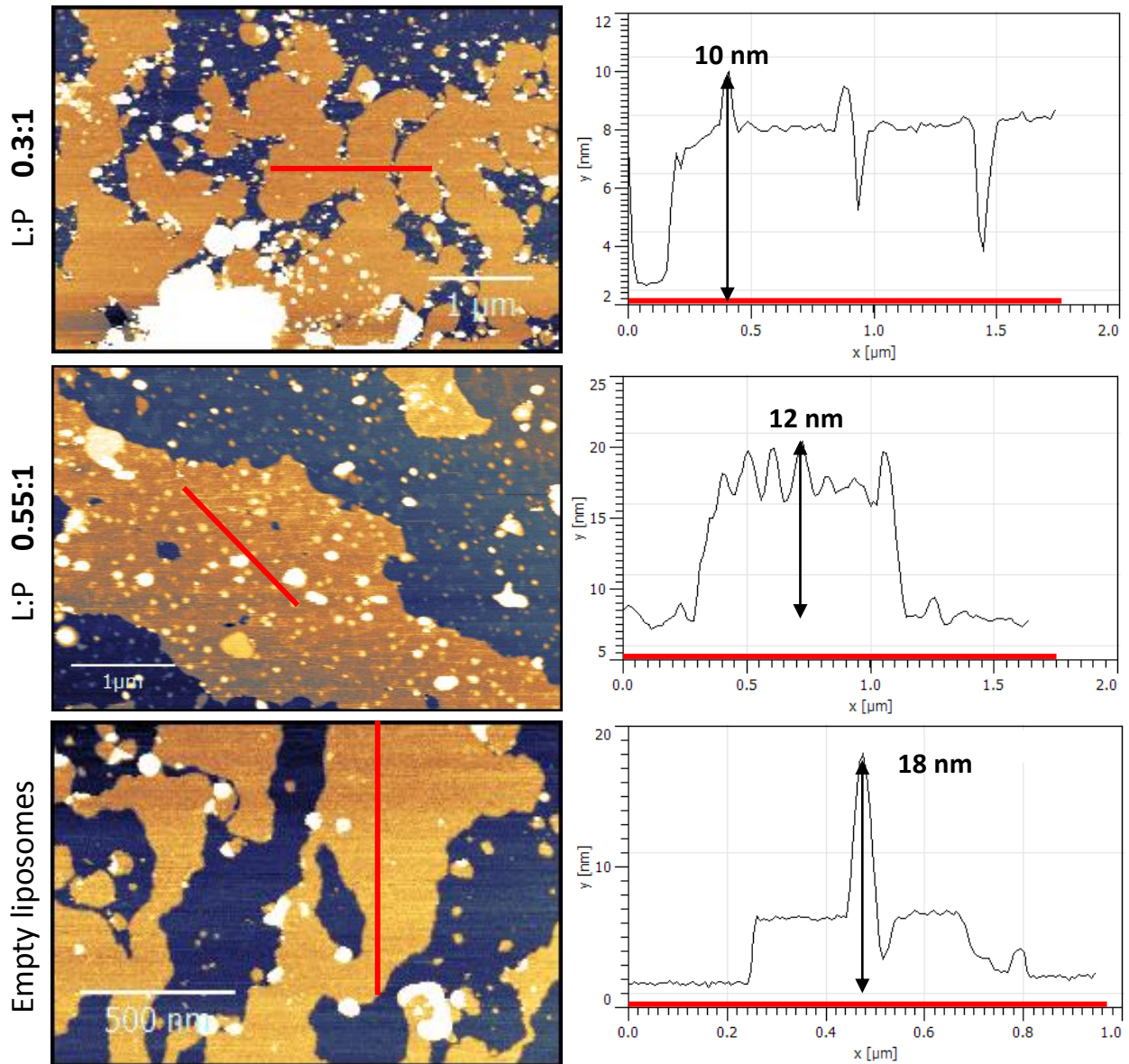
Figure 4.2.10. Octylglucoside-meditated TatAyCy reconstitution into liposomes of DOPC lipid.

TatAyCy proteoliposomes (orange surface on left-hand-side panels) (which have been reconstituted using octylglucoside detergent instead of Triton-X-100) were adsorbed onto mica surface (blue surface on left-hand-side panels) for topography analysis under the atomic force microscope (AFM) tip. Randomly-selected cross-sections (red line) were measured with the AFM and examined for protein reconstitution.

Top panel: TatAyCy protein reconstituted at a lipid-to-protein ratio (L:P) of 0.3:1. AFM measurements (right-hand-side) showed protrusions that are approximately 10 nm in height, consistent with the presence of a protein reconstituted in the lipid bilayer. Scale bar = 1 μm.

Middle panel: TatAyCy protein reconstituted at a L:P ratio of 0.55:1. AFM measurements (right-hand-side) showed protrusions that are approximately ~12 nm in height, consistent with the presence of a protein reconstituted in the lipid bilayer. Scale bar = 1 μm.

Bottom panel: control sample of empty liposomes. This sample was found to possess protrusions from the lipid bilayer of ~18 nm in height, consistent with the presence of protein aggregates. Scale bar = 500 nm.

4.3. Discussion

The results presented in this chapter are the first experimental data for the attempted reconstitution of a Tat protein complex into liposomes; therefore the approach used has been entirely empirical. A detergent-mediated approach was used to attempt to optimise the reconstitution of TatAyCy into liposomes (Figure 4.2.2).

The lack of success in forming TatAyCy-rich proteoliposomes can be attributed to the latter process of reconstitution. Use of cryo-EM to visualise Tat proteoliposomes in their native state confirmed that liposomes were being successfully made, and that their stability was not affected by attempted TatAyCy-protein reconstitution. The small size of the liposomes, if there was successful protein reconstitution, would offer a higher protein density, which is better for AFM analysis where a high density of protein in a lipid bilayer is desired.

During the reconstitution process, numerous parameters proved to be influential on protein incorporation and its analysis. First was the L:P ratio: the ratio of amount of lipid relative to the amount of protein. This ratio is important since it determines whether a sufficient amount of protein is present in order to efficiently reconstitute into a detergent-saturated liposome. Insufficient protein or lipid can result in inactive or aggregated protein which prevents investigation into protein functionality, and/or it can cause ambiguity in structural analysis, as seen in this investigation (discussed later in this section). Owing to the vast range of ratios possible, and variety in properties of the protein to be reconstituted, this parameter is determined empirically for each protein.

Reconstitutions at 60:1 and 1:1 L:P failed to produce liposomes that contained any protein-like features. A further reduction in the amount of lipid (0.3:1 and 0.55:1), in combination with alteration of detergent used for reconstitution (OG versus Triton-X-100), produced proteoliposomes, which contained protein-like features of 10-12 nm that were detectable under the AFM. Clearly this ratio requires further optimisation, and for TatAyCy, lower L:P ratios resulted in, albeit in very low quantities, protein reconstitution into liposomes.

Another important variable is choice of detergent. Two were used in this investigation: Triton-X-100 (low CMC – 0.17 mM) and OG (high CMC – 23 mM).

Both of these are routinely used in detergent-mediated reconstitution, and what is most important is the rate as which these detergent molecules are removed from the sample to drive proteoliposome formation. Samples that were subjected to OG-mediated detergent reconstitution, instead of Triton-X-100, contained protein-like features that were detected by the AFM. SM2 Biobeads have been shown to rapidly remove both of these detergents efficiently, irrespective of initial conditions (Lévy *et al.*, 1990; Paternostre *et al.*, 1988). Therefore, it would seem that the use of a detergent with a high CMC favours detergent-mediated protein reconstitution when using hydrophobic beads. It is likely that slower removal of a detergent minimises the chances of protein aggregation, which would prevent efficient protein reconstitution. Despite this, high-density reconstitution of TatAyCy was still unsuccessful. Perhaps slower removal of the OG detergent would favour reconstitution of all protein complexes.

The choice of lipid was a final parameter that influenced ambiguity of AFM data. DOPC is a bilayer lipid that will form fluid lamellar bilayers (Seddon *et al.*, 2004). Given that it consists of only a single lipid type, this detergent had the potential to aid AFM analysis, since any perturbations in the lipid bilayer should be much less ambiguous than the *E. coli* polar lipid extract, which possesses 3 different types of phospholipid. AFM analysis demonstrated that, for liposomes prepared from DOPC lipid, any protrusions from the lipid bilayer could be clearly discerned from mica surface and/or the surrounding bilayer; thus the 10-12 nm protein-like features detected upon the use of OG in the final reconstitution attempt could be clearly distinguished from the surrounding liposome bilayer and from those detected in the negative control sample.

In light of data from the first chapter of this thesis that showed TatAyCy in protein-detergent complexes to possess diameters of 12-14 nm, it is feasible that the particles of 10-12 nm diameter identified in this investigation would be consistent with TatAyCy lacking contribution of detergent. However, these particles were not abundant and therefore the data is too ambiguous to continue with for detailed topography analysis of the TatAyCy-proteoliposomes; therefore an alternative, more efficient means of direct visualisation of the Tat complex is required.

Chapter 5 - TatA complexes exhibit a marked change in organisation in response to expression of the TatBC complex

5.1 Introduction

Substrates are targeted to the Tat machinery *via* an N-terminal signal peptide (Chaddock *et al.*, 1995; Stanley *et al.*, 2000). At the inner membrane the substrate binds to a TatBC complex (Ma & Cline, 2013; Tarry *et al.*, 2009), which triggers the recruitment of a separate TatA complex (Alami *et al.*, 2003; Mori & Cline, 2002) to form the active translocase through which the substrate can pass. The precise mechanism of translocation is, however, poorly understood and the full translocation system has not been characterised.

It has been proposed that TatA contributes to the translocation process by weakening the membrane, or by forming a transient pore. Electron microscopy generated low-resolution structures of detergent-solubilised TatA protein, which showed TatA to exist as large, homo-oligomeric complexes that possess a cavity-like feature of varying diameter (Gohlke *et al.*, 2005). These data provide support for a role of TatA protein as the pore-forming element of the Tat machinery. However, similar studies on the TatA paralog, TatE, which can functionally substitute for TatA, and TatAd of *B. subtilis* which can also substitute for TatA showed these complexes to be much smaller and more homogeneous than TatA (Baglieri *et al.*, 2012; Beck *et al.*, 2013). Therefore, the biological significance of TatA heterogeneity (as a consequence of sample preparation) remains unclear.

Alternatively, it has been proposed that once TatA protein is recruited to TatBC complex it could serve as a nucleation point for additional TatA proteins (Alami *et al.*, 2003; Mori & Cline, 2002). Cross linking data has shown that the number of cross-links between TatA proteins increases under transport conditions (Dabney-Smith *et al.*, 2006), which is consistent with the idea that substrate binding to the Tat machinery triggers polymerisation of TatA protein. This in turn would alter the immediate environment of the phospholipid bilayer to permit passage of substrate through the inner membrane (Brüser & Sanders, 2003; Cline & McCaffery, 2007; Dabney-Smith *et al.*, 2006; Greene *et al.*, 2007). However, the precise oligomeric state of the TatA protein varies in cell membranes and detergent micelles (Alcock *et al.*, 2013; Gohlke *et al.*, 2005; Leake *et al.*, 2008; Porcelli *et al.*, 2002), which suggests that data from detergent-solubilised complexes are not necessarily a true

reflection of what is occurring in the protein's native cellular environment. Furthermore, cross-linking data are unable to define the distribution of TatA proteins within a given complex.

The distribution of Tat complexes within the membrane is another area that has been difficult to analyse with accuracy. Efforts to investigate the distribution of the two Tat complexes (TatA and Tat(A)BC) have utilised Tat proteins tagged with fluorescent proteins, and there is evidence that the TatB and TatC proteins retain activity with C-terminal fluorescent tags (Ray *et al.*, 2005). This study concluded that these proteins were uniformly distributed when expressed at low levels, although a separate study proposed that Tat complexes exhibit a polar localisation (Berthelmann & Brüser, 2004). However, analysis of TatA is more difficult. One study used GFP-tagged TatA to analyse the oligomeric state of TatA complexes in the membrane (Leake *et al.*, 2008), but another (Ray *et al.*, 2005) showed that a TatA-GFP fusion is prone to proteolysis and release of mature-size TatA. Since even low levels of TatA can support translocation activity, this finding means that it is not possible to determine whether TatA-GFP fusions proteins are active. It has therefore been difficult to reliably gauge TatA protein distribution and/or localisation in two dimensions.

Analysis of the 3-dimensional distribution of Tat complexes within cells is even more problematic. Despite the advent of super-resolution light microscopy bringing opportunity to analyse bacterial protein distribution with high resolution (Bakshi *et al.*, 2012; English *et al.*, 2011; Greenfield *et al.*, 2009), there still remains a lack of visualisation of protein distribution in 3D space. The image acquisition required for techniques such as PALM (photoactivated localisation microscopy) requires hundreds of thousands of X-Y images for every 1 μm deep focal plane; with a resulting trade-off between sample density and image acquisition time (Lidke & Lidke, 2012). Coupled with the above questions regarding TatA-GFP activity, this means that care must be taken when considering light microscopy-based approaches to study Tat localisation.

In this study we have sought to bypass such problems through the use of electron microscopic approaches in which native, unmodified TatA proteins are investigated.

I have developed the novel combinatorial approach of array tomography (Micheva *et al.*, 2010; Micheva & Smith, 2007) (a high-throughput proteometric imaging method) (in collaboration with Andrew Yarwood, JEOL UK) (Figure 5.2.1), with immunogold labelling, to obtain a 3D volume image of *E. coli*; unveiling the unambiguous distribution of TatA protein in the inner membrane. This is the first time that this organism has been analysed using this technique.

Our data show that a proportion of TatA is uniformly distributed in the plasma membrane, whether TatA is over-expressed on its own or together with TatBC. However, another fraction of TatA forms a linear cluster along the membrane in a TatBC-dependent manner, suggesting a mode of organisation not observed before. Despite the data not resolving any of the native structure of the Tat machinery, it does show the localisation and distribution of a Tat component that has been visualised in 3D space, *in situ* – afirst for the Tat field.

Given the ability to unambiguously identify TatA in the inner membrane, the polarity of this protein was investigated. Localisation of specific proteins to the cell poles – the ends of rod-shaped cells – is integral to the spatial organisation of a bacterium's proteome. Such regions play key roles in a multitude of cellular processes including: virulence, cellular differentiation and cell cycle progression (Treuner-Lange & Søgaard-Andersen, 2014). Therefore, knowledge of whether a particular protein localises to the cell poles is not only an essential question in bacterial cell biology, but can also provide insight into the functionality of the specific protein and its interaction partners. Existing data on whether the TatA protein exhibits a polar localisation remains dubious (Berthelmann & Brüser, 2004; Ray *et al.*, 2005; Ridder *et al.*, 2009; Rose *et al.*, 2013). Data presented in this chapter provides evidence for a non-polar localisation of TatA in the inner membrane of *E. coli*.

5.2 Results

5.2.1. Chemical fixation and heavy metal staining of *E. coli* cells for visualisation under the electron microscope

To capture a 'snap shot' of *E. coli* cells (overexpressing TatA or TatABC) with minimal alteration from living state, chemical fixation was required to preserve and protect the biological sample. Subsequent staining with heavy metal salts was necessary to impart high contrast to the cells for visualisation under the scanning/transmission electron microscope (Figure 5.2.1).

Glutaraldehyde was the initial choice of fixative since it is the most frequently used fixative that cross-links proteins efficiently and irreversibly (Melan, 1999). A dual staining approach was used to maximise sample contrast. Osmium tetroxide (OT) and tannic acid (TA) was the first staining protocol tested since osmium has been shown to impart substantial contrast; particularly in lipid-dense regions (Wigglesworth, 1975). However this staining combination produced resin blocks that were very brittle (Figure 5.2.2, panel C) and therefore almost impossible to section. The fragile consistency of the resin block was an indication of unsuccessful staining and resin embedding of the *E.* coli cells. Unsurprisingly, these cells had poor contrast under the SEM (Figure 5.2.2., panel A).

TA has been used as a less severe alternative to osmium tetroxide for the staining lipids in cells (Berryman, 1990), and was therefore used in combination with uranyl acetate (UA) (a conventional heavy metal stain). The combination of TA and UA produced resin blocks that were uniformly stained (Figure 5.2.2, panel D), sectioned well and had good contrast under the SEM (Figure 5.2.2, panel B).

Having optimised a staining protocol and perfected the technique of cutting ultrathin serial sections (Figure 5.2.3., A), the next stage was to optimise the immunolabelling of the sections for the unambiguous identification of TatA or TatABC (Figure 5.2.1., stage 5).
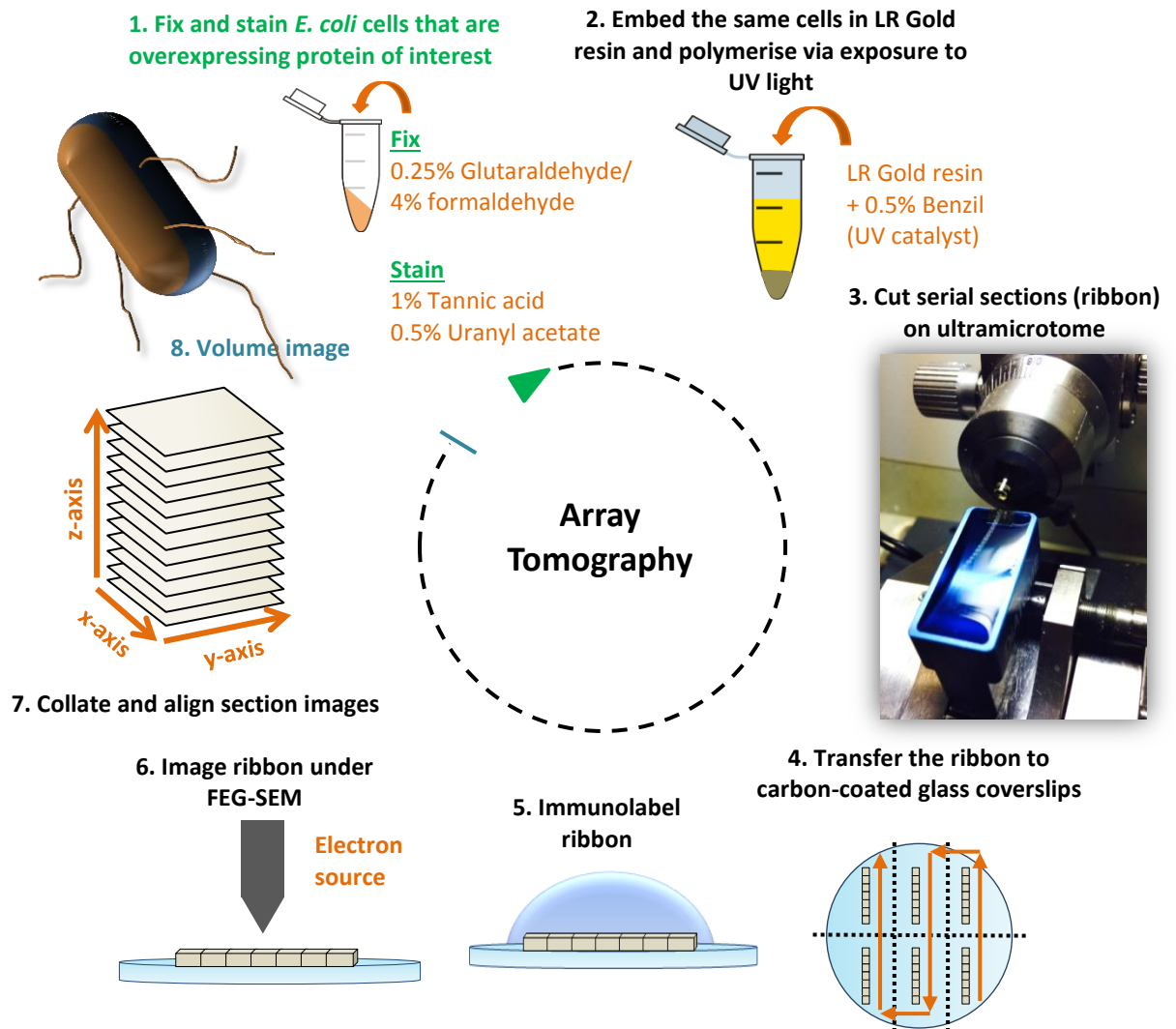
Figure 5.2.1. Overview of the Array Tomography process.
Array tomography is an 8-step technique that results in a volume image of the sample studied, in this case an *E. coli* bacterium. Fixation was necessary to biologically preserve the *E. coli* cells, and staining generated contrast under the electron beam (Step 1). Embedding in a resin forms a solid medium that enables the sample to be imaged in the microscope (Step 2). This requires the *E. coli* bacteria to be cut using a diamond knife (Step 3). Ultrathin (50 nm) serial sections were transferred to a flat, conductive surface for visualisation under the scanning electron microscope (SEM) (Step 4). The protein of interest shall be identified by exploiting the presence of a specific antigen i.e. TatA protein (Step 5). Imaging the ribbon under the SEM (Strep 6) generates an image stack (Step 7) that is to be computationally rendered to generate a 3D reconstruction of an *E. coli* bacterium (Step 8).
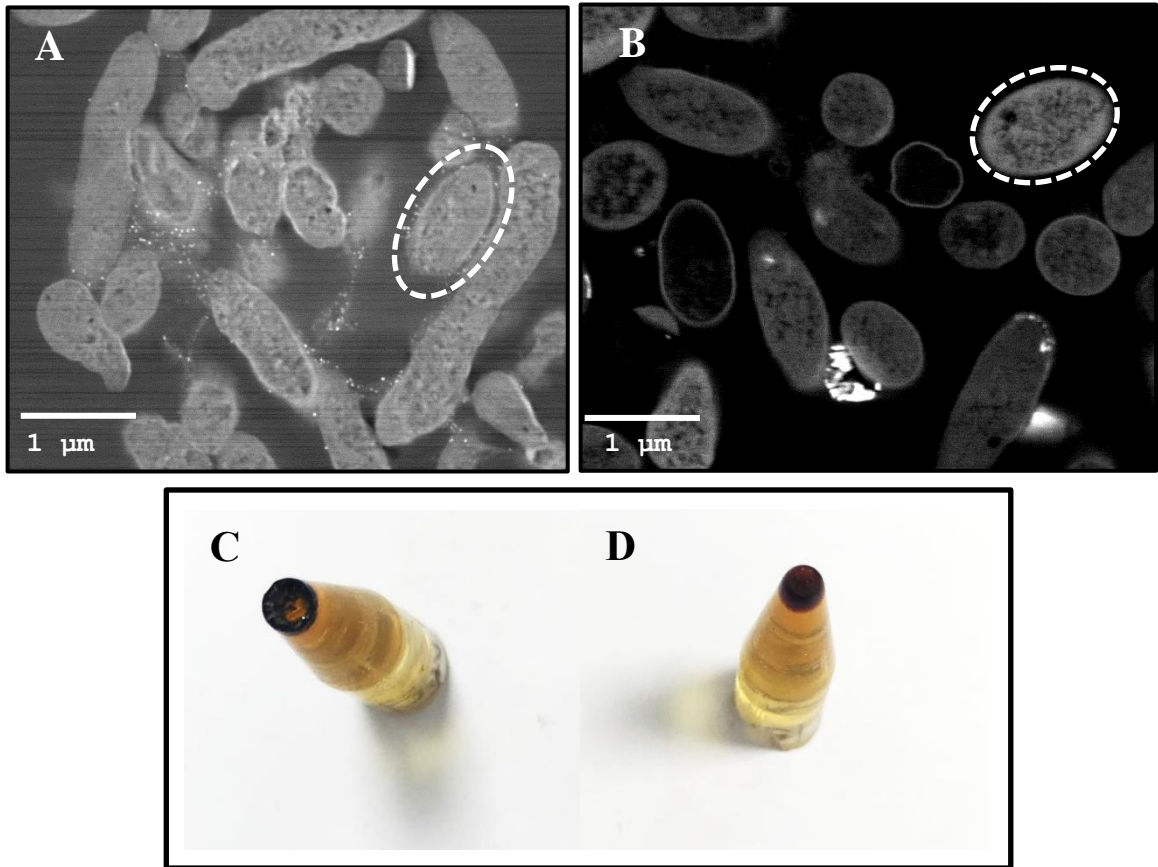
Figure 5.2.2. Optimisation of staining protocol to ensure sufficient contrast of *E. coli* under the electron beam

E. coli cells overexpressing TatA and TatABC were chemically fixed and stained in either osmium tetroxide and TA (A) or TA and UA (B). The latter generated greater contrast of the cells under the SEM (JSM-7500F field emission SEM, 3,000X mag, scale bar= 1 um). (A)-stained resin blocks were brittle and therefore very difficult to cut (C- middle image). (B)-stained resin blocks (D) cut well with glass and diamond knives to generate serial sections of uniform thickness.
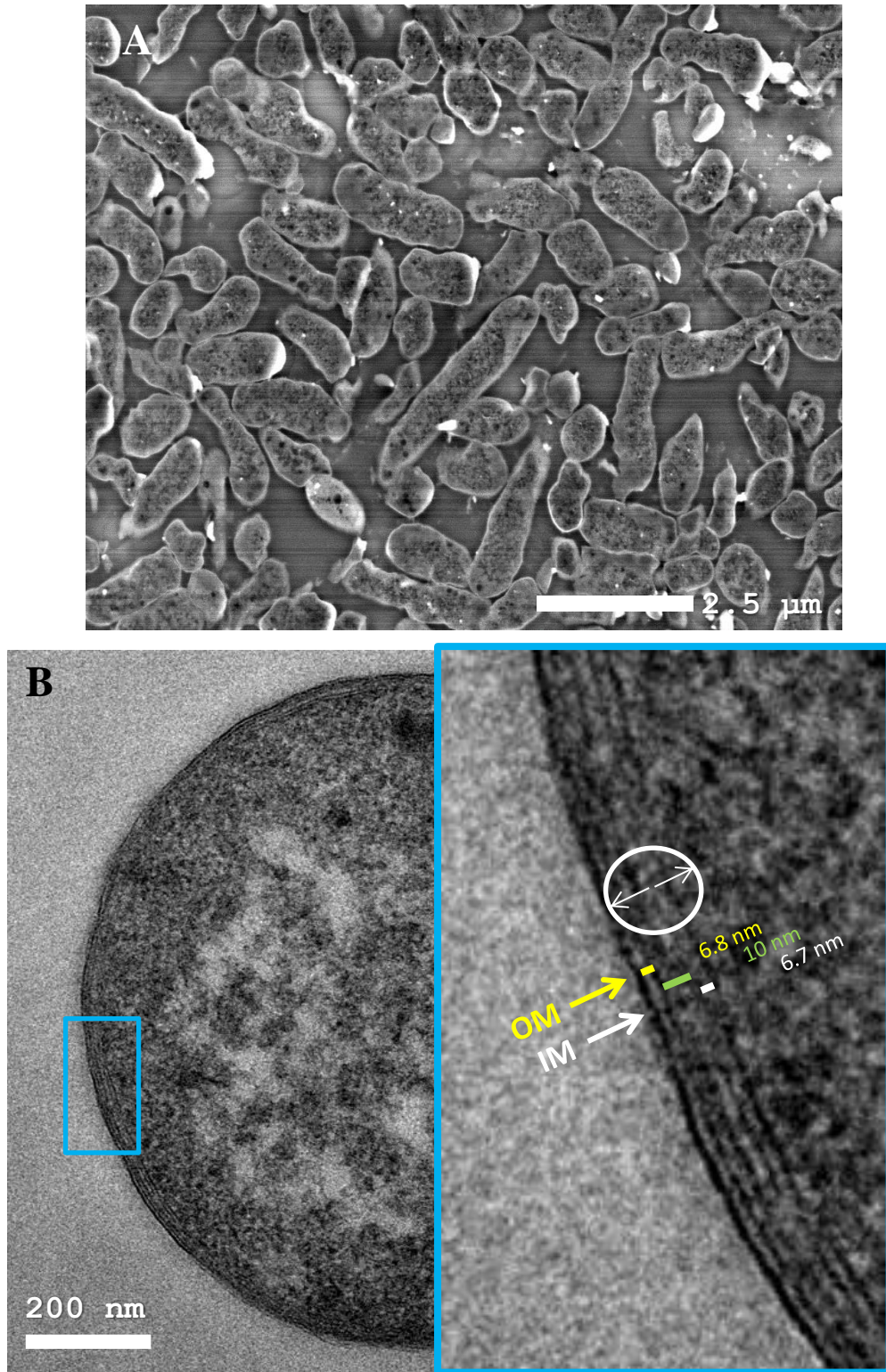
Figure 5.2.3. Electron micrograph of sectioned *E. coli*

A: Electron micrograph of *E. coli* cells stained with tannic acid and uranyl acetate. The cells have good internal contrast with cytoplasmic and cell wall features clearly distinguishable. Image taken on JEOL 7401-F at 5000X mag. Scale bar = 2.5 µm.

B: The *E. coli* bacterium shown has been sectioned through a latitudinal axis with a diamond knife. The outer (OM – yellow line) and inner membrane (IM – white line) can be clearly distinguished as a result of heavy metal staining. Gold particles within 25 nm radius of the section shown (white circle) shall be considered as bound to the inner membrane of *E. coli*. Image taken on JEOL 2010 TEM at 12,000X mag. Scale bar = 200 nm.

115

5.2.2. Optimisation of immunolabelling for the unambiguous identification of TatA protein in *E. coli*

Given that the labelling procedure involves binding of a primary antibody to a gold-conjugated secondary antibody, the electron-dense particle visualised under the EM may not necessarily be localised in the immediate vicinity of the inner membrane. van Weering (van Weering, 2010) elucidated that this "structure" of primary + secondary + 10 nm gold is ~25 nm diameter. Therefore the region considered to be of inner membrane localisation has a 25 nm radius (Figure 5.2.3., B, white circle).

The immunolabelling procedure (§2.10.1.2) consists of many variables, each of which requires optimisation to ensure optimal antibody labelling of desired antigen. The first variables to be tested in this study were: Tris- or phosphate-containing buffer; +/- presence of detergent and +/- blocking of sample prior to antibody incubation.

E. coli cells overexpressing TatA-his or TatABC-strep (hereafter denoted TatA and TatABC) were immunolabelled with each of the above variables changed separately. *E. coli* cells lacking any Tat machinery (Δ*tatABCDE*; hereafter denoted Δ*tat*) were used as controls for non-specific binding. A second negative control was TatA- or TatABC-overexpressing cells immunolabelled with the primary antibody omitted (hereafter denoted (-)).

Cells immunolabelled with PBS and PBS/T buffers yielded higher gold counts versus TBS and TBS/T samples (Figures 5.2.4. to 5.2.7.); however, there is clearly more gold in the negative controls of these phosphate-containing samples and thus more non-specific binding. Since gold is bound in both of the negative controls, it is unclear which of the antibodies are binding non-specifically to the sections, or whether both are.

The orange asterisk in the blocked PBS/T sample (Figure 5.2.4., bottom row, (+)) highlights the presence of UA crystals that have formed upon reaction with phosphate ions in the buffer. These hinder immunogold labelling, and are therefore another justification for omitting phosphate from buffer conditions.

The non-specific binding in the Tris-containing samples (Figure 5.2.6 and 5.2.7), albeit in very low quantity, is mostly in the non-blocked TBS Δ*tat* control where

there is gold bound at the inner membrane (yellow-dashed area) and on the resin (green circle).

Blocked TBS/T samples contained the least amount of non-specific binding and retained a sufficient number of gold particles in the TatA overexpressing sample without any significant signs of gold clustering (Figure 5.2.6., bottom row).

The next step in optimisation focused on increasing the antigenicity of the *E. coli* cells, whilst retaining sufficient internal contrast. A staining procedure was developed that was shown to improve both antigenicity and contrast at the inner membrane (Berryman, 1990). When this protocol was tested on TatA overexpressing *E. coli* cells (Figure 5.2.8., top row), an increased contrast at the inner membrane only occurred upon additional heavy metal counter-staining with lead citrate (Figure 5.2.8., top row, left versus middle panel). However compared to previous imaging results, this level of contrast was attainable without this altered staining protocol. Also, the overall antigenicity of these samples was not markedly improved. In fact-binding at the inner membrane was lacking and the control sample highlighted the capability of the secondary antibody to bind non-specifically (Figure 5.2.8).

To determine whether the lack of gold was attributable to the alteration of staining or immunolabelling procedure, the same "Berryman-stained cells" were immunolabelled using the blocked, TBS/T method optimised in this study (Figure 5.2.8., bottom row). Again, gold was lacking and there were signs of clustering (green circle), which is likely due to alteration in cell preparation/staining. Not only did the "Berryman" preparative technique drastically reduce antigenicity, any increase in membrane contrast was negligible.

What is apparent so far is the presence of cytoplasmic-bound gold. Despite this localisation of TatA being reported previously (Berthelmann *et al.*, 2008), TatABC overexpressing cells were analysed in parallel, since TatC is more hydrophobic than TatA given the six transmembrane helices as opposed to one (§1.3.3). Therefore, we would expect (in line with its calculated membrane localisation), TatABC to reside largely in the inner membrane and thus the amount of cytoplasmic gold to be minimised.
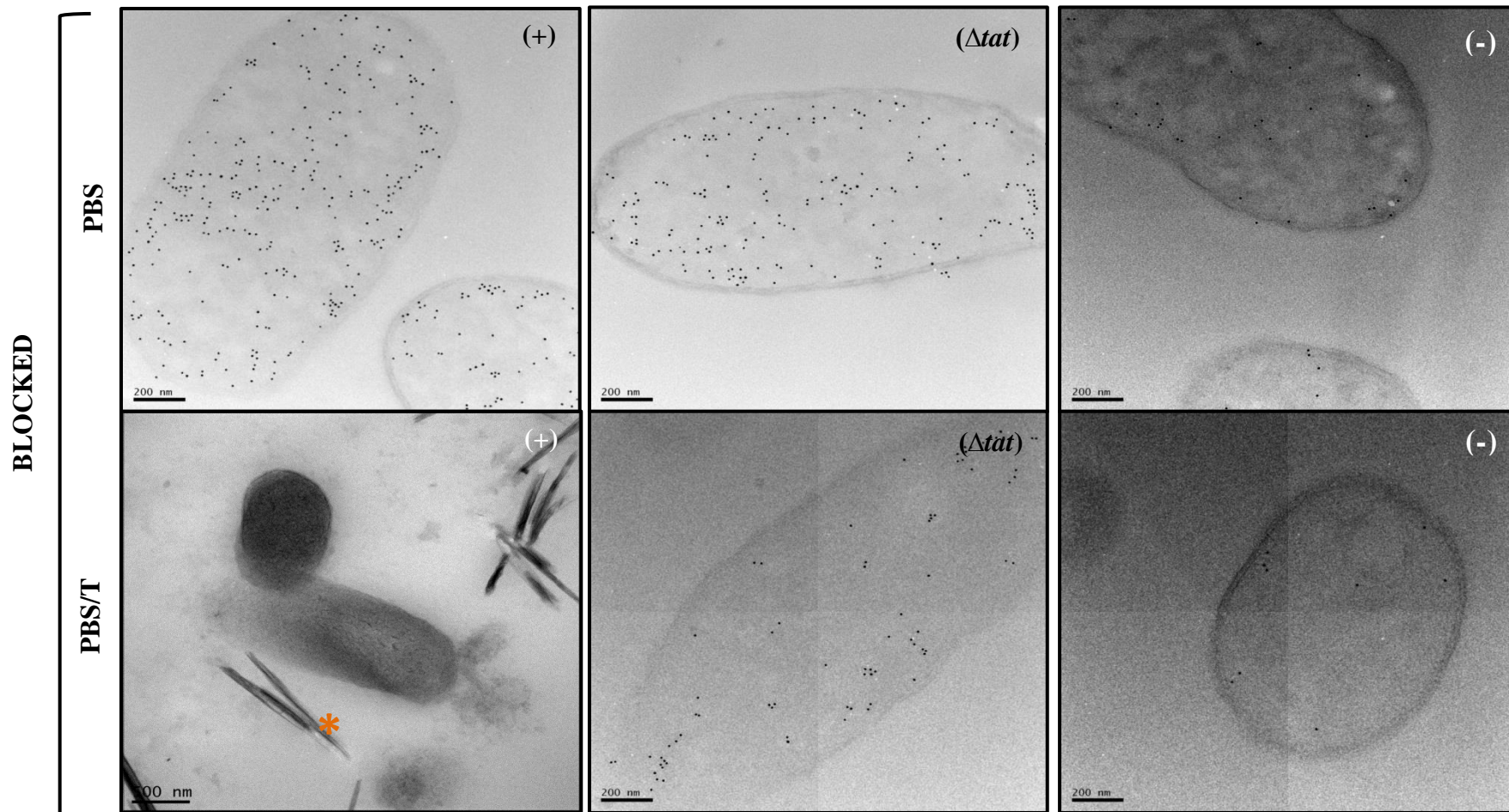
Figure 5.2.4. Electron micrographs of *E. coli* cells, overexpressing TatA, subjected to immunogold labelling with alteration of numerous parameters
Chemically fixed and stained *E. coli* cells overexpressing TatA [labelled **(+)**] were immunogold labelled to detect the presence of his-tagged proteins. Controls: cells that had Tat machinery knocked-out [labelled **(Δ*tat*)**] and (+) cells that had the primary antibody omitted [labelled **(-)**]. Preliminary optimisation of immunolabelling utilised different buffers (PBS or TBS), +/- the presence of 0.1% Tween-20 detergent and +/- blocking of the sections. There was significant non-specific binding at the inner membrane and cytoplasm in each of the controls. Orange asterisk highlights formation of uranyl acetate crystals. Images were taken on a JEOL 2010 TEM at 12,000X mag. Scale bar = 200 nm.
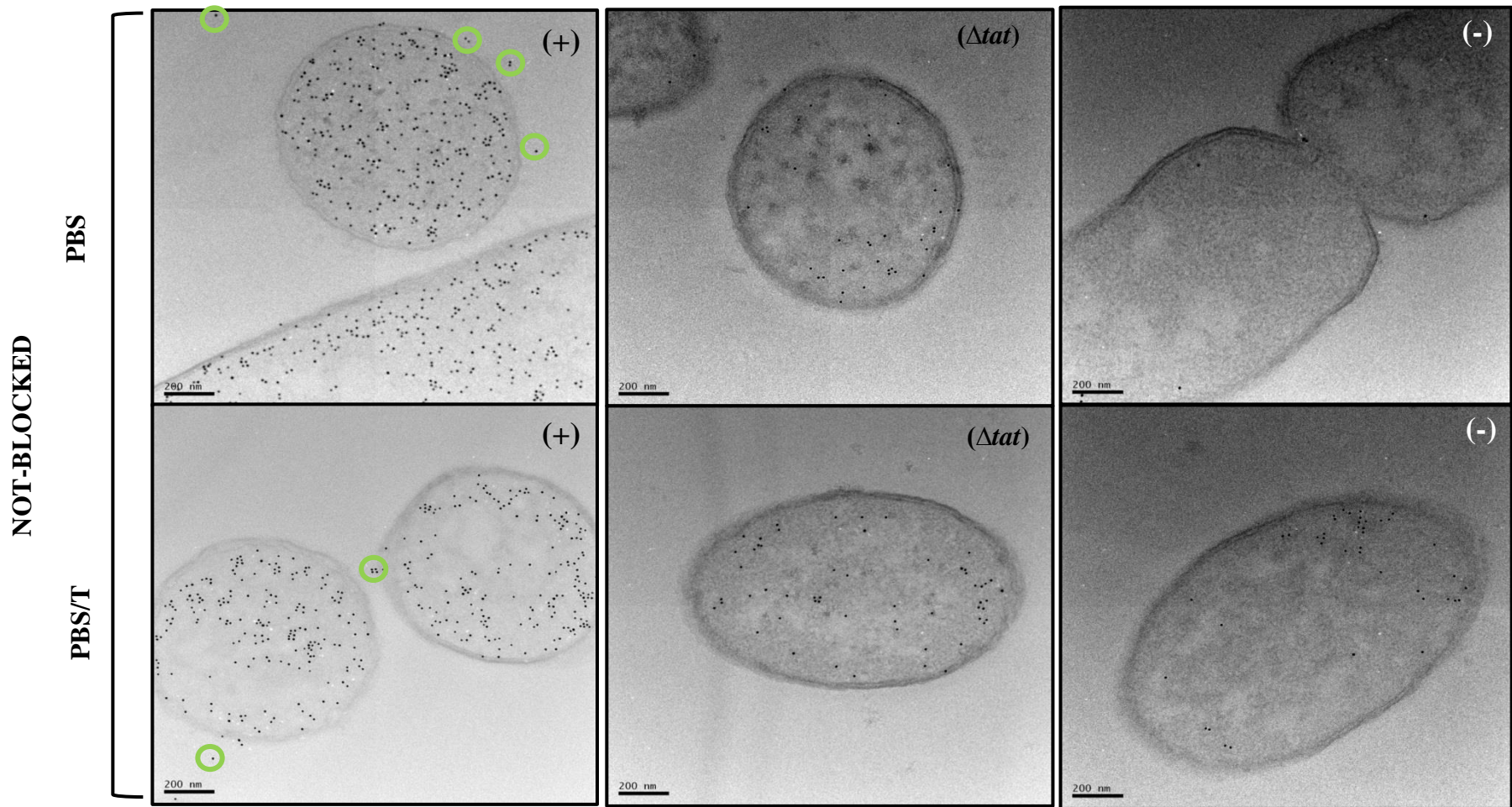
Figure 5.2.5. Electron micrographs of *E. coli* cells, overexpressing TatA, subjected to immunogold labelling with alteration of numerous parameters
Chemically fixed and stained *E. coli* cells overexpressing TatA [labelled **(+)**] were immunogold labelled to detect the presence of his-tagged proteins. Controls: cells that had Tat machinery knocked-out [labelled **(Δtat)**] and (+) cells that had the primary antibody omitted [labelled **(-)**]. Preliminary optimisation of immunolabelling utilised different buffers (PBS or TBS), +/- the presence of 0.1% Tween-20 detergent and +/- blocking of the sections. There was significant non-specific binding at the inner membrane and cytoplasm in each of the controls. Green circles highlight non-specific binding to resin. Images were taken on a JEOL 2010 TEM at 12,000X mag. Scale bar = 200 nm.
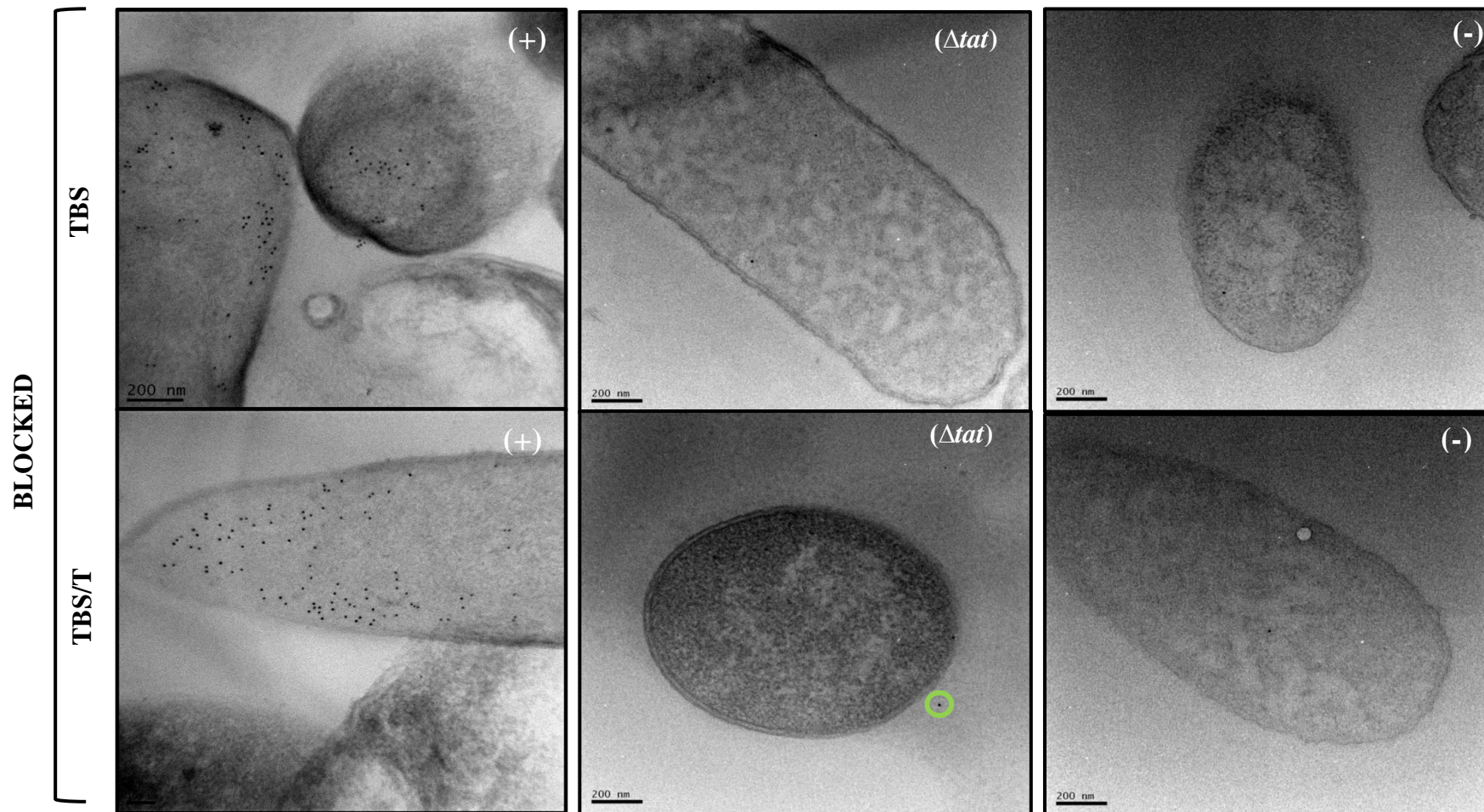
Figure 5.2.6. Electron micrographs of *E. coli* cells, overexpressing TatA, subjected to immunogold labelling with alteration of numerous parameters
Chemically fixed and stained *E. coli* cells overexpressing TatA [labelled **(+)**] were immunogold labelled to detect the presence of his-tagged proteins. Controls: cells that had Tat machinery knocked-out [labelled **(Δ*tat*)**] and (+) cells that had the primary antibody omitted [labelled **(-)**]. Preliminary optimisation of immunolabelling utilised different buffers (PBS or TBS), +/- the presence of 0.1% Tween-20 detergent and +/- blocking of the sections. Use of Tris buffer reduced the amount of non-specific binding. Green circles highlight non-specific binding to resin. Images were taken on a JEOL 2010 TEM at 12,000X mag. Scale bar = 200 nm.
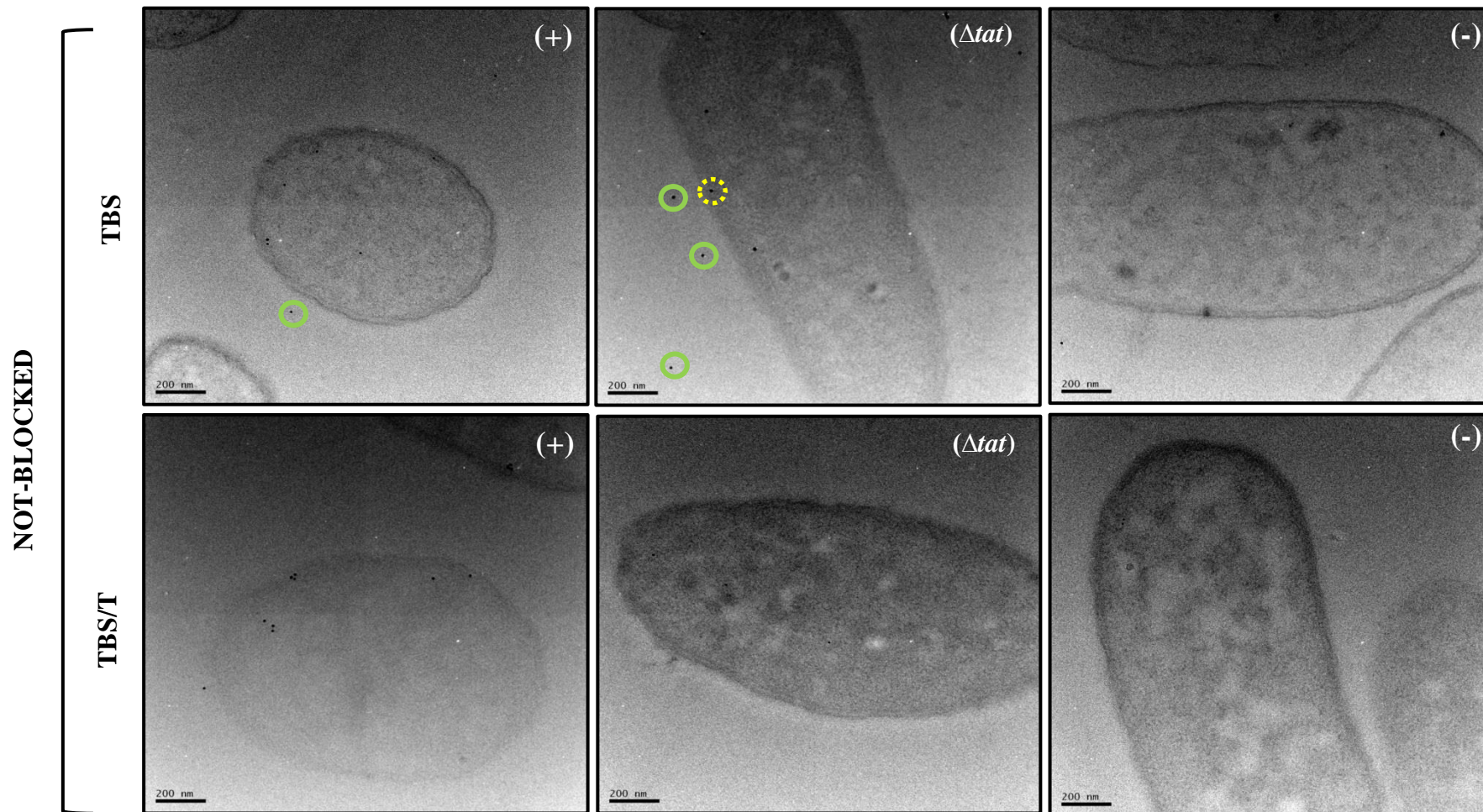
Figure 5.2.7. Electron micrographs of *E. coli* cells, overexpressing TatA, subjected to immunogold labelling with alteration of numerous parameters
Chemically fixed and stained *E. coli* cells overexpressing TatA [labelled **(+)**] were immunogold labelled to detect the presence of his-tagged proteins. Controls: cells that had Tat machinery knocked-out [labelled **(Δtat)**] and (+) cells that had the primary antibody omitted [labelled **(-)**]. Preliminary optimisation of immunolabelling utilised different buffers (PBS or TBS), +/- the presence of 0.1% Tween-20 detergent and +/- blocking of the sections. Use of Tris buffer reduced the amount of non-specific binding. An absence of tween increased non-specific binding to resin (green circles). Yellow circle = inner membrane-bound gold. Images were taken on a JEOL 2010 TEM at 12,000X mag. Scale bar = 200 nm.

121
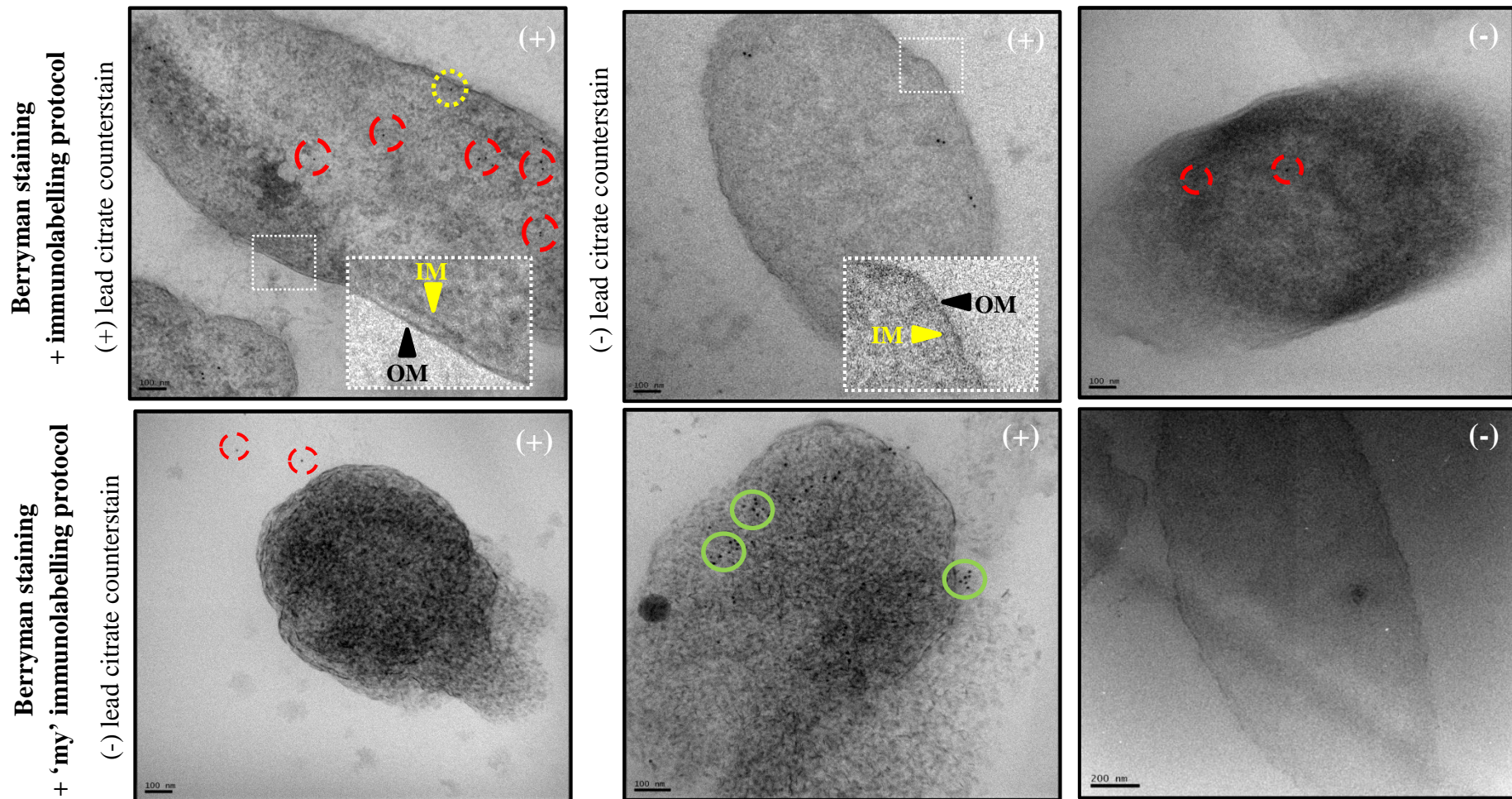
Figure 5.2.8. Alteration of *E. coli* cell fixation and staining to enhance contrast and antigenicity.

E. coli cells overexpressing TatA were fixed in 1% glutaraldehyde/4% formaldehyde and subjected to pre-embedding staining of uranyl acetate and subsequent post-embedding staining of osmium tetroxide (Berryman staining- both rows). The Berryman immunolabelling method (top row) lasted less than 3 hours, avoided use of detergent and +/- counterstaining with lead citrate. Counterstaining marginally increased the contrast of the outer and inner membranes (Left versus right, white-dashed boxes, top row). Berryman staining failed to increase antigenicity relative to previous samples. Images were taken at 12,000X mag using JEOL 2010F TEM Scale bar= 100 nm

To confirm TatA and TatABCs localisation(s), *E. coli* cells overexpressing either TatA-his or TatABC-strep were fractionated into periplasmic, cytoplasmic and membrane fractions and immunoblotted using the same primary antibodies as in the immunogold labelling (Figure 5.2.9). Results showed a lack of His_6-tagged proteins in the cytoplasm of TatA overexpressing cells and unsurprisingly, both regions of Δ*tat* cells (Figure 5.2.9., top panel). These data confirm that the abundance of cytoplasmic gold seen in both cell types is non-specific. Whereas, TatC-strep was detected in both the membrane and cytoplasm of TatABC overexpressing cells (Figure 5.2.9., bottom panel). The fact that TatA-his was not detected in the cytoplasm of TatA-overexpressing cells could be a reflection anti-Strep having a much higher affinity than anti-his hence why it is detecting TatC in the cytoplasm; or the anti-Strep antibody could be non-specific.
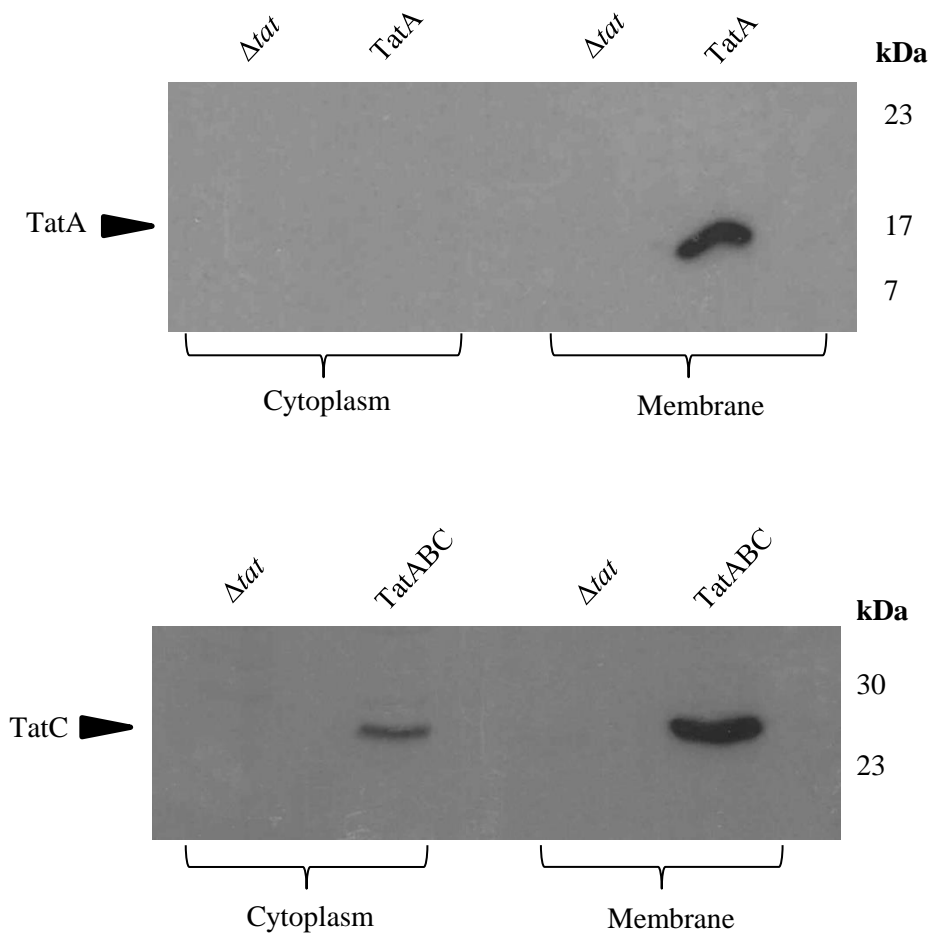
Figure 5.2.9. Cytoplasmic and inner membrane fractions of *E. coli* cells (overexpressing TatA or TatABC) immunoblotted for the detection of his/strep-tagged proteins.
E. coli cells overexpressing TatA (top) and TatABC (bottom) were fractionated into cytoplasmic and membrane fractions. The fractions were resolved by SDS PAGE and immunoblotted to detect for the presence of his/strep-tagged proteins. The control was *E. coli* cells that have had Tat machinery knocked-out (Δ*tat*). Top panel: anti-his antibody identified overexpressed TatA only the membrane fraction of TatA overexpressing cells. Bottom panel: anti-strep antibody identified overexpressed TatABC in the cytoplasm and inner membrane of TatABC over-expressing cells.

In a continued effort to decrease non-specific binding, both TatA and TatABC - overexpressing samples were immunolabelled with increasing dilutions (1:5, 1:10 and 1:15) of anti-his and anti-strep antibody, respectively.

In both samples, an expected decrease in amount of gold upon increasing dilutions of primary antibody was seen (Figures 5.2.10 and 5.2.11). In samples overexpressing TatA or TatABC (denoted (+)), there was an abundance of gold particles in the cytoplasmic region, with little at the inner membrane. The Δ*tat* cells had gold bound, albeit in lower quantities than (+) samples, at all dilutions. This was minimised with 1:20 dilutions. The (+) samples immunolabelled without primary antibody (denoted (-)) both bound gold, demonstrating that the secondary antibody is binding non-specifically. Therefore, the 1:20 dilution of the primary antibody was selected as the optimal dilution in further experiments, with additional efforts required to minimise non-specific binding of gold in both samples.

The next avenue of optimisation was to increase the pH of the TBS/T buffer from 7.2 to ~8.2 (Figure 5.2.12). An increase in pH reduces charge attraction of negatively-charged gold particles to positive sample components. Both (+) samples had binding at the inner membrane (Figure 5.2.12. yellow-dash circles). Whether this had changed relative to previous samples was indistinguishable via qualitative analysis. Gold still bound non-specifically in Δ*tat* cells, so much that they were indistinguishable from the (+) samples; more so for cells overexpressing TatABC. Gold binding to the (-) samples shows that the secondary antibody is also binding non-specifically.

Figure 5.2.10. Electron micrographs of *E. coli* cells, overexpressing TatA, immunolabelled with varying concentrations of primary antibody

E. coli cells overexpressing TatA were immunolabelled using an anti-his primary antibody at 1:5, 1:10 and 1:20 dilutions from stock. Controls: cells that had Tat machinery knocked-out [labelled **(Δ*tat*)**] and (+) cells that had the primary antibody omitted [labelled **(-)**].1:20 was the optimal primary antibody concentration since non-specific binding in (Δ*tat*) cells was minimal compared to 1:5-1:15 dilutions. Images were taken on a JEOL 2010 TEM at 12,000X mag. Scale bar = 200 nm.

Figure 5.2.11. Electron micrographs of *E. coli* cells, overexpressing TatABC, immunolabelled with varying concentrations of primary antibody
E. coli cells overexpressing TatABC were immunolabelled using an anti-strep primary antibody at 1:5, 1:10 and 1:20 dilutions from stock. Controls: cells that had Tat machinery knocked-out [labelled **(Δ*tat*)**] and (+) cells that had the primary antibody omitted [labelled **(-)**].1:20 was the optimal primary antibody concentration since non-specific binding in (Δ*tat*) cells was minimal compared to 1:5-1:15 dilutions. Images were taken on a JEOL 2010 TEM at 12,000X mag. Scale bar = 200 nm. 5.2.1
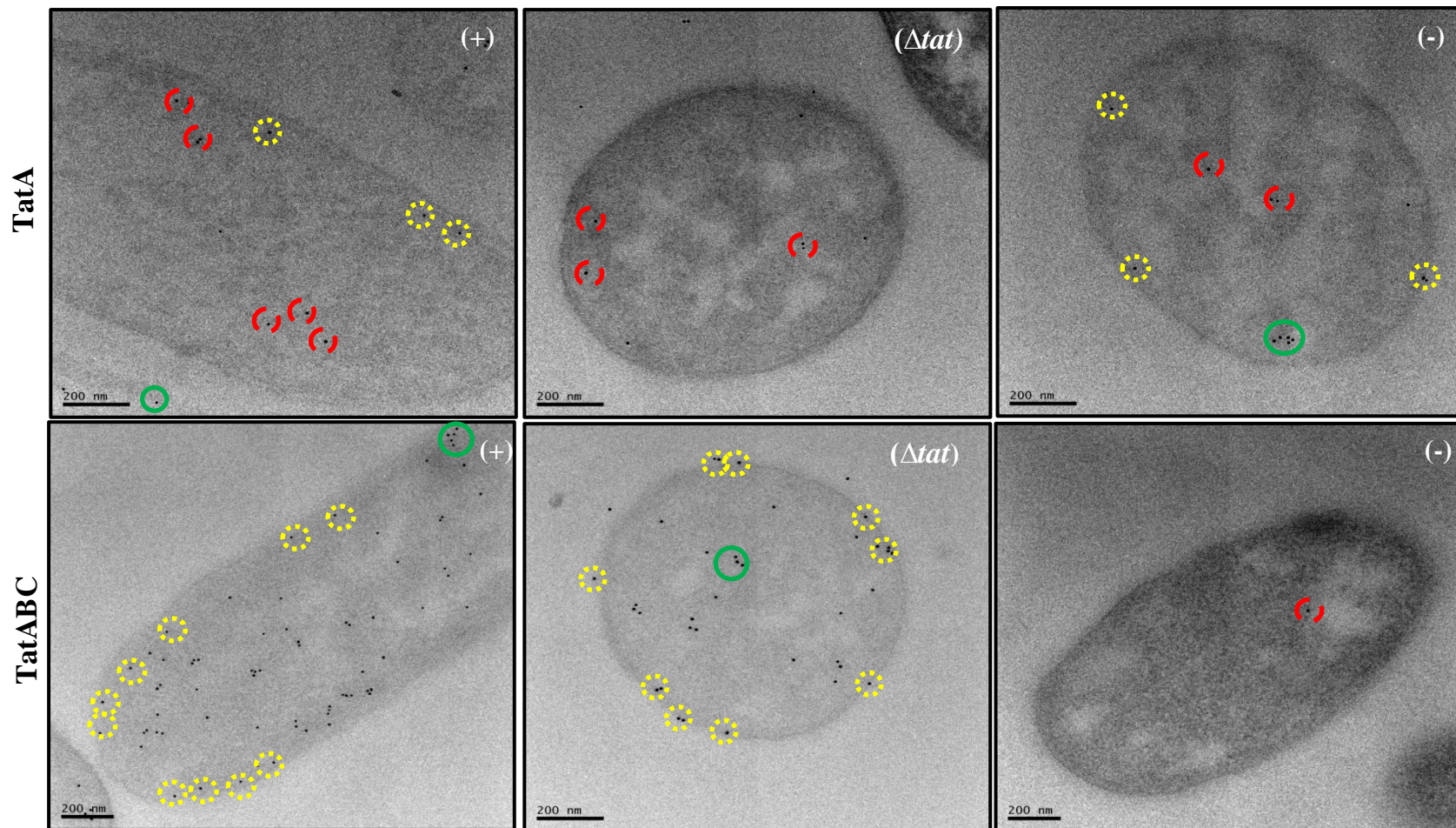
Figure 5.2.12.Electron micrographs of *E. coli* cells immunolabelled with buffers of increased pH
During immunolabelling of cells overexpressing either TatA or TatABC, the pH of the wash buffer was increased from 7.2 to 8.4 in an attempt to minimise non-specific binding. Controls: cells that had Tat machinery knocked-out [labelled **(Δtat)**] and (+) cells that had the primary antibody omitted [labelled **(-)**]. In both cell types, non-specific binding remained in both controls **(Δtat)** and (-). Yellow-dash indicates binding at inner membrane. Red-dash indicates binding in cytoplasmic regions. Green circle highlights signs of gold clustering. Images were taken on a JEOL 2010 TEM at 12,000X mag. Scale bar = 200 nm.

Interim summary:

Despite changing numerous variables such as buffer pH, primary antibody concentrations etc., there is still extensive non-specific labelling of Δ*tat* and (-) cells by the primary and gold-conjugated secondary antibodies.

To address these issues individually, increasing percentages of goat sera (1%, 2% and 4%) were included in the blocking buffer to eradicate non-specific binding of secondary antibody (Figure 5.2.13 and 5.2.14) to TatA and TatABC overexpressing cell. For both samples, only at 4% goat sera was the gold binding in the (-) samples eradicated.

Non-specific binding of primary antibody to Δ*tat* cells remained, thus giving false positives in (+) samples. Avidin was added in the blocking buffer of TatABC overexpressing cells in attempt to stop biotinylated proteins binding non-specifically to the anti-strep antibody (Figure 5.2.15). However, the non-specific binding increased with more gold bound in Δ*tat* and (-) samples. Clustering/aggregation of the gold was abundant (Figure 5.2.15, green circles).
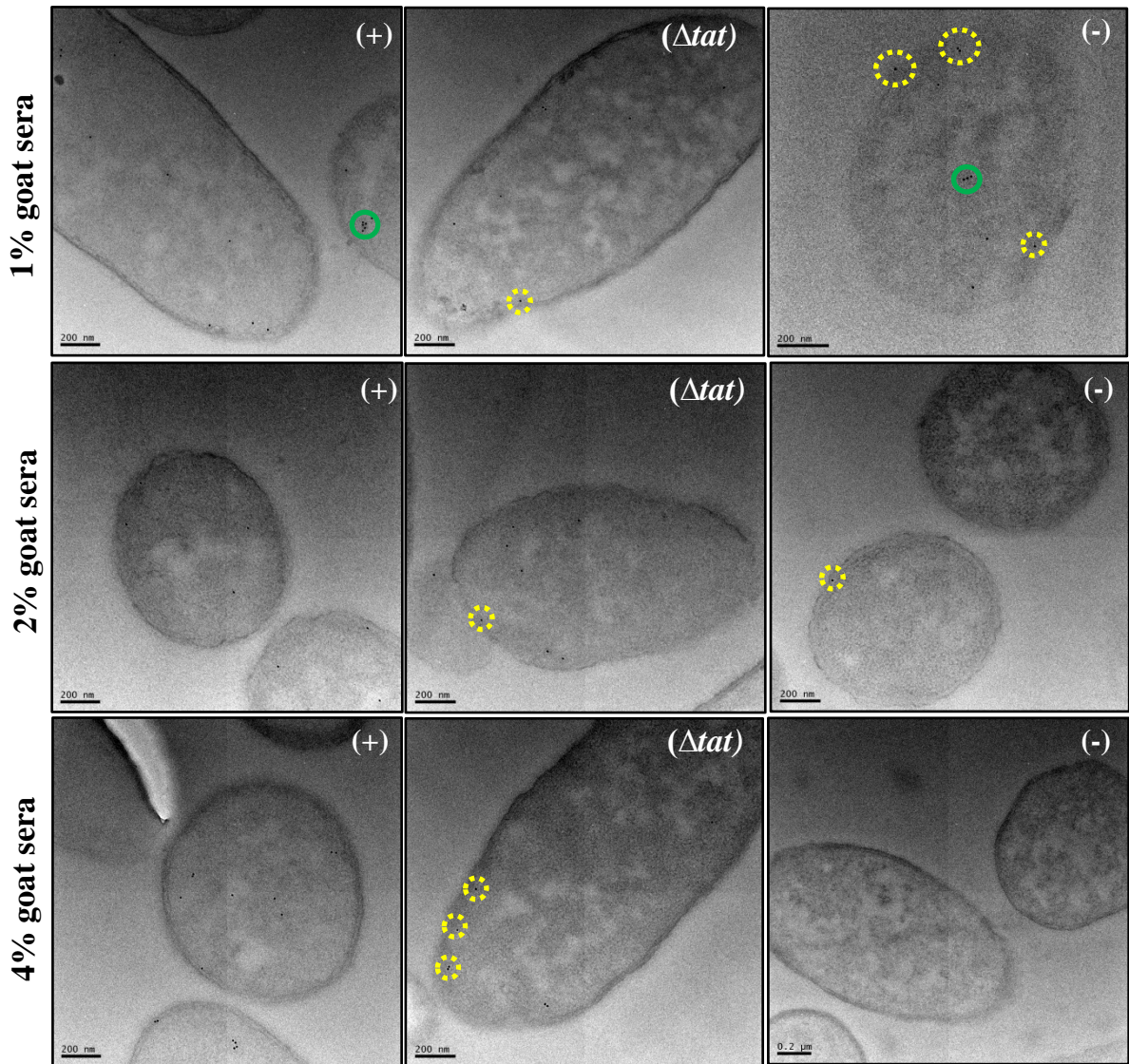
Figure 5.2.13. Electron micrographs of *E. coli* cells, overexpressing TatA, blocked with differing percentages of normal goat sera.

Having been blocked in buffer containing 1, 2 or 4% normal goat sera, *E. coli* cells overexpressing TatA were immunolabelled using an anti-his primary antibody. Controls: cells that had Tat machinery knocked-out [labelled **(Δtat)**] and (+) cells that had the primary antibody omitted [labelled **(-)**]. Yellow-dash = inner membrane binding. 4% goat sera was the optimal concentration of goat sera since it minimised non-specific binding in **(Δtat)** and (-) cells. Images were taken on JEOL 2010F TEM at 12,000X magnification. Scale bar = 200 nm.
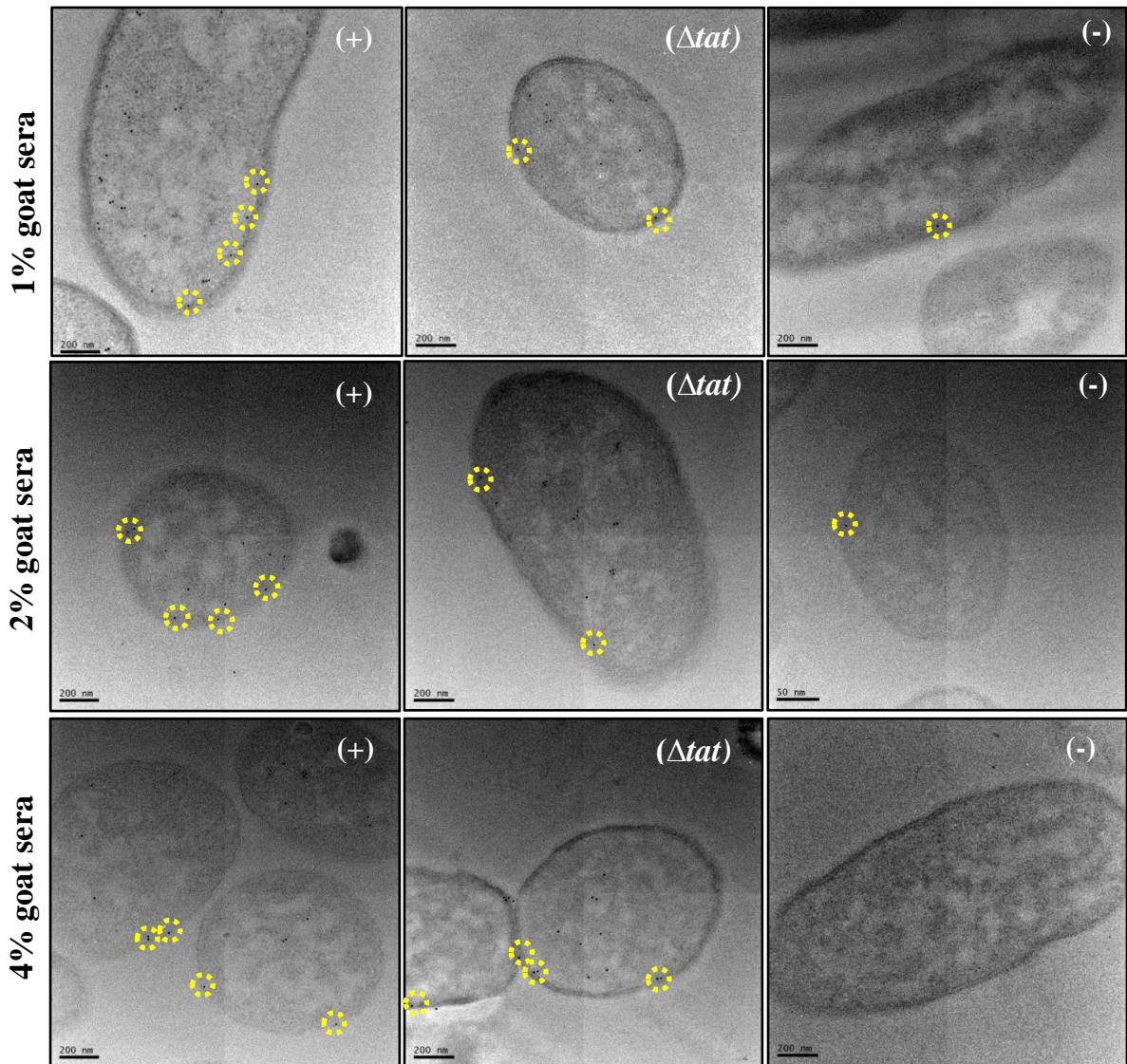
Figure 5.2.14. Electron micrographs of *E. coli* cells, overexpressing TatABC, blocked with differing percentages of normal goat sera.

Having been blocked in buffer containing 1, 2 or 4% normal goat sera, *E. coli* cells overexpressing TatABC were immunolabelled using an anti-strep primary antibody. Controls: cells that had Tat machinery knocked-out [labelled **(Δ*tat*)**] and (+) cells that had the primary antibody omitted [labelled **(-)**]. Yellow-dash = inner membrane binding. 4% goat sera was the optimal concentration of goat sera since it abolished non-specific binding of secondary antibody [bottom row, (-)]. Images were taken on JEOL 2010F TEM at 12,000X magnification. Scale bar = 200 nm.
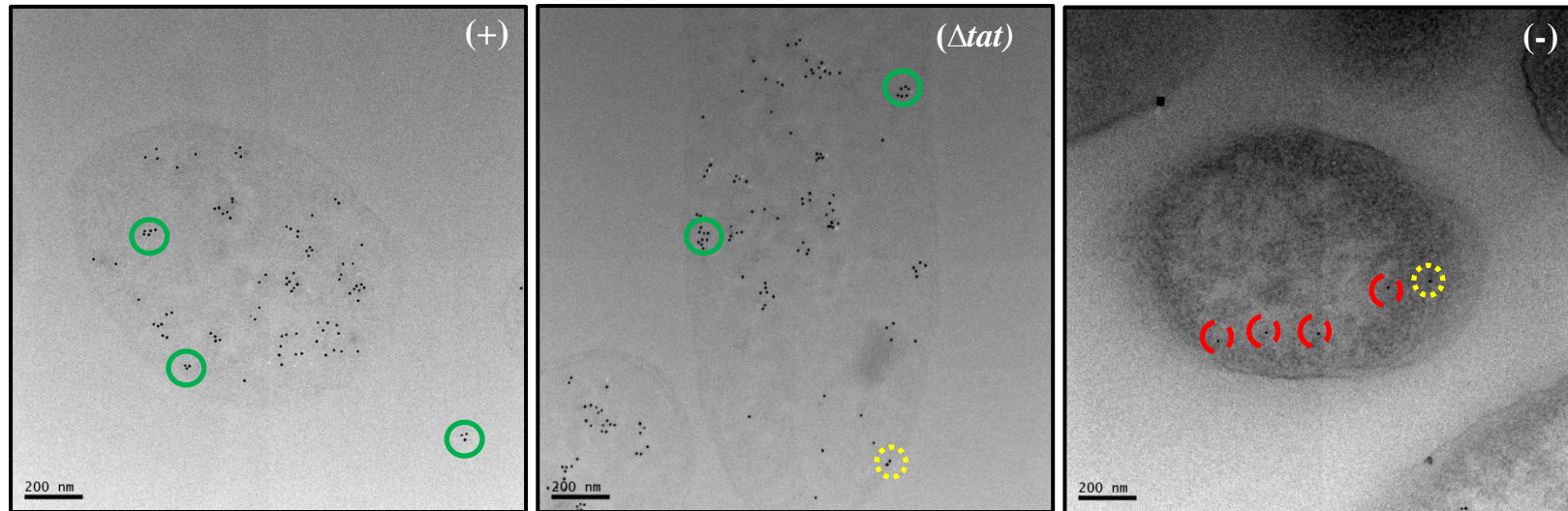
Figure 5.2.15. Electron micrographs of *E. coli* cells, overexpressing TatABC, blocked with an addition of 1% avidin

E. coli cells (overexpressing TatABC) were blocked in buffer containing 4% normal goat sera **and** 1% avidin and subsequently immunolabelled using an anti-strep primary antibody. Controls: cells that had Tat machinery knocked-out [labelled (Δ*tat*)] and (+) cells that had the primary antibody omitted [labelled **(-)**].Yellow-dash = inner membrane binding. Red-dash= cytoplasmic binding. Green= clustering of immunogold. The presence of 1% avidin worsened the non-specific binding in light of the increase in gold in both (Δ*tat*) and (-) samples. Clustering of the gold was noticeable. Images were taken on JEOL 2010F TEM at 12,000X magnification. Scale bar = 200 nm.

132

Next, in attempt to improve antigenicity retained at the end of the chemical fixation and staining process (and thus gold binding at the inner membrane), TatA and TatABC overexpressing cells were prepared in varying concentrations of fixatives (§2.10.1.5). Disappointingly, each new fixative failed to improve antigenicity in both TatA and TatABC samples such that the (+) and Δtat samples were indistinguishable by eye (Figures 5.2.16 and 5.2.17).

From results obtained so far, it is clear that the despite the alteration of numerous variables, the primary antibodies used to label TatA and TatABC overexpressing cells are not suitable for immunogold labelling studies of acrylic sections. Therefore different primary antibodies were tested.

Fractionation of TatABC overexpressing cells and immunoblotting with a different anti-Strep antibody showed TatC-strep to reside solely within the membrane, and Δtat cells to lack any strep-tagged proteins in either compartment (Figure 5.2.18). The corresponding EM micrographs (Figure 5.2.20) show that there was no difference in amount of gold bound to (+) samples, and gold still bound in considerable amounts to the Δtat cells. Therefore the second anti-strep antibody did not produce significant differences in abundance or localisation of gold binding.

TatA was detected only in the cytoplasm and membrane of TatA overexpressing cells (Figure 5.2.19). Electron micrographs of these cells immunolabelled with anti-TatA show a marked improvement in the amount of gold in (+) samples versus Δtat. However, non-specific binding was not completely eradicated since gold bound the inner membrane of Δtat cells (Figure 5.2.21).

In order to maximise antigenicity, TatA overexpressing cells were prepared in different fixatives and immunolabelled using the anti-TatA antibody. A small sampling study was conducted, whereby 50 randomly imaged *E. coli* had their raw gold counts counted. A multi-stage random sampling approach was adopted for unbiased sampling of *E. coli* cells (Figure 5.2.22). Each gold was assigned to the membrane or cytoplasmic region of the cell (Figure 5.2.23) Results show that the second fixative provided the highest ratio of gold at the membrane between (+) and Δtat cells. There were 8.57X more gold at the membrane of each (+) cell compared to Δtat. Therefore this fixative was used for all subsequent preparations of TatA overexpressing cells**.**
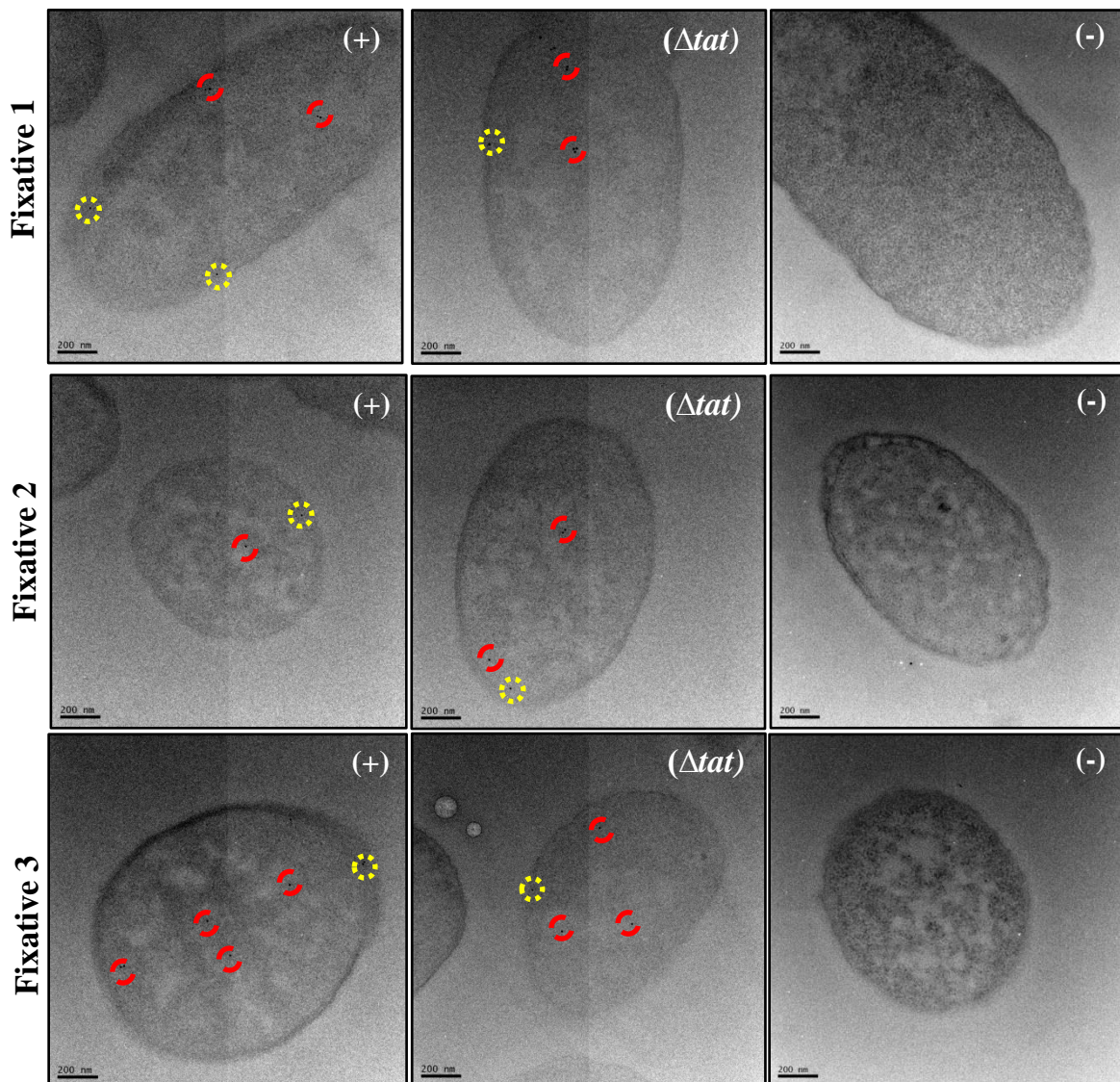
Figure 5.2.16. Electron micrographs of *E. coli* cells, overexpressing TatA, that have been chemically fixed in different combinations of aldehyde.

E. coli cells, overexpressing TatA, were immunolabelled using an anti-his primary antibody. **Fixative 1**: 0.5% glutaraldehyde/2% formaldehyde. **Fixative 2**: 0.25% glutaraldehyde/4% formaldehyde. **Fixative 3**: 2% glutaraldehyde/2% formaldehyde. Controls: cells that had Tat machinery knocked-out [labelled **(Δtat)**] and (+) cells that had the primary antibody omitted [labelled **(-)**]. Yellow-dash = inner membrane binding. Red-dash = cytoplasmic binding. None of the fixatives improved antigenicity. Each fixative had low gold density. Images were taken on JEOL 2010F TEM at 12,000X magnification. Scale bar = 200 nm.

Figure 5.2.17.Electron micrographs of *E. coli* cells, overexpressing TatABC, that have been chemically fixed in different combinations of aldehyde.

E. coli cells, overexpressing TatABC, were immunolabelled using an anti-strep primary antibody. **Fixative 1**: 0.5% glutaraldehyde/2% formaldehyde. **Fixative 2**: 0.25% glutaraldehyde/4% formaldehyde. **Fixative 3**: 2% glutaraldehyde/2% formaldehyde. Controls: cells that had Tat machinery knocked-out [labelled **(Δ*tat*)**] and (+) cells that had the primary antibody omitted [labelled **(-)**]. Yellow-dash = inner membrane binding. Red-dash = cytoplasmic binding. None of the fixatives improved antigenicity. Each fixative had low gold density. Images were taken on JEOL 2010F TEM at 12,000X magnification. Scale bar = 200 nm.

Figure 5.2.18. Cytoplasmic and membrane fractions of *E. coli* cells (overexpressing TatABC) immunoblotted for the detection of strep-tagged proteins using a different anti-Strep antibody. *E. coli* cells overexpressing TatABC were fractionated into cytoplasmic and inner membrane fractions. The fractions were resolved by SDS PAGE and immunoblotted to detect for the presence of strep-tagged proteins. The control was *E. coli* cells that have had Tat machinery knocked-out (Δtat). Strep-tagged TatABC was identified in only the membrane fraction of (+) cells.
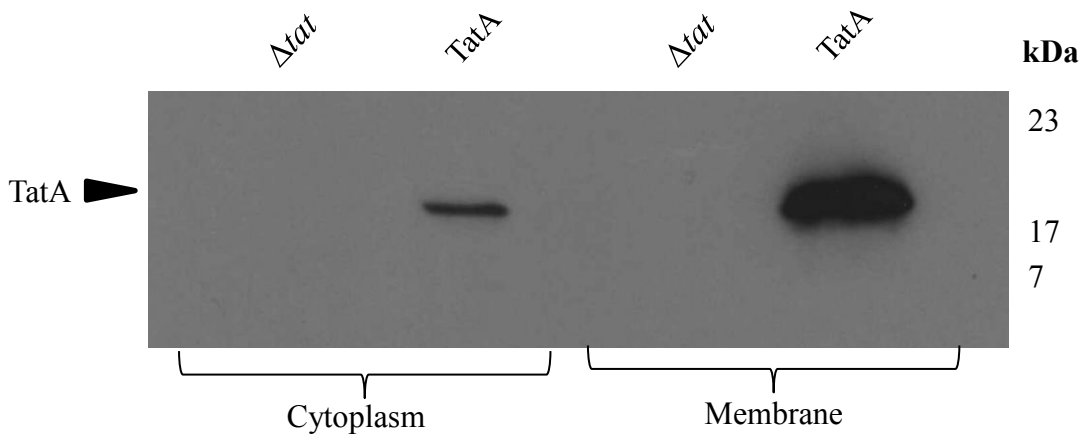
Figure 5.2.19. Cytoplasmic and membrane fractions of *E. coli* cells (overexpressing TatA) immunoblotted for the detection of TatA protein using anti-TatA antibody. *E. coli* cells overexpressing TatA were fractionated into cytoplasmic and inner membrane fractions. The fractions were resolved by SDS PAGE and immunoblotted to detect for the presence of TatA protein. The control was *E. coli* cells that have had Tat machinery knocked-out (Δtat). TatA protein was identified in the cytoplasm and membrane of (+) cells.
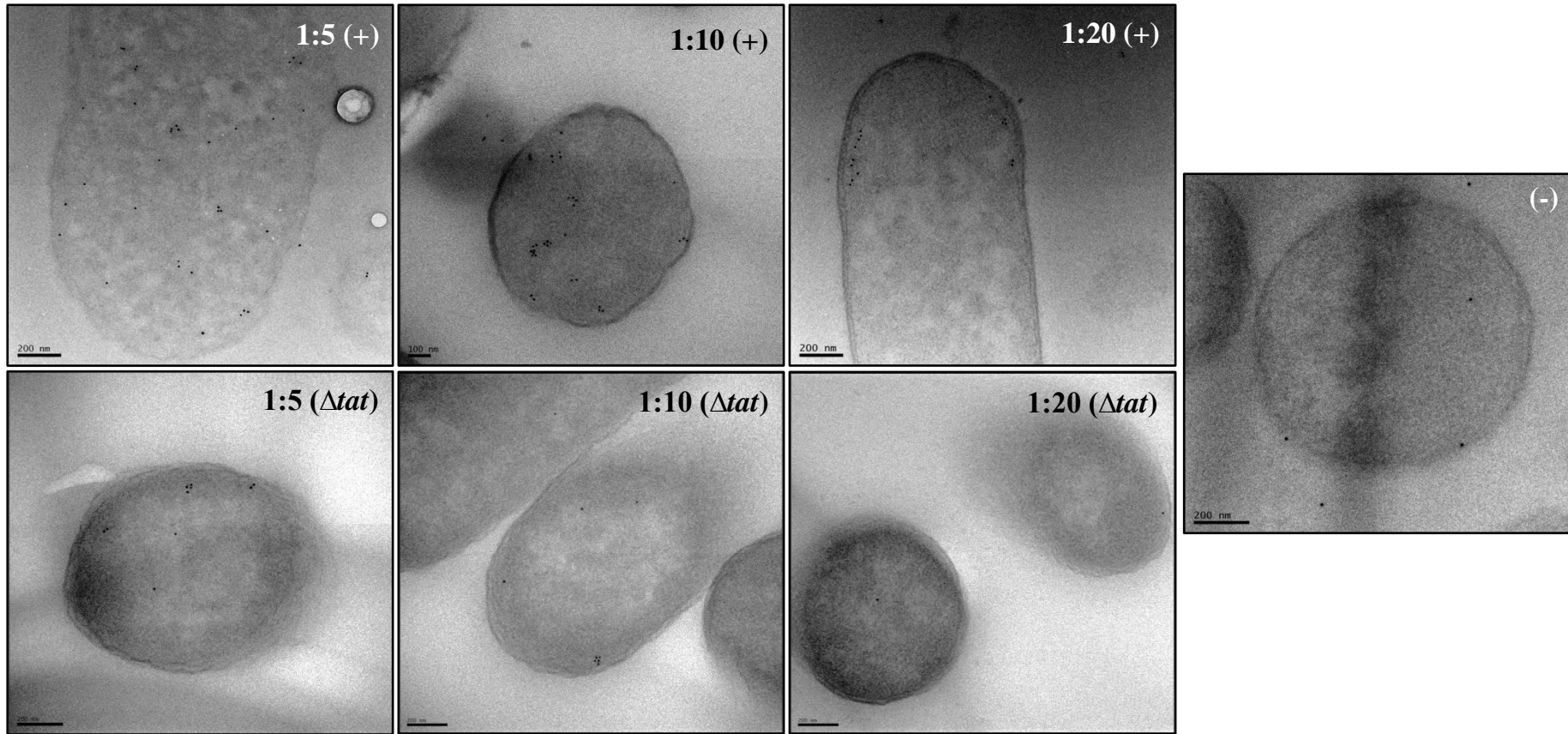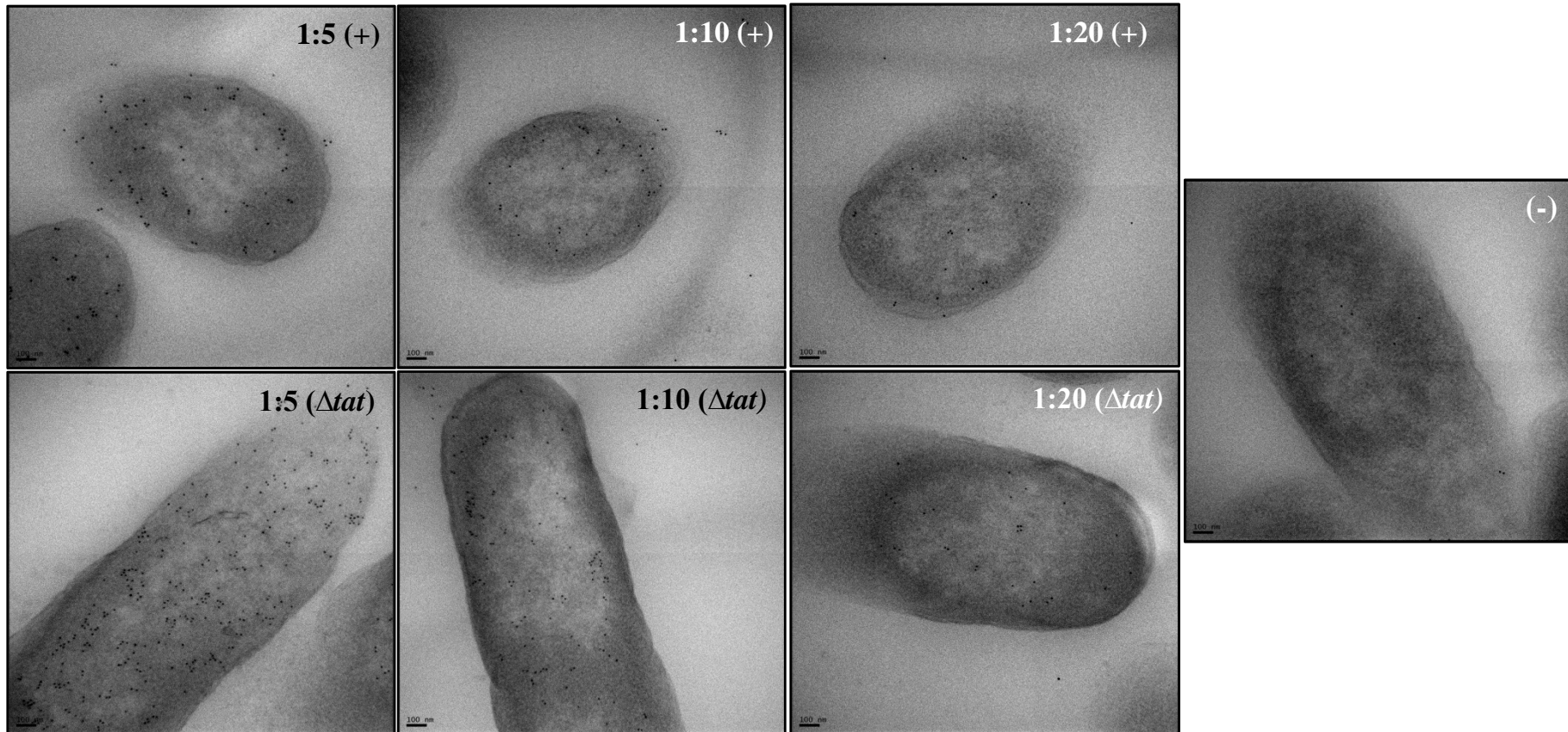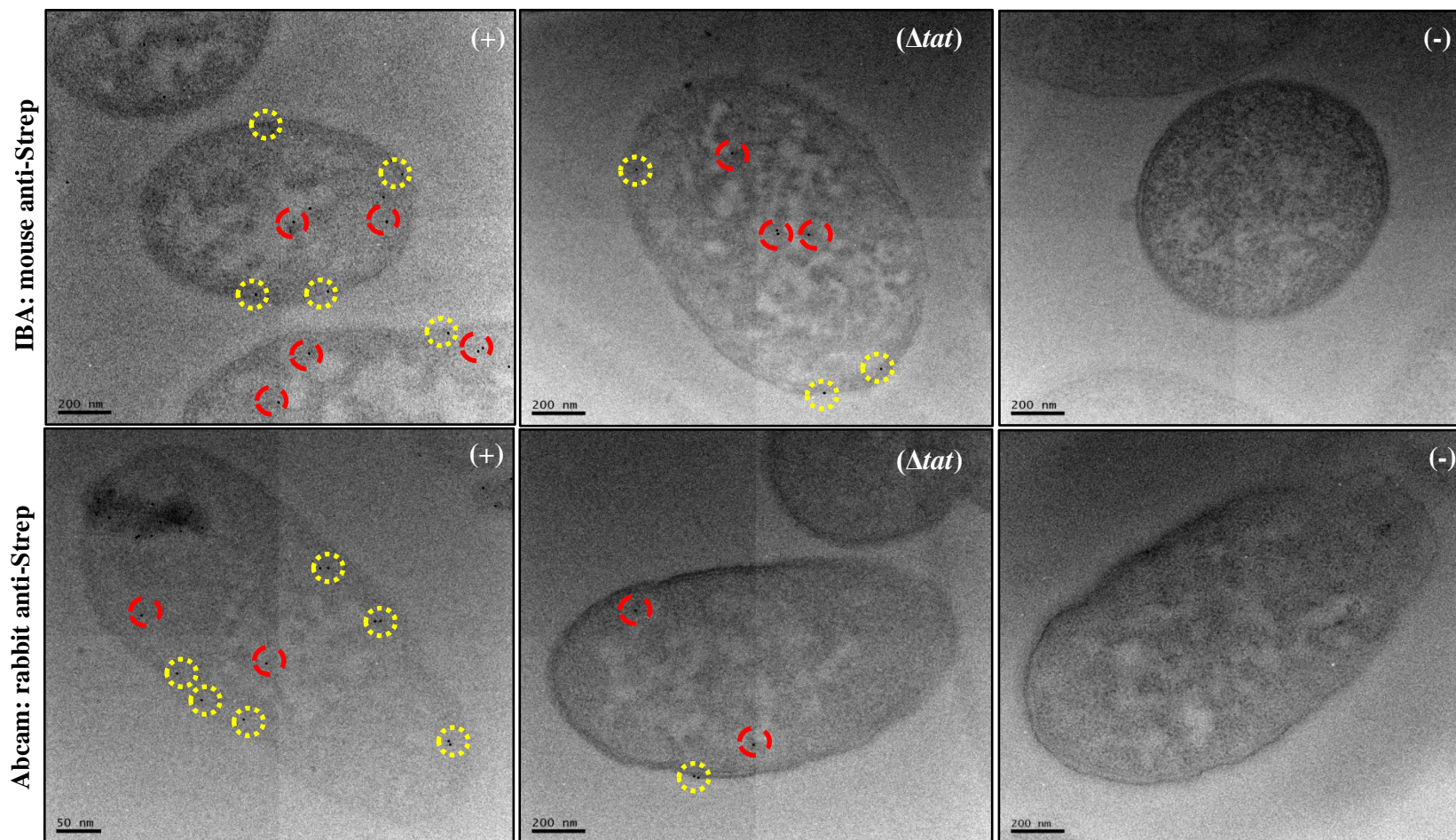
Figure 5.2.20. Electron micrographs of *E. coli* cells, overexpressing TatABC, immunolabelled using a different primary antibody

E. coli cells, overexpressing TatABC, were immunolabelled using a new anti-strep primary antibody. Controls: cells that had Tat machinery knocked-out [labelled (Δ*tat*)] and (+) cells that had the primary antibody omitted [labelled **(-)**].IBA was the provider of the first anti-strep antibody (top row). Abcam was the provider of the second anti-strep antibody (bottom row). Both antibodies had the same final concentrations of 50 ug/ml. Yellow-dash = inner membrane binding. Red-dash = cytoplasmic binding. The 'new' Abcam antibody did not produce significant differences in abundance or localisation of gold binding. Images were taken on JEOL 2010F TEM at 12,000X magnification. Scale bar = 200 nm.
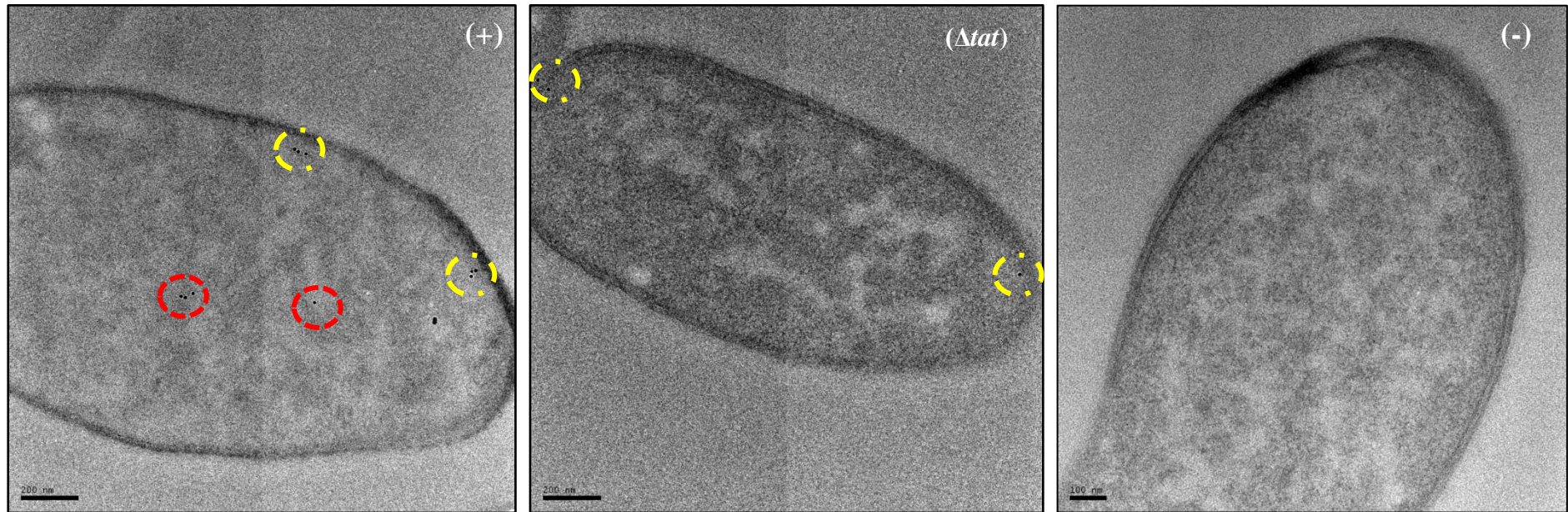
Figure 5.2.21. Electron micrographs of *E. coli* cells, overexpressing TatA, immunolabelled using a different primary antibody
E. coli cells, overexpressing TatA, were immunolabelled using a anti-TatA primary antibody. Controls: cells that had Tat machinery knocked-out [labelled **(Δ*tat*)**] and (+) cells that had the primary antibody omitted [labelled **(-)**]. Despite the anti-TatA antibody binding non-specifically to (Δ*tat*) cells, the cells were distinguishable from (+) cells since they had less gold bound at the inner membrane. No gold bound to (-) sample showed that any non-specific binding in other samples was attributable to primary antibody. Yellow-dash = inner membrane binding. Red-dash = cytoplasmic binding. Images were taken on JEOL 2010F TEM at 12,000X magnification. Scale bar = 200 nm
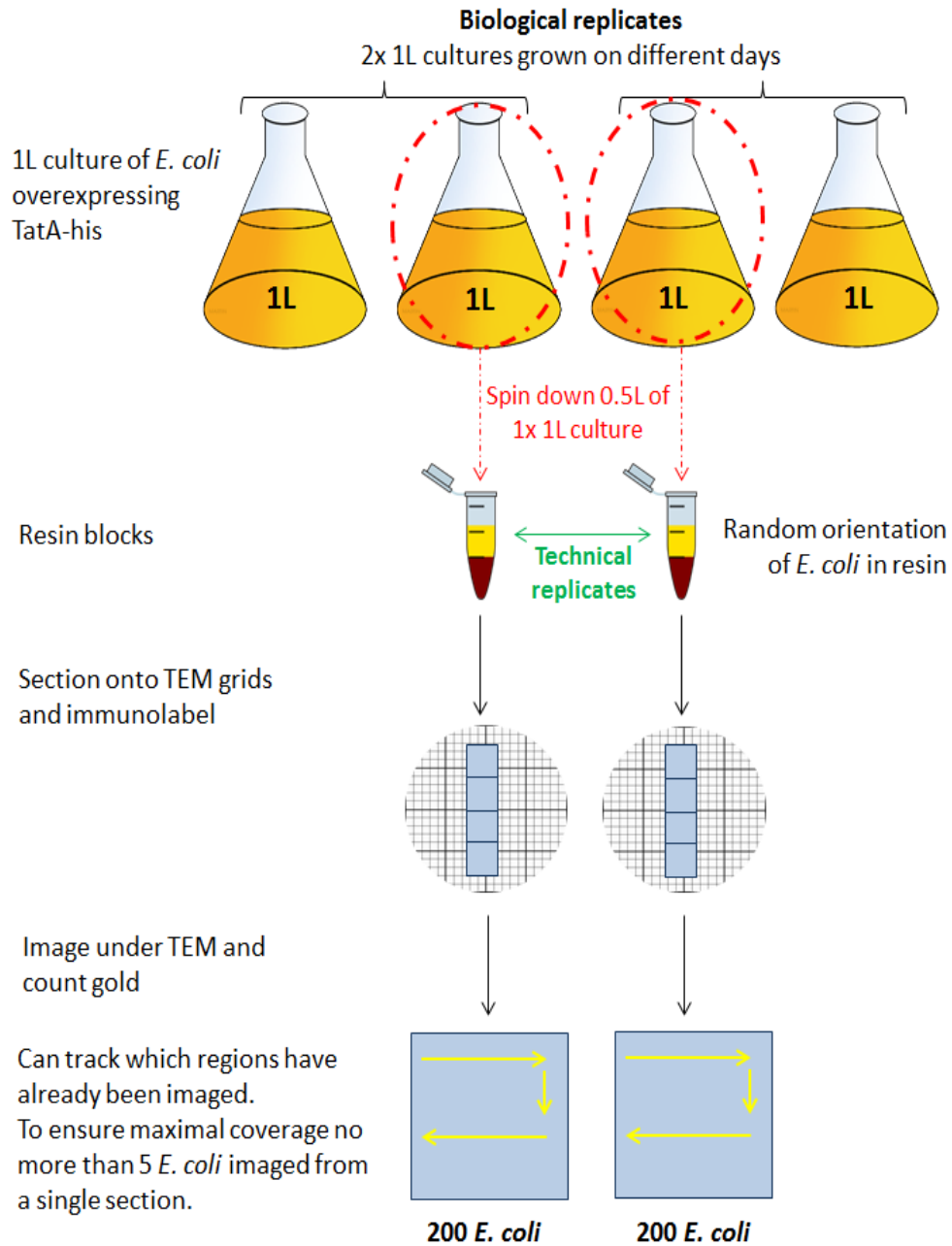
Figure 5.2.22. Schematic depicting the multi-stage random sampling process of *E. coli* cells overexpressing TatA cells.

E. coli specimens are sampled in a hierarchical fashion commencing at the liquid culture stage. Of the two cultures grown, one shall be randomly selected and only 0.5L of that chosen culture shall be harvested for subsequent processing. Since the orientation of *E. coli* within the resin block cannot be controlled, the cellular structures exposed upon sectioning with diamond knife are absolutely random. When under the TEM the top section shall be imaged first and work in a serpentine fashion throughout the sections until 200 *E. coli* are imaged. The sampling experiment shall also be conducted in duplicate.
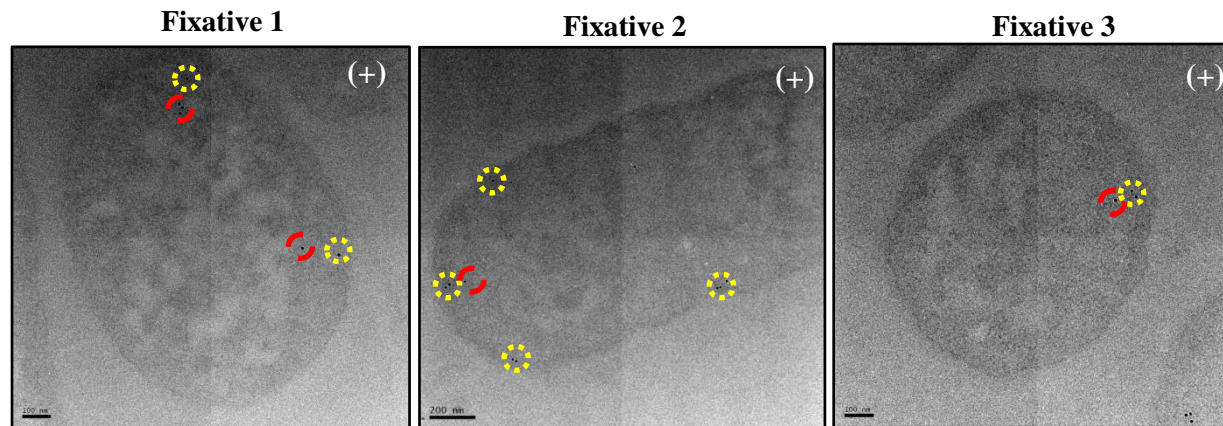
	Fixative 1		Fixative 2		Fixative 3	
	TatA	**Δ*tat***	**TatA**	**Δ*tat***	**TatA**	**Δ*tat***
E. coli	50	50	50	50	50	50
Total gold count	107	25	166	25	102	21
Approx. gold per cell	2.14	0.5	3.32	0.5	2.04	0.42
Total gold at inner membrane	27	11	60	7	29	5
Approx. **inner membrane** gold per cell	0.54	0.22	1.2	0.14	0.58	0.1
Difference in amount of gold at the inner membrane	(0.54)/(0.22)=2.45X		(1.2)/(0.14)=8.57X		(0.58)/(0.1)=5.8X	

Figure 5.2.23. Small-scale sampling of anti-TatA labelled *E. coli* cells that have been chemically fixed in different combinations of aldehydes.

E. coli cells, overexpressing TatA, were immunolabelled using an anti-TatA primary antibody. **Fixative 1**: 0.5% glutaraldehyde/2% formaldehyde. **Fixative 2**: 0.25% glutaraldehyde/4% formaldehyde. **Fixative 3**: 2% glutaraldehyde/2% formaldehyde. Controls were cells that had Tat machinery knocked-out (**Δ*tat***). Raw gold counts were taken from 50 randomly imaged *E. coli* and assigned to one of two cell compartments: inner membrane or cytoplasm. Total gold count was determined and consequently, the approximate gold per cell and gold per inner membrane of each cell was calculated (rows 3 and 5 of table). Quantitative data confirmed fixative 2 retained the best antigenicity since it had the most gold in the inner membrane of each cell (electron micrographs, middle).

Interim summary:

The anti-his and anti-strep antibodies were not good enough for pursuit of array tomography with immunogold labelled *E. coli* cells, since they bound non-specifically to the sections. In contrast, small-scale sampling studies revealed the anti-TatA antibody to unambiguously identify TatA.

5.2.3. TatA exhibits a uniform distribution in the inner membrane of *E. coli* in cells overexpressing only TatA

The distribution of TatA was examined in wild type cells over-expressing TatA. Again, Δtat cells were used as controls for non-specific binding. We first analysed cytoplasmic and membrane fractions to determine the proportion of TatA in the cytoplasm, by immunoblotting cell fractions. The data are shown in Figure 5.2.19, with cells over-expressing TatA. The vast majority of the TatA is found in the membrane fraction as expected. A small proportion (about 10%) is found in the cytoplasm, as observed in previous studies (Berthelmann *et al.*, 2008). As expected, no signal was obtained in blots of Δtat cells.

Immunogold labelling was conducted to identify and localise the Tat complex in *E. coli* cells. Our aim was to achieve unambiguous identification of TatA protein in the inner membrane through immunogold labelling of *E. coli* cells overexpressing TatA. Firstly, the level of non-specific antibody labelling was assessed by comparing the level of gold binding between TatA-overexpressing cells and cells that do not express Tat machinery (Δtat). The images were examined for the presence of gold particles and these were then classified according to their location.

Figure 5.2.25 (montage) shows representative images. The TatA-overexpressing cells (fixed in 0.25% glutaraldehyde/4% formaldehyde (fixative 2)) exhibit a pattern of gold labelling that is predominantly around the periphery and magnification of these images (not shown) confirmed that these particles were almost entirely in the inner membrane. A smaller number of particles are evident in the cell interior (Figure 5.2.24 and 5.2.25, red circles). Analysis of Δtat cells shows the presence of a small

number of gold particles in the cytoplasmic region with hardly any in the membranes (Figure 5.2.24.). These data confirm that the antibody is able to detect TatA with a high degree of specificity. As further controls, TatA-expressing cells were immunolabelled with the primary antibody omitted (Figure 5.2.24, labelled (-)), and TEM analysis showed that these cells lacked any gold binding; confirming that non-specific binding seen in Δ*tat* cells was attributable to the primary antibody. Finally, the same cell type was immunolabelled with a gold conjugated-secondary antibody directed towards a different animal species (Figure 5.2.24, (-)2). TEM analysis showed only unlabelled *E. coli* cells, confirming that the cells do not have a non-specific attraction for gold particles.
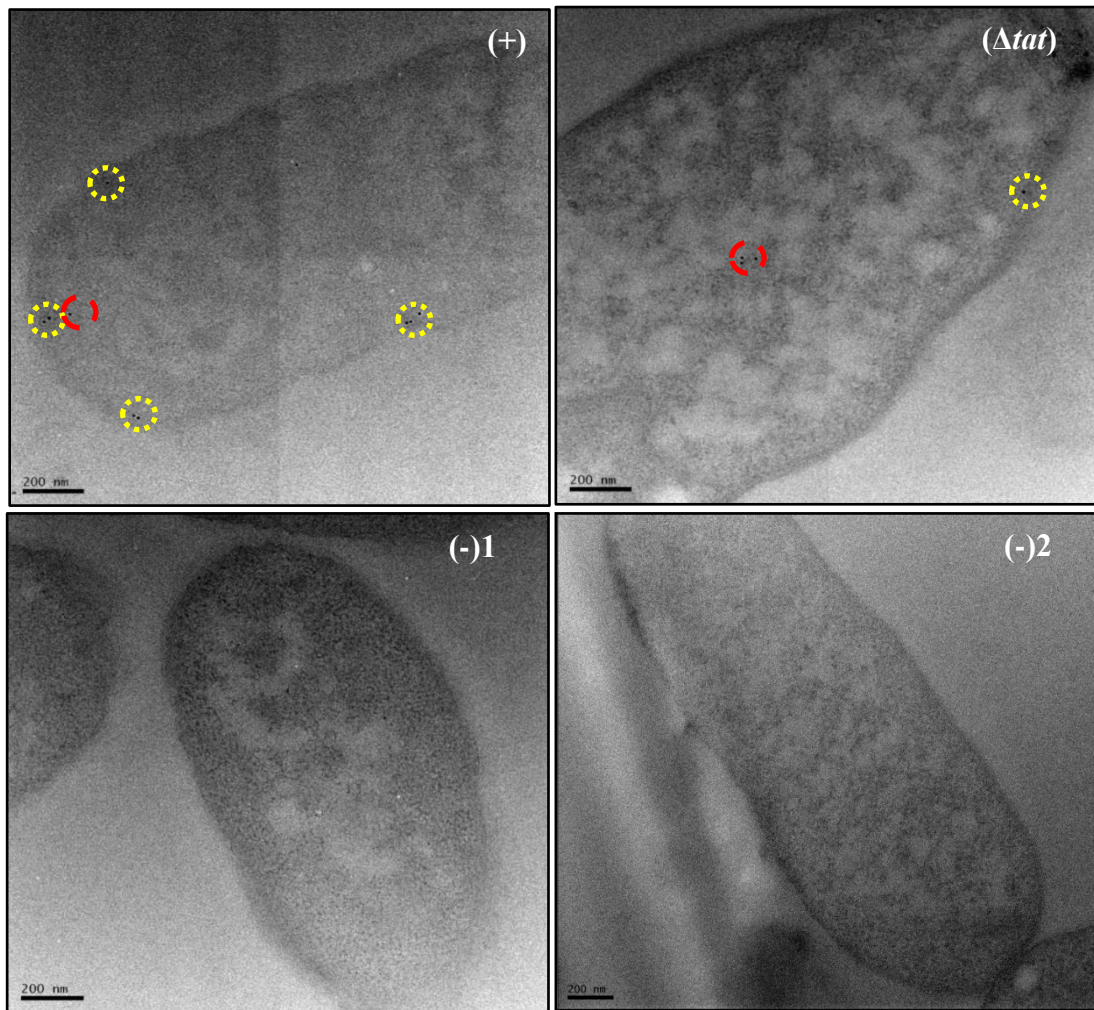
Figure 5.2.24. Electron micrographs of *E. coli* cells, overexpressing TatA, immunogold-labelled following primary antibody detection against TatA protein.

E. coli cells overexpressing TatA, were immunolabelled using a primary antibody raised against the TatA protein [labelled (+)].Controls: cells that had Tat machinery knocked-out [labelled **(Δtat)**]; (+) cells that had the primary antibody omitted [labelled **(-1)**], and (+) cells immunolabelled using a different secondary antibody [labelled **(-2)**]. Raw gold counts were taken from 200 randomly imaged *E. coli* from 2 separate resin blocks. Gold was assigned to either inner membrane compartments (yellow-dotted) or cytoplasm (red-dotted) for subsequent statistical analysis. Images were taken on JEOL 2010F TEM at 12,000X magnification. Scale bar = 200 nm.

Figure 5.2.25. Montage of electron micrographs of *E. coli* cells, overexpressing TatA, immunogold-labelled following primary antibody detection against TatA protein. *E. coli* cells overexpressing TatABC were immunolabelled using a primary antibody raised against the TatA protein. The montage gives an overview of *E. coli* cells sectioned at different angles. TatA protein was found to exhibit a uniform distribution in the inner membrane (yellow circles) with some gold found in the cytoplasm (red circles). Images were taken on JEOL 2010F TEM at 12,000X magnification. Scale bar = 200nm.

Raw gold counts were collected from 200 randomly sampled, immunolabelled *E. coli* TatA-overexpressing and *Δtat E. coli* cells. Gold particles were assigned to either cytoplasmic or inner membrane compartments. Quantification of the gold particles (Figure 5.2.26.) shows that the average number of gold particles per compartment in TatA-overexpressing cells was 1.57 per cell in the cytoplasm and 0.99 per cell in the inner membrane, whereas *Δtat* cells bound approximately 0.595 in the cytoplasm and 0.075 particles in the membrane per cell, respectively (Figure 5.2.26, B). The labelling of the membrane bound TatA is thus highly specific; the inner membrane of TatA-overexpressing cells contains 13.2x more gold particles than the membrane of Δ*tat* cells. To confirm a statistical difference in immunogold labelling between these cells at the cytoplasm and inner membrane, Chi-squared analysis of the raw gold count data was conducted; for a total chi-squared value of 35.25 and 1 degree of freedom, P was less than 0.005. This confirms that the gold labelling distributions between the two cells types are significantly different.

Importantly, the gold particles are randomly distributed within the membrane, with no evidence for a preferential localisation within the *E. coli* cell. The TatA is overexpressed to a considerable extent and is therefore in massive excess over the endogenous TatBC complex, and therefore TatA on its own has no intrinsic preference for a specific location in the membrane.

Analysis of the distribution of gold particles in the cytoplasm shows the presence of 1.57 and 0.595 particles in the TatA-overexpressing and *Δtat* cells, respectively. Since the particle number in *Δtat* cells represents nonspecific binding, and assuming that the level of nonspecific binding in the 2 cell types is identical, this indicates that TatA-overexpressing cells contain an average of 0.975 particles per cell in the cytoplasm, which is approximately the same number as in the inner membrane. Some of these particles can be attributed to genuinely cytoplasmic TatA, as shown in the blots in Figure 5.2.19., but the particle count for the cytoplasmic TatA is still surprising because blots showed the majority of TatA to be in the membrane fraction. It is unclear why the gold particle count is so high in the cytoplasm of these cells and this observation bears further examination. Therefore, the approach provides highly specific detection of TatA in the membrane fraction, whereas labelling of cytoplasmic TatA is higher than expected.

A

	TatA	Δ*tat*
E. coli	200	200
Raw Gold count TOTAL	512	132
Raw Gold count at inner membrane	198	15
Approx. inner membrane gold per cell	0.99	0.075
Difference in the amount of gold at the inner membrane per cell	0.99 / 0.075 = 13.2X	

B
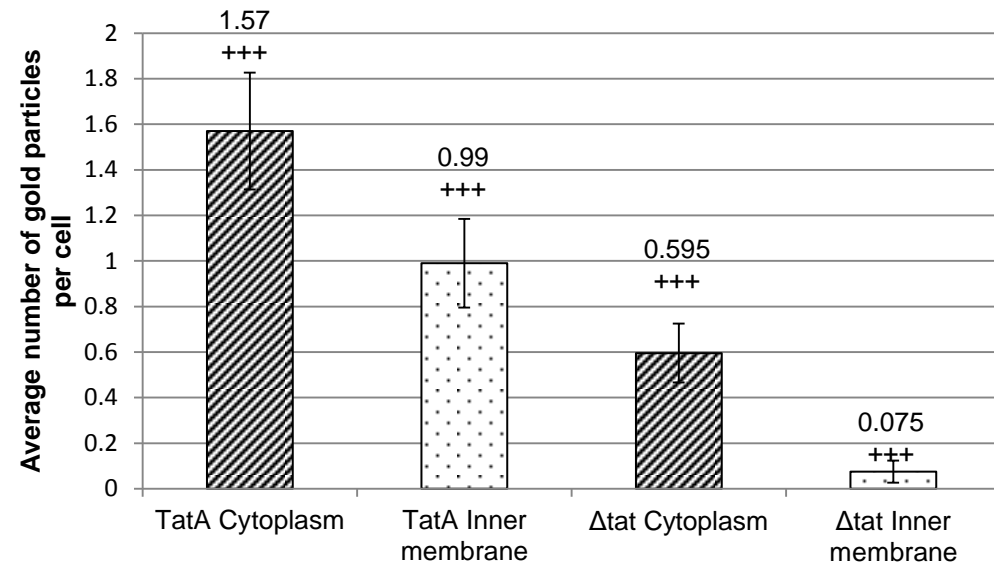
C

Subcellular compartments	TatA		Δ*tat*		Row totals	Chi-squared values	
Inner membrane	198	(169.3)	15	(43.66)	213	4.850	18.81
Cytoplasm	314	(342.6)	117	(88.34)	431	2.397	9.297
Column totals	512		132		644	35.36	

Figure 5.2.26. Quantitative analysis of raw gold counts of *E. coli* cells immunogold labelled with primary antibody detection against TatA protein.
E. coli cells overexpressing TatA, were immunolabelled using a primary antibody raised against the TatA protein. Controls were cells that had Tat machinery knocked-out [labelled **(Δ*tat*)**]. A: Raw gold counts were taken from 200 randomly imaged *E. coli* from 2 separate resin blocks. Gold was assigned to either inner membrane or cytoplasm compartment. The approximate number of gold at the inner membrane and cytoplasm of each cell was calculated, and subsequently the difference between the two cell types. B: The difference in average number of gold particles at the cytoplasm or inner membrane of each cell type is shown. Error bars: CI of 2xSE. C: Statistical analysis of raw gold counts. Values represent observed and (expected) numbers of 10 nm gold particles in the two different cell types. For a total chi-squared of 35.36 and 1 degree of freedom, $P<0.005$ (indicated by +++ on graph); hence the two labelling distributions are significantly different.

5.2.4. Increased expression of TatBC protein alters the distribution of TatA protein in the inner membrane of *E. coli*

The distribution of TatA complexes was also examined in cell overexpressing the TatABC operon. This approach was taken so that we could test whether the presence of stoichiometric levels of the TatBC complex affects the distribution of TatA complexes. Fractionation of *E. coli* cells overexpressing TatABC mirrored the results of previous data showing that TatA is present within the cytoplasmic and membrane fraction of these cells (Figure 5.2.29.). These cells were then immunolabelled with anti-TatA antibody. Analogous to previous immunolabelling experiments, Δ*tat* cells served as important negative controls. These cells showed gold binding, albeit very little, at the cytoplasmic and inner membrane regions (Figure 5.2.27). Representative images are shown in Figure 5.2.28 (montage), with the quantified data shown in Figure 5.2.30. The data show that TatABC-overexpressing cells bound on average 1.25 gold particles per cell in the cytoplasm and 0.85 particles at the inner membrane, whereas Δ*tat* cells bound approximately 0.60 particles per cell in the cytoplasm and 0.075 particles in the membrane. The data thus show that the TatABC cells bind approximately 11.3x more gold at the inner membrane than do Δ*tat* cells, again confirming that the technique is able to detect the TatA with high specificity in these cells. The overall levels of TatA are fairly similar: 0.85 particles per cell in TatABC-overexpressing cells and 0.99 in TatA-overexpressing cells bound, which shows that expression of TatBC does not increase the levels of TatA in the membrane.

Chi-squared analysis confirmed a statistical difference in immunogold labelling between TatABC-overexpressing and Δ*tat* cells in both the cytoplasm and inner membrane: for a total chi-squared of 39.2 and 1 degree of freedom, $P<0.005$. Mirroring the findings of TatA-overexpressing cells, evidence for non-specific binding of the TatA antibody was found, since TatABC-overexpressing cells bound 1.25 particles per cell in the cytoplasm, while Δ*tat* cells bound 0.59 particles. This again, is contrary to the relatively low levels of cytoplasmic TatA observed on the blots.

Figure 5.2.27. Electron micrographs of *E. coli* cells, overexpressing TatABC, immunogold-labelled following primary antibody detection against TatA protein.

E. coli cells overexpressing TatABC, were immunolabelled using a primary antibody raised against the TatA protein [labelled (+)].Controls: cells that had Tat machinery knocked-out [labelled (Δ*tat*)]; (+) cells that had the primary antibody omitted [labelled **(-1)**], and (+) cells immunolabelled using a different secondary antibody [labelled **(-2)**]. Raw gold counts were taken from 200 randomly imaged *E. coli* from 2 separate resin blocks. Gold was assigned to either inner membrane compartments (yellow-dotted) or cytoplasm (red-dotted) for subsequent statistical analysis. Images were taken on JEOL 2010F TEM at 12,000X magnification. Scale bar = 200 nm.

Figure 5.2.28. Montage of electron micrographs of *E. coli* cells, overexpressing TatABC, immunogold-labelled following primary antibody detection against TatA protein. *E. coli* cells overexpressing TatABC were immunolabelled using a primary antibody raised against the TatA protein. The montage gives an overview of *E. coli* cells sectioned at different angles. TatA protein was found to exhibit a uniform distribution in the inner membrane (yellow circles) with some gold found in the cytoplasm (red circles). Images were taken on JEOL 2010F TEM at 12,000X magnification. Scale bar = 200nm.
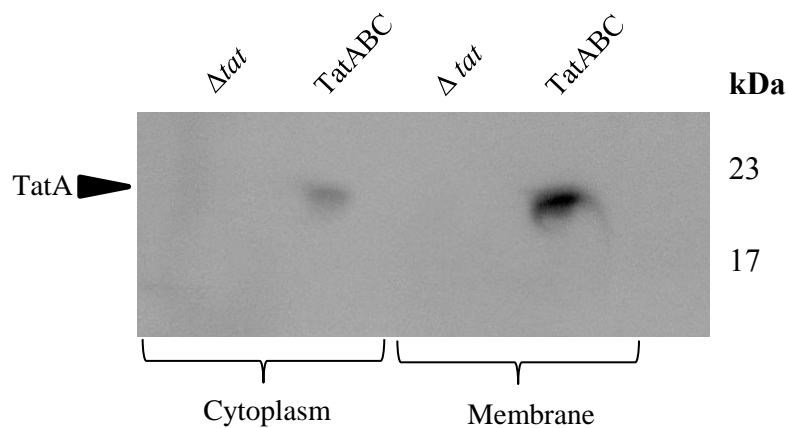
Figure 5.2.29. Cytoplasmic and membrane fractions of *E. coli* cells (overexpressing TatABC) immunoblotted for the detection of TatA protein.

E. coli cells overexpressing TatABC were fractionated into cytoplasmic and inner membrane fractions. The fractions were resolved by SDS PAGE and immunoblotted to detect for the presence of TatA protein. The control was *E. coli* cells that have had Tat machinery knocked-out (Δ*tat)*. Anti-TatA antibody identified TatA protein in both the cytoplasm and membrane of TatABC over-expressing cells.

A

	TatABC	Δ*tat*
E. coli	200	200
Raw Gold count TOTAL	420	132
Raw Gold count at inner membrane	170	15
Approx. inner membrane gold per cell	0.85	0.075
Difference in the amount of gold at the inner membrane per cell	0.85 / 0.075 = 11.3X	

B
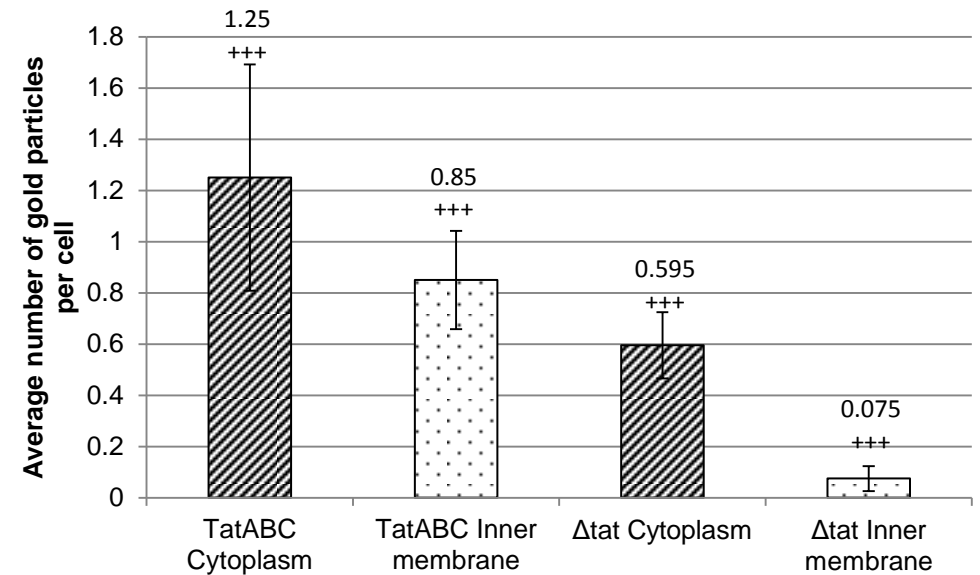
C

Subcellular compartments	TatABC		Δ*tat*		Row totals	Chi-squared values	
Inner membrane	170	(140.2)	15	(44.74)	185	6.309	19.78
Cytoplasm	250	(279.7)	119	(89.25)	369	3.163	9.914
Column totals	420		134		554	39.2	

Figure 5.2.30. Quantitative analysis of raw gold counts of *E. coli* cells immunogold labelled with primary antibody detection against TatA protein.
E. coli cells overexpressing TatABC, were immunolabelled using a primary antibody raised against the TatA protein. Controls were cells that had Tat machinery knocked-out [labelled (Δ*tat)*]. A: Raw gold counts were taken from 200 randomly imaged *E. coli* from 2 separate resin blocks. Gold was assigned to either inner membrane or cytoplasm compartment. The approximate number of gold at the inner membrane and cytoplasm of each cell was calculated, and subsequently the difference between the two cell types. B: The difference in average number of gold particles at the cytoplasm or inner membrane of each cell type is shown. Error bars: CI of 2xSE. C: Statistical analysis of raw gold counts. Values represent observed and (expected) numbers of 10 nm gold particles in the two different cell types. For a total chi-squared of 39.2 and 1 degree of freedom, $P<0.005$ (indicated by +++ on the graph); hence the two labelling distributions are significantly different.

With increased expression of TatBC proteins, immunogold labelling showed the TatA protein to exhibit a uniform distribution around the periphery of the cell in most cells, as shown in Figure 5.2.28. However, in 4% of the cells (4 cells out of 100 imaged) the distribution of TatA protein altered in the inner membrane, with a clustering of gold clearly observed (Figure 5.2.31). This distribution was not observed in any of the TatA-overexpressing cells. Quantitation of the number of TatA clusters in independently-sampled TatA-overexpressing and TatABC-overexpressing cells confirmed that the presence of clusters in the latter cell type was statistically significant (Figure 5.2.32).

Due to the nature of TEM analysis, the images are 2D projections; we do not have any idea of whether this clustering is consistent with an extension of TatA in the inner membrane in 3D space. This is something that array tomography can address.
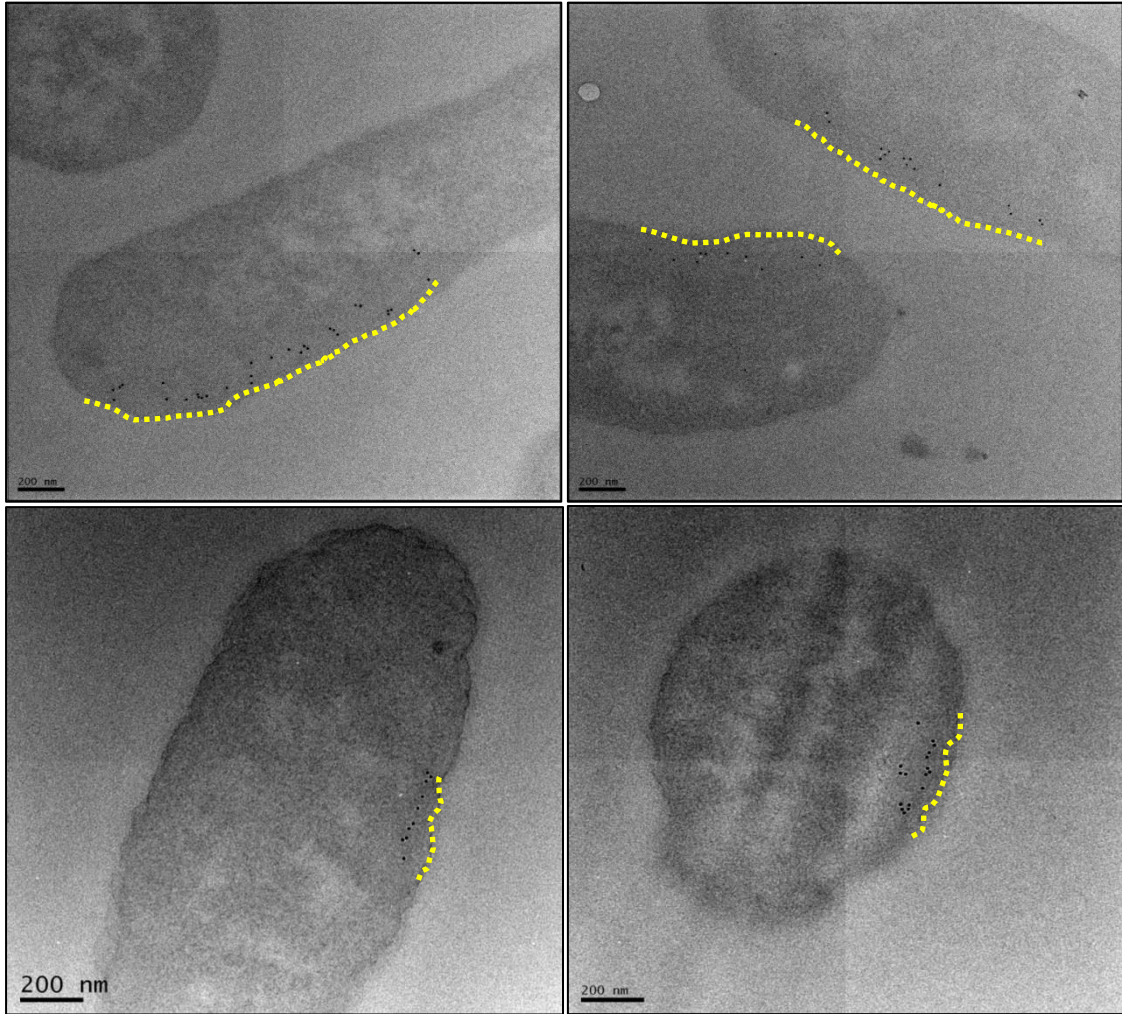
Figure 5.2.31. Electron micrographs of _E. coli_ cells, overexpressing TatABC, immunogold-labelled following primary antibody detection against TatA protein.

A) _E. coli_ cells overexpressing TatABC, were immunolabelled using a primary antibody raised against the TatA protein [labelled (+)].Controls: cells that had Tat machinery knocked-out [labelled (Δ_tat)_]; (+) cells that had the primary antibody omitted [labelled **(-1)**], and (+) cells immunolabelled using a different secondary antibody [labelled **(-2)**]. With increased expression of TatBC, the localisation of the TatA protein altered in approximately 1 in 25 of cells. TatA protein appeared to cluster along the inner membrane (highlighted in yellow). Images were taken on JEOL 2010F TEM at 12,000X magnification. Scale bar = 200 nm.
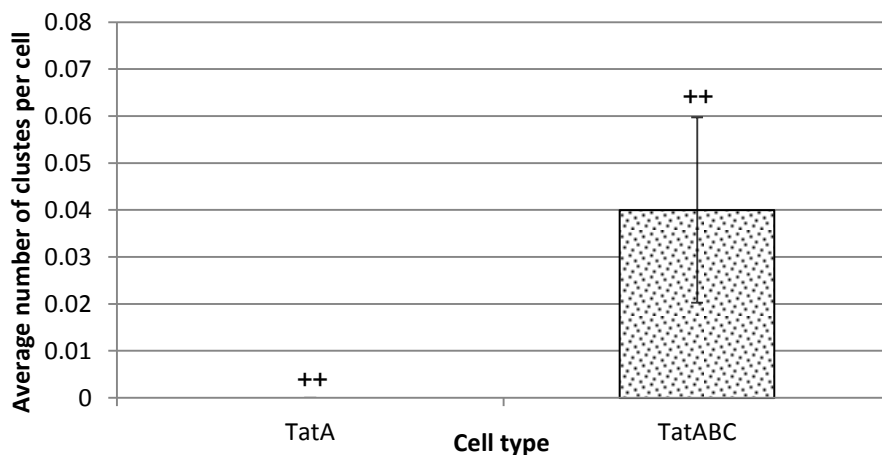
	TatA		TatABC		Row totals	Chi-squared values	
Cluster	0	(2.23)	4	(1.76)	4	2.23	2.83
Non-cluster	100	(97.7)	75	(77.23)	175	0.05	0.06
Column totals	100		79		179	5.18	

Figure 5.2.32 Statistical analysis of clustering of TatA in the inner membrane of *E. coli*. *E. coli* cells overexpressing TatA or TatABC were immunolabelled using a primary antibody raised against TatA protein. Top panel: count data for the presence of gold clustering along the inner membrane was collected from 100 randomly imaged *E. coli* (from 5 independently prepared samples). Subsequently the average number of clusters per cell was calculated for each cell type (top graph). Error bars: CI of 2xSE. Bottom panel: statistical analysis of count data. Values represent observed and (expected) numbers of TatA clustering in the inner membrane. For a total chi-squared of 5.18 and 1 degree of freedom, $P<0.01$ (indicated by ++ on graph); hence the labelling distribution of TatA clustering is significantly different between the two cell types.

5.2.5. The TatA protein of the Tat complex does not exhibit a polar localisation

Given that a protocol to unambiguously identify TatA in the inner membrane of *E. coli* had now been optimised; the polarity of the TatA protein was investigated. TatA-YFP was not found to localise to any sub regions of an *E. coli* cell (Leake *et al.*, 2008), whereas a later study using a TatA-GFP construct found TatA foci (complexed with TatB-mCherry) to have a tendency to move to the cell poles (Rose *et al.*, 2013). Whether the Tat complex or any of its constituents exhibits such localisation remains dubious since TatA-XFP fusions have been shown to be inactive (Alcock *et al.*, 2013; Leake *et al.*, 2008; Ray *et al.*, 2005).

Raw gold counts were taken from 200 randomly-sampled *E. coli* cells that had been longitudinally cross-sectioned (to ensure inner membrane of a polar localisation was captured). Gold was assigned to either a polar or non-polar localisation. A polar region was defined at the point in which the cell wall is non-linear (Figure 5.2.33., F, yellow dashed lines). The TatA protein was found to localise in the entire periphery of the cell (Figure 52.33., yellow circle), with no distinct polarity witnessed. Clustering of the TatA protein was found in both polar and non-polar locations (Figure 5.2.33., red circle). 638 TatA-bound gold was identified, over 70% (454) of which was NOT localised to the poles of the cell (Figure 5.2.34). T-test analysis confirmed a statistically significant difference between these cellular regions (P<0.01).
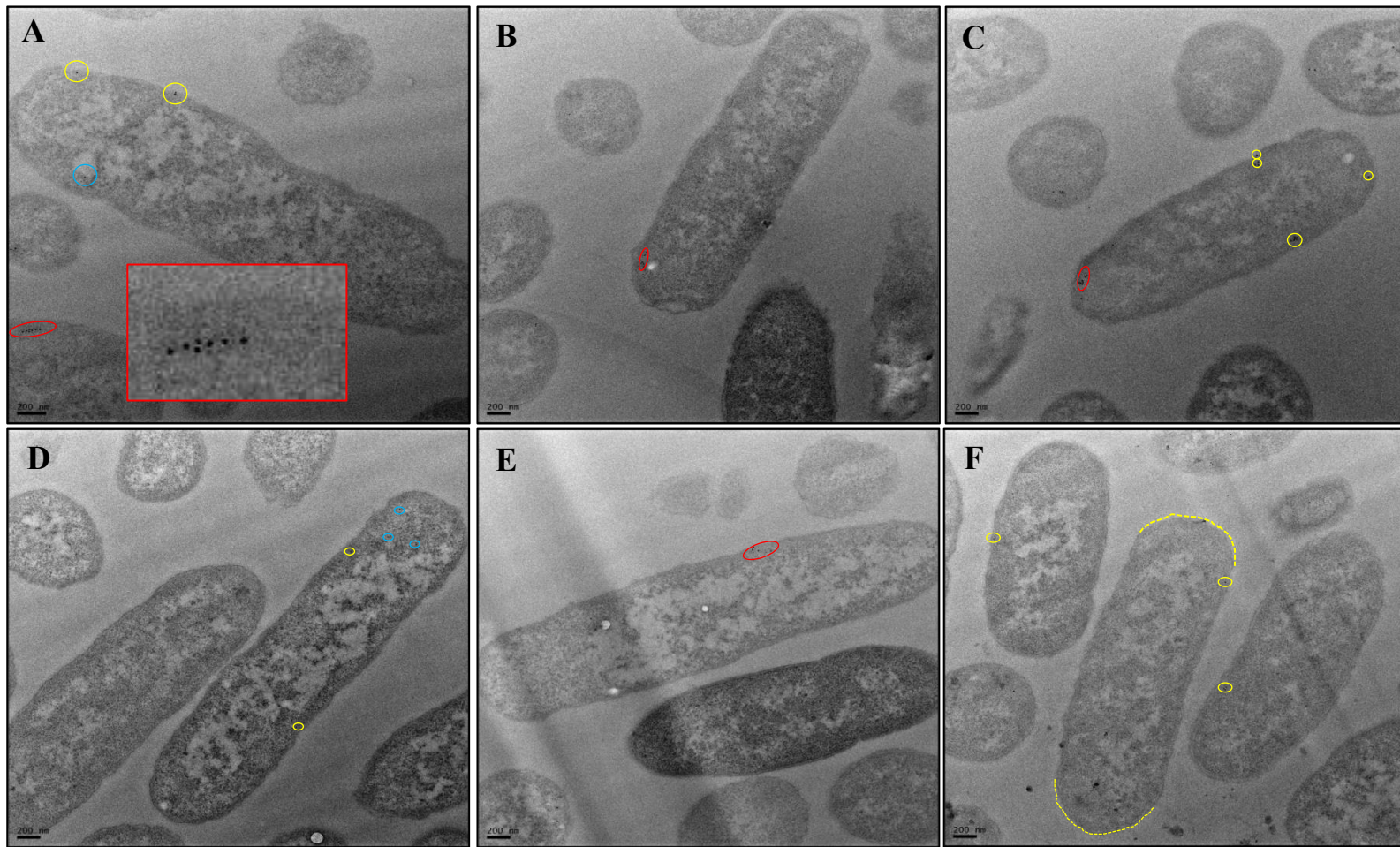
Figure 5.2.33. Electron micrographs of *E. coli* cells, overexpressing TatABC, immunogold-labelled following primary antibody detection against TatA protein to.
E. coli cells overexpressing TatABC, were immunolabelled using a primary antibody raised against the TatA protein [labelled (+)].Raw gold counts were taken from 200 randomly imaged *E. coli* (from 2 separate resin blocks) that had been longitudinally cross-sectioned. Gold was assigned to either polar or non-polar localisation. No polar localisation of TatA protein was apparent. Yellow circle = inner membrane binding. Blue circle = cytoplasmic localisation. Red ellipse = clustering at inner membrane. Images were taken on JEOL 2010F TEM at 12,000X magnification. Scale bar = 200 nm.

E. coli	172
Raw Gold count TOTAL	638
Raw Gold count at poles of cell	184
Raw Gold NOT at poles of the cell	454
Proportion of gold at the poles of the cell	28.84%
Proportion of gold NOT at the poles of the cell	71.16%
	100.00%
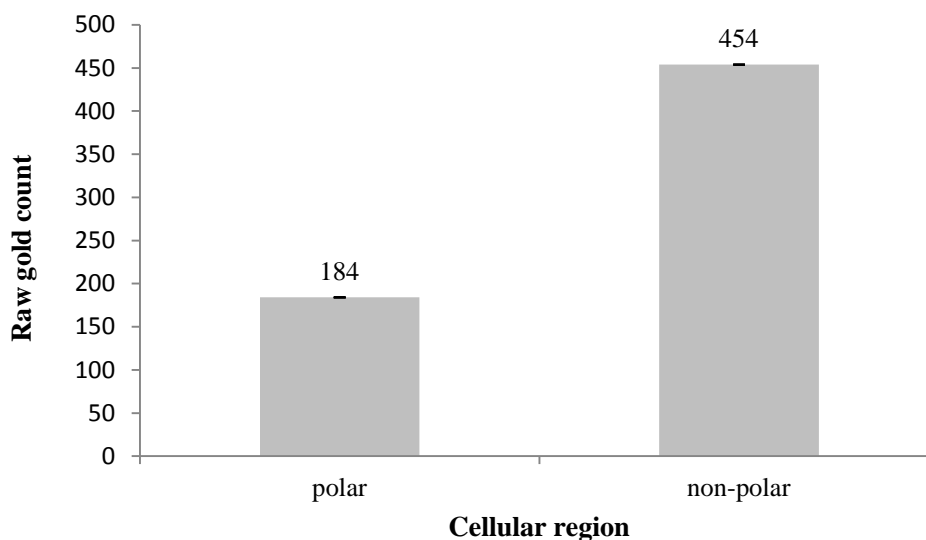
Figure 5.2.34. Quantitative analysis of raw gold counts of immunogold-labelled *E. coli* cells to determine polarity of Tat complex.

E. coli cells overexpressing TatABC were immunolabelled using a primary antibody raised against the TatA protein. Raw gold counts were taken from 200 randomly imaged *E. coli (*from 2 separate resin blocks) that had been longitudinally sectioned. Gold was assigned to either polar or non-polar localisation. The TatA protein does not appear to possess a polar localisation, with only 29% of gold being found at the poles of the bacterial cells. T-test analysis confirms a statistically significant difference between these cellular regions (P<0.01). Error bards = CI of 2x SE.

5.2.6. Wild-type levels of TatA protein are not detectable with immunogold labelling

It is unknown whether overexpression of recombinant Tat proteins alters the distribution or localisation of Tat machinery; therefore *E. coli* cells expressing wild-type levels of TatA were immunogold-labelled to detect any difference in TatA localisation or distribution at the inner membrane. Results show that no gold bound the *E. coli* cells (Figure 5.2.35.) and therefore overexpression of TatA protein is the only way that a sufficient amount of TatA proteins can be detected.
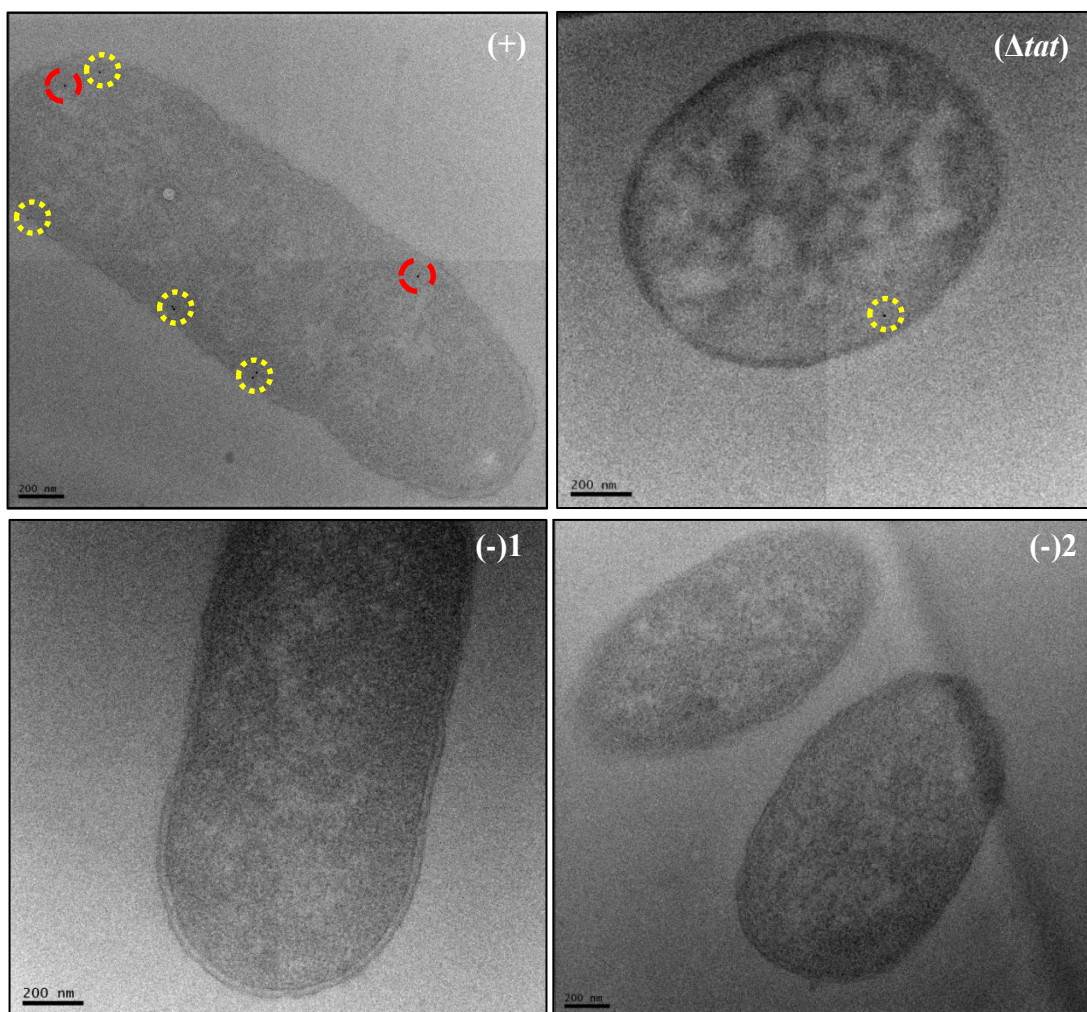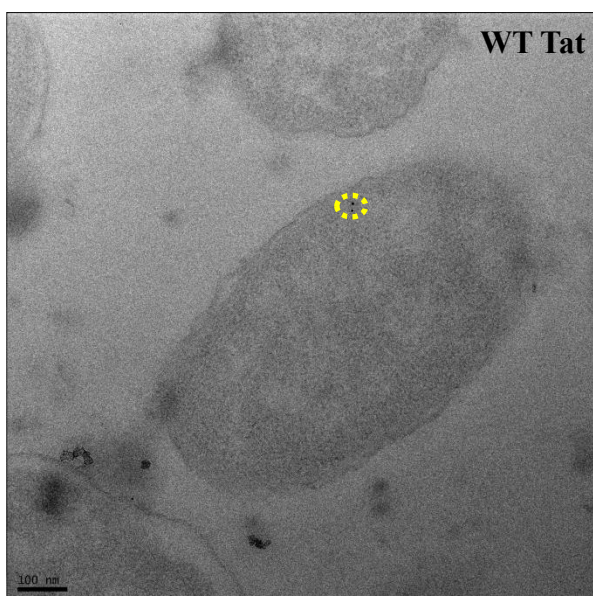

Figure 5.2.35. Electron micrograph of *E. coli* cells, overexpressing WT levels of Tat machinery, immunogold-labelled following primary antibody detection against TatA protein.
E. coli cells expressing WT levels of Tat protein were immunolabelled using a primary antibody raised against the TatA protein. There was an abundance of gold-free cells illustrating a lack of antigenic sites available for anti-TatA binding. Those that had bound antibody, the gold was localised predominantly at the inner membrane (highlighted in yellow). Images were taken on JEOL 2010F TEM at 12,000X magnification. Scale bar = 200 nm.

5.2.7. Array tomography reveals a linear clustering of TatA protein in the inner membrane of *E. coli*.

Having unambiguously identified TatA protein in the inner membrane of *E. coli*, 20 50 nm serial sections of resin-embedded *E. coli* overexpressing TatABC were sequentially imaged in the scanning electron microscope (Figure 5.2.36). A small 3x4 montage was imaged from each of the sections at 5000 x magnification (Figure 5.2.36.). Following alignment of the serial sections, the image stack was computationally segmented such that image stacks of individual *E. coli* cells were input into subsequent image analysis (in IMOD software (Kremer *et al.*, 1996). This was achieved by manually contouring the periphery of each individual bacterium, on each section (Figure 5.2.37., top panel). Simultaneously, the position of any gold particles on the section was also marked (Figure 5.2.37., bottom panel, red circles). This procedure was repeated for 6 cells which were chosen at random.

Having successfully contoured the *E. coli* cells that were visible on all of the 20 sections (Figure 5.2.38., A), 3D reconstructions of individual bacteria were generated (Figure 5.2.38., B). Analysis of the positions of the gold particles (and thus TatA protein) unveiled a cluster of TatA in the inner membrane of each *E. coli* cell (Figure 5.2.39.). Notably, 4 out of 6 of the *E. coli* contoured exhibited a linear cluster of TatA in the inner membrane; whereas with 2D TEM analysis only 4% of cells analysed were seen to possess such a TatA cluster. Therefore, it seems likely that this distribution of TatA is likely to be more common than originally anticipated from TEM analysis (§5.2., Figure 5.2.31). This is the first time that the localisation and distribution of any Tat component has been visualised in 3D space.
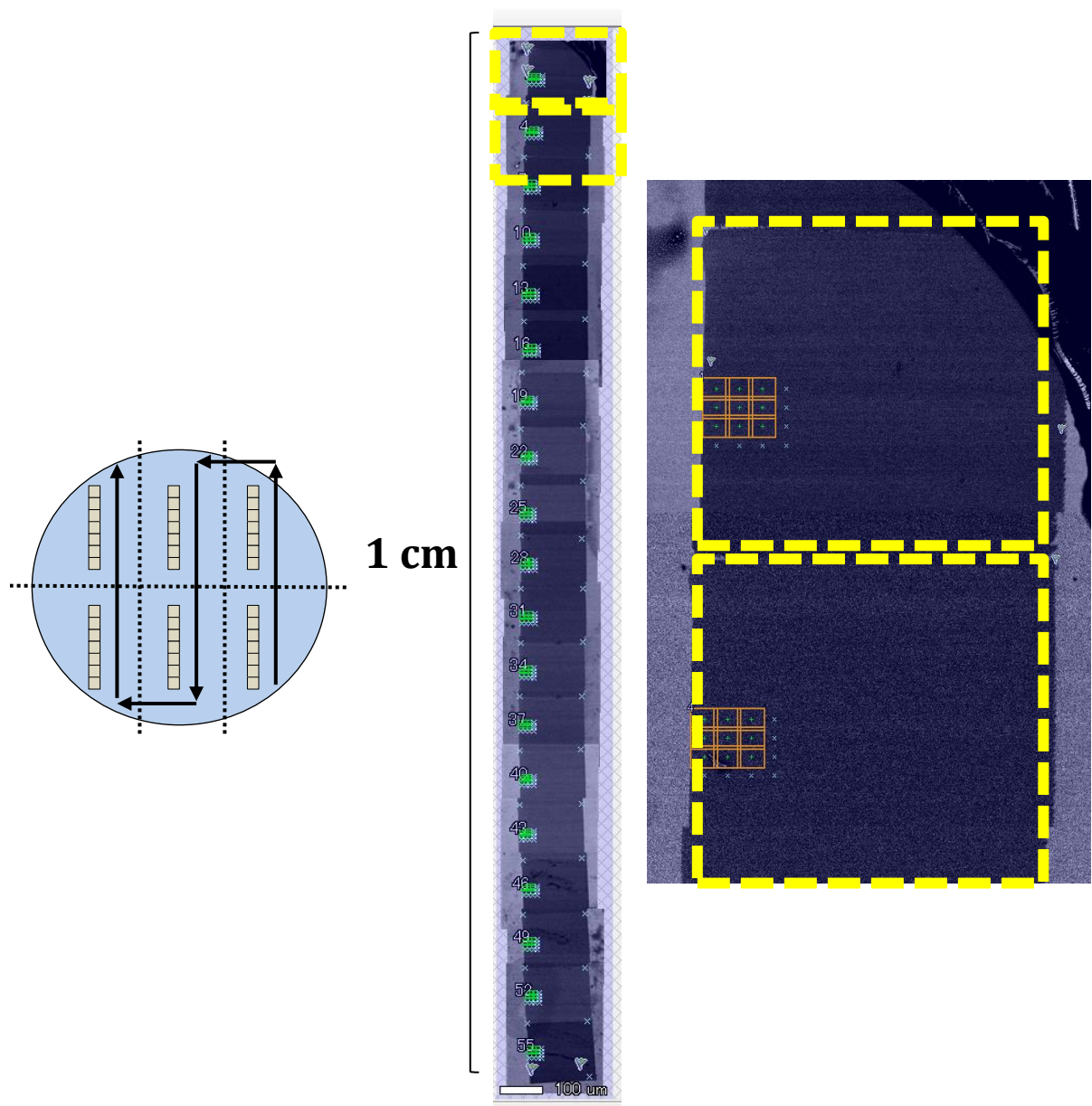
Figure 5.2.36. Serial sections of resin-embedded *E.coli* cells positioned under the electron beam of the scanning electron microscope.

Serial sections of resin-embedded *E. coli* cells, overexpressing TatABC, were transferred onto carbon-coated glass coverslips and placed in the imaging chamber of the SEM. Image acquisition commenced from the top of the ribbon (yellow dashed box) and sequentially moved downwards. A 3x4 montage was collected from each section (orange box), imaging cells at 5000x magnification.
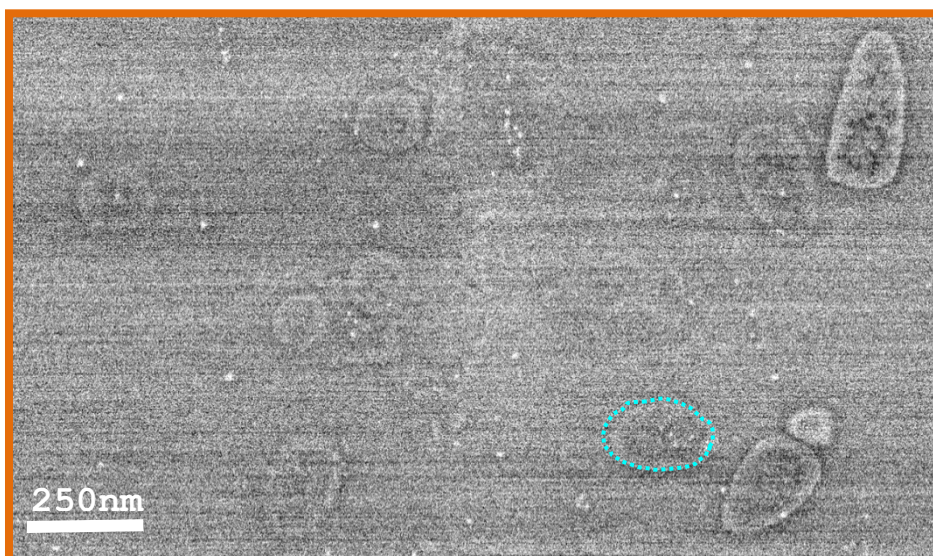
Figure 5.2.37. Manual contouring of individual *E. coli* cells to segment data.
Using IMOD software, individual *E. coli* cells were manually contoured via tracing the entire perimeter of the cell on each section (images 1-16 below). Also, the position of any gold was added (red circles below on images 1-16).Scale bar = 250 nm.
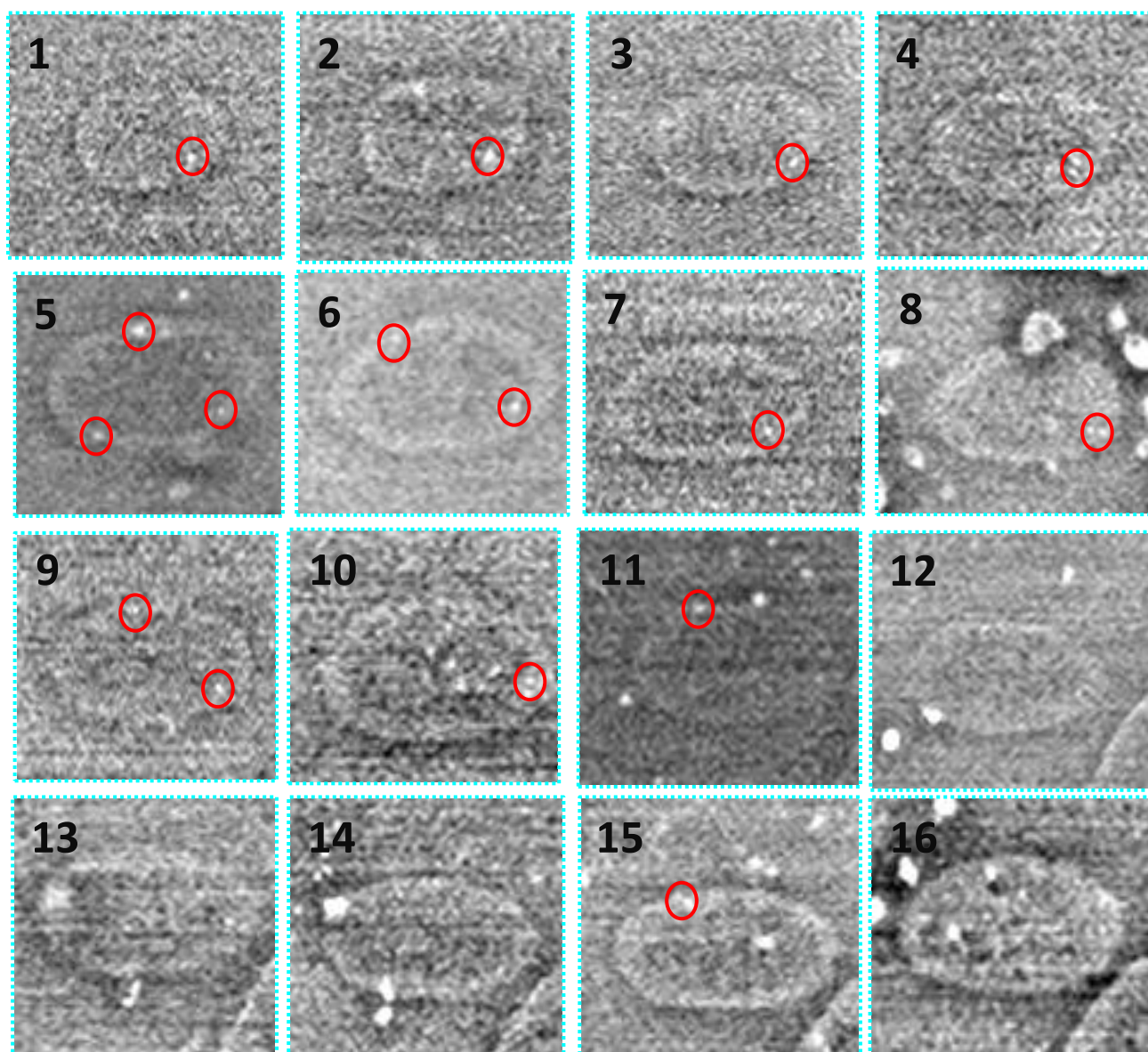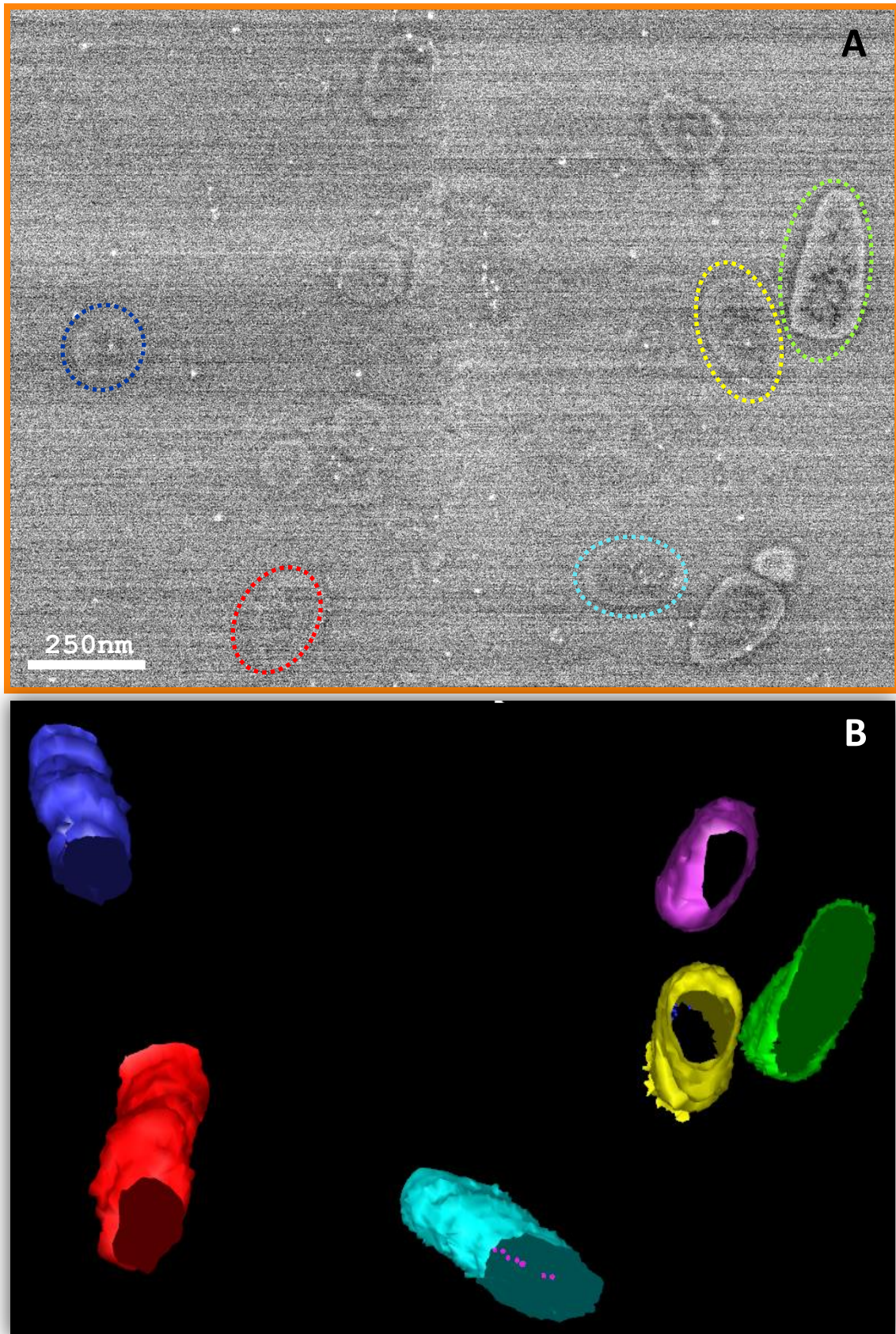
Figure 5.2.38. 3D reconstruction of *E. coli* cells
A) Acquisition of serial electron micrographs of *E. coli* cells (5000X magnification) for subsequent contouring (coloured ellipses). Images taken on Image taken on JEOL 7401-F. B) IMOD software was used to mesh sequential contours for generation of 3D reconstructions of *E. coli*.

162
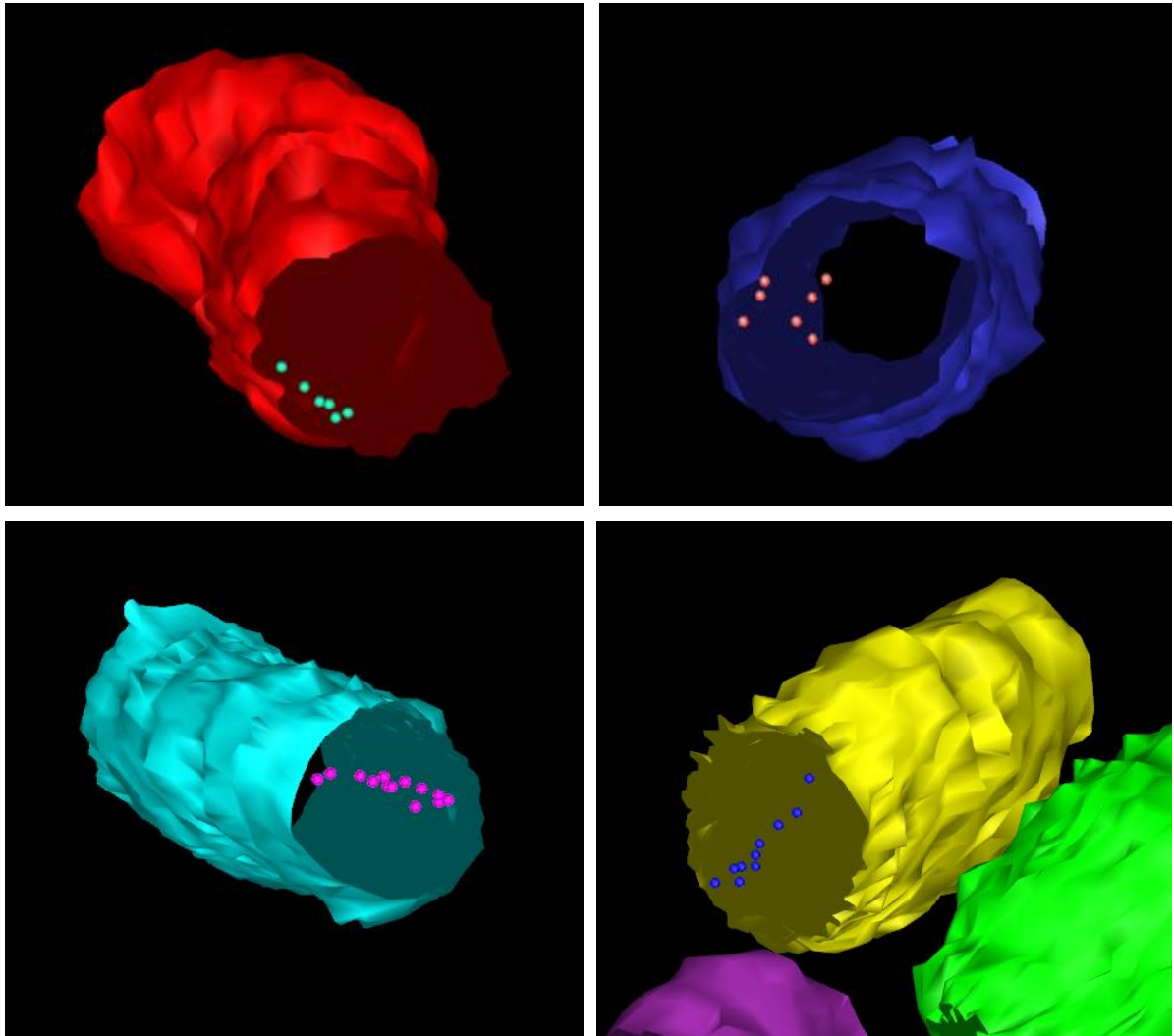
Figure 5.2.39. 3D visualisation of a linear distribution of the TatA protein in the inner membrane of *E. coli*.
Upon reconstruction of individual *E. coli* cells, the position(s) of immunolabelled TatA protein could be deciphered. The above reconstructions illustrate a linear distribution of TatA protein in the inner membrane of *E. coli*.

5.2.8. Optimisation of immunogold labelling of TatB protein in the inner membrane of *E. coli*

Given the novel finding of the distribution of TatA protein in the inner membrane of *E. coli* (§5.2.7., see above), it still remains unknown where the TatB or TatC proteins localise, relative to TatA protein. TatB is known to localise with TatC at 1:1 stoichiometric ratio (Bolhuis *et al.*, 2001), and serves as the substrate-binding complex of the Tat translocase (Cline & McCaffery, 2007; Tarry *et al.*, 2009). It remains elusive whether this TatBC complex serves as a nucleation point for TatA polymerisation and hence TatA extending out into the inner membrane (Frobel *et al.*, 2012), or whether a different conformation of Tat constituents occurs. Therefore immunogold labelling of TatB protein was attempted to gain further insight into the location of this protein in the inner membrane.

Fractionation of TatABC overexpressing cells confirmed the inner membrane localisation of TatB protein (Figure 5.2.41). Initial immunogold labelling of the same cells showed a high density of gold labelling in (+) cells (Figure 5.2.39., A (+)), although there was significant binding to Δ*tat* cells (Figure 5.2.40, B Δ*tat*). Despite efforts to increase ionic and detergent concentrations, and dilution of anti-TatB antibody, the anti-TatB antibody still bound non-specifically to Δ*tat* cells, with clustering of gold seen (Figure 5.2.40., B (+) and Δ*tat*). Therefore reliable, unambiguous insight into the localisation of TatB protein in the inner membrane could not be gained.
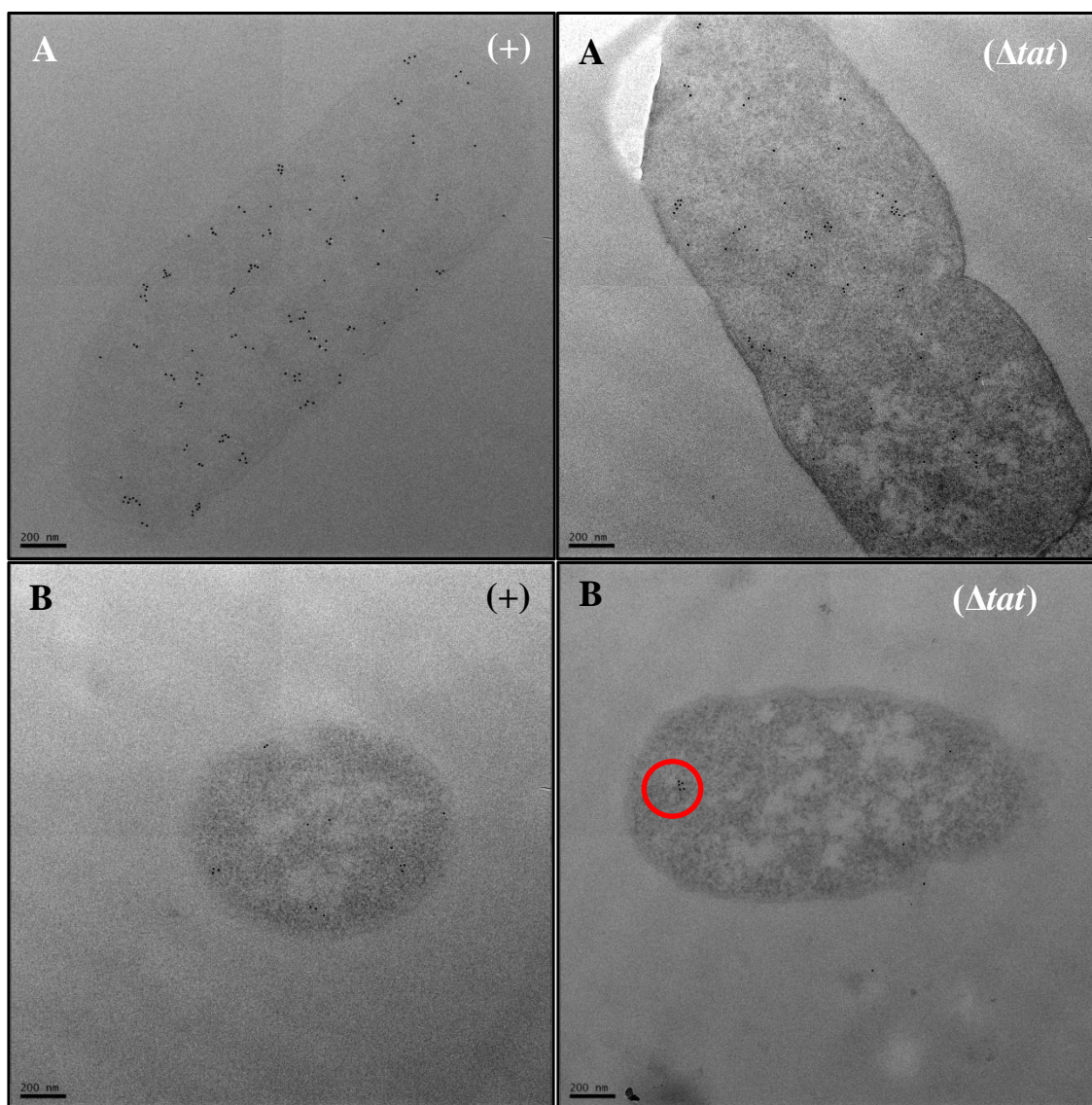
| Variable										
[NaCl] w/v /%	0.8	1.6	0.8	1.6	2	2.5	2	2.5	2.5	2.5
[Tween/20] v/v /%	0.1	0.1	0.5	0.5	1	1	2	2	2	2
Dilution of anti-TatB	1:20	1:20	1:20	1:20	1:20	1:20	1:20	1:20	1:40	1:80
	A								B	

Figure 5.2.40. Electron micrographs of *E. coli* cells, overexpressing TatABC, immunogold-labelled following primary antibody detection against TatB protein.

E. coli cells overexpressing TatABC, were immunolabelled using a primary antibody raised against the TatB protein [labelled (+)].Controls: cells that had Tat machinery knocked-out [labelled (Δ*tat)*]; (+) cells that had the primary antibody omitted [labelled **(-1)]**, and (+) cells immunolabelled using a different secondary antibody [labelled **(-2)]**. The primary antibody bound non-specifically in all areas of *E. coli* (images labelled A). An increase in salt and detergent concentrations (table above) minimised non-specific binding, with an optimal antibody concentration of 1:40 (images labelled B). However, the (+) and (Δ*tat*) samples remained indistinguishable and clustering of gold was present (red circle). Images were taken on JEOL 2010F TEM at 12,000X magnification. Scale bar = 200 nm.
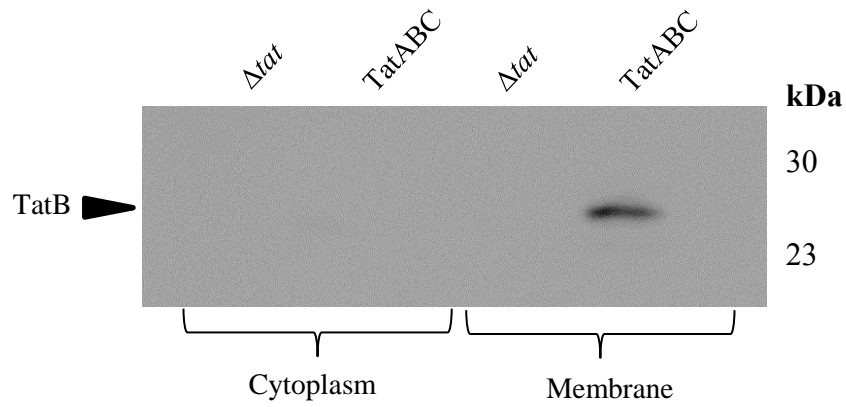
Figure 5.2.41. Cytoplasmic and membrane fractions of *E. coli* cells (overexpressing TatABC) immunoblotted for the detection of TatB protein.

E. coli cells overexpressing TatABC were fractionated into cytoplasmic and inner membrane fractions. The fractions were resolved by SDS PAGE and immunoblotted to detect for the presence of TatB protein. The control was *E. coli* cells that have had Tat machinery knocked-out (Δ*tat*)). Tat anti-TatB antibody identified overexpressed TatB only the membrane fraction of TatABC overexpressing cells.

5.3 Discussion

TatA plays an essential role in the Tat translocation system, and insight into the localisation and distribution of the TatA protein is fundamental to elucidating the mechanism of Tat translocation. Analysis of this membrane protein *in situ* to avoid the use of detergents remains a challenging task; previous experiments have used YFP-labelled TatA proteins in combination with confocal microscopy to analyse Tat distribution in the inner membrane (Alcock *et al.*, 2013; Leake *et al.*, 2008). However, there remains a risk that TatA-XFP fusion proteins may not be properly active (Ray *et al.*, 2005). In this study we have used 2D and 3D EM approaches to study the location and organisation of TatA, which is native, apart from the presence of a C-terminal His tag which has been shown not to affect activity (Bolhuis *et al.*, 2001). This is thus the first study to analyse active TatA complexes and the first to analyse TatA organisation in 3D. Given that this translocase accomplishes the remarkable feat of transporting large, fully-folded proteins without jeopardising membrane integrity, such spatial data is important for a deeper understanding of the system.

To achieve unambiguous immunolabelling of TatA protein, numerous variables were optimised to maximise TatA protein availability for binding at the surface of the section and/or minimise non-specific interactions between the negatively charged antibodies and gold-conjugates to the positively-charged areas of the resin. Such variables included: buffer pH, +/- presence of a blocking agents (BSA and normal sera) and fixative concentrations. Whilst these variables had only a slight impact on the antibody binding; it was alteration of the primary antibody that made the biggest difference. The anti-TatA antibody is a custom-made monoclonal antibody that bound maximally to TatA antigen in *E. coli* cells. The trialling of numerous primary antibodies highlighted a key requirement to the success of this technique: the use of a high-titre, high-affinity antibody to allow the greatest dilution thus minimising non-specific labelling.

The highly-specific, immunogold labelling of TatA in *E. coli* cells shows that this protein is randomly distributed in the inner membrane when overexpressed at levels where it cannot engage in translocation owing to a lack of TatBC complexes. There is no evidence of a preferential localisation of this protein elsewhere within the cell.

167

However, in cells that overexpress TatBC proteins alongside TatA there is a distinguishable alteration in the organisation of TatA protein. A small proportion of cells (4%) exhibit a linear clustering of TatA in the inner membrane. 3D array tomography was able to provide much more insight into the localisation of TatA compared to the 2D data. Array tomography data revealed that TatA forms linear clusters in the inner membrane of *E. coli*.

This is the first demonstration for an organisation of this kind for TatA. Previous studies have identified higher order organisations of TatA previously, including (Berthelmann *et al.*, 2008) who showed TatA to form huge tubules in the cytoplasm of *E. coli*. However, their appearance is completely different under the TEM compared to those in this study. Furthermore, a mutation in the TatA subunit of *B. subtilis* (TatAd) TatAdCd complex triggered the formation of long fibrils. Authors speculated that such fibrils could be an aberrant super-assembly of TatAd. It is possible that the clusters seen in this study could be related to those fibrils.

Other studies have utilised XFP-labelled TatA to analyse its distribution in bacteria. The issue in these instances is the finding that TatA-XFP is inactive (Alcock *et al.*, 2013; Ray *et al.*, 2005). Alcock *et al.* (2013) expressed a Tat-YFP fusion in the presence of TatA paralog, TatE. They observed a doubling of export of native Tat substrate, showing that TatA-YFP could somehow interact with TatE and stimulate its activity; however the underlying reasons for this are unclear. They also observed that TatA can exist in both dispersed and higher oligomer states, and that the distribution of TatA is controlled by other components of the Tat machinery namely TatBC. However, it is impossible to effectively compare the data obtained in this study with the EM data presented in this investigation for two reasons. Firstly, it is possible that Alcock *et al.* could have measured the assembly-disassembly of TatE complexes, with TatA-YFP incorporated. Secondly, it is unclear how inactive TatA-YFP complexes could have contributed to the fluorescence signals.

The ability to identify TatA in the inner membrane allowed investigation into whether the *E. coli* cell poles serve as a prerequisite for the localisation of this protein. Sequestration of Tat constituents could have important implications for the mechanism of Tat machinery. Protein assembly at specific sites is known for other proteins in *E. coli*, which provided fundamental insight into their activity. E.g.

inhibitors of the FtsZ protein (that drives cytokinesis in cell division), localise to the cells poles creating an inhibitor-free zone at the cell centre enabling cell division (Lutkenhaus, 2007).

Rose *et al.,* 2013, showed TatA to colocalise with TatB at the cell poles (Rose *et al.*, 2013). They hypothesise that this colocalisation could benefit the Tat translocase since the cardiolipin-rich cell poles (Huang & Ramamurthi, 2010; Renner & Weibel, 2011) could help position and/or assemble Tat, which is consistent with data showing that export of Tat substrate is severely impaired in *E. coli* cells that have been depleted in cardiolipin phospholipid (Mikhaleva *et al.*, 1999). However, the same results were also found of *E. coli* cells depleted in phosphatidylethanolamine (Mikhaleva *et al.*, 1999), questioning the relevance of this data regarding the polar export of Tat.

Furthermore, fluorescently-labelled proteins can localise to non-biologically relevant regions due to attractive interactions that arise solely as a consequence of this tagging (Tavare *et al.*, 2001). The data presented in this chapter omitted the use of large-recombinant tags and analysed the TatA protein *in situ.* Data shows that there is no preferential localisation of TatA protein at the cell poles of *E. coli.* Further immunogold labelling experiments of other Tat proteins (TatB or –C) could consolidate this finding. Also, it would be interesting to investigate whether this localisation altered upon changing levels of Tat substrate since the immunogold labelling experiments are a "snap-shot" of Tat localisation in the inner membrane.

It is to be remembered that the *E. coli* cells used in this part of the investigation are overexpressing Tat proteins (namely, TatA and TatABC); hence it is important to consider the possibility that the clustering of TatA witnessed in the inner membrane could be a consequence of overexpression of Tat machinery. However Matos *et al.* showed that induction of Tat machinery from a pBAD system (as used in this investigation), relieved saturation of Tat machinery; demonstrating that the Tat proteins expressed upon induction are capable of forming active Tat complexes that are able to transport substrates across the inner membrane of *E. coli.*

To conclude, the data in this chapter show for the first time the localisation and distribution of a Tat component in 3D space, in its native cellular environment. At present we do not know whether the linear clustering of TatA in the inner membrane

is consistent with a pore-forming mechanism of Tat. More specifically, we do not know where the other Tat constituents are localised relative to the TatA labelled in this study. Co-labelling immunogold experiments could identify the localisation of both TatA and TatB, TatC or Tat substrate in the inner membrane, and thus aid the interpretation of data obtained in this chapter. Of course these experiments require a high-titre, high-affinity antibody against any of those additional components listed. The methodology used in this investigation has the potential to be applied to any cellular antigen – not just those of the Tat machinery. The identification of individual proteins can unveil novel levels of organisation and consequently test mechanistic hypotheses.

Chapter 6:

Stable expression of a non-cleavable Tat precursor in the inner membrane of E. coli

6.1 Introduction

The ability of the Tat translocase to transport fully-folded proteins into the periplasmic space has captured the interest and investment of the biotechnology industry, since it offers potential to simplify downstream processing of biotherapeutic proteins (reviewed in section §1.7.2).

The initial studies of (Matos *et al.*, 2012) and (Alanen *et al.*, 2015) tested Tat's capability of transporting a heterologous protein on a large scale. Results showed high levels of TorA-GFP export at ~0.35 g.L^{-1} with no large-scale release of cytoplasmic contents, confirming this translocase's potential as a viable method of producing therapeutic protein. More recent data showed Tat to successfully transport biopharmaceuticals including human growth hormone (hGH), interferon α2b and antibody fragments (Alanen *et al.*, 2015).

The cytoplasm is highly organized with proteins localising to specific regions within this aqueous milieu; therefore knowledge of a preferential localization or distribution of Tat substrate shall enable us to gain deeper insight into Tat transport and potentially assist in the exploitation of this protein machinery for the biotechnology industry.

In this chapter I present the first detailed EM analysis of the export of a biopharmaceutical, hGH, fused to a TorA signal peptide (TorA-hGH) via Tat machinery. hGH is a single polypeptide chain of 191 amino acids and is one of the most important hormones in the human body, possessing vital roles in numerous biological processes including cell metabolism and proliferation (Kassem *et al.*, 1993). Recombinant hGH is used therapeutically to treat hGH deficiency and a range of genetic disorders (Sanchez-Ortiga *et al.*, 2012; Spiliotis, 2008; Takeda *et al.*, 2010; Vogt & Emerick, 2015).

In this study I used two constructs: TorA-hGH and a mutant non–cleavable version, TorA(A39L)-hGH. The latter contained an alanine → leucine substitution at the final residue of the signal peptide, and this is predicted to block processing by leader peptidase. On the basis of previous data on an authentic Tat substrate (Ren *et al.*,

2013), this mutation is expected to result in the mature protein being targeted to the periplasm, after which the protein remains integrated into the inner membrane by means of the uncleaved signal peptide. I used immunogold labelling and TEM analysis to probe the localization and distribution of these Tat substrates *in situ*. Initially, optimisation was carried out to unambiguously identify hGH within the *E. coli* cells. These data highlight the high specificity of the anti-HGH antibody used for labelling.

Results of immunogold labelling experiments show that the TorA-hGH Tat substrate exhibits a random distribution in the cytoplasm and, as has been seen with the Tat machinery (Alcock *et al.*, 2013; Leake *et al.*, 2008; Rose *et al.*, 2013), a uniform distribution in the inner membrane of *E. coli*. Formation of cytoplasmic inclusion bodies was identified, which is common for the heterologous expression of hGH in *E. coli* (Fahnert *et al.*, 2004; Goeddel *et al.*, 1979; Ikehara *et al.*, 1984); however their abundance was very low. Export assays showed that the non-cleavable TorA-hGH precursor was stably expressed at the inner membrane offering potential for the Tat machinery in cell surface display technologies.

6.2 Results

6.2.1. Export of TorA-hGH precursor by Tat machinery

hGH has previously been shown to be exported efficiently into the periplasm of *E. coli* by Tat machinery (Matos *et al.*, 2012). It is synthesized as a 27 kDa precursor protein, and was expressed with a TorA signal peptide that contains features typical of a Tat signal peptide (Figure 6.2.1). These include an N-terminal domain, a hydrophobic core region and a polar C-terminal domain ending with an Ala-Xaa-Ala consensus motif (shown in blue). It is this signal peptide that targets hGH specifically to the Tat machinery. This protein was chosen for this study since it is a high-value therapeutic protein produced by the biotechnology industry for treatment of hGH deficiencies (and associated disorders) in adults and children (Sanchez-Ortiga *et al.*, 2012; Spiliotis, 2008; Takeda *et al.*, 2010; Vogt & Emerick, 2015).

Figure 6.2.2 shows a typical export assay experiment in which synthesis of non-mutated TorA-hGH precursor was induced in wild type (WT) MC4100 *E. coli* cells. At certain time points after the induction of plasmid, cells were fractionated to generate cytoplasm (C), membrane (M) and periplasm (P) samples which were analysed by SDS-PAGE and immunoblotting. Two forms of hGH are detected by immunoblotting of whole cell fractions: 27 kDa precursor protein and 22 kDa mature protein (figure 6.2.2. and 6.2.3.).Some non-specific binding is also observed.
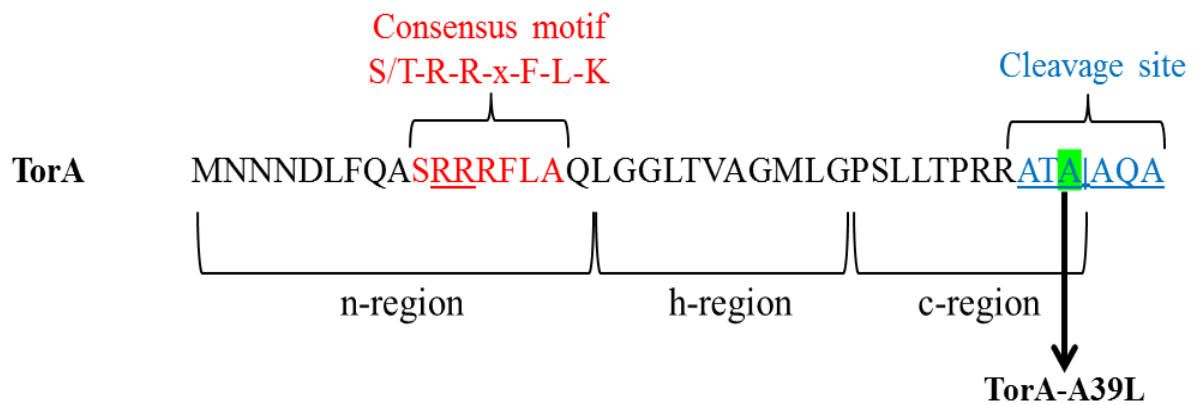
Figure 6.2.1. Structure of the TorA signal peptide and the TorA-A39L variant.
Primary structure of the 42-residue signal peptide of *E. coli* TorA. The consensus motif is highlighted in red (twin-arginine motif underlined), and the peptidase cleavage site is highlighted in blue. The terminal, alanine residue at position 39 (highlighted in green), was substituted by leucine to generate the TorA-A39L variant.

Results in Figure 6.2.2 show that when hGH is fused to a non-mutant signal peptide (TorA-hGH), export of the substrate occurs soon after induction- at 1 hour mature hGH is present in the periplasm. Most hGH detected in the cytoplasm is mature form. This is most likely due to proteolytic cleavage of the precursor protein in the cytoplasm. A minimal amount of precursor protein in this fraction has been observed previously (Alanen *et al.*, 2015), where it was shown precursor TorA-hGH was efficiently exported by the Tat machinery. Therefore, a lack of cytoplasmic precursor protein in this study could be due to the quick turnover of the substrate from the cytoplasm to the periplasm, or due to the fact that most of it is being degraded to mature form. At 1hr 45, the membrane fraction contains precursor TorA-hGH, with mature protein detected at later time points (2hr 15 onwards). The precursor protein is likely Tat substrate at the inner membrane undergoing translocation. The exact nature of mature hGH was investigated further by visualisation under the TEM (§6.2.6 of this chapter).
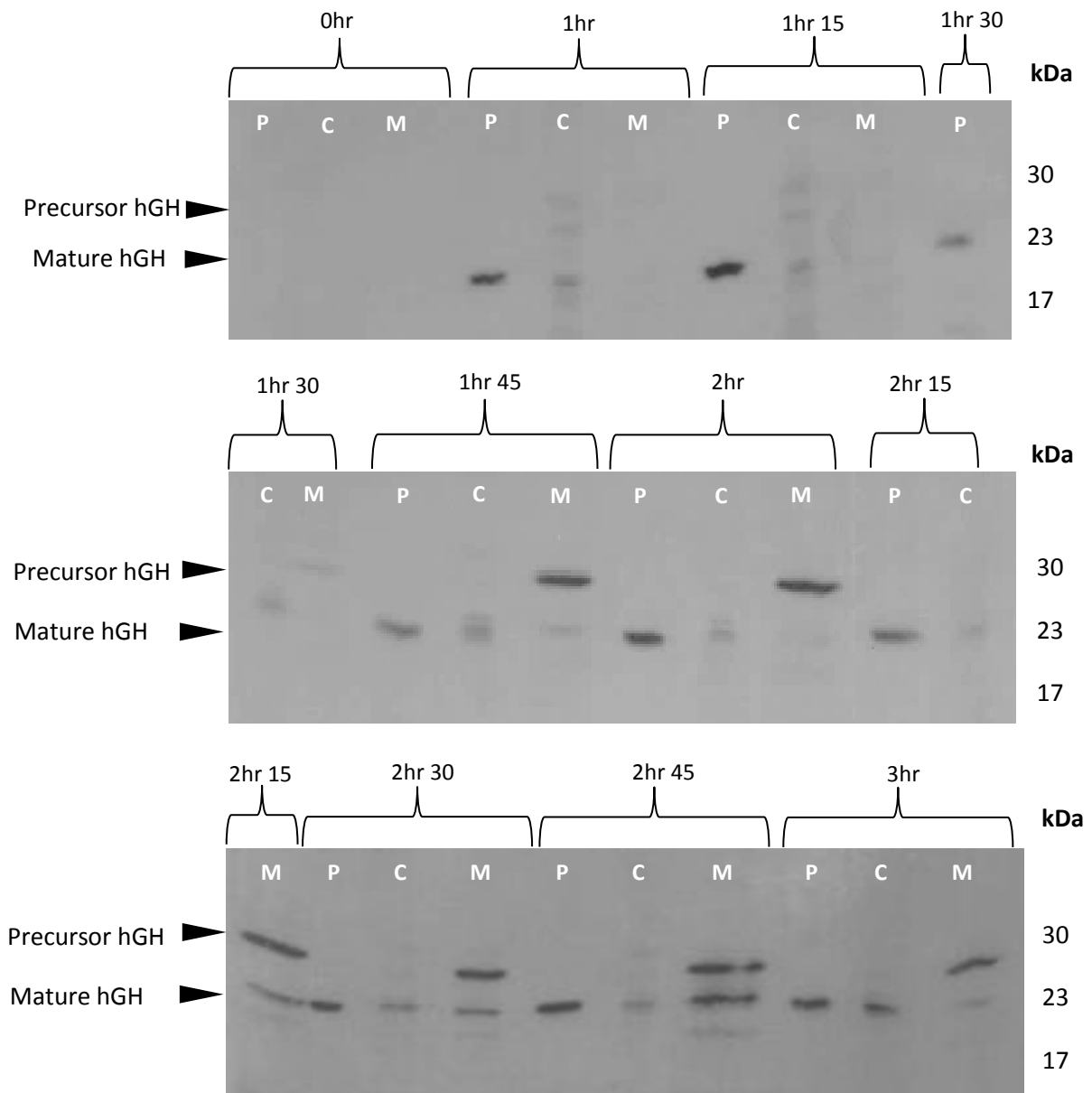
Figure 6.2.2. Export assay of Tat substrate (TorA-hGH) into the periplasm of *E. coli*.
Western Blot to detect the presence of hGH in *E. coli*. Post-induction with 1 mM IPTG
E.coli cells overexpressing hGH fused to a TorA signal peptide (TorA-hGH) were grown at
$37^{\circ}C$ for 3 hours. During this time, cells were periodically harvested, normalised for $OD_{600} =$
10 and subsequently fractionated to periplasm (P), cytoplasm (C) and membrane (M)
fractions. Each fraction was examined for the presence of hGH by immunoblotting with anti-
hGH antibody. Results show there is a good level of export from as early as 1 hour after
induction, shown by the presence of mature hGH (22 kDa) in the periplasm. At each time
point there is a lack of pre-cursor (27kDa) TorA-hGH (i.e. Tat substrate) in the cytoplasmic
fractions, indicating the substrate is either degraded or forming inclusion bodies in the cell.
From 1hr 45min onwards there is a consistent level of precursor TorA-hGH in the membrane
fraction of the *E. coli* cells suggesting to the formation of inclusion bodies.

6.2.2. Substitution at the -1 position of the signal peptide blocks maturation of TorA-hGH

To further examine the export of a Tat precursor protein, the -1 alanine residue in the TorA signal peptide was substituted by leucine (TorA-A39L) (Figure 6.2.1.). This mutated signal peptide was fused to hGH and expressed in *E. coli*. An identical mutation in the TorA signal peptide was performed by (Ren *et al.*, 2013), who showed that the -1 position in the signal peptide is essential for efficient maturation of precursor protein. The mutation completely blocked export of a Tat precursor protein into the periplasmic space. To test whether the same mutation blocks maturation of the hGH protein (and to gain more insight into the export of heterologous Tat substrates), the export assay was repeated with expression of TorA(A39L)-hGH.

Consistent with the findings of (Ren *et al.*, 2013) the precursor protein was not processed to any significant degree and is found almost exclusively in the membrane fraction as precursor protein (Figure 6.2.3., 1hr 15 onwards). The exact nature of this non-cleavable mutant precursor was examined further by visualisation under the EM. Results are presented in section 6.2.7 of this chapter.

As seen with the wild type precursor, mature hGH was detected in the cytoplasm from an early time point (1hr), which most likely represents proteolytic cleavage of hGH protein, and is completely degraded by 2hr 30.
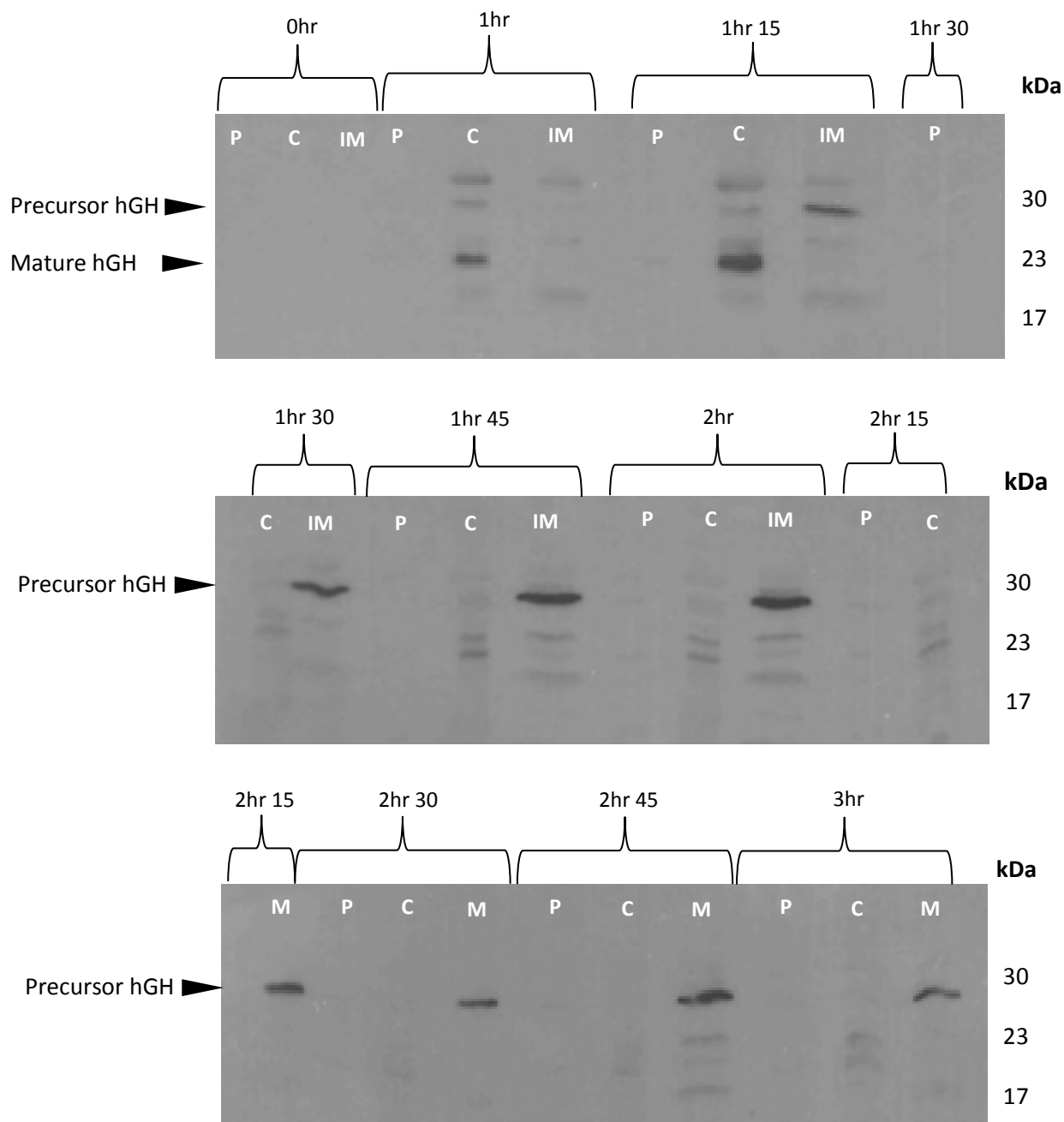
Figure 6.2.3. Export assay of a non-cleavable Tat substrate (TorA(A39L)-hGH) into the periplasm of *E. coli*.

Western Blot to detect the presence of non-cleavable hGH in *E. coli*. Post-induction with 1 mM IPTG *E.coli* cells overexpressing hGH fused to a non-cleavable TorA signal peptide (TorA-hGH) were grown at $37^{o}C$ for 3 hours. During this time, cells were periodically harvested, normalised for $OD_{600} = 10$ and subsequently fractionated to periplasm (P), cytoplasm (C) and membrane (M) fractions. Each fraction was examined for the presence of hGH by immunoblotting with anti-hGH antibody. A lack of hGH protein in the periplasm of any time point confirms that the Tat substrate is non-cleavable and thus remains in the inner membrane fraction. hGH is degraded in the cytoplasm from as early as 1hr indicated by the mature sized hGH (22 kDa). This is degraded by 2hr 15mins. From 1hr 15 min onwards there is a consistent level of precursor TorA-hGH (27 kDa) in the membrane fraction of the *E. coli.*

178

6.2.3. Immunogold labelling of TorA-hGH in *E. coli* cells

To investigate the localisation of the Tat precursor protein further, immunogold labelling and electron microscopy was used to directly visualise these proteins *in situ*. *E. coli* cells overexpressing TorA-hGH or TorA(A39L)-hGH were fixed, stained and resin-embedded for analysis under the EM. The first step was to optimise immunogold labelling of hGH.
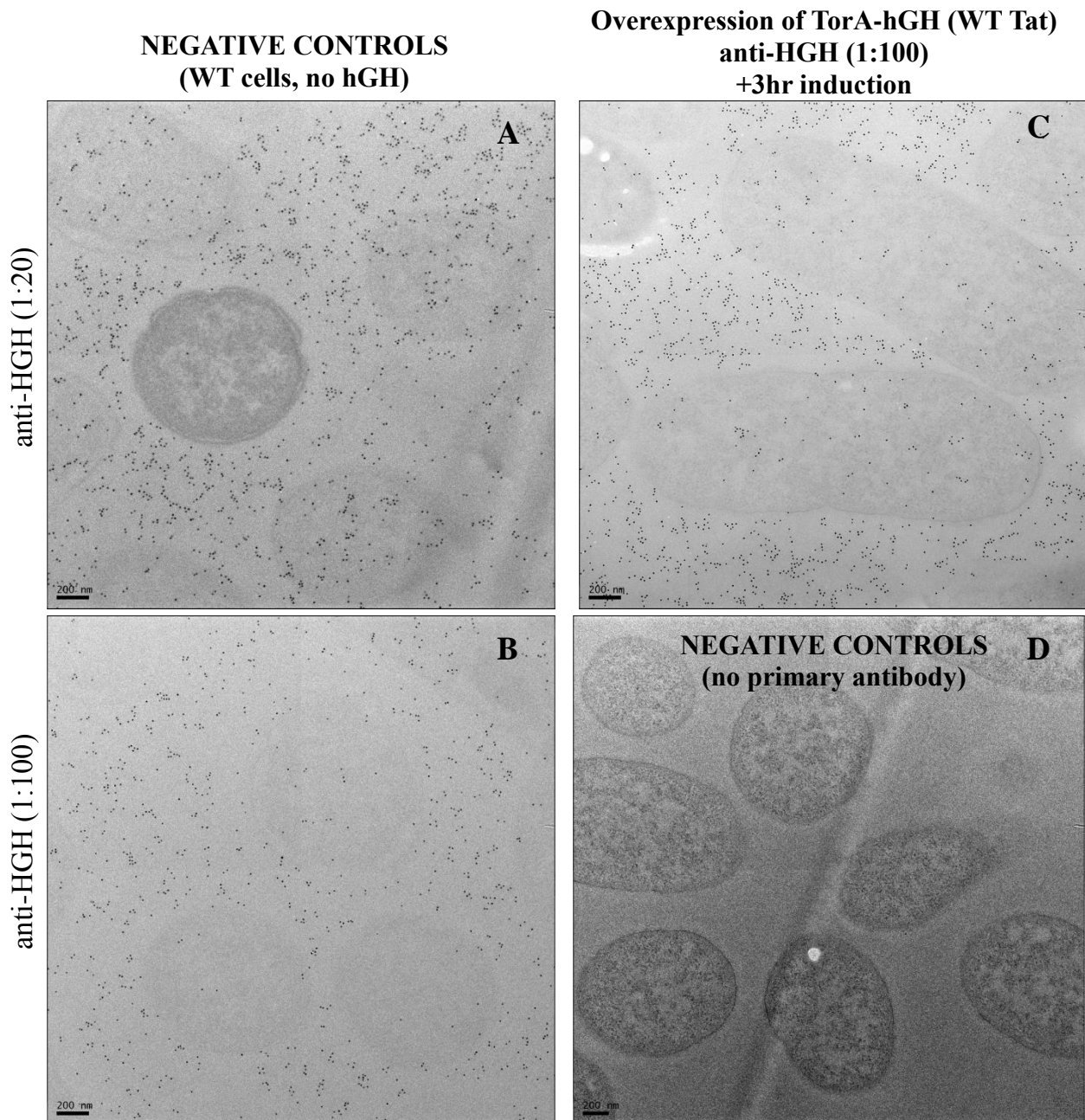
Figure 6.2.4. Optimisation of immunogold labelling of TorA-hGH in *E. coli*
Electron micrograph of resin-embedded, sectioned, immunogold-labelled cells. *E. coli* cells overexpressing TorA-hGH (after 3hrs of induction) were immunogold labelled using anti-hGH antibody (C). Non-specific gold was abundant in the resin, with clustering of gold witnessed inside of the *E. coli* cells. Controls were *E. coli* cells that lacked heterologous expression of the TorA-hGH protein (A+B), and cells that expressed TorA-hGH but lack immunolabelling with primary antibody (D). A and B: labelling of the control cells, irrespective of 1:20 or 1:100 dilution, illustrated the non-specific binding of the anti-hGH antibody since gold was distributed all over the *E. coli* cells and resin. D: non-specific binding was attributable to solely the primary antibody given a lack of gold binding when *E. coli* cells were labelled with the secondary antibody only. Images taken on JEOL 2010F TEM at 15,000X magnification. Scale bar = 200 nm.

6.2.4. Optimisation of immunogold labelling for the unambiguous identification of hGH in *E. coli* cells

hGH expressed in *E. coli* cells was detected using an anti-hGH antibody and subsequently gold-labelled using a gold-conjugated secondary antibody. Gold labelling was performed on resin-embedded cells as described in the Materials and Methods (§2.10.1.14).

Initial immunogold labelling of *E. coli* cells showed a large number of gold particles located randomly throughout the cells and in the resin (Figure 6.2.4, C). Similarly, cells which lacked expression of TorA-hGH and TorA(A39L)-hGH bound gold heavily (Figure 6.2.4, A+B), showing high levels of non-specific antibody binding irrespective of primary antibody dilution. Omitting the primary antibody from the immunolabelling process (Figure 6.2.4., D), confirmed that the non-specific binding observed in other samples was due to the primary anti-hGH antibody.

Increasing salt and detergent concentration in dilution/wash buffers (3X and 20X, respectively) and increasing dilution of primary antibody to 1:1000 gave a marked improvement in immunogold labelling of TorA-hGH and TorA(A39L)-hGH in *E. coli* cells (Figure 6.2.5.). At these concentrations there were minimal non-specific interactions between positively charged tissue components and negatively charged antibodies.

Both TorA-hGH and TorA(A39L)-hGH were found to possess a random distribution in the cytoplasm (Figure 6.2.5., red circle). For the mutant precursor, maturation is blocked; therefore gold bound at the periphery of the cell (Figure 6.2.5, middle, yellow circle) is very likely to be localised at the inner membrane. For the WT precursor, immunoblots (Figure 6.2.2.) showed evidence of maturation of hGH protein and thus localisation to the periplasm. Given the close spatial proximity of the inner membrane and periplasmic space in the *E. coli* cell; gold bound at the periphery of the cell for these samples could be either inner membrane- or periplasm-localised.

Analysis of *E. coli* cells lacking expression of hGH protein revealed gold binding at the cytoplasm and membrane regions (Figure 6.2.5, right); therefore to gauge the extent of non-specific binding of anti-hGH, quantitation of raw gold particles was conducted.
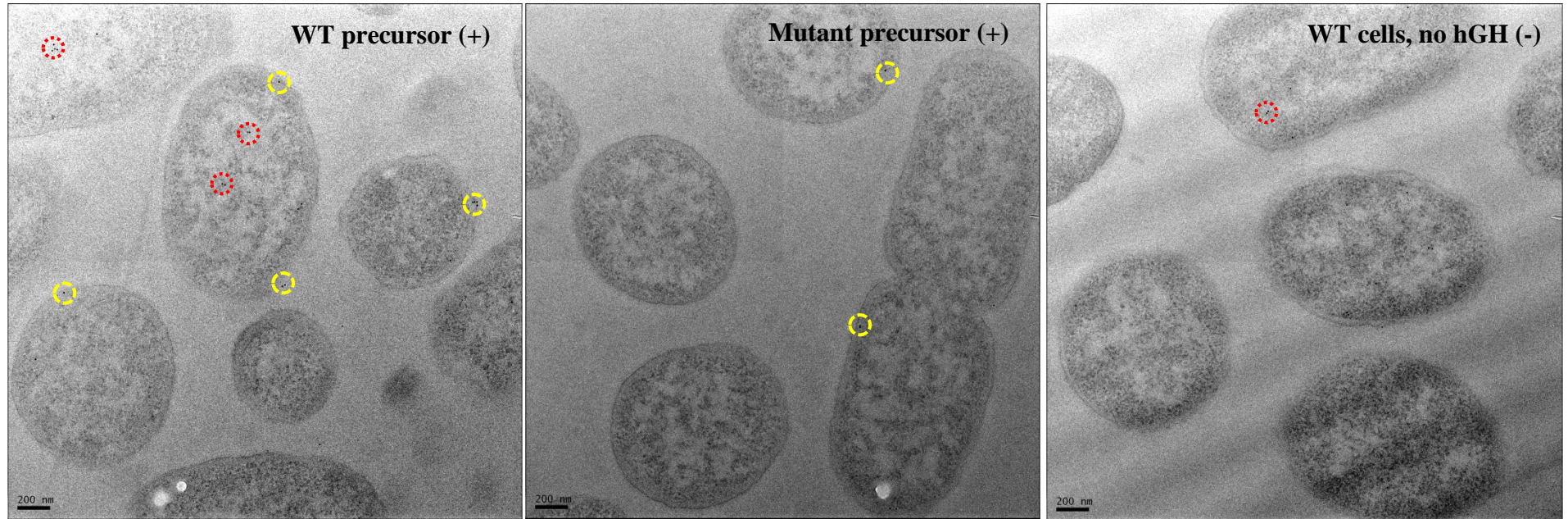
Figure 6.2.5. Unambiguous immunogold labelling of TorA-hGH in *E. coli*
Electron micrographs of resin-embedded, sectioned, immunogold-labelled *E. coli* cells. *E. coli* cells overexpressing WT or mutant precursor TorA-hGH were immunolabelled using anti-hGH antibody (+). Controls were *E. coli* cells that lacked expression of TorA-hGH. After increasing salt and detergent concentrations in wash/dilution buffers to minimise non-specific binding, both (+) cells displayed binding uniformly in the inner membrane (yellow circles) and in the cytoplasm (red circle). Some gold bound the control *E. coli* cells (right-handside image) indicating that non-specific binding, although significantly reduced, was not eradicated.

6.2.5. Quantitative analysis of non-specific binding of anti-hGH antibody to *E. coli* cells

Raw gold counts were collected from 200 randomly sampled, anti-hGH immunolabelled *E. coli* for both TorA-hGH-overexpressing cells and WT *E. coli* cells lacking expression of the hGH protein. Gold was assigned to either cytoplasmic or membrane compartments and the average number of gold particles per cell was calculated (figure 6.2.6., B).

A

	(+)hGH	WT
E. coli	200	200
Raw Gold count TOTAL	1241	263
Raw Gold count at membrane + periplasm	858	91
Approx. membrane + periplasm gold per cell	4.29	0.455
Difference in the amount of gold at the membrane (+ periplasm) per cell	4.29 / 0.455 = 9.42X	

B

C
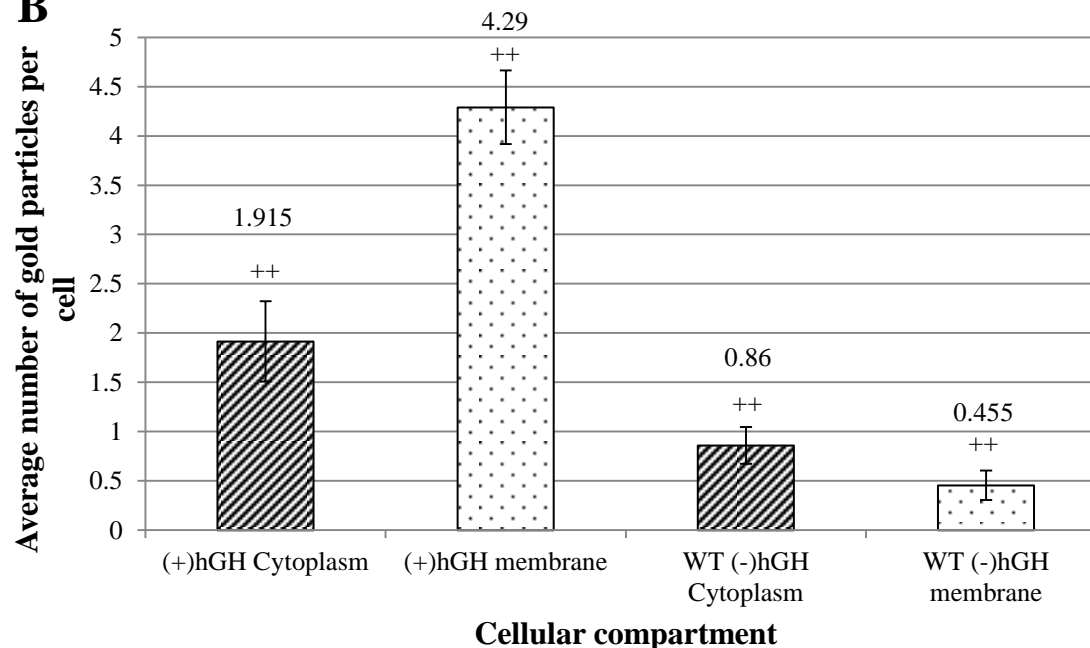
Subcellular compartments	(+)hGH		WT		Row totals	Chi-squared values	
Membrane + periplasm	858	(783.1)	91	(165.9)	949	7.173	33.85
Cytoplasm	383	(457.9)	172	(97.05)	555	12.23	57.88
Column totals	1241		263		1504	111.2	

Figure 6.2.6. Quantitative analysis of raw gold counts of *E. coli* cells immunogold labelled with primary antibody detection against TorA-hGH protein.

E. coli cells overexpressing TorA-hGH were immunolabelled using a primary antibody against the hGH protein. Controls were *E. coli* cells that lacked expression of hGH protein. A: Raw gold counts were taken from 200 randomly imaged *E. coli* from 2 separate resin blocks. Gold was assigned to either 'membrane + periplasm' (labelled membrane in B) or cytoplasm compartment. The approximate number of gold at each compartment was calculated, and subsequently the difference between the two cell types. B: The difference in average number of gold particles at the membrane and cytoplasm of each cell type is shown. Error bars: CI of 2x SE. C: Statistical analysis of raw gold counts. Values represent observed and (expected) number of 10 nm gold particles in the two cell types. For a total chi-squared of 111.2 and 1 degree of freedom, $P<0.005$ (denoted by ++ in graph). The two labelling distributions are significantly different.

Quantification of the gold particles shows that the average number of gold particles per compartment in TorA-hGH-overexpressing cells was 1.9 per cell in the cytoplasm and 4.29 per cell at the membrane, whereas the control, WT cells bound approximately 0.86 in the cytoplasm and 0.45 particles in the membrane per cell, respectively. The labelling of the membrane bound hGH is thus highly specific; the membrane and periplasm of TorA-hGH-overexpressing cells contains 9.42X more gold particles than the membrane and periplasm of WT cells (Figure 6.2.6., A).

To confirm a statistical difference of immunogold labelling between these cells at the cytoplasm and inner membrane, Chi-squared analysis of the raw gold count data was conducted (Figure 6.2.6., C); for a total chi-squared of 111.2 and 1 degree of freedom, P was less than 0.005. This confirms that the gold labelling distributions between the two cell types are significantly different.

Analysis of the distribution of gold particles in the cytoplasm shows the presence of 1.915 and 0.86 particles in the TorA-hGH overexpressing and WT cells, respectively. Since the particle number in WT cells represents non-specific binding, and assuming that the level of non-specific binding in the 2 cell types is identical, this indicates that TorA-hGH overexpressing cells contain an average of 1.055 particles per cell in the cytoplasm, which is less than the number in the membrane (4.29). Given that the immunoblots (Figure 6.2.2.) showed hGH to be present in the cytoplasm, some of these particles can be attributed to genuine cytoplasmic hGH. Therefore, we can conclude that this immunolabelling approach provides highly specific detection of TorA-hGH in the membrane fraction, whereas labelling of the cytoplasmic TorA-hGH is less specific.

6.2.6. Direct visualisation of TorA-hGH *in situ*

The cytoplasm of bacterial cells possesses considerable spatial organisation with many proteins localising to specific sites within the cell (Vendeville *et al.*, 2011). Recent data using fluorescently-tagged TorA showed this substrate to localise uniformly throughout the inner membrane (Rose *et al.*, 2013). However, since there has never been any direct, high resolution visualisation of Tat substrate *in situ*, it is unknown whether any preferential localisation exists.

Having successfully optimised the unambiguous identification of TorA-hGH in the *E. coli* cell to a high degree of specificity, the localisation and distribution of this protein was investigated. *E. coli* cells were induced with IPTG to overexpress TorA-hGH for 1hr 15, 1hr 45 and 3hrs. At the given time point the cells were harvested and fixed, stained and prepared for immunogold analysis under the TEM. The images presented are representative of independent repeats of experiments.

The time points were chosen because previous export assays (Figure 6.2.2.) showed at 1hr 15 there are good levels of export by Tat machinery with mature hGH already in the periplasm. At 1hr 45 mins there is increased precursor at the inner membrane, and at 3 hours there would have been considerable more induction of protein.

In each of the immunogold labelling results (Figure 6.2.7. A-C) TorA-hGH exhibited a uniform distribution around the periphery of the cell (yellow circles), and a random distribution through the cytoplasm (red circles). This is consistent with results showing that the Tat machinery is evenly distributed throughout the inner membrane (Alcock *et al.*, 2013; Leake *et al.*, 2008; Rose *et al.*, 2013).

Qualitative analysis could not discern any differences that arose as a result of increased induction time, nor was there any preferential localisation of substrate to any particular region within the cell. This can be seen clearer in Figure 6.2.8., containing a montage of immunogold-labelled images. Controls of the same cells immunolabelled without a primary anti-hGH antibody did not bind any gold (Figure 6.2.7. D-F), confirming that the secondary antibody did not bind non-specifically.
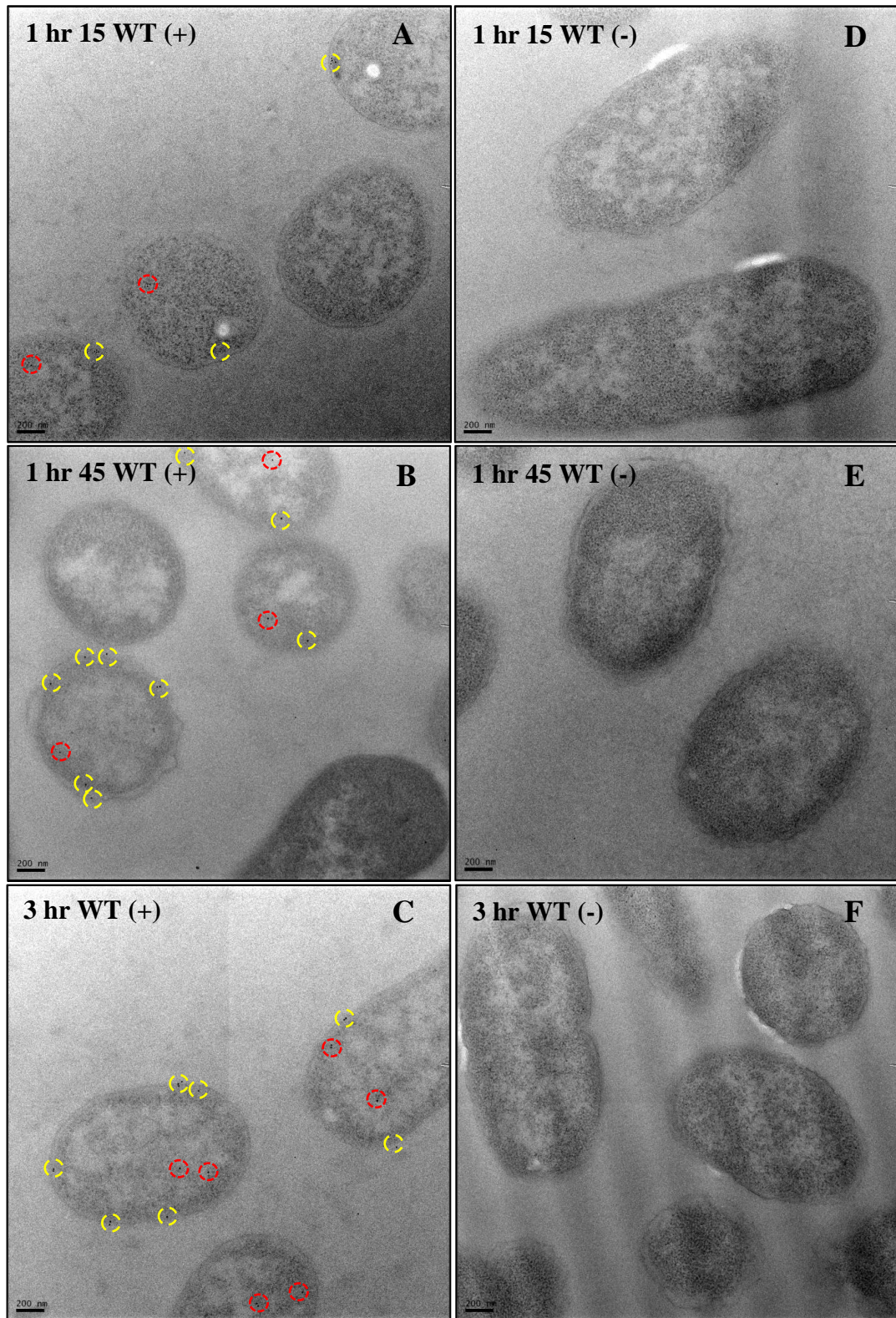
Figure 6.2.7. Immunogold labelling of TorA-hGH (WT precursor) at differing time points
Electron micrographs of resin-embedded, sectioned immunogold-labelled *E. coli* cells. Post-induction with 1 mM IPTG, *E. coli* cells overexpressing TorA-hGH (WT precursor) were harvested at 1hr 15 mins, 1hr 45 min and 3hr. Following biological preservation, resin embedding and serial sectioning, the cells were immunogold labelled using anti-hGH antibody (+). At each time point, the hGH localised to both the cytoplasm (red circle) and even distributions at the inner membrane (yellow circle). Any differences in localisation and/or distribution between each of the time points could not be distinguished qualitatively. Controls were cells that had the primary antibody omitted from the immunolabelling procedure (-).Images were taken on a JEOL 2010F at 15,000X magnification. Scale bar = 200 nm.

188

Figure 6.2.8. Immunogold labelling of TorA-hGH (WT precursor) at 3hrs post-induction

Electron micrographs of resin-embedded, sectioned immunogold-labelled *E. coli* cells. Post-induction with 1 mM IPTG, *E. coli* cells overexpressing TorA-hGH (WT precursor) were harvested at 3hrs. Following biological preservation, resin embedding and serial sectioning, the cells were immunogold labelled using anti-hGH antibody (all images). The TorA-hGH protein localised uniformly throughout the cytoplasm (red circle) and did not exhibit any preferential localisation or distribution at the inner membrane (yellow circles). Images were taken on a JEOL 2010F at 15,000X magnification. Scale bar = 200 nm.

6.2.7. Direct visualisation of TorA(A39L)-hGH *in situ*

E. coli cells overexpressing mutant precursor TorA(A39L)-hGH were immunolabelled to investigate whether differences exist in this protein's localisation and/or distribution compared to the WT precursor. Ren *et al.,* (2013) provided data that showed an unprocessed Tat substrate (possessing identical signal peptide Ala-to-Leu mutation at the -1 position) remains membrane-bound. Immunogold labelling revealed, akin to the WT precursor, TorA(A39L)-hGH protein exhibits a random distribution in the cytoplasm (red circles) and a uniform distribution in the inner membrane (yellow circles) of the *E. coli* cell (Figure 6.2.9. and 6.2.10) (the images presented are representative of independent repeats of experiments). Therefore these data, in combination with immunoblots of export assays, provide additional evidence that an unprocessed Tat precursor remains membrane-associated despite being unable to undergo cleavage by signal peptidases in the periplasm.
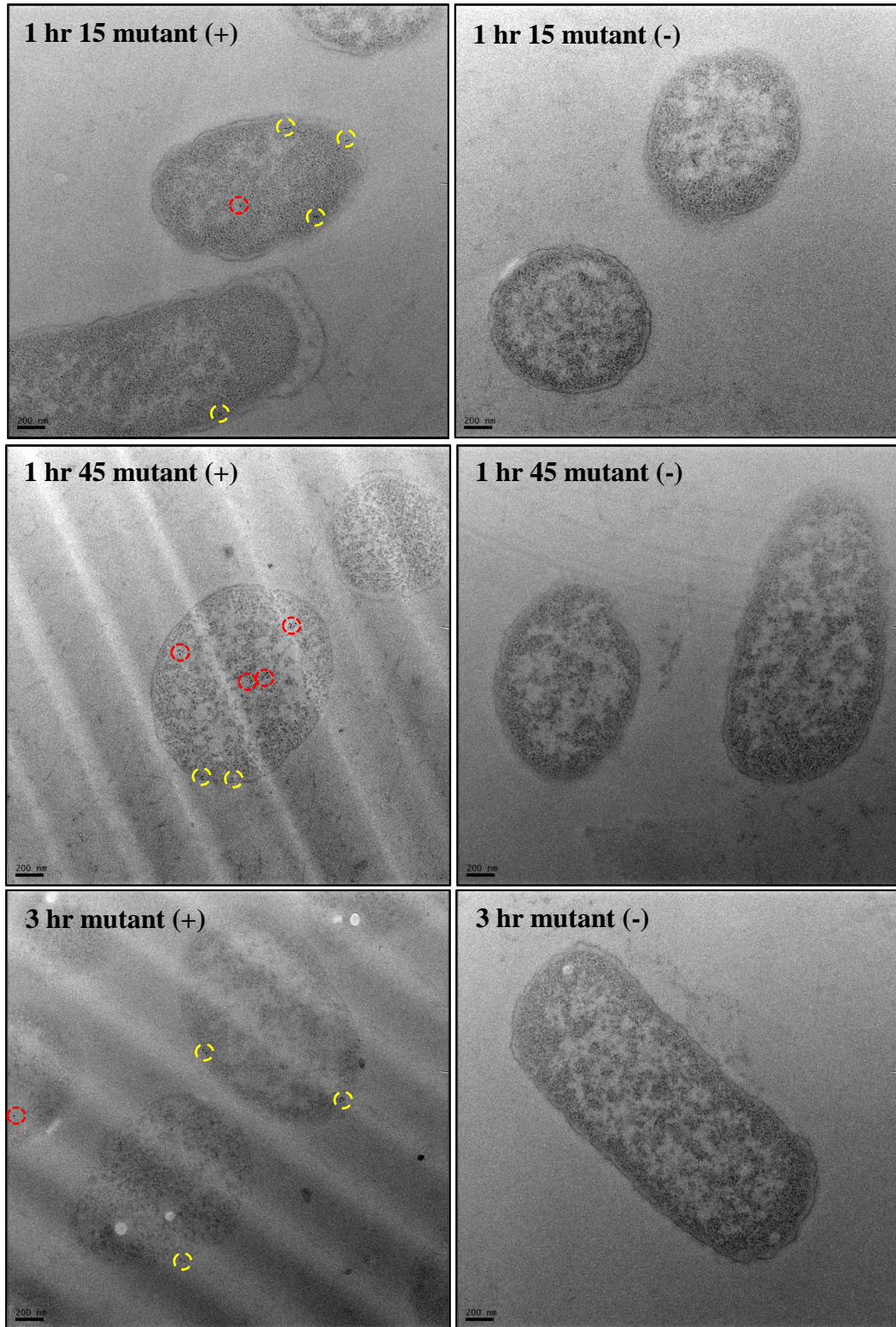
Figure 6.2.9. Immunogold labelling of TorA-hGH (mutant precursor) at different time points

Electron micrographs of resin-embedded, sectioned immunogold-labelled *E. coli* cells. Post-induction with 1 mM IPTG, *E. coli* cells overexpressing TorA-hGH (mutant precursor) were harvested at 1hr 15 mins, 1hr 45 min and 3hr. Following biological preservation, resin embedding and serial sectioning, the cells were immunogold labelled using anti-hGH antibody (+). At each time point, the hGH localised to both the cytoplasm (red circle) and even distributions at the inner membrane (yellow circle). Any differences in localisation and/or distribution between each of the time points could not be distinguished qualitatively. Controls were cells that had the primary antibody omitted from the immunolabelling procedure (-).Images were taken on a JEOL 2010F at 15,000X magnification. Scale bar = 200 nm.

191

Figure 6.2.10. Immunogold labelling of TorA-hGH (mutant precursor) at 3hrs post-induction

Electron micrographs of resin-embedded, sectioned immunogold-labelled *E. coli* cells. Post-induction with 1 mM IPTG, *E. coli* cells overexpressing TorA-hGH (mutant precursor) were harvested at 3hrs. Following biological preservation, resin embedding and serial sectioning, the cells were immunogold labelled using anti-hGH antibody (all images). The TorA-hGH protein localised uniformly throughout the cytoplasm (red circle) and did not exhibit any preferential localisation or distribution at the inner membrane (yellow circles). Images were taken on a JEOL 2010F at 15,000X magnification. Scale bar = 200 nm.

6.2.8. TorA-hGH and TorA(A39L) form cytoplasmic inclusion bodies

Extensive analysis of *E. coli* cells overexpressing TorA-hGH and TorA(A39L)-hGH showed some cells to possess insoluble aggregates of hGH protein, termed - inclusion bodies (IBs). The images presented are representative of independent repeats of experiments. These are electron-dense regions in the cytoplasm of the cell (Figure 6.2.11., blue box) and heavily labelled with the anti-hGH antibody. The IBs were present in all 3 time points imaged with no apparent variation in their abundance.

This is the first time that IBs have been seen for heterologous proteins that are to be exported by Tat machinery. Such details could only be identified by this direct visualisation of *E. coli* cells. These bodies are found in the 'membrane' fraction in the export assays shown earlier (Figure 6.2.2. and 6.2.3.), but this more direct method shows that at some proportion of the protein in this fraction is in insoluble IBs.

IBs complicate the production of therapeutic proteins since they contain inactive, denatured aggregated protein (Yamaguchi & Miyazaki, 2014), making purification of a biologically active therapeutic protein inefficient and costly. However, the cells imaged in this study had a very low abundance of IBs, present in only 10 of 200 cells sampled.

It is to be remembered that visualisation of IBs is reliant on a part of the inclusion body being exposed when sectioned. Given that analysis under the TEM is a 2D projection of only 50 nm of a whole cell *E. coli* cell (up to 3 μm in length), a cell not possessing an IB via TEM analysis, does not mean it does not contain one. Therefore to gain a better understanding of the abundance of these inclusion bodies further examination of these cells will have to be conducted.
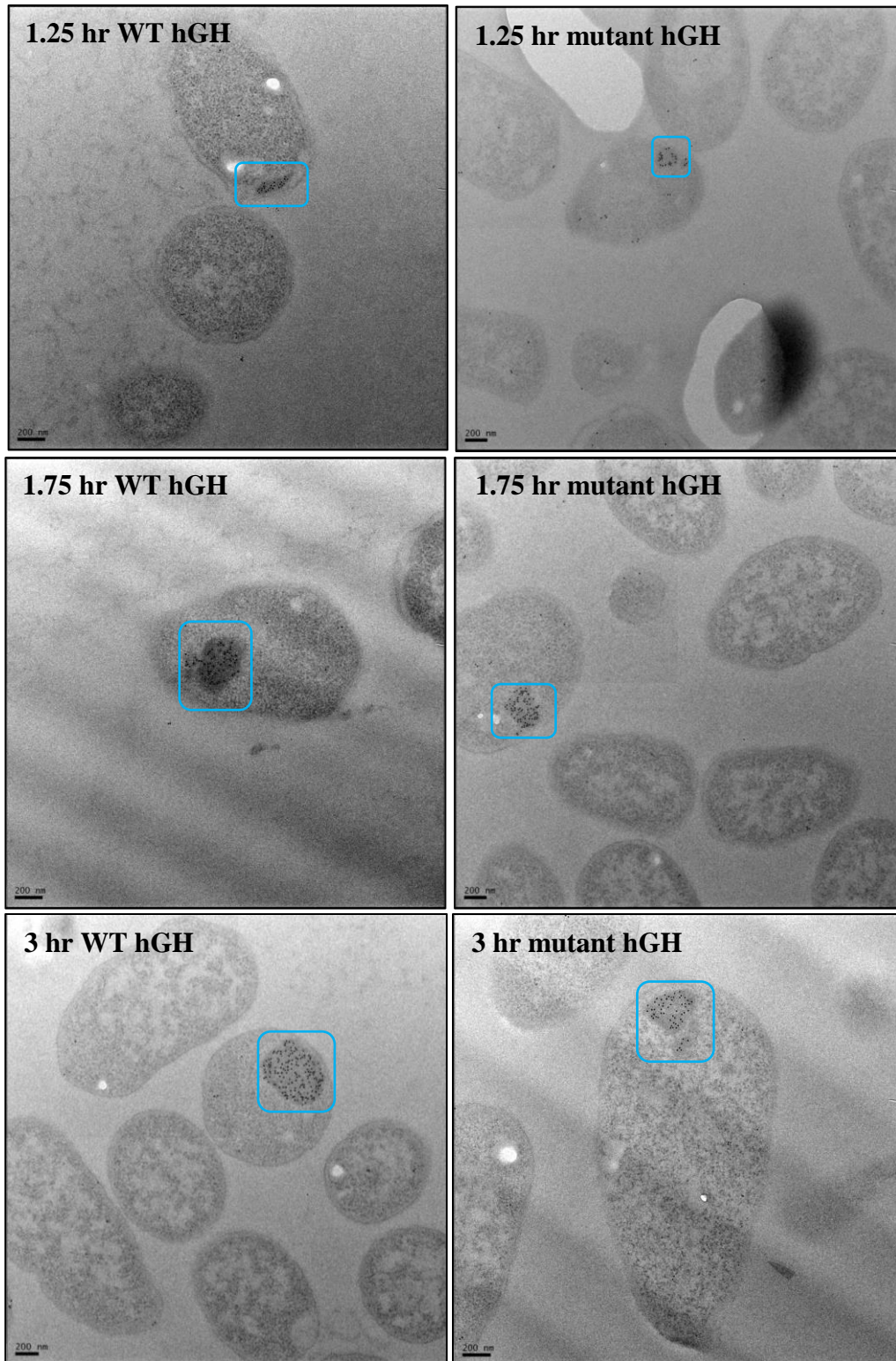
Figure 6.2.11. Immunogold labelling of TorA-hGH (WT and mutant precursor) at different time points

Electron micrographs of resin-embedded, sectioned immunogold-labelled *E. coli* cells. Post-induction with 1 mM IPTG, *E. coli* cells overexpressing TorA-hGH (WT and mutant precursor) were harvested at 1hr 15 mins, 1hr 45 min and 3hr. Following biological preservation, resin embedding and serial sectioning, the cells were immunogold labelled using anti-hGH antibody (+). At each time point, for both WT and mutant precursor, the hGH aggregated to form inclusion bodies (IBs) in the cytoplasm of the cells. The abundance of IBs between the two substrates and time points was not discernible. Images were taken on a JEOL 2010F at 15,000X magnification. Scale bar = 200 nm.

194

6.2.9. Increased expression of Tat machinery does not alter localisation or distribution of Tat substrate in *E. coli*

Experiments in this study have used WT levels of Tat machinery and overexpressed substrate. No preferential localisation or distribution of Tat substrates within the cytoplasm or membrane could be detected. Therefore, to investigate whether substrate localisation and/or distribution is affected by the amount of Tat machinery available, export assays of *E. coli* cells overexpressing both TatABC machinery and TorA-hGH substrate were conducted.

TatABC and TorA-hGH were induced simultaneously in *E. coli* cells that have had the Tat operon knocked out (i.e. Δ*tat* cells). At certain times after induction of plasmids, cells were fractionated to generate cytoplasm (C), membrane (M) and periplasm (P) samples which were analysed by SDS-PAGE and immunoblotting.

Immunoblotting using an anti-Strep antibody confirmed expression of Tat machinery: from 1hr 45 onwards TatC-strep was present in the inner membrane (Figure 6.2.14). A second immunoblot using an anti-TatA antibody provided additional confirmation of Tat machinery expression. Again, from 1hr 45 onwards TatA was expressed in the membrane fraction (Figure 6.2.13). This protein also partially localised to the cytoplasm, which has been seen previously (Berthelmann *et al.*, 2008).

To check that the overexpressed Tat machinery was capable of translocation, the same fractions were immunoblotted for the presence of substrate (Figure 6.2.12). Precursor TorA-hGH was detected in the cytoplasm and membrane from very early on (1hr); however no mature hGH was detected in the periplasm until 1hr 45. The expression of mature hGH in the periplasm was short-lived with it being degraded by the next time point.
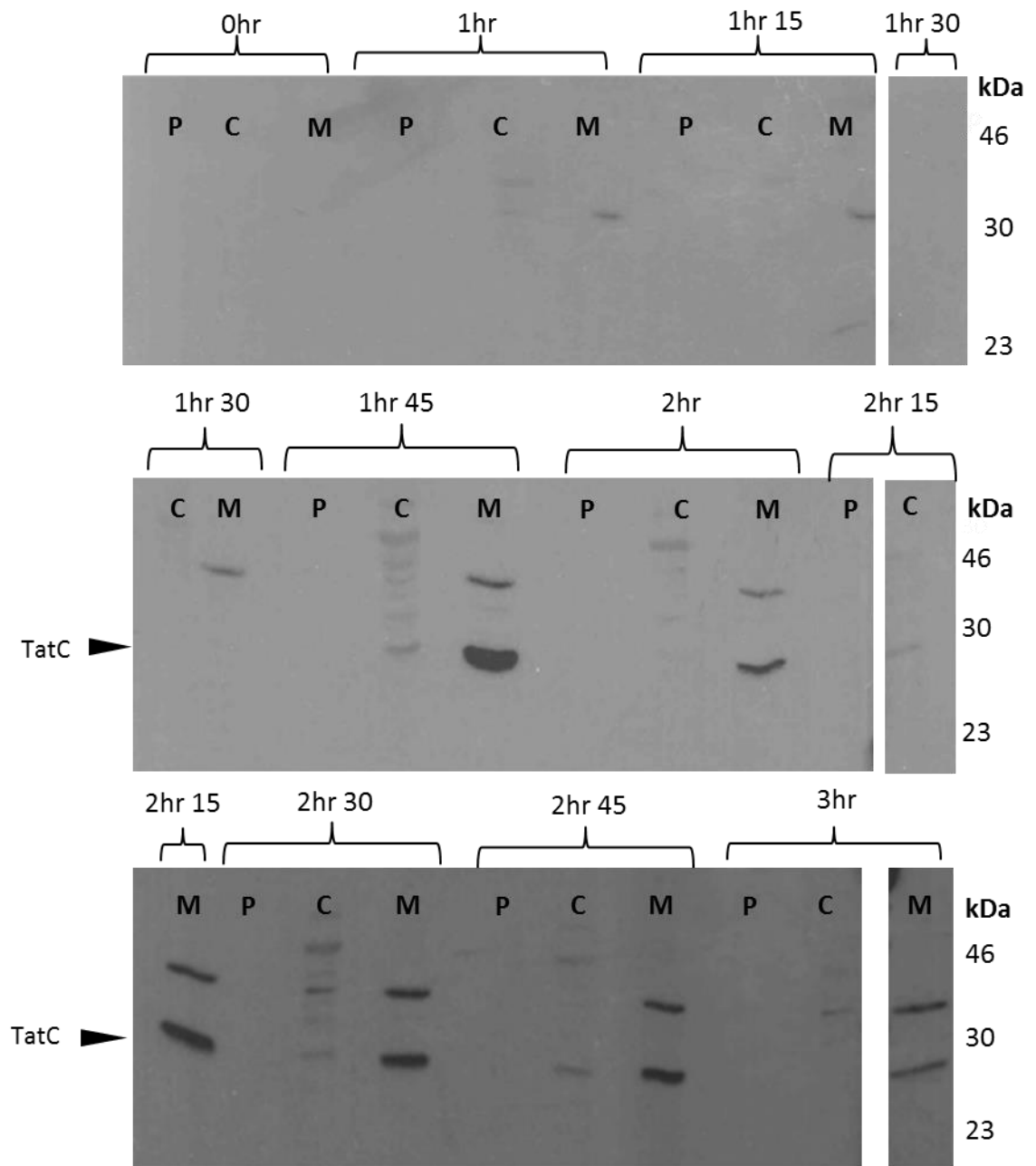
Figure 6.2.12. Export assay of Tat substrate (TorA-hGH) into the periplasm of *E. coli* with increased expression of Tat machinery: immunoblotting for detection of TatC
Western Blot to detect the presence of hGH in *E. coli*. Post-induction with 1 mM IPTG *E.coli* cells overexpressing hGH fused to a TorA signal peptide (TorA-hGH), and TatABC were grown at 37°C for 3 hours. During this time, cells were periodically harvested, normalised for $OD_{600} = 10$ and subsequently fractionated to periplasm (P), cytoplasm (C) and membrane (M) fractions. To check for successful expression of Tat machinery, each fraction was examined for the presence of TatC by immunoblotting with anti-Strep antibody. Results show TatA to reside within the membrane fraction from 1hr 45 mins after induction until 3hrs.
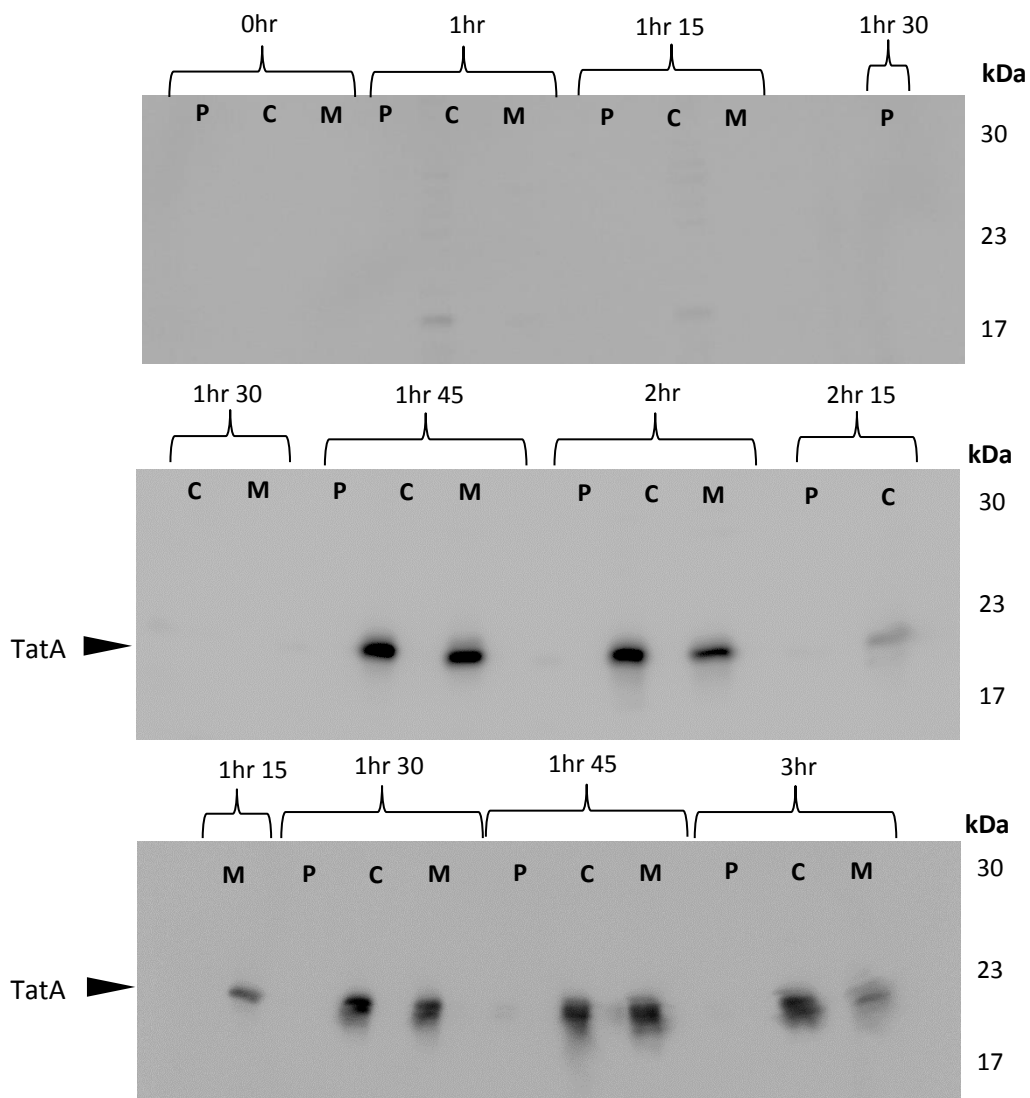
**Figure 6.2.13. Export assay of Tat substrate (TorA-hGH) into the periplasm of *E. coli*
with increased expression of Tat machinery: immunoblotting for detection of TatA**
Western Blot to detect the presence of hGH in *E. coli*. Post-induction with 1 mM IPTG
E.coli cells overexpressing hGH fused to a TorA signal peptide (TorA-hGH), and TatABC
were grown at 37°C for 3 hours. During this time, cells were periodically harvested,
normalised for $OD_{600} = 10$ and subsequently fractionated to periplasm (P), cytoplasm (C) and
membrane (M) fractions. Each fraction was examined for the presence of TatA by
immunoblotting with anti-TatA antibody. TatA was present in both the cytoplasm and
membrane fractions from 1hr 45 min until 3hrs.
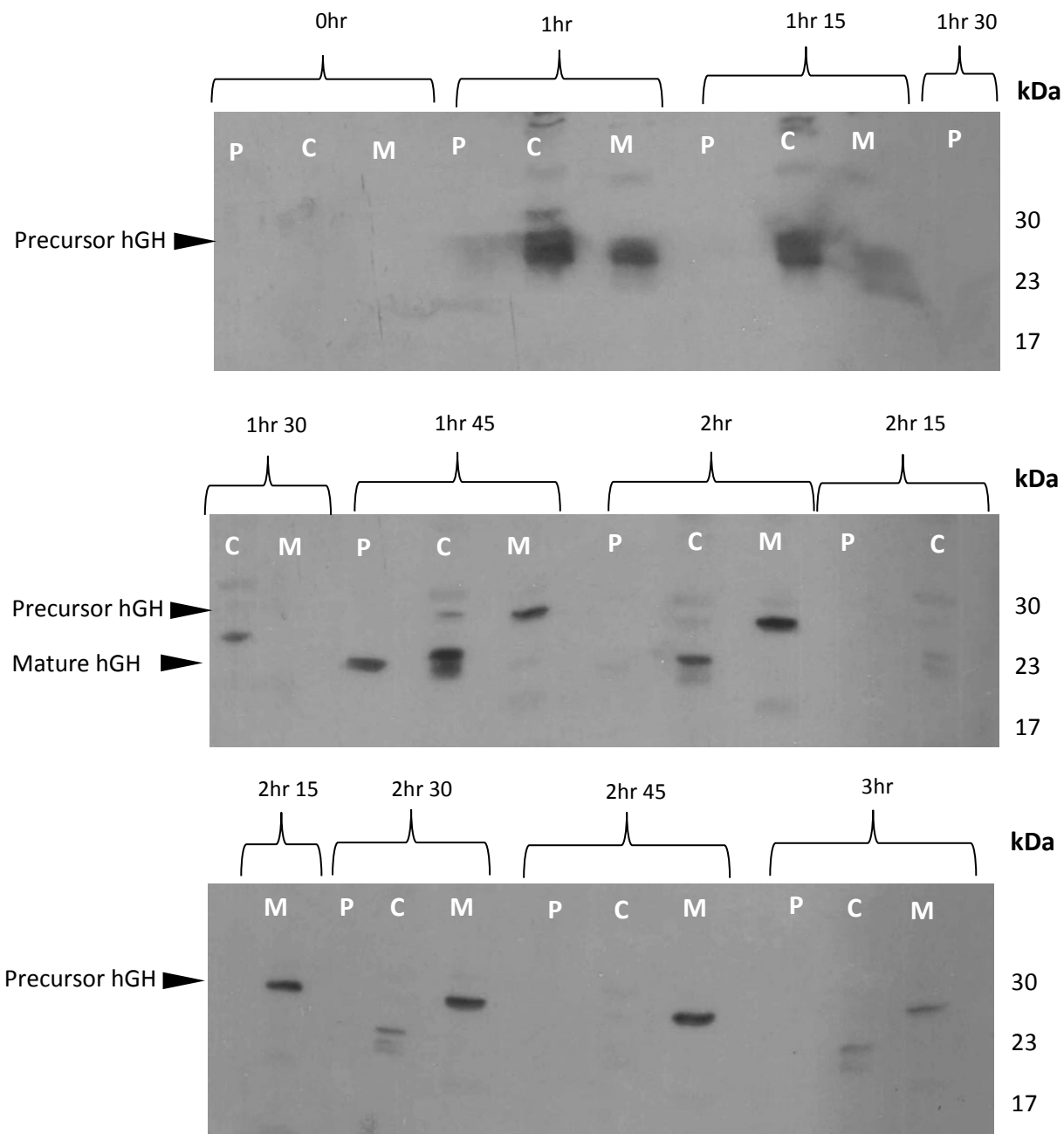
Figure 6.2.14. Export assay of Tat substrate (TorA-hGH) into the periplasm of *E. coli* with increased expression of Tat machinery: immunoblotting for detection of hGH
Western Blot to detect the presence of hGH in *E. coli*. Post-induction with 1 mM IPTG *E.coli* cells overexpressing hGH fused to a TorA signal peptide (TorA-hGH), and TatABC were grown at 37°C for 3 hours. During this time, cells were periodically harvested, normalised for $OD_{600} = 10$ and subsequently fractionated to periplasm (P), cytoplasm (C) and membrane (M) fractions. Each fraction was examined for the presence of hGH by immunoblotting with anti-hGH antibody. Results show that after 1 hour, precursor hGH (27 kDa) is present in both cytoplasmic and membrane fractions. The substrate remains in the membrane fraction until 3hrs. At 1hr 45, the cytoplasmic substrate is degraded into its mature form (22 kDa), and the amount of this protein gradually decreases over the remainder of the experiment. Only at 1hr 45 is the mature substrate seen in the periplasmic fraction.
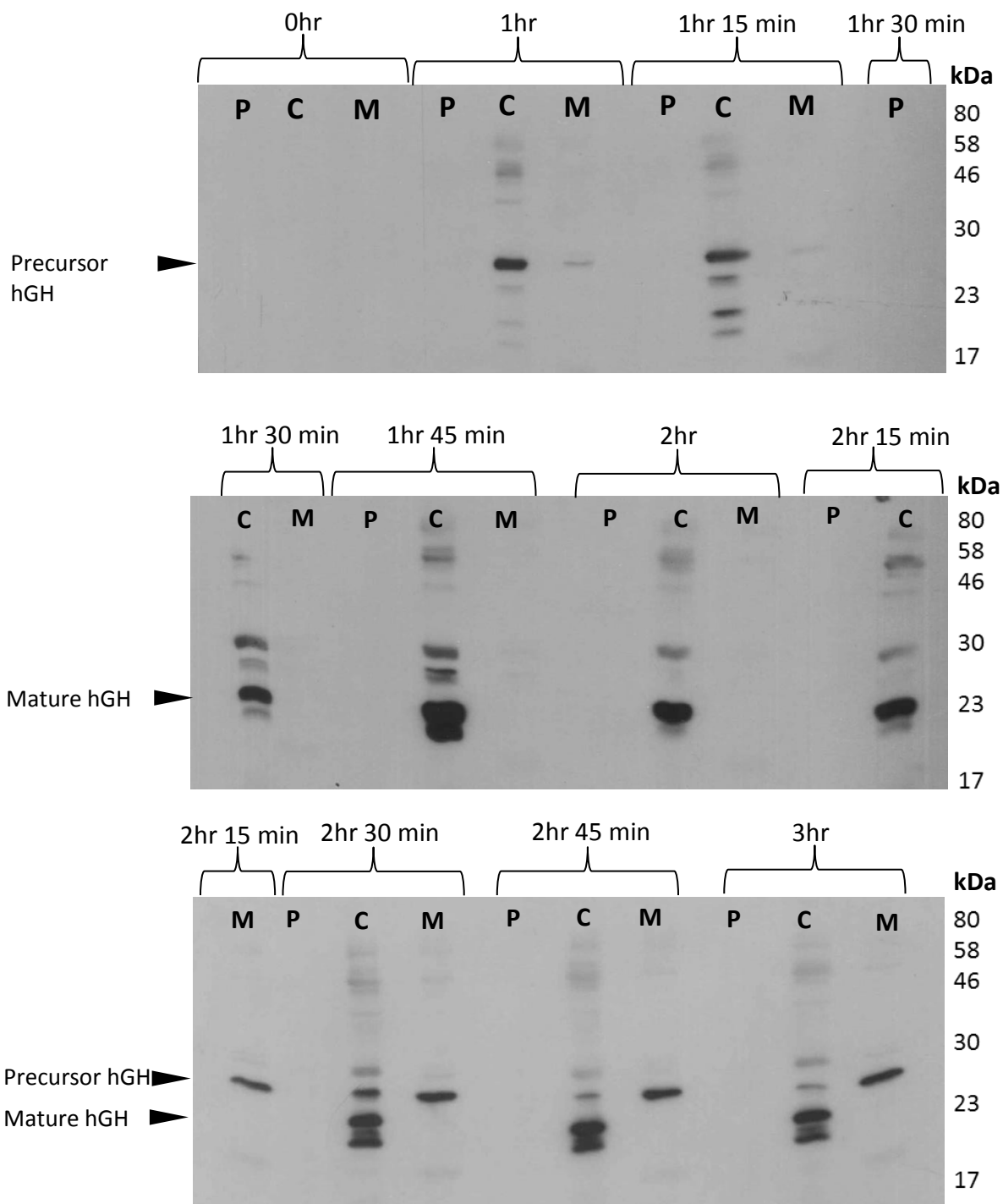
Figure 6.2.15. Export assay of TorA-hGH into the periplasm of *E. coli* cells lacking expression of Tat machinery

Western Blot to detect the presence of hGH in *E. coli*. Post-induction with 1 mM IPTG *E.coli* cells overexpressing hGH fused to a TorA signal peptide (TorA-hGH) and lacking expression of Tat machinery i.e. Δ*tat* were grown at 37°C for 3 hours. During this time, cells were periodically harvested, normalised for $OD_{600} = 10$ and subsequently fractionated to periplasm (P), cytoplasm (C) and membrane (M) fractions. Each fraction was examined for the presence of hGH by immunoblotting with anti-hGH antibody. Results show that mature hGH (22 kDa) is present in the cytoplasm from very early on (1 hr). Precursor Hgh (27 kDa) expression increases at 1hr 30. Membranous hGH is detected at 2hr 15 onwards. As expected, given the lack of Tat machinery, no hGH is located in the periplasm.
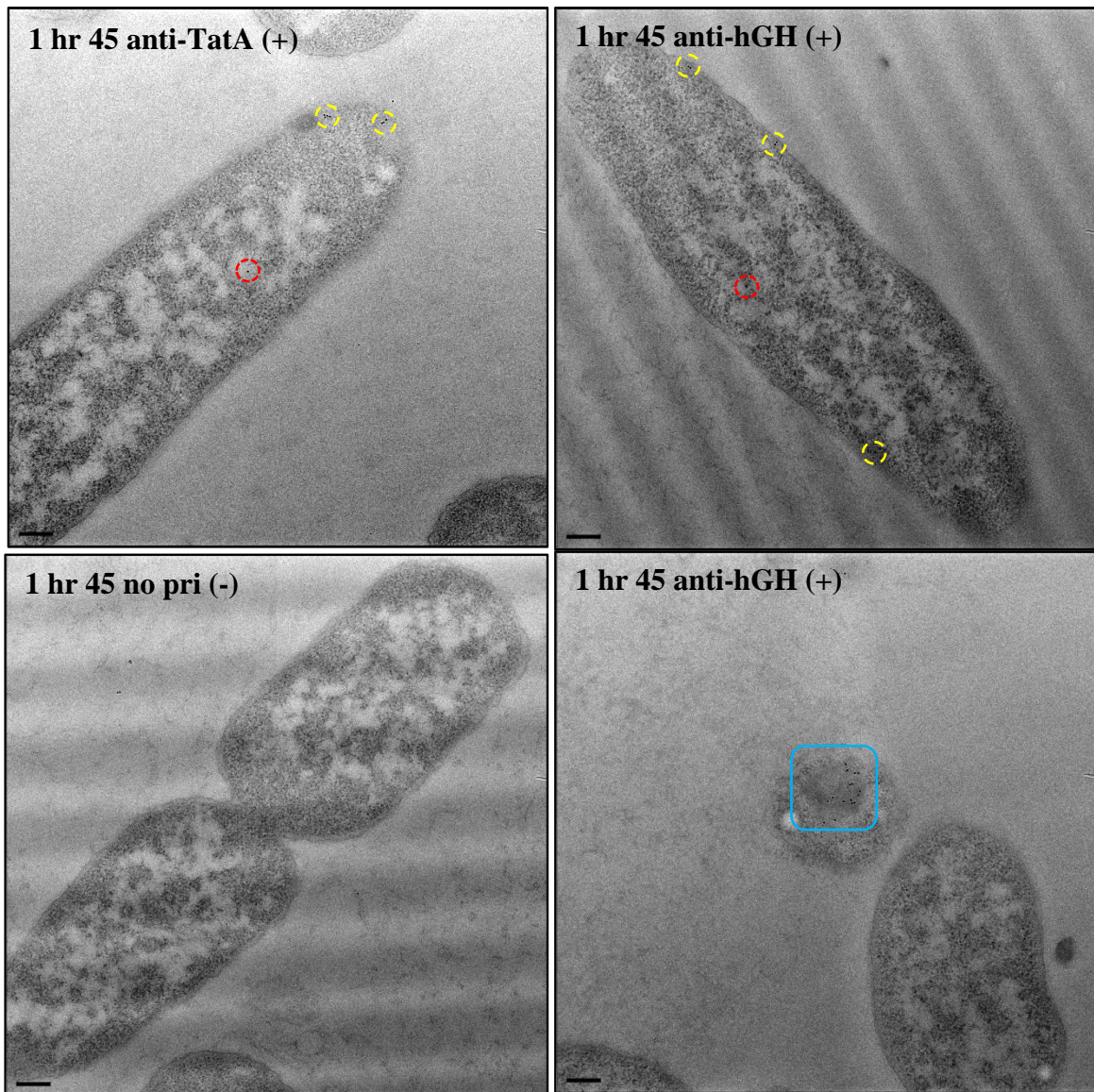
Figure 6.2.16. Immunogold labelling of TorA-hGH and TatA with increased expression of Tat machinery, 1hr 45 min post-induction.

Electron micrographs of resin-embedded, sectioned immunogold-labelled *E. coli* cells. Post-induction with 1 mM IPTG, *E. coli* cells overexpressing TorA-hGH and TatABC were harvested at 1hr 45 min. Following biological preservation, resin embedding and serial sectioning, the cells were immunogold labelled using anti-hGH antibody (top right and bottom right) and anti-TatA antibody (top left). Top-right: despite increased expression of Tat machinery, there was no alteration in the localisation and distribution of the hGH protein in either the cytoplasm (red circle) or membrane (yellow circle). hGH still aggregated into inclusion bodies (bottom right). Top-left: the TatA protein localised to both the cytoplasm (red circle) and inner membrane regions (yellow circle), with no preferential distribution or localisation witnessed. Controls were cells that had the primary antibody omitted from the immunolabelling procedure (-). These cells lacked gold binding, confirming no non-specific binding of gold-conjugated secondary antibody. Images were taken on a JEOL 2010F at 15,000X magnification. Scale bar = 200 nm.

At 2hrs the cytoplasmic precursor TorA-hGH started to degrade. Some precursor remained membrane-localised throughout the duration of the export assay. Given that successful transport was only seen for a short period, and based on previous data IN this chapter, it is likely that these bands represent inclusion bodies. Since the cells are co-expressing two plasmids it is likely that they are being subjected to considerable stress. To test whether this is the case, the export assay was repeated but with only expression of TorA-hGH in Δ*tat* background. *E. coli* cells overexpressing TorA-hGH (Δ*tat* background) were fractionated to generate cytoplasm (C), membrane (M) and periplasm (P) samples which were analysed by SDS-PAGE and immunoblotting with anti-hGH antibody. Some non-specific binding was observed.

As expected, results show that there is no mature hGH in the periplasm since Tat machinery is not expressed. As with co-expression experiments (Figure 6.2.15.), precursor TorA-hGH is expressed in the cytoplasm from as early as 1 hour after plasmid induction and is cleaved to mature hGH from 1hr 30 onwards. However, this mature hGH is more stable than in the co-expression experiment (Figure 6.2.12), residing in the cytoplasm until 3 hours. Therefore it is sensible to infer that expression of a second plasmid confers stress to the cell, and the heterologous protein was either degraded or aggregated into inclusion bodies.

Despite significant degradation of hGH upon co-expression of Tat machinery and substrate, export was observed, albeit briefly, at 1hr 45. Analysis of this sample by immunogold labelling and EM imaging revealed no difference in localisation and/or distribution of TatA protein (Figure 6.2.16, top-left) or hGH substrate (Figure 6.2.16, top right). A negative control in which primary antibody was omitted during immunolabelling showed that the secondary gold-conjugated antibody was not binding non-specifically (Figure 6.2.16, bottom left). As anticipated, inclusion bodies formed (Figure 6.2.16, bottom right).

6.3. Discussion

E. coli is one of the most widely-used prokaryotic organisms for the production of heterologous proteins for therapeutic or commercial uses; it is exploited for the production of over a third of currently-licensed therapeutic proteins (Walsh, 2010). Purification of such proteins from the periplasm offers two main advantages: firstly, there are fewer proteins in this cellular compartment, which simplifies downstream processing. Secondly, the oxidising environment facilitates disulphide bond formation. Heterologous proteins reach the periplasm by virtue of a signal peptide fused to its N-terminus. Once the protein is in the periplasm the signal peptide is cleaved off by specific proteases to release the mature protein into the periplasmic space (reviewed in: (Miot & Betton, 2004)).

To maximise periplasmic yields it is important to identify limiting factors to the high-yield production of heterologous proteins. Conventionally, the protein of interest is fused to a Sec-signal peptide to target it to the inner membrane (Georgiou & Segatori, 2005; Pugsley, 1993); however a pre-requisite of translocation is that the protein is unfolded. The limitation here is that once the protein is in the periplasm, it has to refold correctly. The Tat translocase bypasses this issue by transporting fully-folded proteins across the inner membrane into the periplasm.

Initial studies confirmed the capability of the Tat system to transport a heterologous protein to a high-yield (Matos *et al.*, 2012), and more recent data has shown that substrates are not limited to GFP with Tat being able to transport human growth hormone (hGH), scFV and interferon α2b (Alanen *et al.*, 2015). It is currently unknown whether Tat is capable of transporting these proteins on a large, industrial scale.

The data presented in this chapter investigated the export of a heterologous substrate – hGH – fused to a TorA signal peptide (**TorA-hGH**). Also, a substrate with a subtle mutation in the signal peptide was analysed in parallel: **TorA(A39L)-hGH**. This mutation has been shown to block maturation of the precursor at the inner membrane (Ren *et al.*, 2013). This is the first time that the export of a heterologous Tat substrate has been analysed in detail with direct, 2D visualisation of the substrate *in situ*.

Results of export assays presented in this chapter showed, for the first time, that precursor hGH is being degraded in the cytoplasm from as early as 1 hour after plasmid induction. This degradation is detrimental to the yield of hGH because the availability of precursor for Tat transport is significantly reduced.

E. coli contains many cytoplasmic proteases that play vital roles in regulating protein levels and eliminating damaged or abnormal proteins. Heterologous proteins can be regarded as unwanted by the cell, and thus stress proteins are induced to rapidly degrade the protein (Baney & Mujacic, 2004; Goff & Goldberg, 1985).

Whilst Tat has already been shown to export TorA-hGH (Matos *et al.*, 2012), previous studies have only taken a "snap shot" of protein localisation at 3 hours post-induction of plasmid (Alanen *et al.*, 2015). The data presented in this chapter is the first time export of the TorA-hGH has been studied in detail over the course of its induction. Detection of this early degradation provides vital preliminary insight into hGH export, and this degradation is something that can be minimised prior to large-scale trials.

Strategies for minimising the proteolysis of heterologous recombinant proteins have been studied (Murby *et al.*, 1996). A favoured approach, already adopted in this study, is targeting the protein to the periplasm where proteolysis is less extensive (Georgiou & Segatori, 2005). Alternately, alteration of host cell can be tested. For example, an *E. coli* strain that lacks expression of La protease (cytoplasmic protease responsible for degradation of non-native proteins) has been shown to stabilise recombinant proteins (Gottesman, 1990).

Export assays of mutant precursor showed that the Ala → Leu mutation at -1 position of the signal peptide successfully blocked maturation of TorA-hGH. Further analysis, using immunogold labelling and TEM visualisation, showed that the blocked precursor localised to the inner membrane. Further confirmation of this localisation is required by repeating the export assay of mutant precursor, but in cells with the Tat operon knocked-out (Δ*tat* cells). A lack of gold binding at the periphery of the cell would confirm that mutant precursor is stably expressed at the inner membrane in Tat-expressing cells.

From a bioprocessing perspective, the stable expression of a non-cleavable Tat precursor (which is exposed at the periplasmic face of the inner membrane (Karlsson *et al.*, 2012; Ren *et al.*, 2013), offers potential for the Tat system to be exploited for the development of cell surface display technologies.

Bacterial cell surface display involves expressing recombinant, heterologous proteins on the surface of cells. It is a versatile technique that has wide applicability, implicated in numerous technologies such as library screening, protein engineering or use as whole cell biocatalysts.

In *E. coli* proteins are usually displayed on the outer membrane (OM) surface-however: incorporation of foreign proteins in the OM can be toxic to the cell; the presence of lipopolysaccharides can sterically hinder interactions between expressed protein and binding-partner, and assembly at cellular appendages (e.g. flagella or pilli) can disrupt assembly of the recombinant protein (Chen & Georgiou, 2002). Therefore, expression on the inner membrane of spheroblasts (*E. coli* cells that have had their OM removed), has been shown to be a viable alternative: a technique termed 'Anchored Periplasmic Expression' (APEx).

APEx involves the N- or C-terminal fusion of heterologous proteins to the plasma membrane of bacteria. Initially single chain fragment variables (scFVs) were expressed when the technique was first developed (Harvey *et al.*, 2004), but whole antibodies and other proteins have since been expressed to significantly develop this technique for uses such as protein library screening (Lee *et al.*, 2013). Conventional means of expressing proteins at the surface of spheroblasts by N- or C-terminal fusions often encounters the uncertainty as to which side of the cytoplasmic membrane the recombinant protein is expressed i.e. the cytoplasmic side where the protein is rendered inaccessible or the periplasmic side where it is available for binding. The same could be argued for proteins expressed by the Tat machinery; however recent protease accessibility experiments confirmed that heterologous proteins (that have mutated signal peptides), are expressed solely on the periplasmic side of the cytoplasmic membrane (Ren *et al,.* 2013).

scFV has recently been shown to be exported by Tat machinery (Karlsson *et al.*, 2012), simplifying the APEx technique by bypassing requirement of an N- or C-terminal fusion and instead using an endogenous inner membrane protein complex:

Tat. The data presented in this chapter present preliminary evidence that this is now possible with another heterologous protein exported by the Tat machinery: hGH.

Prokaryotic production of recombinant hGH has its drawbacks: recombinant, overexpressed hGH aggregates to form inclusion bodies which require expensive denaturation and refolding steps to recover a biologically-active hormone. Also, Gram-negative bacteria possess an outer membrane bilayer which contains LPS. These are immunogenic and have to be removed prior to administering to humans or animals (Demain & Vaishnav, 2009). APEx expression of hGH in *E. coli* spheroblasts would avoid these issues and offers the possibility for Tat-expressed hGH to be implicated in cell surface display technology such as affinity maturation of hGH (Levin & Weiss, 2006).

Visualisation of hGH-overexpressing cells showed the formation of inclusion bodies that contained insoluble, aggregated hGH. These bodies limit the recoverable yield of active hGH and protein recovery from them is costly. However- IBs were not abundant in the sample, present in only 5% of cells visualised (10 out of 200 cells imaged); therefore there is a need to gain further insight into their prevalence.

Identifying IBs relies on exposing a portion of the IB during sectioning. Therefore more cells need to be analysed, or whole cell reconstructions of numerous *E. coli* obtained to gauge a better idea of the abundance of these IB. Also, these cells were only induced for 3 hours – in the biotechnology industry the cells undergo batch fermentation with expression lasting in excess of 10 hours. It would be interesting to see whether the prevalence of IBs increased significantly with increased induction of TorA-hGH and how it compared to conventional cytoplasmic expression systems of hGH. If there is indeed a low abundance of IBs when TorA-hGH is secreted into the periplasm this would give a strong advantage to using Tat machinery for the production of recombinant hGH, since downstream processing would be much more time- and cost-efficient.

Finally- visualisation of the TorA-hGH precursor revealed a random distribution in the cytoplasm and a uniform distribution in the inner membrane. These data mirror previous results of substrate localisation studies which used fluorescently tagged TorA (Rose *et al.*, 2013). TorA-mCherry exhibited a uniform staining throughout the inner membrane of *E. coli* suggesting the lack of a preferential localisation of this

substrate within the cell. A similar distribution was also seen in the cytosol. To increase the resolution obtained from the data presented in this chapter, which is only a 2D projection of cells, a 3D reconstruction of whole *E. coli* cells has the potential to provide deeper insight into the organisation of substrate in the cytoplasm and at the inner membrane.

To conclude, the data presented in this chapter have provided further insight into export of heterologous substrates via tat machinery. The identification of early precursor degradation and formation of inclusion bodies in the cytoplasm has highlighted specific activities that require further investigation and/or optimisation prior to large-scale expression of recombinant hGH. The stable expression of a non-cleavable Tat precursor highlights potential for Tat machinery to be exploited for bacterial cell surface display technologies.

Chapter 7:

Final discussion

7.0 Final Discussion

A considerable proportion of our knowledge regarding the Tat translocase has originated from studies on the Tat system of *E. coli*. This translocase is highly conserved amongst Gram-negative bacteria (Oates *et al.*, 2003), and is comprised of 3 essential proteins: TatA, TatB and TatC (Bogsch *et al.*, 1998; Sargent *et al.*, 1998; Sargent *et al.*, 1999). The organisation of this translocase in the inner membrane and its structure has been the focus of many studies over the past years (reviewed in chapter 1). In a steady-state situation, when there is no substrate to be transported, this translocase consists of a substrate-binding 370 kDa Tat(A)BC complex, and a separate heterogeneous TatA complex that ranges in size from 100 kDa to over 500 kDa (Oates *et al.*, 2005).

Low resolution structures of the TatA complex generated from EM analysis showed that these complexes have ring-shaped structures of variable diameter (9 – 13 nm), with an internal channel large enough to accommodate even the largest Tat substrate, TorA (90 kDa) (Gohlke *et al.*, 2005). It was the identification of an internal channel that has underpinned the currently most accepted mechanism of Tat translocation: the pore-forming mechanism. This mechanism predicts that substrate binding to the Tat(A)BC complex (Alami *et al.*, 2003; Alami *et al.*, 2002; Cline & Mori, 2001; McDevitt *et al.*, 2006) triggers the recruitment of TatA proteins (Mori & Cline, 2002) to form the active size-fitting translocase, TatABC, through which the substrate can traverse the inner membrane, and gain entry to the periplasmic space (Gohlke *et al.*, 2005; Oates *et al.*, 2005). However in light of more recent evidence from biochemical and structural studies, which indicate that such variation in TatA size and structure (Baglieri *et al.*, 2012; Barnett *et al.*, 2008; Beck *et al.*, 2013; van der Ploeg *et al.*, 2011) is not common to all Tat complexes, the validity of the pore-forming model is uncertain. Therefore, the mechanism of Tat translocation is still very much unresolved. Further insight into the structure and localisation of Tat complexes from both Gram-positive and Gram–negative bacteria will undoubtedly play key roles in elucidating more information on how this remarkable protein machinery operates.

In this investigation, electron microscopy has been used to gain novel insight into the structure, localisation and distribution of Tat complexes from both Gram-negative

and Gram–positive bacteria. Preliminary structural characterisation of TatAyCy complex from *B. subtilis* was conducted alongside further investigation into the localisation and distribution of TatABC and its substrates in the inner membrane. The work presented in this thesis largely supports previous biochemical and microscopy-based observations on these Tat complexes from both Gram-positive and Gram–negative bacteria.

In the first chapter presented in this thesis, the TatAyCy complex from *B. subtilis* was isolated and purified for direct visualisation under the TEM. Despite being smaller than its Gram-negative counterpart, this complex's arrangement in the inner membrane is parallel to that of TatABC in *E. coli*, whereby a substrate-binding complex TatAyCy (200 kDa) is expressed alongside a separate pool of TatAy (200 kDa) (Barnett *et al.*, 2009).

Preliminary 2D structural characterisation of detergent-solubilised TatAyCy complexes revealed circular particles, ranging from 12 - 14 nm in diameter. It remains uncertain whether this observed heterogeneity under the electron microscope is inherent and important for Tat translocase function or is an artefact of sample preparation. However, in light of this data showing that a Tat complex from a Gram-positive bacterium is able to functionally complement the Gram-negative system of *E. coli*, it highlights that there are no system-specific factors in the Gram-positive *B. subtilis* which contribute to the operation of Tat machinery. Therefore, it is sensible to assume that these Tat machineries operate by the same mechanism and the heterogeneity observed between the two is an artefact if their isolation (i.e. detergent extraction) and is therefore not likely to be necessary for function. For example, there could be differing lipid retention during the purification of Gram-positive versus Gram-negative Tat complexes. This variation could affect stability of the protein-detergent complexes and thus induce heterogeneity in the detergent-solubilised Tat complexes. Alternatively, the heterogeneity of Tat complexes could be a consequence of the protein's sensitivity to proteolysis, whereby the Tat proteins/complexes would be cleaved into by-products of varying sizes.

3D EM structures of TatAd showed this protein complex lacks a pore large enough to support translocation on its own (Beck *et al.*, 2013). Together, this and the aforementioned findings question the biological significance of the large

heterogeneity seen for *E. coli* TatA, and are instead in favour of an alternative model of Tat that is flexible enough to transport a wide range of substrates. For example- the coalescence of numerous relatively homogeneous TatA/TatAy/TatAd and TatBC/TatAyCy/TatAdCd complexes to form Tat translocases of differing sizes. The inherent heterogeneity of TatAyCy revealed in this study is likely to be an identification of the flexibility of this complex, and could explain why this complex is capable of transporting substrates other than its endogenous YwbN (45 kDa) (Barnett *et al.*, 2009).

A control of serially diluted TatAyCy complexes was necessary to gauge the true population of TatAyCy complexes under the TEM. Results showed that as the dilution of the TatAyCy protein increased, the average diameter of the particles also increased. This detergent-induced variation in complex appearance (i.e. size) under the EM is supported by evidence showing that detergent-solubilised TatA forms complexes even when expressed in the absence of TatBC components (Porcelli *et al.*, 2002). Furthermore, detergent-only samples were found to contain particles, albeit in lower abundance than TatAyCy complexes, which were of the same diameter to the TatAyCy PDCs. Together these results demonstrate the implications that detergent-solubilisation has on the structural analysis of membrane proteins, and reiterates the need to circumvent the use of detergents in this field of research. Therefore the remainder of findings presented in this thesis endeavoured to analyse the Tat machinery and/or its substrates avoiding the analysis of detergent-solubilised complexes.

The next avenue of research involved the reconstitution of TatAyCy into liposomes for topography analysis via AFM. Liposomes are synthetic membrane mimetics; therefore reconstitution of an integral membrane protein into these vesicles provides a lipid bilayer for the protein- an environment more natural than detergent-solubilised complexes. Reconstitution of TatAyCy into liposomes proved difficult. I identified numerous parameters that are important for reconstitution of Tat complexes into liposomes. From the data presented in this chapter, it seems that lower L:P ratios, liposomes consisting of single lipid type (i.e. DOPC) and use of detergent with high CMC (i.e. OG), provide conditions that favour protein reconstitution.

Analysis of the Tat proteoliposomes under the AFM tip was ambiguous, with very few protein-like features detected. The lack of such features is owed to the difficulty in reconstituting a high density of Tat proteins into liposomes. Protein reconstitution involves a complex interplay between the aforementioned parameters, and successful reconstitution of Tat protein would require significant further empirical optimisation. Therefore, an alternative means for directly visualising Tat in the inner membrane, circumventing the use of detergent, was desired. To achieve this, I developed the novel combinatorial approach of array tomography with immunogold labelling to unambiguously identify TatA in the inner membrane of *E. coli*.

TatA plays an essential role in the translocation system, and any hypothesis regarding Tat's mechanism of translocation makes predictions about the localisation and distribution of TatA in the inner membrane. Therefore, insight into the arrangement of this protein is fundamental to elucidating the mechanism of Tat translocation.

Direct visualisation of the TatA protein in its native cellular environment, in 3D space, revealed TatA to cluster along the inner membrane in a TatBC-dependent manner. This is the first time that the localisation and distribution of a Tat component has been visualised in 3D space, *in situ*.

Previous efforts to gain this level of insight have utilised TatA-XFP fusion proteins. Data derived from these studies are complicated by the fact that fluorescently-tagged TatA proteins are inactive and can aggregate at the membrane (Alcock *et al.*, 2013; Ray *et al.*, 2005). Therefore, we are unable to compare data from such studies to those obtained in this study.

The higher resolution of labelling in this study in combination with the 3D appreciation of the localisation of TatA provided further insight into the Tat translocase. Remembering that we are labelling specifically for TatA, current models of the mechanism of Tat protein transport make specific predictions about the oligomeric state of TatA and whether or how this changes during the transport cycle. For example, the pore-forming model of Tat translocation predicts that there is a 'pool' of TatA protein positioned in the membrane "waiting" for a substrate to binding the Tat(A)BC complex (Gohlke *et al.*, 2005; Sargent *et al.*, 2001) (Figure 7.1, top panel). The identification of individual TatA proteins in a linear cluster in the

inner membrane in this study could be consistent with the pore-forming model of Tat, whereby a 'pool' of TatA protein is required for complex assembly (Gohlke *et al.*, 2005; Sargent *et al.*, 2001).

However, since I have only labelled for a single protein and sectioned the *E. coli* at 50 nm intervals (hence each protein in the TatA cluster is 50 nm apart from the next TatA protein), one of two situations could be represented with this clustering of TatA. Either: a single TatBC serves as a nucleation site with a row of TatA along the inner membrane (Figure 7.1., middle panel); or there are separate Tat complexes awaiting substrate binding (Figure 7.1., bottom panel). Given that the higher order oligomer formation of the TatA complex is absolutely dependent on the presence of TatBC (Mori and Cline., 2002), and that I only see this clustering of TatA along the inner membrane when TatBC are co-expressed with TatA (not TatA alone), this localisation of TatA could be a higher order oligomeric structure of TatA. Furthermore, TatBC exists in a 1:1 ratio with TatA being expressed at an ~20-fold excess (Bolhius *et al.,* 2001; Sargent *et al.,* 2001), it is possible that there could be a single TatBC complex serving as a single nucleation site for subsequent binding of multiple TatA protomers upon substrate binding. The observed heterogeneity in the number of TatA proteins in each cluster could reflect the dynamic polymerisation of TatA protein for substrates of different sizes (Gohlke *et al.*, 2005).
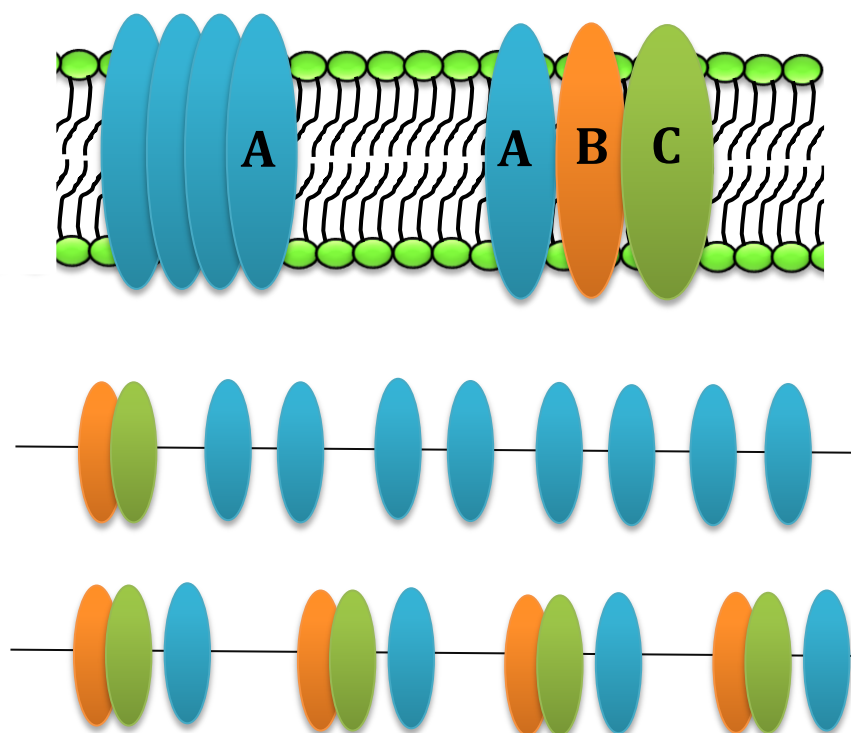
Figure 7.1. Arrangement of TatA in the inner membrane of *E. coli*
According to the pore-forming model of Tat translocation, a pool of heterogeneous TatA proteins are located in close proximity to the Tat(A)BC substrate-binding complex. Upon substrate binding, it is predicted that TatA proteins are recruited to the Tat(A)BC complex to form the active translocase through which the substrate is transported (top panel). The arrangement of Tat constituents in the inner membrane is ambiguous. It is unknown whether the TatA proteins are located adjacent to each other with TatBC forming a nucleation point (middle panel), or multiple Tat complexes are located adjacent to each other (bottom panel).

The relative location of other Tat proteins remains unknown. Such information would add further detail to the distribution of TatA observed in this investigation; and therefore remains an important avenue for future work. Previous array tomography studies have only ever utilised fluorescently-conjugated proteins to quantitatively determine the protein composition of synaptic vesicles (Collman *et al.*, 2015; Horstmann *et al.*, 2012; Kay *et al.*, 2013; Reichelt *et al.*, 2012). However, the resolution of labelling in these experiments it not as high as what has been achieved in this study; and the use of immunogold avoids the requirement of fluorescently conjugated tags onto the protein of interest.

Until now, the technique of array tomography has been used almost exclusively in the field of neuroscience; however our novel development of array tomography, in

combination with the high-resolution immunogold labelling of proteins, has the potential to be applied to any cellular antigen- not just those of Tat machinery or of *E. coli.*

The identification of individual proteins can unveil novel levels of organisation and consequently test mechanistic hypotheses. For example, Besson *et al.* (2015) identified an alteration in localisation of the PAR protein complex: the polarisation of this complex in mother cells is an essential process for cell division and thus development of fly notum in *Drosophila* (Besson *et al., 2015).* Alternatively, alterations in subcellular protein distributions patterns was ascertained to specific adhesive and mechanical properties of human fibroblast cells, and consequently able to identify metastasizing tumour cells (Rönnlund *et al.*, 2013).

The high-resolution of labelling afforded by the combinatorial technique used in this study, in combination with the efficiency of image acquisition and lack of requirement for fluorescently-conjugated proteins (such as those used in the aforementioned studies (Besson *et al.*, 2015; Rönnlund *et al.*, 2013)), has the potential to reveal novel insight into specific proteins. Additionally, the immunogold labelling of serially sectioned samples overcomes the difficulties of protein labelling in electron tomography. For example, a sufficient density of gold particles is required on the section surface to allow accurate reconstruction of a 3D volume.

In a continued effort to gain further insight into the Tat translocase in the inner membrane, the technique of immunogold labelling was further utilised to analyse Tat substrates, *in situ,* directly under the EM. In the final chapter of this thesis, the export of a heterologous Tat substrate was analysed. A TorA signal peptide was fused to the hGH protein to form a 26 kDa precursor. Given the potential application of the Tat system to the biotech industry (Alanen *et al.*, 2015; Matos *et al.*, 2012) the export of this biotechnologically-relevant precursor protein was investigated. This was the first time that the export of a heterologous Tat substrate has been analysed in detail with direct, 2D visualisation of the substrate, *in situ.*

Results of export assays revealed that the precursor protein was degraded from an early time point. This novel insight implicates the exploitation of the Tat translocase for export of biotherapeutic proteins: degradation of the heterologous precursor reduces the amount of protein available for export and hence decreases the final yield

of hGH. Additionally, inclusion bodies (IBs) containing aggregates of hGH protein were visualised under the TEM. Similarly, this affects the biotechnological application of Tat machinery since IBs of hGH are likely to contain aggregated, denatured hGH and thus limit the yield of recoverable hGH (Yamaguchi & Miyazaki, 2014). Strategies to minimise precursor degradation and to further investigate the true abundance of the IBs remains important future work.

A mutant precursor protein with a subtle mutation in the signal peptide was analysed in parallel to the wild-type. In support of previous biochemical data (Ren *et al.*, 2013), this mutation blocked maturation of the precursor protein and was consequently expressed at the inner membrane for the duration of the expression period. The stable expression of a non-cleavable precursor at periplasmic face of the inner membrane (Karlsson *et al.*, 2012; Ren *et al.*, 2013) offers potential for the Tat system to be exploited for the development of bacterial cell surface display technologies. The ability to express hGH on the periplasmic face of the inner membrane offers the possibility that Tat-exported hGH can be utilised in affinity maturation experiments. Future work remains to see the possible yield of Tat-exported hGH on a large scale.

Additionally, it remains to be seen whether Tat is capable of stably expressing other signal peptide mutants on the periplasmic face of the inner membrane. scFV has already been identified as a substrate capable of Tat export (Alanen *et al.*, 2015). Stable expression of this protein, via the APEx technology, has already been employed in library screening studies (Jung *et al.*, 2007; Qiu *et al.*, 2010); Tat offers potential as a system capable of overexpressing large, heterologous protein at the inner membrane without becoming saturated (Ren *et al.*, 2013). This would facilitate and accelerate the potential of APEx technology for high-throughput screening of protein libraries to identify novel antibodies against disease cell surface antigens.

Direct visualisation of hGH permitted novel insight into the localisation and distribution of a Tat substrate in an *E. coli* cell. Immunogold labelling revealed TorA-hGH to exhibit a random distribution in the cytoplasm and a uniform distribution in the inner membrane, which mirrors results of previous substrate localisation experiments (Rose *et al.*, 2013). Deeper insight into the organisation of the Tat substrate in the cytoplasm and inner membrane would be provided through

3D reconstruction(s) of whole *E. coli* cells, and thus remains as future work; whilst Tat would be too small to see as a complex, the immunogold labelling could reveal any larger structures/arrangements that it forms inside the cell.

To conclude, the initial part of this investigation illustrated how detergent solubilisation of an integral membrane protein implicates structural analysis, and the structural information gained must be treated with caution. Therefore, I successfully circumvented the use of detergent to analyse the Tat machinery in its native cellular environment. The novel development of array tomography in combination with immunogold labelling enabled the direct, unambiguous visualisation of TatA in the inner membrane of *E. coli*. The 3D visualisation of this protein unveiled, for the first time, that the TatA protein forms a linear cluster in the inner membrane, in a TatBC-dependent manner. Capitalising on the ability of the immunogold labelling to identify any cellular antigen, the stable expression of a non-cleavable Tat precursor substrate demonstrated the potential for this translocase to be exploited for cell-surface display technologies. The visualisation of other Tat proteins, its substrates or possible neighbouring constituents remains important future work and will enable higher levels of understanding regarding the arrangement, and thus activity, of this translocase in the inner membrane.

Chapter 8:
References

8.0 References

Alami, M., Lüke, I., Deitermann, S., Eisner, G., Koch, H.-G., Brunner, J. & Müller, M. (2003) Differential Interactions between a Twin-Arginine Signal Peptide and Its Translocase in Escherichia coli. *Molecular Cell*, **12** (4): 937-946.

Alami, M., Trescher, D., Wu, L. F. & Müller, M. (2002) Separate analysis of twin-arginine translocation (Tat)-specific membrane binding and translocation in Escherichia coli. *Journal of Biological Chemistry*, **277** (23): 20499.

Alanen, H. I., Walker, K. L., Lourdes Velez Suberbie, M., Matos, C. F. R. O., Bönisch, S., Freedman, R. B., Keshavarz-Moore, E., Ruddock, L. W. & Robinson, C. (2015) Efficient export of human growth hormone, interferon α2b and antibody fragments to the periplasm by the Escherichia coli Tat pathway in the absence of prior disulfide bond formation. *Biochimica et Biophysica Acta (BBA) - Molecular Cell Research*, **1853** (3): 756-763.

Albiniak, A. M., Baglieri, J. & Robinson, C. (2012) Targeting of lumenal proteins across the thylakoid membrane. *Journal of Experimental Botany*, **63** (4): 1689-1698.

Alcock, F., Baker, M. A. B., Greene, N. P., Palmer, T., Wallace, M. I. & Berks, B. C. (2013) Live cell imaging shows reversible assembly of the TatA component of the twin-arginine protein transport system. *Proceedings of the National Academy of Sciences of the United States of America*, **110** (38): E3650-E3659.

Aldridge, C., Ma, X., Gerard, F. & Cline, K. (2014) Substrate-gated docking of pore subunit Tha4 in the TatC cavity initiates Tat translocase assembly. *The Journal of Cell Biology*, **205** (1): 51-65.

Allen, S. C. H., Barrett, C. M. L., Ray, N. & Robinson, C. (2002) Essential cytoplasmic domains in the Escherichia coli TatC protein. *Journal of Biological Chemistry*, **277** (12): 10362.

Bachmann, J., Bauer, B., Zwicker, K., Ludwig, B. & Anderka, O. (2006) The Rieske protein from Paracoccus denitrificans is inserted into the cytoplasmic membrane by the twin-arginine translocase. *FEBS Journal*, **273** (21): 4817-4830.

Baglieri, J., Beck, D., Vasisht, N., Smith, C. & Robinson, C. (2012) Structure of the TatA paralog, TatE, suggests a structurally homogeneous form of Tat protein translocase that transports folded proteins of differing diameter. *Journal of Biological Chemistry*, **287** (10): 7335 - 7344.

Bakshi, S., Siryaporn, A., Goulian, M. & Weisshaar, J. C. (2012) Superresolution Imaging of Ribosomes and RNA Polymerase in Live Escherichia coli Cells. *Molecular Microbiology*, **85** (1): 21-38.

Baney, F. & Mujacic, M. (2004) Recombinant protein folding and misfolding in Escherichia coli. *Nature Biotechnology*, **22** 1399 - 1408.

Barnett, J., Eijlander, R. & Kuipers, O. (2008) A minimal Tat systems from a Gram-positive organism: a bifunctional TatA subunit participates in discrete TatAC and TatA complexes. *Journal of Biological Chemistry*, **283** 2534 - 2542.

Barnett, J. P., van der Ploeg, R., Eijlander, R. T., Nenninger, A., Mendel, S., Rozeboom, R., Kuipers, O. P., van Dijl, J. M. & Robinson, C. (2009) The twin-arginine translocation (Tat) systems from Bacillus subtilis display a conserved mode of complex organization and similar substrate recognition requirements. *FEBS journal*, **276** (1): 232-243.

Barrett, C. M. L., Freudl, R. & Robinson, C. (2007) Twin Arginine Translocation (Tat)-dependent Export in the Apparent Absence of TatABC or TatA Complexes Using Modified Escherichia coli TatA Subunits That Substitute for TatB. *Journal of Biological Chemistry*, **282** (50): 36206-36213.

Barrett, C. M. L., Mangels, D. & Robinson, C. (2005) Mutations in Subunits of theEscherichia coli Twin-arginine Translocase Block Function via Differing Effects on Translocation Activity or Tat Complex Structure. *Journal of Molecular Biology*, **347** (2): 453-463.

Barrett, C. M. L., Mathers, J. E. & Robinson, C. (2003) Identification of key regions within the Escherichia coli TatAB subunits. *FEBS Letters*, **537** (1-3): 42-46.

Batey, R. T., Rambo, R. P., Lucast, L., Rha, B. & Doudna, J. A. (2000) Crystal Structure of the Ribonucleoprotein Core of the Signal Recognition Particle. *Science*, **287** (5456): 1232-1239.

Beck, D., Vasisht, N., Baglieri, J., Monteferrante, C. G., van Dijl, J. M., Robinson, C. & Smith, C. J. (2013) Ultrastructural characterisation of Bacillus subtilis TatA complexes suggests they are too small to form homooligomeric translocation pores. *Biochimica et Biophysica Acta (BBA) - Molecular Cell Research*, **1833** (8): 1811-1819.

Beckmann, R., Spahn, C. M. T., Eswar, N., Helmers, J., Penczek, P. A., Sali, A., Frank, J. & Blobel, G. (2001) Architecture of the Protein-Conducting Channel Associated with the Translating 80S Ribosome. *Cell*, **107** (3): 361-372.

Behrendt, J., Standar, K., Lindenstrauß, U. & Brüser, T. (2004) Topological studies on the twin-arginine translocase component TatC. *FEMS Microbiology Letters*, **234** (2): 303-308.

Belin, D., Plaia, G., Boulfekhar, Y. & Silva, F. (2015) Escherichia coli SecG Is Required for Residual Export Mediated by Mutant Signal Sequences and for SecY-SecE Complex Stability. *Journal of Bacteriology*, **197** (3): 542-552.

Berg, B. v. d., Clemons, W. M., Collinson, I., Modis, Y., Hartmann, E., Harrison, S. C. & Rapoport, T. A. (2004) X-ray structure of a protein-conducting channel. *Nature*, **427** (6969): 36-44.

Berks, B. (1996) A common export pathway for proteins binding complex redox cofactors? *Molecular Microbiology*, **22** (3): 393-404.

Berks, B. C., Palmer, T. & Sargent, F. (2003) The Tat protein translocation pathway and its role in microbial physiology. *Advances in microbial physiology*, **47** 187-254.

Bernhardt, T. G. & De Boer, P. A. J. (2003) The Escherichia coli amidase AmiC is a periplasmic septal ring component exported via the twin-arginine transport pathway. *Molecular Microbiology*, **48** (5): 1171-1182.

Bernstein, H. D., Poritz, M. A., Strub, K., Hoben, P. J., Brenner, S. & Walter, P. (1989) Model for signal sequence recognition from amino-acid sequence of 54K subunit of signal recognition particle. *Nature*, **340** (6233): 482-486.

Berryman, M. A., Rodewald, R.D., (1990) An enhanced method for post-embedding immunocytochemical staining which preserves cells membranes. *The Journal of Histochemistry and Cytochemistry*, **38** (2): 159-170.

Berthelmann, F. & Brüser, T. (2004) Localization of the Tat translocon components in Escherichia coli. *FEBS letters*, **569** (1-3): 82-88.

Berthelmann, F., Mehner, D., Richter, S., Lindenstrauss, U., Lunsdorf, H., Hause, G. & Bruser, T. (2008) Recombinant Expression of tatABC and tatAC Results in the Formation of Interacting Cytoplasmic TatA Tubes in Escherichia coli. *J. Biol. Chem.*, **283** (37): 25281-25289.

Besson, C., Bernard, F., Corson, F., Rouault, H., Reynaud, E., Keder, A., Mazouni, K. & Schweisguth, F. (2015) Planar Cell Polarity Breaks the Symmetry of PAR Protein Distribution prior to Mitosis in Drosophila Sensory Organ Precursor Cells. *Current Biology*, **25** (8): 1104-1110.

Blaudeck, N., Kreutzenbeck, P., Freudl, R. & Sprenger, G. A. (2003) Genetic Analysis of Pathway Specificity during Posttranslational Protein Translocation across the Escherichia coli Plasma Membrane. *Journal of Bacteriology*, **185** (9): 2811-2819.

Blaudeck, N., Kreutzenbeck, P., Muller, M., Sprenger, G. A. & Freudl, R. (2005) Isolation and Characterization of Bifunctional Escherichia coli TatA Mutant Proteins That Allow Efficient Tat-dependent Protein Translocation in the Absence of TatB. *Journal of Biological Chemistry*, **280** (5): 3426-3432.

Blümmel, A.-S., Haag, L. A., Eimer, E., Müller, M. & Fröbel, J. (2015) Initial assembly steps of a translocase for folded proteins. *Nature Communications*, **6** 7234.

Bogsch, E., Brink, S. & Robinson, C. (1997) Pathway specificity for a delta-pH-dependent precursor thylakoid lumen protein is governed by 'Sec-avoidance' motif in the transfer peptide and a 'Sec-incompatible' mature protein. *EMBO*, **16** 3851-3859.

Bogsch, E. G., Sargent, F., Stanley, N. R., Berks, B. C., Robinson, C. & Palmer, T. (1998) An Essential Component of a Novel Bacterial Protein Export System with Homologues in Plastids and Mitochondria. *Journal of Biological Chemistry*, **273** (29): 18003-18006.

Bolhuis, A. (2002) Protein transport in the halophilic archaeon Halobacterium sp. NRC-1: a major role for the twin-arginine translocation pathway? *Microbiology*, **148** (11): 3335-3346.

Bolhuis, A., Mathers, J. E., Thomas, J. D., Barrett, C. M. L. & Robinson, C. (2001) TatB and TatC form a functional and structural unit of the twin-arginine translocase from Escherichia coli. *Journal of Biological Chemistry*, **276** (23): 20213.

Bruch, M. D., McKnight, C. J. & Gierasch, L. M. (1989) Helix formation and stability in a signal sequence. *Biochemistry*, **28** (21): 8554 - 8561.

Brüser, T. & Sanders, C. (2003) An alternative model of the twin arginine translocation system. *Microbiological research*, **158** (1): 7-17.

Buchanan, G., de Leeuw, E., Stanley, N. R., Wexler, M., Berks, B. C., Sargent, F. & Palmer, T. (2002) Functional complexity of the twin-arginine translocase TatC component revealed by site-directed mutagenesis. *Molecular microbiology*, **43** (6): 1457-1470.

Buchanan, G., Sargent, F., Berks, B. C. & Palmer, T. (2001) A genetic screen for suppressors of Escherichia coli Tat signal peptide mutations establishes a critical role for the second arginine within the twin-arginine motif. *Archives of microbiology*, **177** (1): 107-112.

Caldelari, I., Mann, S., Crooks, C. & Palmer, T. (2006) The Tat Pathway of the Plant Pathogen Pseudomonas syringae is Required for Optimal Virulence. *Molecular Plant-Microbe Interactions*, **19** (2): 200-212.

Chaddock, A. M., Mant, A., Karnauchov, I., Brink, S., Herrmann, R. G., Klösgen, R. B. & Robinson, C. (1995) A new type of signal peptide: central role of a twin-arginine motif in transfer signals for the delta pH-dependent thylakoidal protein translocase. *The EMBO Journal*, **14** (12): 2715.

Chan, C. S., Haney, E. F., Vogel, H. J. & Turner, R. J. (2011) Towards understanding the Tat translocation mechanism through structural and biophysical studies of the amphipathic region of TatA from Escherichia coli. *Biochimica et Biophysica Acta (BBA) - Biomembranes*, **1808** (9): 2289-2296.

Chan, C. S., Zlomislic, M. R., Tieleman, D. P. & Turner, R. J. (2007) The TatA subunit of Escherichia coli twin-arginine translocase has an N-in topology. *Biochemistry*, **46** (25): 7396-7404.

Chen, W. & Georgiou, G. (2002) Cell-Surface Display of Heterologous Proteins: From High-Throughput Screening to Environmental Applications *Biotechnology and Bioengineering*, **79** (5): 496 - 503.

Clark, S. A. & Theg, S. M. (1997) A folded protein can be transported across the chloroplast envelope and thylakoid membranes. *Molecular Biology of the Cell*, **8** (5): 923-934.

Cline, K. (2015) Mechanistic aspects of folded protein transport by the Twin Arginine Translocase (Tat). *The Journal of Biological Chemistry*, **290** (27): 16530 - 16538.

Cline, K. & McCaffery, M. (2007) Evidence for a dynamic and transient pathway through the TAT protein transport machinery. *EMBO J*, **26** (13): 3039 - 3049.

Cline, K. & Mori, H. (2001) Thylakoid ΔpH-dependent precursor proteins bind to a cpTatC–Hcf106 complex before Tha4-dependent transport. *The Journal of cell biology*, **154** (4): 719-730.

Collman, F., Buchanan, J., Phend, K. D., Micheva, K. D., Weinberg, R. J. & Smith, S. J. (2015) Mapping Synapses by Conjugate Light-Electron Array Tomography. *The Journal of Neuroscience*, **35** (14): 5792-5807.

Creighton, A. M., Hulford, A., Mant, A., Robinson, D. & Robinson, C. (1995) A Monomeric, Tightly Folded Stromal Intermediate on the pH-dependent Thylakoidal Protein Transport Pathway. *Journal of Biological Chemistry*, **270** (4): 1663-1669.

Cristóbal, S., de Gier, J.-W., Nielsen, H. & von Heijne, G. (1999) Competition between Sec- and TAT-dependent protein translocation in Escherichia coli. *EMBO journal*, **18** 2982-2990.

Dabney-Smith, C., Mori, H. & Cline, K. (2006) Oligomers of Tha4 organize at the thylakoid Tat translocase during protein transport. *Journal of Biological Chemistry*, **281** (9): 5476-5483.

Dalbey, R. E., Wang, P. & Kuhn, A. (2011) Assembly of Bacterial Inner Membrane Proteins. *Annual Review of Biochemistry*, **80** (1): 161-187.

De Buck, E., Maes, L., Meyen, E., Van Mellaert, L., Geukens, N., Anné, J. & Lammertyn, E. (2005) Legionella pneumophila Philadelphia-1 tatB and tatC affect intracellular replication and biofilm formation. *Biochemical and Biophysical Research Communications*, **331** (4): 1413-1420.

De Buck, E., Vranckx, L., Meyen, E., Maes, L., Vandersmissen, L., Anné, J. & Lammertyn, E. (2007) The twin-arginine translocation pathway is necessary for correct membrane insertion of the Rieske Fe/S protein in Legionella pneumophila. *FEBS Letters*, **581** (2): 259-264.

de Leeuw, E., te Kaat, K., Moser, C., Menestrina, G., Demel, R., de Kruijff, B., Oudega, B., Luirink, J. & Sinning, I. (2000) Anionic phospholipids are involved in membrane association of FtsY and stimulate its GTPase activity. *The EMBO Journal*, **19** (4): 531-541.

De Paul, A. L., Torres, A. I., Quintar, A. A., Maldonado, C. A., Mukdsi, J. H., Petiti, J. P. & Gutiérrez, S. (2012) *Immunoelectron microscopy: a reliable tool for the analysis of cellular processes*. INTECH Open Access Publisher.

DeLisa, M. P., Samuelson, P., Palmer, T. & Georgiou, G. (2002) Genetic Analysis of the Twin Arginine Translocator Secretion Pathway in Bacteria. *Journal of Biological Chemistry*, **277** (33): 29825-29831.

Demain, A. L. & Vaishnav, P. (2009) Production of recombinant proteins by microbes and higher organisms. *Biotechnology Advances*, **27** (3): 297-306.

Ding, Z. & Christie, P. J. (2003) Agrobacterium tumefaciens Twin-Arginine-Dependent Translocation Is Important for Virulence, Flagellation, and Chemotaxis but Not Type IV Secretion. *Journal of Bacteriology*, **185** (3): 760-771.

du Plessis, D. J. F., Nouwen, N. & Driessen, A. J. M. (2011) The Sec translocase. *Biochimica et Biophysica Acta (BBA) - Biomembranes*, **1808** (3): 851-865.

Dorwart, M. R., Wray, R., Brautigam, C. A., Jiang, Y. & Blount, P. (2010) S. aureus MscL Is a Pentamer In Vivo but of Variable Stoichiometries In Vitro: Implications for Detergent-Solubilized Membrane Proteins. *PLoS Biology*, **8** (12): e1000555.

Egea, P. F. & Stroud, R. M. (2010) Lateral opening of a translocon upon entry of protein suggests the mechanism of insertion into membranes. *Proceedings of the National Academy of Sciences of the United States of America*, **107** (40): 17182-17187.

English, B. P., Hauryliuk, V., Sanamrad, A., Tankov, S., Dekker, N. H. & Elf, J. (2011) Single-molecule investigations of the stringent response machinery in living bacterial cells. *Proceedings of the National Academy of Sciences*, **108** (31): E365-E373.

Fahnert, B., Lilie, H. & Neubauer, P. (2004) Inclusion bodies: formation and utilisation. *Adv Biochem Eng Biotechnol.*, **89** 93 - 142.

Fekkes, P., de Wit, J. G., Boorsma, A., Friesen, R. H. E. & Driessen, A. J. M. (1999) Zinc Stabilizes the SecB Binding Site of SecA. *Biochemistry*, **38** (16): 5111-5116.

Franke, W., Krien, S. & Brown, R. M., Jr. (1969) Simultaneous glutaraldehyde-osmium tetroxide fixation with postosmication. *Histochemie*, **19** (2): 162-164.

Frobel, J., Rose, P., Lausberg, F., Blummel, A.-S., Freudl, R. & Muller, M. (2012) Transmembrane insertion of twin-arginine signal peptides is driven by TatC and regulated TatB. *Nature Communications,* **3**: 1311.

Fröbel, J., Rose, P. & Müller, M. (2011) Early Contacts between Substrate Proteins and TatA Translocase Component in Twin-arginine Translocation. *Journal of Biological Chemistry*, **286** (51): 43679-43689.

Georgiou, G. & Segatori, L. (2005) Preparative expression of secreted proteins in bacteria: status report and future prospects. *Current Opinion in Biotechnology*, **16** (5): 538-545.

Gerard, F. & Cline, K. (2006) Efficient Twin Arginine Translocation (Tat) Pathway Transport of a Precursor Protein Covalently Anchored to Its Initial cpTatC Binding Site. *Journal of Biological Chemistry*, **281** (10): 6130-6135.

Goeddel, D., Heyneker, H., Hozumi, T., Arentzen, R., Itakura, K., Yansura, D., Ross, M., Miozzari, G., Crea, R. & Seeburg, P. (1979) Direct expression in Escherichia coli of a DNA sequence coding for human growth hormone. *Nature*, **281** (5732): 544 - 548.

Goff, S. A. & Goldberg, A. L. (1985) Production of abnormal proteins in E. coli stimulates transcription of ion and other heat shock genes. *Cell*, **41** (2): 587-595.

Gohlke, U., Pullan, L., McDevitt, C. A., Porcelli, I., De Leeuw, E., Palmer, T., Saibil, H. R. & Berks, B. C. (2005) The TatA component of the twin-arginine protein transport system forms channel complexes of variable diameter. *Proceedings of the National Academy of Sciences*, **102** (30): 10482.

Gottesman, S. (1990) Minimizing proteolysis in Escherichia coli: genetic solutions. In: eds. *Methods in Enzymology*, **185**: 119-129.

Gouffi, K., Gérard, F., Santini, C. L. & Wu, L. F. (2004) Dual topology of the Escherichia coli TatA protein. *Journal of Biological Chemistry*, **279** (12): 11608.

Greene, N. P., Porcelli, I., Buchanan, G., Hicks, M. G., Schermann, S. M., Palmer, T. & Berks, B. C. (2007) Cysteine Scanning Mutagenesis and Disulfide Mapping Studies of the TatA Component of the Bacterial Twin Arginine Translocase. *Journal of Biological Chemistry*, **282** (33): 23937-23945.

Greenfield, D., McEvoy, A. L., Shroff, H., Crooks, G. E., Wingreen, N. S., Betzig, E. & Liphardt, J. (2009) Self-Organization of the Escherichia coli Chemotaxis Network Imaged with Super-Resolution Light Microscopy. *PLoS Biology*, **7** (6): e1000137.

Harvey, B. R., Georgiou, G., Hayhurst, A., Jeong, K. J., Iverson, B. L. & Rogers, G. K. (2004) Anchored periplasmic expression, a versatile technology for the isolation of high-affinity antibodies from Escherichia coli-expressed libraries. *Proceedings of the National Academy of Sciences of the United States of America*, **101** (25): 9193-9198.

Hatzixanthis, K., Palmer, T. & Sargent, F. (2003) A subset of bacterial inner membrane proteins integrated by the twin-arginine translocase. *Molecular Microbiology*, **49** (5): 1377-1390.

Heijne, G. v. (1986) The distribution of positively charged residues in bacterial inner membrane proteins correlates with the trans-membrane topology. *The EMBO Journal*, **5** (11): 3021-3027.

Helenius, A. & Simons, K. (1975) Solubilization of membranes by detergents. *Biochimica et Biophysica Acta (BBA) - Reviews on Biomembranes*, **415** (1): 29-79.

Hicks, M. G., de Leeuw, E., Porcelli, I., Buchanan, G., Berks, B. C. & Palmer, T. (2003) The Escherichia coli twin-arginine translocase: conserved residues of TatA and TatB family components involved in protein transport. *FEBS Letters*, **539** (1-3): 61-67.

Holland, I. B. (2004) Translocation of bacterial proteins—an overview. *Biochimica et Biophysica Acta (BBA) - Molecular Cell Research*, **1694** (1–3): 5-16.

Holzapfel, E., Eisner, G., Alami, M., Barrett, C. M. L., Buchanan, G., Lüke, I., Betton, J. M., Colin Robinson, O., Palmer, T. & Moser, M. (2007) The entire N-terminal half of TatC is involved in twin-arginine precursor binding. *Biochemistry*, **46** (10): 2892-2898.

Horstmann, H., Körber, C., Sätzler, K., Aydin, D. & Kuner, T. (2012) Serial Section Scanning Electron Microscopy on Silicon Wafers for Ultra-Structural Volume Imaging of Cells and Tissues. *PLoS ONE*, **7** (4): e35172.

Hu, Y., Zhao, E., Li, H., Xia, B. & Jin, C. (2010) Solution NMR Structure of the TatA Component of the Twin-Arginine Protein Transport System from Gram-Positive Bacterium Bacillus subtilis. *Journal of the American Chemical Society*, **132** (45): 15942-15944.

Huang, C., Jr., Lin, H. & Yang, X. (2012) Industrial production of recombinant therapeutics in Escherichia coli and its recent advancements. *Journal of Industrial Microbiology & Biotechnology*, **39** (3): 383-399.

Huang, K. C. & Ramamurthi, K. S. (2010) Macromolecules that prefer their membranes curvy. *Molecular microbiology*, **76** (4): 822-832.

Hynds, P. J., Robinson, D. & Robinson, C. (1998) The Sec-independent Twin-arginine Translocation System Can Transport Both Tightly Folded and Malfolded Proteins across the Thylakoid Membrane. *Journal of Biological Chemistry*, **273** (52): 34868-34874.

Ikehara, M., Ohtsuka, E., Tokunaga, T., Taniyama, Y., Iwai, S., Kitano, K., Miyamoto, S., Ohgi, T., Sakuragawa, Y. & Fujiyama, K. (1984) Synthesis of a gene for human growth hormone and its expression in Escherichia coli *Proceedings of the National Academy of Science*, **81** (19): 5956 - 5960.

Ize, B., Gérard, F., Zhang, M., Chanal, A., Voulhoux, R., Palmer, T., Filloux, A. & Wu, L.-F. (2002) In vivo dissection of the Tat translocation pathway in Escherichia coli. *Journal of Molecular Biology*, **317** (3): 327-335.

Ize, B., Porcelli, I., Lucchini, S., Hinton, J. C., Berks, B. C. & Palmer, T. (2004) Novel Phenotypes of Escherichia coli tat Mutants Revealed by Global Gene Expression and Phenotypic Analysis. *Journal of Biological Chemistry*, **279** (46): 47543-47554.

Ize, B., Stanley, N. R., Buchanan, G. & Palmer, T. (2003) Role of the Escherichia coli Tat pathway in outer membrane integrity. *Molecular Microbiology*, **48** (5): 1183-1193.

Jack, R. L., Buchanan, G., Dubini, A., Hatzixanthis, K., Palmer, T. & Sargent, F. (2004) Coordinating assembly and export of complex bacterial proteins. *EMBO journal*, **23** 3962-3972.

Jack, R. L., Sargent, F., Berks, B. C., Sawers, G. & Palmer, T. (2001) Constitutive expression of Escherichia coli tat genes indicates an important role for the twin-arginine translocase during aerobic and anaerobic growth. *Journal of bacteriology*, **183** (5): 1801.

Jongbloed, J., Grieger, U., Antelmann, H., Hecker, M., Nijland, R., Bron, S. & van Dijl, J. (2004) Two minimal Tat translocases in Bacillus. *Molecular Microbiology*, **54** (5): 1319 - 1325.

Jongbloed, J. D. H., Antelmann, H., Hecker, M., Nijland, R., Bron, S., Airaksinen, U., Pries, F., Quax, W. J., van Dijl, J. M. & Braun, P. G. (2002) Selective Contribution of the

Twin-Arginine Translocation Pathway to Protein Secretion in Bacillus subtilis. *Journal of Biological Chemistry*, **277** (46): 44068-44078.

Jongbloed, J. D. H., van der Ploeg, R. & van Dijl, J. M. (2006) Bifunctional TatA subunits in minimal Tat protein translocases. *Trends in Microbiology*, **14** (1): 2-4.

Jormakka, M., Törnroth, S., Byrne, B. & Iwata, S. (2002) Molecular Basis of Proton Motive Force Generation: Structure of Formate Dehydrogenase-N. *Science*, **295** (5561): 1863-1868.

Joshi, M. V., Mann, S. G., Antelmann, H., Widdick, D. A., Fyans, J. K., Chandra, G., Hutchings, M. I., Toth, I., Hecker, M., Loria, R. & Palmer, T. (2010) The twin arginine protein transport pathway exports multiple virulence proteins in the plant pathogen Streptomyces scabies. *Molecular Microbiology*, **77** (1): 252-271.

Jung, S. T., Jeong, K. J., Iverson, B. L. & Georgiou, G. (2007) Binding and enrichment of Escherichia coli spheroplasts expressing inner membrane tethered scFv antibodies on surface immobilized antigens. *Biotechnology and Bioengineering*, **98** (1): 39-47.

Karlsson, A. J., Lim, H.-K., Xu, H., Rocco, M. A., Bratkowski, M. A., Ke, A. & DeLisa, M. P. (2012) Engineering Antibody Fitness and Function Using Membrane-Anchored Display of Correctly Folded Proteins. *Journal of Molecular Biology*, **416** (1): 94-107.

Kassem, M., Blum, W., Ristelli, J., Mosekilde, L. & Eriksen, E. (1993) Growth hormone stimulates proliferation and differentiation of normal human osteoblast-like cells in vitro. *Calcified Tissue International*, **52** (3): 222 - 226.

Kay, K. R., Smith, C., Wright, A. K., Serrano-Pozo, A., Pooler, A. M., Koffie, R., Bastin, M. E., Bak, T. H., Abrahams, S., Kopeikina, K. J., McGuone, D., Frosch, M. P., Gillingwater, T. H., Hyman, B. T. & Spires-Jones, T. L. (2013) Studying synapses in human brain with array tomography and electron microscopy. *Nat. Protocols*, **8** (7): 1366-1380.

Kihara, A., Akiyama, Y. & Ito, K. (1995) FtsH is required for proteolytic elimination of uncomplexed forms of SecY, an essential protein translocase subunit. *Proceedings of the National Academy of Sciences of the United States of America*, **92** (10): 4532-4536.

Klösgen, R. B., Brock, I. W., Herrmann, R. G. & Robinson, C. (1992) Proton gradient-driven import of the 16 kDa oxygen-evolving complex protein as the full precursor protein by isolated thylakoids. *Plant Molecular Biology*, **18** (5): 1031-1034.

Koch, H. G., Moser, M. & Müller, M. (2003) Signal recognition particle-depencent protein targeting, universal to all kingdoms of life. In: eds. *Reviews of Physiology, Biochemistry and Pharmacology*. Springer Berlin Heidelberg: 55-94.

Kremer, J. R., Mastronarde, D. N. & McIntosh, R. (1996) Computer Visualisation of Three-Dimensional Image Data Using IMOD. *Journal of Structural Biology*, **116** 71 - 76.

Kreutzenbeck, P., Kroger, C., Lausberg, F., Blaudeck, N., Sprenger, G. A. & Freudl, R. (2007) Escherichia coli Twin Arginine (Tat) Mutant Translocases Possessing Relaxed Signal Peptide Recognition Specificities. *Journal of Biological Chemistry*, **282** (11): 7903-7911.

Kudva, R., Denks, K., Kuhn, P., Vogt, A., Müller, M. & Koch, H.-G. (2013) Protein translocation across the inner membrane of Gram-negative bacteria: The Sec and Tat dependent protein transport pathways. *Research in microbiology*, **164** (6): 505-534.

Lange, C., Müller, S. D., Walther, T. H., Bürck, J. & Ulrich, A. S. (2007) Structure analysis of the protein translocating channel TatA in membranes using a multi-construct approach. *Biochimica et Biophysica Acta (BBA)-Biomembranes*, **1768** (10): 2627-2634.

Lausberg, F., Fleckenstein, S., Kreutzenbeck, P., Frobel, J., Rose, P., Muller, M. & Freudl, R. (2012) Genetic evidence for a tight cooperation of TatB and TatC during productive recognition of Twin-Arginine (Tat) signal peptides in *Escherichia coli. PLoS One,* **7** (6): e39867.

Leake, M. C., Greene, N. P., Godun, R. M., Granjon, T., Buchanan, G., Chen, S., Berry, R. M., Palmer, T. & Berks, B. C. (2008) Variable stoichiometry of the TatA component of the twin-arginine protein transport system observed by in vivo single-molecule imaging. *Proceedings of the National Academy of Sciences*, **105** (40): 15376.

Lee, P. A., Buchanan, G., Stanley, N. R., Berks, B. C. & Palmer, T. (2002) Truncation Analysis of TatA and TatB Defines the Minimal Functional Units Required for Protein Translocation. *The Journal of Bacteriology*, **184** (21): 5871-5879.

Lee, P. A., Orriss, G. L., Buchanan, G., Greene, N. P., Bond, P. J., Punginelli, C., Jack, R. L., Sansom, M. S. P., Berks, B. C. & Palmer, T. (2006) Cysteine-scanning Mutagenesis and Disulfide Mapping Studies of the Conserved Domain of the Twin-arginine Translocase TatB Component. *Journal of Biological Chemistry*, **281** (45): 34072-34085.

Lee, J. H., Velmurugan, N. & Jeong, K. J. (2013) Novel strategy for production of aggregation-prone proteins and lytic enzymes in Escherichia coli based on an anchored periplasmic expression system. *Journal of Bioscience and Bioengineering*, **116** (5): 638-643.

Levin, A. & Weiss, G. (2006) Optimising the affinity and specificity of proteins with molecular display. *Molecular BioSystems*, **2** 49 - 57.

Lévy, D., Bluzat, A., Seigneuret, M. & Rigaud, J.-L. (1990) A systematic study of liposome and proteoliposome reconstitution involving Bio-Bead-mediated Triton X-100 removal. *Biochimica et Biophysica Acta (BBA) - Biomembranes*, **1025** (2): 179-190.

Lichtenberg, D., Ahyayauch, H. & Goñi, Félix M. (2013) The Mechanism of Detergent Solubilization of Lipid Bilayers. *Biophysical Journal*, **105** (2): 289-299.

Lidke, D. S. & Lidke, K. A. (2012) Advances in high-resolution imaging – techniques for three-dimensional imaging of cellular structures. *Journal of Cell Science*, **125** (11): 2571-2580.

Lüke, I., Handford, J., Palmer, T. & Sargent, F. (2009) Proteolytic processing of Escherichia coli twin-arginine signal peptides by LepB. *Archives of Microbiology*, **191** (12): 919-925.

Lutkenhaus, J. (2007) Assembly Dynamics of the Bacterial MinCDE System and Spatial Regulation of the Z Ring. *Annual Review of Biochemistry*, **76** (1): 539-562.

Ma, X. & Cline, K. (2010) Multiple precursor proteins bind individual Tat receptor complexes and are collectively transported. *EMBO J*, **29** (9): 1477-1488.

Ma, X. & Cline, K. (2013) Mapping the Signal Peptide Binding and Oligomer Contact Sites of the Core Subunit of the Pea Twin Arginine Protein Translocase. *The Plant Cell*, **25** (3): 999-1015.

Matos, C., Branston, S., Albinak, A., Dhanoya A, Freedman R, Keshavarz-Moore, E. & Robinson, C. (2012) High-yield export of a native heterologous protein to the periplasm by the tat translocation pathway in Escherichia coli. *Biotechnology & Bioengineering*, **109** (10): 2533 - 2542.

Matos, C., Di Cola, A. & Robinson, C. (2009) TatD is a central component of a Tat translocon-initiated quality control system for exported FeS proteins in Escherichia coli. *EMBO reports*, **10** (5): 474-479.

Maurer, C., Panahandeh, S., Jungkamp, A.-C., Moser, M. & Müller, M. (2010) TatB functions as an oligomeric binding site for folded Tat precursor proteins. *Molecular biology of the cell*, **21** (23): 4151-4161.

McDevitt, C. A., Buchanan, G., Sargent, F., Palmer, T. & Berks, B. C. (2006) Subunit composition and in vivo substrate binding characteristics of Escherichia coli Tat protein complexes expressed at native levels. *FEBS journal*, **273** (24): 5656-5668.

McDonough, J. A., Hacker, K. E., Flores, A. R., Pavelka, M. S. & Braunstein, M. (2005) The Twin-Arginine Translocation Pathway of Mycobacterium smegmatis Is Functional and Required for the Export of Mycobacterial β-Lactamases. *Journal of Bacteriology*, **187** (22): 7667-7679.

Miot, M. & Betton, J.-M. (2004) Protein quality control in the bacterial periplasm. *Microbial Cell Factories*, **3** 4-4.

Melan, M. (1999) Overview of Cell Fixatives and Cell Membrane Permeants. In: Javois, L. eds. *Immunocytochemical Methods and Protocols*. Humana Press: 45-55.

Meloni, S., Rey, L., Sidler, S., Imperial, J., Ruiz-Argüeso, T. & Palacios, J. M. (2003) The twin-arginine translocation (Tat) system is essential for Rhizobium–legume symbiosis. *Molecular Microbiology*, **48** (5): 1195-1207.

Mendel, S., McCarthy, A., Barnett, J. P., Eijlander, R. T., Nenninger, A., Kuipers, O. P. & Robinson, C. (2008) The Escherichia coli TatABC System and a Bacillus subtilis TatAC-type System Recognise Three Distinct Targeting Determinants in Twin-arginine Signal Peptides. *Journal of Molecular Biology*, **375** (3): 661-672.

Micheva, K. D., O'Rourke, N., Busse, B. & Smith, S. J. (2010) Array Tomography: Immunostaining and Antibody Elution. *Cold Spring Harbor Protocols*, 2010 (11): pdb.prot5525.

Micheva, K. D. & Smith, S. J. (2007) Array tomography: A new tool for imaging the molecular architecture and ultrastructure of neural circuits. *Neuron*, **55** (1): 25-36.

Mickael, C. S., Lam, P.-K. S., Berberov, E. M., Allan, B., Potter, A. A. & Köster, W. (2010) Salmonella enterica Serovar Enteritidis tatB and tatC Mutants Are Impaired in Caco-2 Cell Invasion In Vitro and Show Reduced Systemic Spread in Chickens. *Infection and Immunity*, **78** (8): 3493-3505.

Mikhaleva, N. I., Santini, C. L., Giordano, G., Nesmeyanova, M. A. & Wu, L. F. (1999) Requirement for phospholipids of the translocation of the trimethylamine N-oxide reductase through the Tat pathway in Escherichia coli. *FEBS letters*, **463** (3): 331-335.

Miller, H. R. (1972) Fixation and tissue preservation for antibody studies. *The Histochemical journal*, **4** (4): 305 - 320.

Milne, J. L. S., Borgnia, M. J., Bartesaghi, A., Tran, E. E. H., Earl, L. A., Schauder, D. M., Lengyel, J., Pierson, J., Patwardhan, A. & Subramaniam, S. (2013) Cryo-electron microscopy: A primer for the non-microscopist. *The FEBS journal*, **280** (1): 28-45.

Monteferrante, C. G., Baglieri, J., Robinson, C. & van Dijl, J. M. (2012) TatAc, the Third TatA Subunit of Bacillus subtilis, Can Form Active Twin-Arginine Translocases with the TatCd and TatCy Subunits. *Applied and Environmental Microbiology*, **78** (14): 4999-5001.

Mori, H., Summer, E. J., Ma, X. & Cline, K. (1999) Component Specificity for the Thylakoidal Sec and Delta Ph–Dependent Protein Transport Pathways. *The Journal of Cell Biology*, **146** (1): 45-56.

Mori, H. & Cline, K. (2002) A twin arginine signal peptide and the pH gradient trigger reversible assembly of the thylakoid ΔpH/Tat translocase. *The Journal of cell biology*, **157** (2): 205-210.

Mould, R. M. & Robinson, C. (1991) A proton gradient is required for the transport of two lumenal oxygen-evolving proteins across the thylakoid membrane. *Journal of Biological Chemistry*, **266** (19): 12189.

Müller, S. D., De Angelis, A. A., Walther, T. H., Grage, S. L., Lange, C., Opella, S. J. & Ulrich, A. S. (2007) Structural characterization of the pore forming protein TatAd of the twin-arginine translocase in membranes by solid-state 15N-NMR. *Biochimica et Biophysica Acta (BBA)-Biomembranes*, **1768** (12): 3071-3079.

Murby, M., Uhlén, M. & Ståhl, S. (1996) Upstream Strategies to Minimize Proteolytic Degradation upon Recombinant Production inEscherichia coli. *Protein Expression and Purification*, **7** (2): 129-136.

Ng, D. T., Brown, J. D. & Walter, P. (1996) Signal sequences specify the targeting route to the endoplasmic reticulum membrane. *The Journal of Cell Biology*, **134** (2): 269-278.

Nishiyama, K., Hanada, M. & Tokuda, H. (1994) Disruption of the gene encoding p12 (SecG) reveals the direct involvement and important function of SecG in the protein translocation of Escherichia coli at low temperature. *The EMBO Journal*, **13** (14): 3272-3277.

Nolandt, O. V., Walther, T. H., Roth, S., Bürck, J. & Ulrich, A. S. (2009) Structure analysis of the membrane protein TatCd from the Tat system of *Bacillus subtilis* by circular dichroism. *Biochimica et Biophysica Acta (BBA)-Biomembranes*, **1788** (10): 2238-2244.

Northfield, J., Whitty, C. J. M. & MacPhee, I. A. M. (2002) Burkholderia pseudomallei infection, or melioidosis, and nephrotic syndrome. *Nephrology Dialysis Transplantation*, **17** (1): 137-139.

Oates, J., Barrett, C. M. L., Barnett, J. P., Byrne, K. G., Bolhuis, A. & Robinson, C. (2005) The Escherichia coli twin-arginine translocation apparatus incorporates a distinct form of TatABC complex, spectrum of modular TatA complexes and minor TatAB complex. *Journal of molecular biology*, **346** (1): 295-305.

Oates, J., Mathers, J., Mangels, D., Kühlbrandt, W., Robinson, C. & Model, K. (2003) Consensus structural features of purified bacterial TatABC complexes. *Journal of molecular biology*, **330** (2): 277-286.

Ochsner, U. A., Snyder, A., Vasil, A. I. & Vasil, M. L. (2002) Effects of the twin-arginine translocase on secretion of virulence factors, stress response, and pathogenesis. *Proceedings of the National Academy of Sciences of the United States of America*, **99** (12): 8312-8317.

Palmer, T., Sargent, f. & Berks, B. (2010) The Tat protein export pathway. *In EcoSal— Escherichia coli and Salmonella: Cellular and Molecular Biology.* American Society for Microbiology Press.

Park, E. & Rapoport, T. (2012) Mechanisms of Sec61/SecY-mediated protein translocation across membranes. *Annual Review of Biophysics*, **41** 21 - 40.

P**armar, M. M., Edwards, K. & Madden, T. D.** (1999) Incorporation of bacterial membrane proteins into liposomes: factors influencing protein reconstitution. *Biochimica et Biophysica Acta (BBA) - Biomembranes*, **1421** (1): 77-90.

Patel, R., Smith, S.M., Robinson, C. (2014) Protein transport by the bacterial Tat pathway. *Biochimica et Biophysica Acta (BBA),* **1843** 1620-1628.

Patel, R., Vasilev, C., Beck, D., Monteferrante, C. G., van Dijl, J. M., Hunter, C. N., Smith, C. & Robinson, C. (2014) A mutation leading to super-assembly of twin-arginine translocase (Tat) protein complexes. *Biochimica et Biophysica Acta (BBA) - Molecular Cell Research*, **1843** (9): 1978-1986.

Paternostre, M. T., Roux, M. & Rigaud, J. L. (1988) Mechanisms of membrane protein insertion into liposomes during reconstitution procedures involving the use of detergents. 1. Solubilisation of large unilamellar liposomes (prepared by reverse-phase evaporation) by triton-X-100, octyl glucoside and sodium cholate. . *Biochemistry*, **27** (8): 2668 - 2677.

Philimonenko, V. V., Janacek, J. & Hozak, P. (2002) LR White is preferable to Unicryl of immunogold detection of fixation-sensitive nuclear antigens. *European journal of histochemistry*, **46** (4): 359 - 364.

Pohlschröder, M., Dilks, K., Hand, N. J. & Wesley Rose, R. (2004) Translocation of proteins across archaeal cytoplasmic membranes. *FEMS Microbiology Reviews*, **28** (1): 3-24.

Pohlschröder, M., Prinz, W. A., Hartmann, E. & Beckwith, J. (1997) Protein Translocation in the Three Domains of Life: Variations on a Theme. *Cell*, **91** (5): 563-566.

Pooley, H. M., Merchante, R. & Karamata, D. (1996) Overall Protein Content and Induced Enzyme Components of the Periplasm of Bacillus subtilis. *Microbial Drug Resistance*, **2** (1): 9-15.

Pop, O., Martin, U., Abel, C. & Muller, J. P. (2002) The Twin-arginine Signal Peptide of PhoD and the TatAd/Cd Proteins of Bacillus subtilis Form an Autonomous Tat Translocation System. *Journal of Biological Chemistry*, **277** (5): 3268-3273.

Porcelli, I., de Leeuw, E., Wallis, R., Els van den Brink-van der, L., de Kruijff, B., Wallace, B. A., Palmer, T. & Berks, B. C. (2002) Characterization and membrane assembly of the TatA component of the Escherichia coli twin-arginine protein transport system. *Biochemistry*, **41** (46): 13690-13697.

Pradel, N., Ye, C., Livrelli, V., Xu, J., Joly, B. & Wu, L.-F. (2003) Contribution of the Twin Arginine Translocation System to the Virulence of Enterohemorrhagic Escherichia coli O157:H7. *Infection and Immunity*, **71** (9): 4908-4916.

Pugsley, A. P. (1993) The complete general secretory pathway in gram-negative bacteria. *Microbiological Reviews*, **57** (1): 50-108.

Punginelli, C., Maldonado, B., Grahl, S., Jack, R., Alami, M., Schroder, J., Berks, B. C. & Palmer, T. (2007) Cysteine Scanning Mutagenesis and Topological Mapping of the Escherichia coli Twin-Arginine Translocase TatC Component. *The Journal of Bacteriology*, **189** (15): 5482-5494.

Qiu, J.-K., Jung, S.-T., Georgiou, G. & Hang, H.-Y. (2010) Enrichment of Escherichia coli spheroplasts displaying scFv antibodies specific for antigens expressed on the human cell surface. *Applied Microbiology and Biotechnology*, **88** (6): 1385-1391.

Ramasamy, S., Abrol, R., Suloway, C. J. M. & Clemons Jr, W. M. (2013) The Glove-like Structure of the Conserved Membrane Protein TatC Provides Insight into Signal Sequence Recognition in Twin-Arginine Translocation. *Structure*, **21** (5): 777-788.

Ray, N., Nenninger, A., Mullineaux, C. W. & Robinson, C. (2005) Location and Mobility of Twin Arginine Translocase Subunits in the Escherichia coli Plasma Membrane. *Journal of Biological Chemistry*, **280** (18): 17961-17968.

Reichelt, M., Joubert, L., Perrino, J., Koh, A. L., Phanwar, I. & Arvin, A. M. (2012) 3D Reconstruction of VZV Infected Cell Nuclei and PML Nuclear Cages by Serial Section Array Scanning Electron Microscopy and Electron Tomography. *PLoS Pathogens*, **8** (6): e1002740.

Ren, C., Patel, R. & Robinson, C. (2013) Exclusively membrane-inserted state of an uncleavable Tat precursor suggests lateral transfer into the bilayer from the translocon. *FEBS Journal*, **280** (14): 3354 - 3364.

Renner, L. D. & Weibel, D. B. (2011) Cardiolipin microdomains localize to negatively curved regions of Escherichia coli membranes. *Proceedings of the National Academy of Sciences of the United States of America*, **108** (15): 6264-6269.

Rholl, D. A., Papp-Wallace, K. M., Tomaras, A. P., Vasil, M. L., Bonomo, R. A. & Schweizer, H. P. (2011) Molecular Investigations of PenA-mediated β-lactam Resistance in Burkholderia pseudomallei. *Frontiers in Microbiology*, **2**: 139.

Richter, S. & Brüser, T. (2005) Targeting of unfolded PhoA to the TAT translocon of Escherichia coli. *Journal of Biological Chemistry*, **280** (52): 42723.

Ridder, A. N. J. A., de Jong, E. J., Jongbloed, J. D. H. & Kuipers, O. P. (2009) Subcellular localization of TatAd of Bacillus subtilis depends on the presence of TatCd or TatCy. *Journal* of bacteriology, **191** (13): 4410-4418.

Robinson, C., Matos, C. F. R. O., Beck, D., Ren, C., Lawrence, J., Vasisht, N. & Mendel, S. (2011) Transport and proofreading of proteins by the twin-arginine translocation (Tat) system in bacteria. *Biochimica et Biophysica Acta (BBA) - Biomembranes*, **1808** (3): 876-884.

Rodrigue, A., Chanal, A., Beck, K., Müller, M. & Wu, L. F. (1999) Co-translocation of a periplasmic enzyme complex by a hitchhiker mechanism through the bacterial Tat pathway. *Journal of Biological Chemistry*, **274** (19): 13223.

Rodriguez, F., Rouse, S. L., Tait, C. E., Harmer, J., De Riso, A., Timmel, C. R., Sansom, M. S. P., Berks, B. C. & Schnell, J. R. (2013) Structural model for the protein-translocating element of the twin-arginine transport system. *Proceedings of the National Academy of Sciences*, **110** (12): E1092-E1101.

Rollauer, S. E., Tarry, M. J., Graham, J. E., Jääskeläinen, M., Jäger, F., Johnson, S., Krehenbrink, M., Liu, S.-M., Lukey, M. J. & Marcoux, J. (2012) Structure of the TatC core of the twin-arginine protein transport system. *Nature*, **492** (7428): 210-214.

Rönnlund, D., Gad, A. K. B., Blom, H., Aspenström, P. & Widengren, J. (2013) Spatial organization of proteins in metastasizing cells. *Cytometry Part A*, **83** (9): 855-865.

Rose, P., Frobel, J., Graumann, P. & Muller, M. (2013) Substrate-dependent assembly of the Tat translocase as observed in live Escherichia coli cells. *PLoS One*, **8** (8): e69488.

Rose, W., Bruser, T., Kissinger, J.T., Pohlschroder, M. (2002) Adaptation of protein secretion to extremely high-salt conditions by extensive use of the twin-arginine translocation pathway. *Molecular Microbiology*, **45** (4): 943-950.

Saint-Joanis, B., Demangel, C., Jackson, M., Brodin, P., Marsollier, L., Boshoff, H. & Cole, S. T. (2006) Inactivation of Rv2525c, a Substrate of the Twin Arginine Translocation (Tat) System of Mycobacterium tuberculosis, Increases β-Lactam Susceptibility and Virulence. *Journal of Bacteriology*, **188** (18): 6669-6679.

Sanchez-Ortiga, R., Klibanski, A. & Tritos, N. (2012) Effects of recombinant human growth hormone therapy in adults with Prader-Willi syndrome: a meta-analysis. *Clinical Endocrinology*, **77** (1): 86 - 93.

Santini, C. L., Ize, B., Chanal, A., Müller, M., Giordano, G. & Wu, L. F. (1998) A novel Sec-independent periplasmic protein translocation pathway in Escherichia coli. *The EMBO journal*, **17** (1): 101-112.

Sargent, F., Bogsch, E. G., Stanley, N. R., Wexler, M., Robinson, C., Berks, B. C. & Palmer, T. (1998) Overlapping functions of components of a bacterial Sec-independent protein export pathway. *The EMBO journal*, **17** (13): 3640-3650.

Sargent, F., Gohlke, U., de Leeuw, E., Stanley, N. R., Palmer, T., Saibil, H. R. & Berks, B. C. (2001) Purified components of the Escherichia coli Tat protein transport system form a double-layered ring structure. *European Journal of Biochemistry*, **268** (12): 3361-3367.

Sargent, F., Stanley, N. R., Berks, B. C. & Palmer, T. (1999) Sec-independent protein translocation in Escherichia coli. *Journal of Biological Chemistry*, **274** (51): 36073.

Sasaki, S., Matsuyama, S. & Mizushima, S. (1990) In vitro kinetic analysis of the role of the positive charge at the amino-terminal region of signal peptides in translocation of secretory protein across the cytoplasmic membrane in Escherichia coli. *Journal of Biological Chemistry*, **265** (8): 4358-4363.

Sauvé, V., Bruno, S., Berks, B. C. & Hemmings, A. M. (2007) The SoxYZ Complex Carries Sulfur Cycle Intermediates on a Peptide Swinging Arm. *Journal of Biological Chemistry*, **282** (32): 23194-23204.

Schaerlaekens, K., Schierova, M., Lammertyn, E., Geukens, N., Anne, J. & Van Mellaert, L. (2001) Twin-Arginine Translocation Pathway in Streptomyces lividans. *The Journal of Bacteriology*, **183** (23): 6727-6732.

Schiebel, E., Driessen, A. J. M., Hartl, F.-U. & Wickner, W. (1991) ΔμH+ and ATP function at different steps of the catalytic cycle of preprotein translocase. *Cell*, **64** (5): 927-939.

Schuck, P. (2005) Analytical Ultracentrifugation: Techniques and Methods.

Seddon, A. M., Curnow, P. & Booth, P. J. (2004) Membrane proteins, lipids and detergents: not just a soap opera. *Biochimica et Biophysica Acta (BBA) - Biomembranes*, **1666** (1–2): 105-117.

Settles, A. M., Yonetani, A., Baron, A., Bush, D. R., Cline, K. & Martienssen, R. (1997) Sec-independent protein translocation by the maize Hcf106 protein. *Science*, **278** (5342): 1467.

Smit, J. W., Meijer, C. J. L. M., Decary, F. & Feltkamp-vroom, T. M. (1974) Paraformaldehyde fixation in immunofluorescence and immunoelectron microscopy: Preservation of tissue and cell surface membrane antigens. *Journal of Immunological Methods*, **6** (1–2): 93-98.

Smith, E. & Pickels, E. (1940) Micelle formation in aqueous solutions of digitonin. *Proceedings of the National Academy of Sciences of the United States of America* **26** 27 - 35.

Spiliotis, B. (2008) Recombinant human growth hormone in the treatment of Turner syndrome. *Therapeutics and Clinical Risk Management*, **4** (6): 1177 - 1183.

Stanley, N. R., Palmer, T. & Berks, B. C. (2000) The twin arginine consensus motif of Tat signal peptides is involved in Sec-independent protein targeting in Escherichia coli. *Journal of Biological Chemistry*, **275** (16): 11591-11596.

Takeda, A., Cooper, K., Bird, A., Baxter, L., Frampton, G., Gospodarevskaya, E., Welch, K. & Bryant, J. (2010) Recombinant human growth hormone for the treatment of growth disorders in children: a systematic review and economic evaluation. *Health Technology Assessment*, **14** (42): 1-209.

Tarry, M. J., Schäfer, E., Chen, S., Buchanan, G., Greene, N. P., Lea, S. M., Palmer, T., Saibil, H. R. & Berks, B. C. (2009) Structural analysis of substrate binding by the TatBC component of the twin-arginine protein transport system. *Proceedings of the National Academy of Sciences*, **106** (32): 13284.

Tavare, J. M., Fletcher, L. M. & Welsh, G. I. (2001) Using green fluorescent protein to study intracellular signalling. *Journal of Endocrinology*, **170** (2): 297-306.

Tjalsma, H., Bolhuis, A., Jongbloed, J. D. H., Bron, S. & van Dijl, J. M. (2000) Signal Peptide-Dependent Protein Transport in Bacillus subtilis: a Genome-Based Survey of the Secretome. *Microbiology and Molecular Biology Reviews*, **64** (3): 515-547.

Tokuyasu, K. T. (1984) Immuno-cryoultramicrotomy: immunolabelling for electron microscopy. *Elsevier*, 71 - 96.

Tomkiewicz, D., Nouwen, N., van Leeuwen, R., Tans, S. & Driessen, A. J. M. (2006) SecA Supports a Constant Rate of Preprotein Translocation. *Journal of Biological Chemistry*, **281** (23): 15709-15713.

Treuner-Lange, A. & Søgaard-Andersen, L. (2014) Regulation of cell polarity in bacteria. *The Journal of Cell Biology*, **206** (1): 7-17.

Tsukazaki, T., Mori, H., Fukai, S., Ishitani, R., Mori, T., Dohmae, N., Perederina, A., Sugita, Y., Vassylyev, D. G., Ito, K. & Nureki, O. (2008) Conformational transition of Sec machinery inferred from bacterial SecYE structures. *Nature*, **455** (7215): 988-991.

Valent, Q. A., Scotti, P. A., High, S., de Gier, J. W., von Heijne, G., Lentzen, G., Wintermeyer, W., Oudega, B. & Luirink, J. (1998) The Escherichia coli SRP and SecB targeting pathways converge at the translocon. *The EMBO Journal*, **17** (9): 2504-2512.

VanAken, T., Foxall-VanAken, S., Castleman, S. & Ferguson-Miller, S. (1986) Alkyl glycoside detergents: synthesis and applications to the study of membrane proteins. *Methods in Enzymology*, **125** 27 - 35.

van der Ploeg, R., Barnett, J. P., Vasisht, N., Goosens, V. J., Pöther, D. C., Robinson, C. & van Dijl, J. M. (2011) Salt Sensitivity of Minimal Twin Arginine Translocases. *Journal of Biological Chemistry*, **286** (51): 43759-43770.

van Weering, J., Brown, E., Sharp, T., Mantell, J., Cullen, P., Verkade, P., (2010) Intrecellular Membrane Traffic at High Resolution. *Methods in Cell Biology,* **96**: 619 - 648.

Vasil, M. L., Tomaras, A. P. & Pritchard, A. E. (2012) Identification and Evaluation of Twin-Arginine Translocase Inhibitors. *Antimicrobial Agents and Chemotherapy*, **56** (12): 6223-6234.

Vendeville, A., Lariviere, D. & Fourmentin, E. (2011) An inventory of the bacterial macromolecular components and their spatial organisation *FEMS Microbiology Reviews*, **35** (2): 395 - 414.

Vogt, K. & Emerick, J. (2015) Growth hormone therapy in adults with Prader-Willi syndrome. *Diseases*, **3** 56 - 67.

Walker, M. B., Roy, L. M., Coleman, E., Voelker, R. & Barkan, A. (1999) The Maize tha4 Gene Functions in Sec-Independent Protein Transport in Chloroplasts and Is Related to hcf106, tatA, and tatB. *The Journal of Cell Biology*, **147** (2): 267-276.

Walsh, G. (2010) Post-translational modifications of protein biopharmaceuticals. *Drug Discovery Today*, **15** (17–18): 773-780.

Walther, T. H., Grage, S. L., Roth, N. & Ulrich, A. S. (2010) Membrane alignment of the pore-forming component TatAd of the twin-arginine translocase from Bacillus subtilis resolved by solid-state NMR spectroscopy. *Journal of the American Chemical Society*, **132** (45): 15945-15956.

Wang, P. & Dalbey, R. E. (2011) Inserting membrane proteins: The YidC/Oxa1/Alb3 machinery in bacteria, mitochondria, and chloroplasts. *Biochimica et Biophysica Acta (BBA) - Biomembranes*, **1808** (3): 866-875.

Warner, J. M., Pelowa, D. B., Currie, B. J. & Hirst, R. G. (2007) Melioidosis in a rural community of Western Province, Papua New Guinea. *Transactions of The Royal Society of Tropical Medicine and Hygiene*, **101** (8): 809-813.

Weiner, J. H., Bilous, P. T., Shaw, G. M., Lubitz, S. P., Frost, L., Thomas, G. H., Cole, J. A. & Turner, R. J. (1998) A Novel and Ubiquitous System for Membrane Targeting and Secretion of Cofactor-Containing Proteins. *Cell*, **93** (1): 93-101.

Welte, T., Kudva, R., Kuhn, P., Sturm, L., Braig, D., Müller, M., Warscheid, B., Drepper, F. & Koch, H.-G. (2012) Promiscuous targeting of polytopic membrane proteins to SecYEG or YidC by the Escherichia coli signal recognition particle. *Molecular Biology of the Cell*, **23** (3): 464-479.

Wexler, M., Sargent, F., Jack, R. L., Stanley, N. R., Bogsch, E. G., Robinson, C., Berks, B. C. & Palmer, T. (2000) TatD is a cytoplasmic protein with DNase activity. *Journal of Biological Chemistry*, **275** (22): 16717.

White, G. F., Schermann, S. M., Bradley, J., Roberts, A., Greene, N. P., Berks, B. C. & Thomson, A. J. (2010) Subunit Organization in the TatA Complex of the Twin Arginine Protein Translocase. *Journal of Biological Chemistry*, **285** (4): 2294.

Widdick, D. A., Dilks, K., Chandra, G., Bottrill, A., Naldrett, M., Pohlschröder, M. & Palmer, T. (2006) The twin-arginine translocation pathway is a major route of protein

export in Streptomyces coelicolor. *Proceedings of the National Academy of Sciences*, **103** (47): 17927-17932.

Wigglesworth, V. B. (1975) Lipid staining for electron microscopy: a new method. *Journal of Cell Science*, **19** 425 - 437.

Yahr, T. L. & Wickner, W. T. (2001) Functional reconstitution of bacterial Tat translocation in vitro. *EMBO journal*, **20** 2472-2479.

Yamaguchi, H. & Miyazaki, M. (2014) Refolding Techniques for Recovering Biologically Active Recombinant Proteins from Inclusion Bodies. *Biomolecules*, **4** (1): 235-251.

Yen, M.-R., Tseng, Y.-H., Nguyen, E., Wu, L.-F. & Saier, M. (2002) Sequence and phylogenetic analyses of the twin-arginine targeting (Tat) protein export system. *Archives of Microbiology*, **177** (6): 441-450.

Zhang, Y., Hu, Y., Li, H. & Jin, C. (2014a) Structural basis for TatA oligomerisation: an NMR study of Escherichia coli TatA dimeric structure. *PLoS One*, **9** (8): e103157.

Zhang, Y., Wang, L., Hu, Y. & Jin, C. (2014b) Solution structure of the TatB component of the Twin-arginine translocation system. *Biochimica et Biophysica Acta (BBA) - Biomembranes* **1838** (7): 1881 - 1888.

Zheng, N. & Gierasch, L. M. (1997) Domain Interactions in E. coli SRP: Stabilization of M Domain by RNA Is Required for Effective Signal Sequence Modulation of NG Domain. *Molecular Cell*, **1** (1): 79-87.

Zoufaly, S., Fröbel, J., Rose, P., Flecken, T., Maurer, C., Moser, M. & Müller, M. (2012) Mapping Precursor-binding Site on TatC Subunit of Twin Arginine-specific Protein Translocase by Site-specific Photo Cross-linking. *Journal of Biological Chemistry*, **287** (16): 13430-13441.

Appendix:
Published work

Review

Protein transport by the bacterial Tat pathway ☆

Roshani Patel [a,1], Sarah M. Smith [a,1], Colin Robinson [b,*]

[a] *School of Life Sciences, University of Warwick, Coventry CV4 7AL, United Kingdom*
[b] *Centre for Molecular Processing, School of Biosciences, University of Kent, Canterbury CT2 7NJ, United Kingdom*

ARTICLE INFO

ABSTRACT

The twin-arginine translocation (Tat) system accomplishes the remarkable feat of translocating large – even dimeric – proteins across tightly sealed energy-transducing membranes. All of the available evidence indicates that it is unique in terms of both structure and mechanism; however its very nature has hindered efforts to probe the core translocation events. At the heart of the problem is the fact that two large sub-complexes are believed to coalesce to form the active translocon, and 'capturing' this translocation event has been too difficult. Nevertheless, studies on the individual components have come a long way in recent years, and structural studies have reached the point where educated guesses can be made concerning the most interesting aspects of Tat. In this article we review these studies and the emerging ideas in this field. This article is part of a Special Issue entitled: Protein trafficking and secretion in bacteria. Guest Editors: Anastassios Economou and Ross Dalbey.

© 2014 Published by Elsevier B.V.

1. Introduction

The twin arginine translocase (Tat) is a protein transport pathway that exists in Archaea, bacteria and plant chloroplasts. In bacteria, it exports proteins across the plasma membrane and is important for many processes including energy metabolism, formation of the cell envelope, biofilm formation, heavy metal resistance, nitrogen-fixing symbiosis, bacterial pathogenesis and others [1,2]. What makes this protein transport system unusual compared to other transport systems (such as the general secretory, or Sec pathway) is its ability to transport fully folded proteins across membranes. This remarkable feat has no requirement for ATP as an energy source, and relies solely on the proton motive force (PMF) [3–5].

The mechanism of translocation remains poorly understood, in part due to a lack of high resolution structural information on this complex and its individual components. That said, a number of recent biophysical and structural studies have provided a more detailed picture of the action and composition of this translocase, particularly with respect to the early events prior to the actual translocation event. This review discusses the key information from each of these studies. Much of this article will focus on the *Escherichia coli* (*E. coli*) Tat system, but relevant data on the Gram-positive homologs from *Bacillus subtilis* (*B. subtilis*) and the chloroplast Tat system are also mentioned. A more detailed analysis of Gram-positive Tat systems is given elsewhere in this volume by Goosens et al. [6].

2. The Tat system's substrates

The extent to which different organisms utilise the Tat pathway varies significantly. Gram-positive bacteria such as *Staphylococcus aureus* or *B. subtilis* have few predicted substrates [7–9], whereas enteric bacteria typically possess around 20–30 substrates [10]. Whilst the rationale for using this translocase remains unclear for some Tat substrates, three key underlying factors have been identified. The first is a requirement for the enzymatic insertion of complex cofactors in the cytoplasm prior to transport, thereby bypassing the requirement for extra mechanisms to firstly, separately export the cofactor and then subsequently catalyse its insertion in the periplasm [1]. The second motive is avoidance of metal ions that compete for insertion into the active site, and lastly, the transport of hetero-oligomeric complexes that optimally assemble in the cytoplasm [11,12]. The latter is achieved through proteins forming complexes with other proteins that possess an N-terminal Tat signal peptide [13].

Navigation to the Tat translocase is dictated by the presence of an N-terminal signal peptide that possesses an overall tripartite architecture of: a polar amino terminal (N) domain, hydrophobic core (H) region and a polar carboxyl (C) domain (Fig. 1). Despite the Sec- and Tat-type signal peptides having the same basic structure and a similar terminal Ala-X-Ala motif, studies on Tat signals revealed a highly conserved SRRxFLK motif [14,15] located at the junction of the N- and H-domains. The twin-arginine motif gives this translocase its name. Both arginines are critical in chloroplast Tat signals [16], but less so in bacteria, where mutation of a single arginine in bacteria only affects the rate of translocation, whereas mutation of both completely abolishes transport [17–19]. Within the SRRxFLK motif, three determinants are important: the twin-arginine pair, the hydrophilic −1 residue
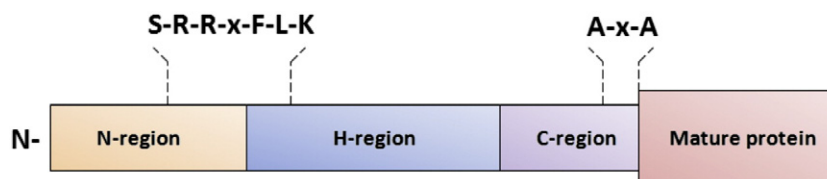

Fig. 1. The Tat signal peptide. A polar amino domain (N-region), hydrophobic core (H-region), and polar carboxyl domain (C-region) comprise the tripartite structure of a Tat signal peptide, which is located at the N-terminus of the substrate protein. On average they are less hydrophobic than Sec-specific signals, as well as being longer (on average 38 to 24 amino acids, respectively). Tat signal peptides are distinguished by their conserved twin-arginine motif in the N-region. The C-terminal region houses an A-x-A motif, which is a consensus cleavage site for removal of the signal peptide by signal peptidase.

and the hydrophobic +2 residue (+/− relative to the twin-arginine pair). However, while Tat and Sec signal peptides share a similar overall architecture, it is not the twin arginine pair alone that prevents mistargeting to the Sec pathway. Tat signal peptides are less hydrophobic than those used in Sec-targeting [20], and the C-region of certain Tat signal peptides houses basic residues, which are seldom found in the same region of Sec signal peptides. The latter is believed to hinder engagement with Sec machinery [21–23].

3. Tat Translocase components and complexes

3.1. The Tat subunits

Three integral membrane proteins form the minimal set of components for the assembly of the Tat translocase in *E. coli*: TatA, TatB and TatC. These proteins are expressed from the *tatABC* operon and reside in the cytoplasmic membrane arranged as a Tat(A)BC substrate binding complex and a separate TatA complex (Fig. 2). TatA is an 89 amino acid protein (9.6 kDa) that consists of a short periplasmic N-terminal region, a transmembrane helix that is linked via a hinge region to a cytosolically exposed amphipathic helix (APH), and a highly unstructured, cytoplasmically-exposed C-terminal region [24–26]. This arrangement is supported by spectroscopy studies, which indicate that the APH lies along the surface of the membrane [27,28]. Additionally, solid-state NMR has shown the TMH to cross the cytoplasmic membrane at a 17° tilt [29]. An N-out topology is the favoured orientation of TatA in the cytoplasmic membrane and is supported by recent NMR data of the TatA component of a Gram-positive homolog, TatAd [30,31]. Some studies have predicted that TatA may also have a dual topology, on the

basis of data that suggest the N-terminal region of TatA can also be accessed from the cytoplasm [32]. Moreover, there is evidence of soluble TatA in bacteria and chloroplasts [33–39]; however the functional relevance of this soluble TatA pool remains controversial.

TatB consists of 171 amino acids with a molecular mass of 18.5 kDa. Despite sharing a 20% sequence similarity with TatA [40] and a very similar predicted secondary structure (Fig. 2), TatB and TatA carry out functionally distinct roles within the Tat translocase [41].

TatC consists of 258 amino acids with a molecular mass of 28.9 kDa. As predicted by its secondary structure, this protein traverses the membrane 6 times, possessing an N-in C-in topology [42]. The *tatABC* gene products form two distinct membrane complexes at steady state: a TatBC-containing substrate binding complex and a separate TatA complex. It is in this former 370 kDa Tat(A)BC complex where most of TatB and -C are found at a 1:1 stoichiometric ratio [43]. TatA (found at ~ 25 and 50 fold higher concentrations than TatB and TatC, respectively [44]), is present as highly heterogeneous complexes ranging from 100–500 kDa [43,45,46] and is not required for TatBC complex assembly [47].

The composition of the Tat system differs significantly in most Gram-positive bacteria; all except Streptomycetes contain only *tatAC* genes [48,49]. In those examples studied to date, the TatA protein is bifunctional [50]. The best characterised Tat system in this type of bacteria is found in *B. subtilis* — a non-pathogenic soil bacterium, which contains two discrete Tat systems that operate in parallel, yet possess different substrate specificities [48]. The first of the two is TatAdCd, whose only substrate identified at present is the phosphodiesterase, PhoD [49]. The second translocase is TatAyCy, which exports YwbN, an iron-dependent DyP-peroxidase [49]. There is a third *tatA* gene encoding the TatAc protein, which like TatAd, was recently shown to form small homogeneous complexes and restore export of TorA in a Δ*AE* mutant [51].

Reminiscent of the situation in *E. coli*, the TatAyCy system is composed of two types of membrane protein complexes: TatAyCy and TatAy that have been reported to form ~200 kDa complexes (as judged by gel filtration chromatography) [37,52]. Likewise, TatAdCd exists as a ~230 kDa complex, alongside a separate and discrete TatAd complex of ~160 kDa[50,53]. The TatAd and TatAy proteins are bifunctional fulfilling the role of the TatB protein that would otherwise be present in Gram-negative bacteria [50,54].

In addition to these bacterial TatAC-containing complexes being smaller than their *E. coli* counterparts (TatABC is ~370 kDa on BN gels [43,45,55]), the lack of a *tatB* gene and TatA heterogeneity appear to be conserved features of Gram-positive bacteria. This is an important point because the remarkable heterogeneity of *E. coli* TatA complexes has been considered to be a key element of current translocation models (see below)[53].

Finally, *E. coli* also possesses a TatA paralogue, TatE. This 67 amino acid protein possesses 57% sequence identity to TatA [25] and is thought to have arisen from a gene duplication of *tatA* [56]. Whilst it can fulfil TatA activity if overexpressed [41], there is no evidence for a specific role for this protein, and indeed many Gram-negative bacteria lack a *tatE* gene [46,57].
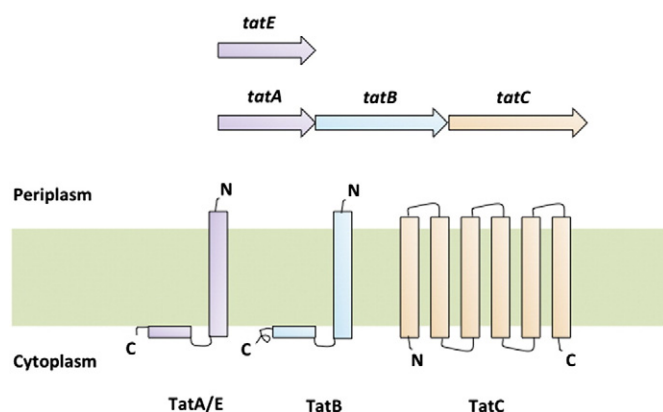
Fig. 2. Component organisation of the *E. coli* Tat system. In Gram-negative bacteria the Tat translocase system is usually made up of three integral membrane proteins, encoded by the *tatABC* operon. Both TatA and TatB are single-span transmembrane proteins that possess: a short periplasmic N-terminal region; single-span transmembrane helix; hinge region; amphipathic helix lying along the cytoplasm-membrane interface and a highly charged, unstructured C-terminus. In contrast, TatC is a polytopic protein that is predicted to contain 6 transmembrane spans, with both the N- and C- termini in the cytoplasm. In *E. coli* a TatA paralog exists, TatE, which is encoded elsewhere in the genome.

3.2. The TatBC complex

3.2.1. Structural characterisation of the TatBC complex

Early cross-linking studies conducted in chloroplasts demonstrated that a Tat-dependent substrate could be cross-linked to the Hcf106-cpTatC complex (equivalent to TatBC in bacteria) [58], demonstrating that this is the initial receptor for the Tat pathway. Similar binding characteristics were observed for the TatBC complex of *E. coli* [59]. In both instances full translocation was prevented by the absence of a PMF, and these studies represent good evidence that the TatBC complex does indeed carryout the binding of a substrate [58]. These complexes were initially shown to be large (370–500 kDa), multi-subunit entities using Blue Native Polyacrylamide Gel Electrophoresis [43,46,60].

Electron microscopy characterisation of the TatBC complex presented a hemispherical complex ranging from 11–17 nm in diameter [60]. It was inferred by Tarry et al. that the size of the complex is large enough to accommodate 7 copies of TatB and TatC in equimolar ratio [43,60]. The central cavity within the hemisphere was not large enough to accommodate the substrate; although it was shown to expand upon substrate binding [60]. The functional role of this cavity is not clearly understood, however it is predicted to be implicated in signal peptide insertion once the precursor protein has been recognised by Tat [61,62]. The substrate itself is shown to bind to the periphery of the TatBC complex with a maximum of two substrates bound per complex, which possibly indicates a negatively cooperative binding event. In this review we have presented a feasible assembly for the TatBC complex, using the structure of TatC recently resolved by Ramasamy et al. [63]. In this hypothetical assembly, the substrate binding would have a knock on effect on the adjacent TatC monomers by "closing off" binding sites to neighbouring TatC proteins. The second substrate binding would therefore be most favourable on the opposite side of the complex, similar to that observed by Tarry et al. [60].

Recent structural characterisation of the individual TatC components has hugely contributed to the understanding of its functional role. TatC is the largest and most conserved component of the Tat machinery in both bacteria and chloroplasts [54]. It plays a central role in the translocation event, ranging from substrate recognition and binding, to the recruitment of other Tat components [36]. The predicted topology of TatC shows the protein to form 6 transmembrane helices with the N- and C-termini residing in the cytoplasm (Fig. 3) [64]. Recent 3D crystallisation studies on TatC from *Aquifex aeolicus* present a "glove-like structure" [63,65], where TatC appeared to assemble into a concave structure as a result of transmembrane helix (TMH) TMH5 and TMH6 being shorter in length relative to the remaining helices (Fig. 3)[65]. Data showing that TMH5 could interact with the TMH of TatB suggests that a functional role for the "groove" of TatC is possible: it could accommodate a single TatB protein- or at least in part (Fig. 3B). Additionally, the interaction of TatC's periplasmic loops with TMHs of neighbouring TatC proteins, suggests they most likely possess a role of maintaining the stability of the complex (Fig. 3)[65].

The residues that line the groove of this glove-like structure are predominantly aromatic with the potential to bind the lysine on the amphipathic helix of the signal peptide [63]. This characteristic shape and residue environment may imply a possible site for signal peptide insertion into the bilayer [61]. In compliment, mutation within the N terminus of TMH1 and the first cytoplasmic loop are involved in substrate binding. Compilation of these studies and recent studies suggest the substrate is bound inside the TatC protein with the linker region forming a hairpin around TMH4 of TatC. The possible association of the TatBC unit with the substrate bound is shown in Fig. 4.

3.2.2. Recent mechanistic studies on the TatBC complex

It has been well documented that the Tat substrate-binding site in *E. coli* consists of a hetero-oligomeric complex of TatB and TatC (Hcf106 and cpTatC in the thylakoid Tat system). Whilst it is known that the Tat-dependent precursor binds to this complex for subsequent
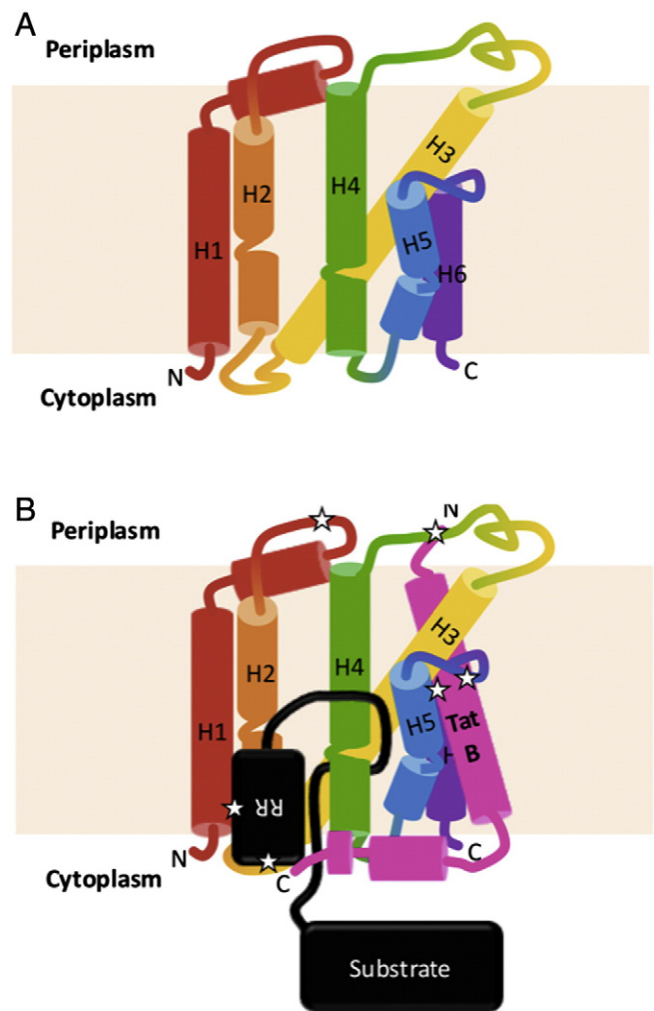
Fig. 3. The topology of TatC within the cytoplasmic membrane +/− the presence of TatB and precursor protein. A. Shows the N-in C-in arrangement of the multi-spanning TatC protein within the cytoplasmic membrane. B. Shows how the TatBC complex may arrange itself within the cytoplasmic membrane upon precursor binding. Critical interactions identified from cross linking studies are starred. TatB makes three vital contacts to TatC. Namely: to TMH 5 of TatC (blue) and its second periplasmic loop (green/yellow). TatB (pink) could be accommodated within the groove of TatC which was shown to exist from recent crystallisation data (§3.2.1). The first periplasmic loop (red/orange) fails to make contact with TatB, yet is in close proximity to a neighbouring TatC; lending to the idea that this loop is implicated in self-assembly and maintaining the stability of the TatBC complex. Recent data allude to a hairpin-like insertion of the precursor signal peptide (shown in black). The signal peptide makes vital contacts to the extreme N-terminus of TatC and its first cytoplasmic loop (orange/yellow).

translocation into the periplasm/thylakoid lumen, the precise details of this interaction have only started coming to light in recent years. This information is vital for elucidating the most ambiguous topic of this translocase — its mechanism of translocation.

TatC is known to be the primary site of interaction between a Tat RR-precursor protein and the substrate-binding complex [59,60,62,66–71]. Site specific cross-linking has elucidated that RR-precursors make contact to the cytosolically exposed extreme N-terminus and first cytosolic loop of TatC (Fig. 3B) [72]. This data is in agreement with results demonstrating that the signal sequences of membrane-bound Tat substrates are still accessible to proteases and can be detached by disrupting electrostatic interactions [73,74].

To gain further insight into this interaction between TatC and RR-precursor proteins, a random mutagenesis study was performed with the aim of identifying regions within TatC that are essential for protein transport [75]. Mirroring the results mentioned previously, conserved residues of TatC that are essential for its activity were identified in its
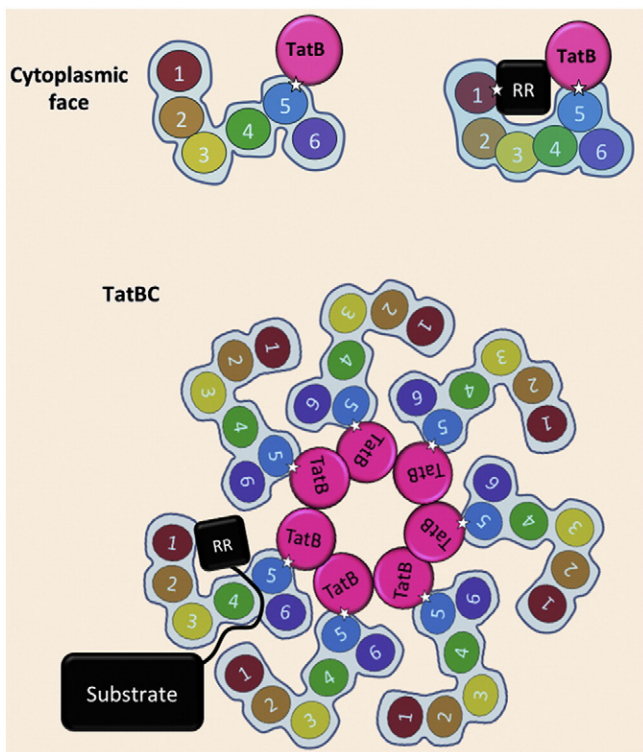
Fig. 4. Cytoplasmic-view of a Tat RR-precursor protein binding to the TatBC substrate-binding complex. This schematic amalgamates available structural and cross-linking data on the TatBC complex to hypothesise how TatB and TatC could arrange themselves in the cytoplasmic membrane upon precursor binding. We hypothesise that for Tat precursors to bind an individual binding site, whilst the complex still accommodates 7 copies of TatBC in equimolar ratio, the TatBC complex could arrange itself as shown. Not only would this satisfy the aforementioned cross-linking data, an arrangement such as this would be in agreement with EM data of SufI-bound TatBC; in that the Tat precursor would bind to the periphery of the TatBC complex. It is plausible that precursor binding to the shown position could alter the accessibility of neighbouring binding sites and therefore result in the Tat translocase exhibiting negative cooperativity.

first cytoplasmic loop. However an abundance of this study's inactivating mutations localised in the first two periplasmic loops of TatC (P1 and P2). Whilst additional insertion and deletion analysis supported the idea that these regions are essential for transport, it remains unclear as to what roles they may fulfil. Inactivating mutations in P1 and P2 did not affect insertion of TatC into the membrane or make it unstable, nor did they inhibit the formation of TatBC substrate-binding complexes. More specifically, the P1 loop fails to make contact with TatB, yet is in close proximity to a neighbouring TatC (Fig. 3B) [75]. The P2 loop makes contact with neighbouring TatC [42], TatB and TatA [72]. Zoufaly et al. [72] inferred that the P2 loop of TatC may be involved in maintaining the stability and functional interaction between TatB and TatC, since a P142S substitution mutation in this region suppressed the defective transport of a mutant KK-precursor protein [76]. Mutational studies on the TatC protein in chloroplasts revealed the functional significance of the stromal loops, where the 1st and 2nd loops are involved in self-assembly as well as interaction with other Tat components [77].

Despite it being well documented that TatB and TatC form a stable, substrate-binding complex, there is a deficiency of molecular details on specific sites of contact between the two proteins and the precursor protein. In the aforementioned study [75], in addition to the N-terminal region of TatC making contact with the RR-signal peptide, cross-linking analysis also revealed that this region comes into close contact with TatB; reinforcing the molecular neighbourhood of these two proteins [75]. In light of the data showing that TatB possesses the capability to directly interact with RR signal peptides [59,68,70,71,78], including residues flanking the RR-pair [59,68], it is suggested that TatB functionally cooperates with TatC by forming part of the signal binding pocket [72].

Lausberg et al. found evidence for a tight cooperation of TatB and TatC during recognition of Tat signal peptides. To analyse which regions are involved in the substrate binding event, this study searched for suppressor TatB or TatC mutants that successfully supressed the translocation defect of mutant precursor TorA(D^{2+})-MalE [79]. Three mutations were found (TatC K18E, TatB L**9**P and TatB L**9**Q) which each displayed clear synergies with a L9F mutation of TatC i.e. restored export of TorA(D^{2+})-MalE; adding strong genetic evidence for a tight cooperation of TatB and TatC during signal peptide recognition, and for the participation of both components in the formation of a specific signal peptide binding site [79].

According to the topology model of TatB, position **9** is located at the periplasmic-oriented end of the TatB TMH. Such a location reflects one of two situations. Either the effects of these mutations are long-range conformational ones in that they are transmitted via the TMH of TatB to a binding pocket located on the cytoplasmic face of the TatBC receptor complex. Or, they could affect precursor binding at a stage when the signal peptide and the early mature part of the precursor had been transferred to an advanced-stage binding site that would reach out as far as the periplasmic end of the TMH of TatB.

Beyond recognition of the RR-precursor, it has remained questionable as to which component of the TatBC substrate-binding complex mediates the transmembrane insertion of the RR-signal peptide; commencing translocation of the protein. Frobel et al. showed that despite a lack of TatB, the signal sequence of translocation-incompetent substrates was removed, in addition to the premature cleavage of the signal sequence from a substrate capable of translocation [80]. This lends itself to the idea that when a precursor protein interacts with TatB, it prevents the premature cleavage of the signal peptide; revealing a potential insertase activity of TatC in addition to further evidence for the concerted activity of TatB and TatC in recognising Tat substrates.

Although it is well established that TatB is part of the substrate binding site, its precise function in the substrate-binding process has remained elusive. Maurer et al. demonstrated that upon precursors being targeted to the cytoplasmic membrane via their RR-motif they become surrounded by TatB and make contact to its TMH and APH [62]. This interaction is then lost upon translocation, lending itself to the idea that the close vicinity of TatB and precursor is an intermediate binding step that occurs prior to translocation [62]. This same study found homooligomeric complexes of TatB, containing potentially 2 or 3 TatB monomers, bound to a single precursor molecule. Dimerisation of TatB has previously been demonstrated [81], and this suggests that TatB may assemble into an oligomeric binding site that is capable of transiently accommodating large parts of the folded precursor protein [62]. A model of TatB-precursor protein interaction is speculated in Maurer et al., which is in line with a hairpin-like insertion of Tat signal peptides [62].

In recent years there has been frequent mention of a hairpin-like insertion of Tat-dependent signal sequences into the cytoplasmic and thylakoid membrane (Fig. 3B). It is proposed that once the RR-signal sequence is recognised by the TatBC substrate-binding complex, it is threaded deep into the receptor complex reaching out as far as the periplasmic end of the TatB TMH; resulting in the formation of a hairpin loop topology of the signal peptide and early mature region of the precursor protein. This hypothesis is experimentally supported by numerous studies. In *E. coli*, the N-terminus of TatB was found to cross-link to precursors TorA and SufI prior to translocation completion [62]. For the same region of TatB, suppressor mutations were found to compensate the translocation defect of mutant TorA precursors [70,79]. Finally, translocation can progress to completion despite the N-terminus of an RR signal peptide being covalently bound to TatC in thylakoids [68].

Until recently there had been a lack of information regarding the precise logistics of substrate binding. A recent study by Ma and Cline gained insight into the topology of bound precursors [82]. They found that Cys residues inserted into the signal peptide failed to produce dimers, proposing that each signal peptide is bound to an individual

binding site (Fig. 4). It was also identified that the Tat substrate binding complex has the capability of binding more than one precursor protein. More interestingly, they identified that cross-linked dimer and tetramer were readily transported into the lumen without breaking the linkage, concluding that multiple occupied receptor units operate coordinately to transport the oligomer [82].

A later study conducted by Celedon and Cline performed binding analyses on both intact membranes and purified thylakoid Tat complexes in an attempt to further elucidate the stoichiometry of binding to this complex [83]. Their results very much mirrored that of the aforementioned study in that they found the Tat complex bound multiple precursor proteins [82]. More specifically, each Tat substrate-binding complex had the capability of binding 8 precursor proteins that were each independently functional for transport. With sufficient Tha4, all sites were active for simultaneous transport [83]. Despite evidence for simultaneous transport of Tat substrates occurring [82], it is not certain whether this occurs for all Tat substrates; perhaps each site has the same probability of undertaking translocation [83].

On a different note, it still remains to be determined whether this protein transport system displays any form of cooperativity during substrate binding i.e. does Tat's affinity for its RR-precursor proteins alter upon a substrate already having bound the translocase? In agreement with Cline et al., Celedon and Cline found no evidence of cooperativity when examining the binding step [83,84]. However, Tarry et al. inferred that Tat displayed a negative cooperativity for the *E. coli* Tat system in light of evidence that TatBC complexes possessed only one or two bound precursors [60]. Again in contrast, Alder and Theg described a positive cooperativity for the translocation of a Tat precursor. This study kinetically characterised cpTat-mediated protein translocation, where the protein transport displayed a sigmoidal rate-substrate relationship; indicating allosteric proteins. The measured Hill coefficient of 1.8 was postulated to result from 2 binding sites per translocation with strong cooperativity. However, it could not be determined whether such characteristics were exhibited at the binding or translocation step [85]. Clearly more research needs to be employed in this area to absolutely identify which form of cooperativity is displayed during substrate-binding to the Tat translocase.

Once the precursor protein has been recognised by and subsequently bound to TatBC, it is still unclear as to how the Tat-dependent substrate traverses the membrane. A real-time FRET experiment analysed the kinetics of precursor interactions with the Tat translocase [86]. Results showed that once the membrane becomes energised there is a delay in cargo migration away from the binding site; suggesting that the Δ is not directly responsible for promoting migration of the Tat precursor across the membrane [86]. Moreover, it was found that TatA increases the affinity of the TatBC receptor complex for the precursor in the presence of a membrane potential [86]. These data are in agreement with the hypothesis that TatBC and TatA oligomerisation occurs in the presence of a Δ with or without the cargo. It is plausible that this oligomerisation process is responsible for the lag phase observed. The subsequent loss of FRET signal after such phase is rapid, signifying that migration of the mature domain from TatABC is fairly quick post-oligomerisation [86]. Despite this, it still remains unclear whether the mature domain of the Tat-dependent protein proceeds directly across the membrane after oligomerisation of TatABC or whether there is an additional kinetic intermediate e.g. the protein residing within a pore [86].

Whilst a wealth of information regarding substrate binding focuses on the TatBC complex, there is evidence for the involvement of TatA during the early stages of translocation. Since *E. coli* TatBC complexes contain TatA when purified [46,87], it is unsurprising that Frobel et al. reported TatA to be an early interacting partner of the TatBC receptor complex [88]. The finding that cross-links between TatA and Tat-dependent precursors were not obtained in the absence of TatBC, not only highlights the intramembrane proximity of TatBC and TatA, but also strongly suggests that a functional hierarchy exists between Tat precursors and Tat subunits i.e. the interaction with TatA requires that

the precursor has already been recognised by the TatBC substrate binding complex [88]. Moreover, the precursor contacts to TatA were sensitive to the dissipation of the PMF. Hence, this interaction with TatA does not directly correspond with the precursor binding to the TatBC but instead represents a subsequent targeting event that is dependent on the presence of a PMF [88].

More specifically, the RR-precursors made contact to the N-proximal region of the TMH of TatA. Considering data that showed the precursor protein to make contact with the N-terminal region of TatB [62], a possible explanation for this interaction would be the deep insertion of a Tat signal sequence prior to translocation. Furthermore, once a TatA monomer is recruited to the TatBC receptor, it is possible it could serve as a 'nucleation point' for the subsequent recruitment of additional TatA to form the active translocase [88]. This is supported by the finding that oligomerisation of Tha4 (the thylakoid TatA homolog) occurred upon binding of a Tat signal peptide [89].

3.3. The TatA complex

Vital to elucidating the mechanism of the twin arginine translocase is gaining structural insight into the individual Tat components. TatA is one such component, which through oligomerisation with other TatA protomers has been predicted to form the 'pore' of this translocase in the cytoplasmic membrane, permitting the passage of fully-folded proteins into the periplasm.

Whilst electron microscopy structures of TatA showed ring-like complexes, there is a lack of detail on the arrangement of TatA oligomers within this ring. Nor is there any information on how TatA facilitates the transport of fully-folded proteins with such an arrangement [90]. Through the use of solution NMR, Rodriguez at al. generated a model for the TatA oligomer, which was subsequently utilised to propose a structure of the oligomeric complex [91]. Combination of these structures with molecular dynamic simulations permitted predictions as to how TatA might mediate the translocation of Tat-dependent precursors across the membrane.

The precise oligomeric state of TatA varies in cell membranes and detergent micelles [60,90,92,93]. The interfacial contacts obtained between TatA TMHs and dodecylphosphocholine (DPC) micelles in Rodriguez et al. are consistent with previous EPR studies of TatA in $C_{12}E_9$ [27]. For the 9-mer repeat of a TatA oligomer, the crossing angle of each subunit's TMH is 4.2°, meaning there is a narrow contact surface whereby large increase in subunit numbers results in small changes in intersubunit contacts. However, the APH extend out from the pore axis meaning that the varying subunit number in this instance would avoid APHs making contact. These components of TatA may provide an upper limit to oligomer size in light of the fact that inter-APH distances decrease upon the addition of subunits.

On a different note, TatA proteins possess a conserved polar residue at the N-terminal end of the TMH [40]. Through molecular dynamics conducted in this study it is postulated that when TatA oligomerises, this residue resides in the centre of a TatA pore and is water accessible [94]. The position of this residue results in a pore that is only hydrophobic for 3 turns of the TMH; approximately half that of a typical membrane bilayer [94]. Further simulations indicated that this pore can house lipids, but they are distorted relative to those in the surrounding membrane. It is predicted that these lipids could provide an energetic barrier to the loss of protons during transport [94]. This thinned and distorted membrane within the pore of a TatA oligomer would provide a clear pathway for the translocation of the substrate protein, giving a reasonable explanation for how substrates traverse the cytoplasmic membrane through the pore of TatA.

Additionally, when TatA oligomerises during translocation, it must reorient in the cytoplasmic membrane to generate the 4.2° shallow crossing angles for TMH packing. Such movement would result in the entire APH of TatA lying along the surface of the membrane, which is in agreement with data that found changes in accessibility of Tha4

APH upon substrate binding [95]. This relocalisation would pull the TMH of TatA into the cytoplasmic leaflet of the membrane, reducing the length of the TMH. Further shortening occurs due to the presence of a conserved polar residue at position 8 in the N-terminal region of the TMH. As a consequence, a hydrophobic mismatch is generated within the membrane bilayer resulting in its thinning and lipid disordering within the pore of TatA. Therefore, to add to the model of translocation for Tat, this study suggests that a bound substrate is located over a thinned and disordered patch of membrane that is susceptible to rupture [94].

To continue the theme of subunit organisation of TatA within the lipid bilayer, a site-directed spin labelling study shed light on how the TMHs of TatA are arranged in the membrane [27]. As already mentioned, single-molecule electron microscopy of detergent-solubilised TatA has shown TatA to exist as ring-shaped structures with variable diameters [90]. The largest of these complexes contained cavities that could accommodate large, folded Tat substrates, leading to models that proposed TatA complexes to provide the translocation pore in the assembling translocase. With the assumption that the TatA ring has a transmembrane orientation, it is likely that the TMH of TatA forms part of the ring wall. However, the extent to which the APH and C-terminal tail of TatA contribute to this wall structure as opposed to the cap is unclear. It also remains unknown as to how the TMH of this Tat component may pack together to form rings of variable diameter, nor do we know which residues within the TMH lie at the inter-helical binding surfaces [27].

White et al. hypothesise that the TMH of TatA are positioned side-by-side during pore formation. Their EPR study detected interactions between Ile112 on one side of each TMH and Val14 on the other, suggesting a Ile112-Val14 arrangement of helices for TatA during pore formation [27]. Of course, other regions of TatA could be positioned within the ring or on either side of the wall of TMHs.

However, the exact nature and functionality of TatA-type complexes was made more confusing by recent structural studies that showed the TatE component of E. coli, which can functionally substitute for TatA, to form complexes that are much smaller and more homogeneous than TatA complexes [93]. More specifically, the solubilised TatE forms ring-shaped complexes of 6–8 nm in diameter that are much too small to accommodate the larger Tat substrates like TorA that is 90 kDa. The small size of TatE complexes would appear to preclude this protein from possessing a pore-forming role, suggesting another mechanism of Tat translocation whereby TatABC contributes the bulk of the translocation channel and TatA/E activates it [93]. This is supported by data illustrating that the thylakoidal TatC is actively involved in the translocation event as opposed to solely being the primary binding site for the substrate protein [68].

Another possibility is that multiple TatA or TatE complexes bind to the TatABC complex once the substrate has bound, with flexibility in pore size arising from different number of TatA/E protomers [93]. This model is supported by the identification of multi-ringed structures of TatE i.e. modular interaction of smaller rings to produce a larger super-structure [93]. In agreement with the inferences from TatE electron microscopy data, ultrastructural characterisation of TatAd complexes from B. subtilis suggests that these too are smaller and more homogeneous than E. coli TatA complexes, with no indication of a pore that would be large enough to translocate large fully-folded Tat substrates. In this study, it was shown that TatAd, which can also substitute for TatA, forms a ring-shaped structure of ~7.5–9 nm in diameter, possessing a potential cavity or pore of 2.5–3 nm that is occluded at one end by a lid-like structure [51]. The authors speculate that this lid structure is comprised of the APH and C-terminal tails of TatAd since these are the most flexible regions of the protein. It is predicted that this lid serves to seal the translocation channel, maintaining the integrity of the membrane.

As for TatE, the small size of the pore has major implications on the mechanism of translocation and supports the above model of the coalescence of relatively homogeneous Tat(A)BC and multiple TatA or TatE complexes. It also questions the functional relevance of TatA heterogeneity in E. coli. Simply put, additional functional studies are required to understand the nature and role of TatA-type complexes with respect to the overall Tat mechanism.

4. Mechanism of translocation — summary and emerging ideas

There appears to be a general agreement that the substrate binds initially to TatBC (Hcf106-cpTatC in thylakoids), and this binding is independent of other Tat components [58]. Once the precursor is bound to the substrate-binding TatBC complex, the TatA complex associates with the TatBC complex in the presence of a ΔpH [66]. It is likely that the initial binding of the substrate requires only TatB and TatC, while the TatA is recruited once substrate binding has occurred. It is at this point that uncertainty starts in earnest: the active translocon has never been 'captured' in any sense apart from cross-linking studies and our understanding of the core translocation event is accordingly vague, but the recent structural data have led to plausible models for the mechanism of translocation (Fig. 5): the translocation pore model and the membrane destabilisation model [96].
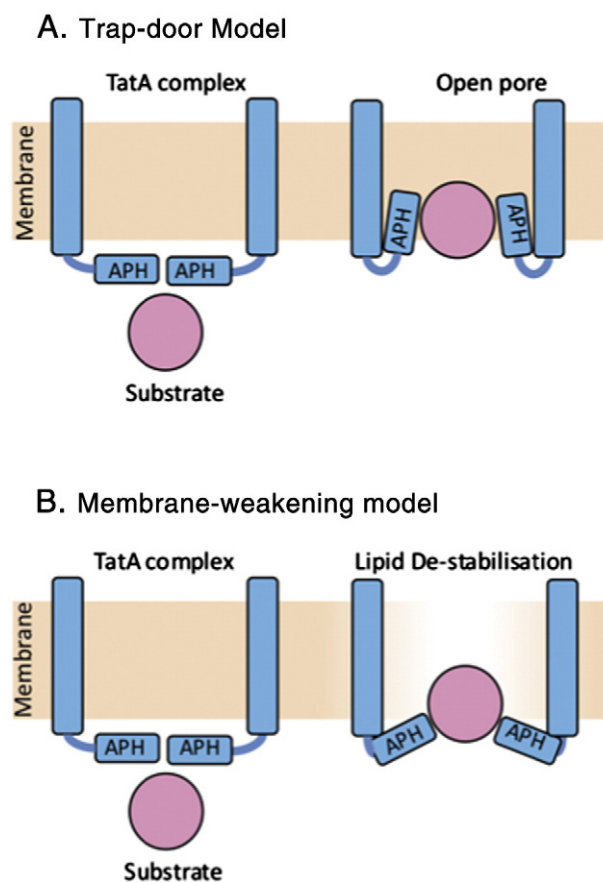
Fig. 5. Mechanism of Tat translocation. A substrate bearing a twin-arginine signal peptide is recognised by the TatBC complex in a resting membrane. The figure shows two proposed models for the subsequent translocation event involving the TatA complex. A. Trap-door model: the amphipathic helix (APH) of the TatA protein has dual topology. In a resting membrane the APH lies along the cytoplasmic face, to form a one-sided lid complex. Upon substrate recognition the APH flips into the bilayer, providing a tightly regulated pore for the translocation of the substrate in the presence of a membrane potential. B. Membrane-weakening model: The APH of TatA in the resting state aligns parallel to the cytoplasmic membrane. The recognition of a substrate induces a topological change in the APH so that it partially perturbs the lipid bilayer, leading to the de-stabilisation of the lipid bilayer. Subsequently, this permits the translocation of the substrate in a less regulated manner.

4.1. Trapdoor model

The "trapdoor mechanism" is based on the hypothesis that the topology of TatA has the ability of to flip its amphipathic helix (APH) domain into the membrane from its resting position along the cytoplasmic face of the membrane [97]. In *E. coli*, TatA is a highly abundant protein relative to TatB and TatC and its ability to form complexes of variable size suggested a possible role as translocation pore [46,98].

The idea of a "Trap door" gained prominence with the first 3D model of the TatA complex constructed by single particle electron microscopy. This study showed two main points: the presence of a cupped pore-like structure was generated and the presence of a range of complex sizes [46,90,99].

In a more recent study, Walther et al. explored the concept of a "Charge Zipper mechanism", portraying a simulated model where the C-terminus region of TatA permits a hairpin fold between the C-terminus and APH using complementary charge interactions [100]. This theoretical work is more inclined to the pore-forming model where the APH C-terminus hairpin flips into the membrane, to provide an internal hydrophilic coating of the pore.

In addition, the substrate itself has been shown to carry a motif which is capable of interacting with TatA [62]. This study suggests the binding conformation between the substrate and TatA is what is expected if TatA was to surround the substrate as if it were a pore. This suggests that TatA may be interacting with the substrate which then leads to a seeding of monomeric TatA to form a pore. In a recent review this substrate interaction and seeding process of TatA is interpreted as mode of pore formation using the PMF [61].

4.2. Membrane weakening model

The concept of membrane weakening was first presented by Bruser and Sanders, who hypothesised that TatA's role is not to form a pore but instead aggregate in an unordered manner, which would result in the formation of Tat complexes large enough to destabilise the membrane [101]. One reason for proposing an alternative mechanism is due to the relatively low abundance of Tha4 (TatA ortholog) found in the membrane of chloroplast, as opposed to the excessive level detected in *E. coli*. As a result, making it more difficult for Tha4 to bind to substrate and rapidly form a membrane-inserting structure round it.

As structural data on the Tat components has mounted over the recent years, this mode of transport is now considered more feasible. Walther et al. resolved the structure of TatAd using NMR, where the amphipathic helix was shown to partially incorporate into the membrane bilayer during a conformational change [31]. In contrast to the otherwise predicted flip topology in the pore model, these NMR studies suggest that the topology of TatA may not be as flexible during the conformation change as initially anticipated [31,97,102]. The swing of the APH from the cytoplasmic face into the bilayer would imply a 'lipid disrupting property' [31].

Another structural characterisation of the TatAd complex performed 3D reconstruction using single particle electron microscopy. Mirroring the results of Gohlke et al., this study also identified the one-sided lid structure in TatA [90]. However, the structural characterisation of this TatAd pore, suggests it may not be able to accommodate substrate [103]. This implies that the pore-like structure assembled from TatA may not actually function as a pore and instead function in membrane destabilisation or active translocon stabilisation after it has been recruited to the substrate-bound complex [104].

When membrane destabilisation is considered as a possible mode of mechanism it must be emphasised that the specificity of substrate transport is also compromised. Therefore for this mechanism to function correctly there must be a maintenance system in place to counteract the destabilisation and prevent leakage of ions. It was proposed that this is mediated by a phage shock protein PspA in *E. coli* and its homolog VIPPI in chloroplasts [105,106]. From the evidence of phylogenetic

conservation and ability of TatA to interact with PspA, this method of membrane stabilisation during export could conceivably be a core element of this proposed membrane weakening model [107].

In summary, we are still a long way from understanding Tat. Structural advances have helped a great deal, but the transient nature of the elusive 'super-complex' has presented a huge barrier to more rapid progress. Studies on other protein translocases were revolutionised by experimental tricks to trap substrates within the translocation channel. Unfortunately, the Tat system has resolutely refused to play this game and substrates are either rapidly translocated or completely rejected. Nevertheless, real advances have been made in the last few years and some of the most essential pieces of the jigsaw are coming into place. Further efforts in this direction may enable us to catch this remarkable system *in flagrante* and understand its unique mechanism.

References

[1] B. Berks, A common export pathway for proteins binding complex redox cofactors? Mol. Microbiol. 22 (3) (1996) 393–404.

[2] T. Palmer, F. Sargent, B.C. Berks, Export of complex cofactor-containing proteins by the bacterial Tat pathway, Trends Microbiol. 13 (4) (2005) 175–180.

[3] K. Cline, W.F. Ettinger, S.M. Theg, Protein-specific energy requirements for protein transport across or into thylakoid membranes. Two lumenal proteins are transported in the absence of ATP, J. Biol. Chem. 267 (4) (1992) 2688–2696.

[4] M. Alami, et al., Separate analysis of twin-arginine translocation (Tat)-specific membrane binding and translocation in Escherichia coli, J. Biol. Chem. 277 (23) (2002) 20499.

[5] T.L. Yahr, W.T. Wickner, Functional reconstitution of bacterial Tat translocation in vitro, EMBO J. 20 (2001) 2472–2479.

[6] V.J. Goosens, C.G. Monteferrante, J.M. van Dijl, The Tat system of Gram-positive bacteria, Biochim. Biophys. Acta (2013 Oct 16) pii: S0167-4889(13)00353-4. http://dx.doi.org/10.1016/j.bbamcr.2013.10.008 [Epub ahead of print].

[7] K. Dilks, et al., Prokaryotic utilization of the twin-arginine translocation pathway: a genomic survey, J. Bacteriol. 185 (4) (2003) 1478–1483.

[8] H. Tjalsma, et al., Proteomics of protein secretion by Bacillus subtilis: separating the "secrets" of the secretome, Microbiol. Mol. Biol. Rev. 68 (2) (2004) 207–233.

[9] M. Sibbald, et al., Mapping the pathways to staphylococcal pathogenesis by comparative secretomics, Microbiol. Mol. Biol. Rev. 70 (3) (2006) 755–788.

[10] T. Palmer, f. Sargent, B. Berks, The Tat protein export pathway, *Escherichia coli and Salmonella*: Cellular and Molecular Biology, American Society for Microbiology Press, 2010.

[11] C.C. Monteferrante, et al., Specific targeting of the metallophosphoesterase YkuE to the bacillus cell wall requires the twin-arginine translocation system, J. Biol. Chem. 287 (35) (2012) 29789–29800.

[12] S. Tottey, et al., Protein-folding location can regulate manganese-binding versus copper- or zinc-binding, Nature 455 (7216) (2008) 1138–1142.

[13] A. Rodrigue, et al., Co-translocation of a periplasmic enzyme complex by a hitch-hiker mechanism through the bacterial tat pathway, J. Biol. Chem. 274 (19) (1999) 13223–13228.

[14] B.C. Berks, F. Sargent, T. Palmer, The Tat protein export pathway, Mol. Microbiol. 35 (2) (2000) 260–274.

[15] F. Sargent, B. Berks, T. Palmer, Assembly of membrane-bound respiratory complexes by the Tat protein-transport system, Arch. Microbiol. 178 (2) (2002) 77–84.

[16] A.M. Chaddock, A. Mant, I. Karnauchov, S. Brink, R.G. Herrmann, R.B. Klösgen, C. Robinson, A new type of signal peptide: central role of a twin-arginine motif in transfer signals for the ΔpH-dependent thylakoidal protein translocase, EMBO J. 14 (1995) 2715–2722.

[17] G. Buchanan, et al., A genetic screen for suppressors of Escherichia coli Tat signal peptide mutations establishes a critical role for the second arginine within the twin-arginine motif, Arch. Microbiol. 177 (1) (2001) 107–112.

[18] M.P. DeLisa, et al., Genetic Analysis of the Twin Arginine Translocator Secretion Pathway in Bacteria, J. Biol. Chem. 277 (33) (2002) 29825–29831.

[19] S. Mendel, et al., The *Escherichia coli* TatABC system and a bacillus subtilis TatAC-type system recognise three distinct targeting determinants in twin-arginine signal peptides, J. Mol. Biol. 375 (3) (2008) 661–672.

[20] C. Sanders, N. Wethkamp, H. Lill, Transport of cytochrome c derivatives by the bacterial Tat protein translocation system, Mol. Microbiol. 41 (2) (2001) 241–246.

[21] S. Cristóbal, et al., Competition between Sec- and TAT-dependent protein translocation in Escherichia coli, EMBO J. 18 (1999) 2982–2990.

[22] N. Blaudeck, et al., Genetic Analysis Of Pathway Specificity During Posttranslational Protein Translocation Across The Escherichia Coli Plasma Membrane, J. Bacteriol. 185 (9) (2003) 2811–2819.

[23] E. Bogsch, S. Brink, C. Robinson, Pathway specificity for a delta-pH-dependent precursor thylakoid lumen protein is governed by 'Sec-avoidance' motif in the transfer peptide and a 'Sec-incompatible' mature protein, EMBO 16 (1997) 3851–3859.

[24] J.H. Weiner, et al., A novel and ubiquitous system for membrane targeting and secretion of cofactor-containing proteins, Cell 93 (1) (1998) 93–101.

[25] F. Sargent, et al., Overlapping functions of components of a bacterial Sec-independent protein export pathway, EMBO J. 17 (1998) 3640–3650.

[26] A.M. Settles, et al., Sec-independent protein translocation by the maize Hcf106 protein, Science 278 (5342) (1997) 1467–1470.

[27] G.F. White, et al., Subunit organization in the TatA complex of the twin arginine protein translocase, J. Biol. Chem. 285 (4) (2010) 2294–2301.

[28] C. Lange, et al., Structure analysis of the protein translocating channel TatA in membranes using a multi-construct approach, Biochim. Biophys. Acta Biomembr. 1768 (10) (2007) 2627–2634.

[29] S.D. Müller, et al., Structural characterization of the pore forming protein TatAd of the twin-arginine translocase in membranes by solid-state ^{15}N NMR, Biochim. Biophys. Acta Biomembr. 1768 (12) (2007) 3071–3079.

[30] Y. Hu, et al., Solution NMR Structure of the TatA Component of the Twin-Arginine Protein Transport System from Gram-Positive Bacterium Bacillus subtilis, J. Am. Chem. Soc. 132 (45) (2010) 15942–15944.

[31] T.H. Walther, et al., Membrane alignment of the pore-forming component TatAd of the twin-arginine translocase from Bacillus subtilis resolved by solid-state NMR spectroscopy, J. Am. Chem. Soc. 132 (45) (2010) 15945–15956.

[32] C.S. Chan, et al., The TatA Subunit of Escherichia coli Twin-Arginine Translocase Has an N-in Topology†, Biochemistry 46 (25) (2007) 7396–7404.

[33] O. Pop, et al., The Twin-arginine Signal Peptide of PhoD and the TatAd/Cd Proteins of Bacillus subtilis Form an Autonomous Tat Translocation System, J. Biol. Chem. 277 (5) (2002) 3268–3273.

[34] S. De Keersmaeker, et al., Functional analysis of TatA and TatB in Streptomyces lividans, Biochem. Biophys. Res. Commun. 335 (3) (2005) 973–982.

[35] M. Westermann, et al., The TatAd component of the Bacillus subtilis twin-arginine protein transport system forms homo-multimeric complexes in its cytosolic and membrane embedded localisation, Biochim. Biophys. Acta Biomembr. 1758 (4) (2006) 443–451.

[36] S. Schreiber, et al., Affinity of TatCd for TatAd elucidates its receptor function in the Bacillus subtilis twin arginine translocation (Tat) translocase system, J. Biol. Chem. 281 (29) (2006) 19977–19984.

[37] J.P. Barnett, et al., The twin-arginine translocation (Tat) systems from Bacillus subtilis display a conserved mode of complex organization and similar substrate recognition requirements, FEBS J. 276 (1) (2009) 232–243.

[38] F. Berthelmann, et al., Recombinant Expression of tatABC and tatAC Results in the Formation of Interacting Cytoplasmic TatA Tubes in Escherichia coli, J. Biol. Chem. 283 (37) (2008) 25281–25289.

[39] S. Frielingsdorf, M. Jakob, R.B. Klosgen, A stromal pool of TatA promotes Tat-dependent protein transport across the thylakoid membrane, J. Biol. Chem. (2008) M806334200.

[40] M.G. Hicks, et al., The Escherichia coli twin-arginine translocase: conserved residues of TatA and TatB family components involved in protein transport, FEBS Lett. 539 (1–3) (2003) 61–67.

[41] F. Sargent, et al., Sec-independent Protein Translocation in Escherichia coli. A DISTINCT AND PIVOTAL ROLE FOR THE TatB PROTEIN, J. Biol. Chem. 274 (51) (1999) 36073–36082.

[42] C. Punginelli, et al., Cysteine scanning mutagenesis and topological mapping of the Escherichia coli twin-arginine translocase TatC component, J. Bacteriol. 189 (15) (2007) 5482–5494.

[43] A. Bolhuis, et al., TatB and TatC form a functional and structural unit of the twin-arginine translocase from Escherichia coli, J. Biol. Chem. 276 (23) (2001) 20213–20219.

[44] R.L. Jack, et al., Constitutive expression of Escherichia coli Tat genes indicates an important role for the twin-arginine translocase during aerobic and anaerobic growth, J. Bacteriol. 183 (5) (2001) 1801–1804.

[45] J. Oates, et al., Consensus structural features of purified bacterial TatABC complexes, J. Mol. Biol. 330 (2) (2003) 277–286.

[46] J. Oates, et al., The Escherichia coli twin-arginine translocation apparatus incorporates a distinct form of TatABC Complex, Spectrum of Modular TatA complexes and minor TatAB complex, J. Mol. Biol. 346 (1) (2005) 295–305.

[47] G.L. Orriss, et al., TatBC, TatB, and TatC form structurally autonomous units within the twin arginine protein transport system of Escherichia coli, FEBS Lett. 581 (21) (2007) 4091–4097.

[48] J.D.H. Jongbloed, R. van der Ploeg, J.M. van Dijl, Bifunctional TatA subunits in minimal Tat protein translocases, Trends Microbiol. 14 (1) (2006) 2–4.

[49] J.D.H. Jongbloed, et al., Two minimal Tat translocases in Bacillus, Mol. Microbiol. 54 (5) (2004) 1319–1325.

[50] J.P. Barnett, et al., A minimal Tat system from a gram-positive organism: A bifunctional TatA SUBUNIT PARTICIPATES IN DISCRETE TatC AND TatA complexes, J. Biol. Chem. 283 (5) (2008) 2534–2542.

[51] D. Beck, et al., Ultrastructural characterisation of Bacillus subtilis TatA complexes suggests they are too small to form homooligomeric translocation pores, Biochim. Biophys. Acta (BBA) Mol. Cell Res. 1833 (8) (2013) 1811–1819.

[52] R. van der Ploeg, et al., Salt sensitivity of minimal twin arginine translocases, J. Biol. Chem. 286 (51) (2011) 43759–43770.

[53] C.C. Monteferrante, et al., TatAc, the third TatA subunit of Bacillus subtilis, can form active twin-arginine translocases with the TatCd and TatCy subunits, Appl. Environ. Microbiol. 78 (14) (2012) 4999–5001.

[54] J.D.H. Jongbloed, et al., TATC is a specificity determinant for protein secretion via the twin-arginine translocation pathway, J. Biol. Chem. 275 (52) (2000) 41350–41357.

[55] M. Miethke, et al., The Bacillus subtilis EfeUOB transporter is essential for high-affinity acquisition of ferrous and ferric iron, Biochim. Biophys. Acta (BBA) 1833 (10) (2013) 2267–2278.

[56] M.-R. Yen, et al., Sequence and phylogenetic analyses of the twin-arginine targeting (Tat) protein export system, Arch. Microbiol. 177 (6) (2002) 441–450.

[57] E. de Leeuw, et al., Oligomeric properties and signal peptide binding by Escherichia coli tat protein transport complexes, J. Mol. Biol. 322 (5) (2002) 1135–1146.

[58] H. Mori, K. Cline, A twin arginine signal peptide and the pH gradient trigger reversible assembly of the thylakoid ΔpH/Tat translocase, J. Cell Biol. 157 (2) (2002) 205–210.

[59] M. Alami, et al., Differential interactions between a twin-arginine signal peptide and its translocase in Escherichia coli, Mol. Cell 12 (4) (2003) 937–946.

[60] M.J. Tarry, et al., Structural analysis of substrate binding by the TatBC component of the twin-arginine protein transport system, Proc. Natl. Acad. Sci. 106 (32) (2009) 13284.

[61] J. Fröbel, P. Rose, M. Müller, Twin-arginine-dependent translocation of folded proteins, Philos. Trans. R. Soc. Lond. B Biol. Sci. 367 (1592) (2012) 1029–1046.

[62] C. Maurer, et al., TatB functions as an oligomeric binding site for folded Tat precursor proteins, Mol. Biol. Cell 21 (23) (2010) 4151–4161.

[63] S. Ramasamy, et al., The Glove-like Structure of the conserved membrane protein TatC provides insight into signal sequence recognition in twin-arginine translocation, Structure 21 (2013) 777–788.

[64] J. Behrendt, et al., Topological studies on the twin-arginine translocase component TatC, FEMS Microbiol. Lett. 234 (2) (2004) 303–308.

[65] S.E. Rollauer, et al., Structure of the TatC core of the twin-arginine protein transport system, Nature 492 (7428) (2012) 210–214.

[66] K. Cline, H. Mori, Thylakoid ΔpH-dependent precursor proteins bind to a cpTatC–Hcf106 complex before Tha4-dependent transport, J. Cell Biol. 154 (4) (2001) 719–730.

[67] S. Richter, T. Brüser, Targeting of unfolded PhoA to the TAT translocon of Escherichia coli, J. Biol. Chem. 280 (52) (2005) 42723.

[68] F. Gerard, K. Cline, Efficient Twin Arginine Translocation (Tat) Pathway Transport of a Precursor Protein Covalently Anchored to Its Initial cpTatC Binding Site, J. Biol. Chem. 281 (10) (2006) 6130–6135.

[69] C.A. McDevitt, et al., Subunit composition and in vivo substrate binding characteristics of Escherichia coli Tat protein complexes expressed at native levels, FEBS J. 273 (24) (2006) 5656–5668.

[70] P. Kreutzenbeck, et al., Escherichia coli Twin arginine (Tat) Mutant Translocases Possessing Relaxed Signal Peptide Recognition Specificities, J. Biol. Chem. 282 (11) (2007) 7903–7911.

[71] S. Panahandeh, et al., Following the path of a twin-arginine precursor along the TatABC translocase of Escherichia coli, J. Biol. Chem. (2008) M804225200.

[72] S. Zoufaly, et al., Mapping Precursor-binding Site on TatC Subunit of Twin Arginine-specific Protein Translocase by Site-specific Photo Cross-linking, J. Biol. Chem. 287 (16) (2012) 13430–13441.

[73] F. Gerard, K. Cline, The Thylakoid Proton Gradient Promotes an Advanced Stage of Signal Peptide Binding Deep within the Tat Pathway Receptor Complex, J. Biol. Chem. 282 (8) (2007) 5263–5272.

[74] V. Fincher, M. McCaffery, K. Cline, Evidence for a loop mechanism of protein transport by the thylakoid Delta pH pathway, FEBS Lett. 423 (1) (1998) 66–70.

[75] H. Kneuper, et al., Molecular dissection of TatC defines critical regions essential for protein transport and a TatB–TatC contact site, Mol. Microbiol. 85 (5) (2012) 945–961.

[76] E.-M. Strauch, G. Georgiou, Escherichia coli tatC Mutations that Suppress Defective Twin-Arginine Transporter Signal Peptides, J. Mol. Biol. 374 (2) (2007) 283–291.

[77] X. Ma, K. Cline, Mapping the signal peptide binding and oligomer contact sites of the core subunit of the pea twin arginine protein translocase, Plant Cell 25 (3) (2013) 999–1015.

[78] E. Holzapfel, et al., The entire N-terminal half of TatC is involved in twin-arginine precursor binding, Biochemistry 46 (10) (2007) 2892–2898.

[79] F. Lausberg, et al., Genetic evidence for a tight cooperation of TatB and TatC during productive recognition of Twin-Arginine (Tat) signal peptides in Escherichia coli, PLoS One 7 (6) (2012) e39867, http://dx.doi.org/10.1371/journal.pone.0039867 [Epub 2012 Jun 26].

[80] J. Frobel, et al., Transmembrane insertion of twin-arginine signal peptides is driven by TatC and regulated TatB, Nat. Commun. (2012) 1311.

[81] P.A. Lee, et al., Cysteine-scanning mutagenesis and disulfide mapping studies of the conserved domain of the twin-arginine translocase TatB component, J. Biol. Chem. 281 (45) (2006) 34072–34085.

[82] X. Ma, K. Cline, Multiple precursor proteins bind individual Tat receptor complexes and are collectively transported, EMBO J. 29 (9) (2010) 1477–1488.

[83] J.M. Celedon, K. Cline, Stoichiometry for binding and transport by the twin arginine translocation system, J. Cell Biol. 197 (4) (2012) 523–534.

[84] K. Cline, et al., Multiple pathways for protein transport into or across the thylakoid membrane, EMBO 12 (11) (1993) 4105–4114.

[85] N.N. Alder, S.M. Theg, Energetics of Protein Transport across Biological Membranes: A Study of the Thylakoid [Delta]pH-Dependent/cpTat Pathway, Cell 112 (2) (2003) 231–242.

[86] N. Whitaker, U. Bageshwar, S. Musser, kinetics of precursor interaction with the bacterial Tat translocase detected by real-time FRET, J. Biol. Chem. 287 (14) (2012) 11252–11260.

[87] C.A. McDevitt, et al., Characterisation of Tat protein transport complexes carrying inactivating mutations, Biochem. Biophys. Res. Commun. 329 (2) (2005) 693–698.

[88] J. Fröbel, P. Rose, M. Müller, Early contacts between substrate proteins and TaTa translocase component in twin-arginine translocation, J. Biol. Chem. 286 (51) (2011) 43679–43689.

[89] C. Dabney-Smith, K. Cline, Clustering of C-terminal stromal domains of Tha4 homo-oligomers during translocation by the Tat protein transport system, Mol. Biol. Cell 20 (7) (2009) 2060–2069.

[90] U. Gohlke, et al., The TatA component of the twin-arginine protein transport system forms channel complexes of variable diameter, Proc. Natl. Acad. Sci. 102 (30) (2005) 10482.

[91] F. Rodriguez, et al., Structural model for the protein-translocating element of the twin-arginine transport system, Proc. Natl. Acad. Sci. 110 (12) (2013) E1092–E1101.

[92] M.C. Leake, et al., Variable stoichiometry of the TatA component of the twin-arginine protein transport system observed by in vivo single-molecule imaging, Proc. Natl. Acad. Sci. 105 (40) (2008) 15376.

[93] J. Baglieri, et al., Structure of TatA Paralog, TatE, Suggests a Structurally Homogeneous Form of Tat Protein Translocase That Transports Folded Proteins of Differing Diameter, J. Biol. Chem. 287 (10) (2012) 7335–7344.

[94] C.S. Chan, et al., Towards understanding the Tat translocation mechanism through structural and biophysical studies of the amphipathic region of TatA from Escherichia coli, Biochim. Biophys. Acta Biomembr. 1808 (9) (2011) 2289–2296.

[95] C. Aldridge, et al., The chloroplast twin arginine transport (Tat) component, Tha4, undergoes conformational changes leading to tat protein transport, J. Biol. Chem. 287 (41) (2012) 34752–34763.

[96] R.S. Hauer, et al., Enough is enough: TatA demand during Tat-dependent protein transport, Biochim. Biophys. Acta (BBA) Mol. Cell Res. 1833 (2013) 957–965.

[97] K. Gouffi, et al., Dual topology of the Escherichia coli TatA protein, J. Biol. Chem. 279 (12) (2004) 11608.

[98] E. De Leeuw, et al., Membrane interactions and self-association of the TatA and TatB components of the twin-arginine translocation pathway, FEBS Lett. 506 (2) (2001) 143–148.

[99] D. Beck, et al., Ultrastructural characterisation of Bacillus subtilis TatA complexes suggests they are too small to form homooligomeric translocation pores, Biochim. Biophys. Acta (BBA) 1833 (8) (2013) 1811–1819.

[100] T.H. Walther, et al., Folding and self-assembly of the TatA translocation pore based on a charge zipper mechanism, Cell 152 (1) (2013) 316–326.

[101] T. Brüser, C. Sanders, An alternative model of the twin arginine translocation system, Microbiol. Res. 158 (1) (2003) 7–17.

[102] I. Porcelli, et al., Characterization and membrane assembly of the TatA component of the escherichia coli twin-arginine protein transport system†, Biochemistry 41 (46) (2002) 13690–13697.

[103] D. Beck, et al., Ultrastructural characterisation of Bacillus subtilis TatA complexes suggests they are too small to form homooligomeric translocation pores, Biochim. Biophys. Acta (BBA) Mol. Cell Res. 1833 (2013) 1811–1819.

[104] J. Froebel, P. Rose, M. Mueller, Twin-arginine translocation: early contacts between substrate proteins and TatA, J. Biol. Chem. 71 (2011) 656–668.

[105] S.M. Lo, S.M. Theg, Role of vesicle-inducing protein in plastids 1 in cpTat transport at the thylakoid, Plant J. 71 (4) (2012) 656–668.

[106] M.P. DeLisa, et al., Phage shock protein PspA of Escherichia coli relieves saturation of protein export via the Tat pathway, J. Bacteriol. 186 (2) (2004) 366–373.

[107] R. Kudva, et al., Protein translocation across the inner membrane of Gram-negative bacteria: The Sec and Tat dependent protein transport pathways, Res. Microbiol. 164 (2013) 505–534.